

SUBDUCTION ZONE SEGMENTATION

ALONG THE SUNDA MARGIN,

INDONESIA

Dissertation

zur Erlangung des Doktorgrades
der Mathematisch-Naturwissenschaftlichen Fakultät
der Christian-Albrechts-Universität zu Kiel
vorgelegt von

Alexey Shulgin

Kiel, 2012

Referent: Prof. Dr. H. Kopp

Koreferent: Prof. Dr. E.R. Flüh

Date of the defense: 21 June 2012

Contents

| | |
|---|----|
| Contents | 3 |
| Abstract | 4 |
| Zusammenfassung..... | 6 |
| 1. Motivation | 8 |
| 2. Factors controlling subduction dynamics: the Sunda margin..... | 8 |
| 2.1 Rate and direction of convergence..... | 9 |
| 2.2 Sediment thickness and the seafloor age..... | 9 |
| 2.3 Anomalous relief (geometry, topography) of subducting plate | 10 |
| 2.4 Forearc high | 11 |
| 2.5 Structure of the overriding plate | 13 |
| 2.6 Seismicity along the Sunda margin..... | 13 |
| 2.7 Summary | 15 |
| 3. The objectives of the study..... | 20 |
| Part 1: the Sindbad Project offshore eastern Java | 20 |
| Part 2: the SeaCause project offshore northern Sumatra | 21 |
| 4. Data and methodology..... | 21 |
| 5. Major Results and Novelty | 23 |
| 6. Prospects in subduction system research..... | 27 |
| 7. Acknowledgements | 29 |
| 8. References | 30 |
| 9. Peer-reviewed papers produced during the study..... | 32 |

Abstract

The Sunda margin marks the eastern termination of the Indian Ocean along the Indonesian archipelago, where the subduction of the Indo-Australian plate below Eurasia is taking place. The convergence direction changes from orthogonal in the eastern part of the margin to a more oblique convergence towards the north-west offshore Sumatra. Along the margin, a wide range of subduction scenarios is observed, which makes this margin a perfect natural laboratory to study the role of various physical and geological parameters on subduction dynamics.

This work builds on geophysical and tectonic interpretations of data acquired along eight seismic/gravity and several MCS marine profiles, distributed along the Sunda margin. The data include wide-angle seismic records, multi-channel seismic data, and gravity data. Data interpretation and modeling include a joint reflection/refraction seismic tomography used to constrain geophysical models across the subduction complex at several locations, further constrained by geological information from the multichannel seismic data. Additionally, other geophysical information including gravity modeling and bathymetry data is employed to refine geodynamic models based on seismic interpretations.

Excellent data quality allows detailed structural models of the subduction complex to be constrained in several locations along the Sunda margin. The geophysical models obtained in this study show significant variations of the crustal and upper mantle structure of the subduction complex along-strike and across-strike of the margin. The study revealed an increased thickness of the crystalline crust in the Savu Sea, attributed to the approach of the

Australian shelf to the trench. Offshore Lombok Island, the oceanic crust thickness is found to be 7 km, and heavily fractured by normal faults. The crustal structure of the Roo Rise oceanic plateau was modeled for the first time, revealing the crustal thickness of 15 km. Its subduction is causing inhomogeneous deformation of the forearc and complex evolution of the entire subduction processes. In addition, large variability in the amount of sediment on the incoming plate is found in adjacent sectors of the margin, ranging from ~3 km in the Savu Sea to almost absence in the Lombok and East Java areas. Offshore north Sumatra, comparison of the crustal-scale profiles located on different sides of the segment boundary between 2004 and 2005 earthquakes rupture areas, showed variability of the structure of the oceanic plate and the amount of sediment present at the trench, resulting in the principally different sizes of the accretionary prisms and the width of the seismogenic zone. A comparison of the subduction complex along the adjacent profiles shows that changes in the structure of the incoming oceanic plate result in drastic changes in the structure of the subduction complex and its evolution. New crustal-scale geophysical models enable analysis of the geodynamic effects caused by the transition from oceanic subduction to continental shelf collision, the presence of anomalous relief on the oceanic plate, variations in the morphology of the incoming oceanic plate, and the presence of segment boundaries, and thus provide a solid basis for geodynamic interpretations of subduction processes and the associated geohazards.

Zusammenfassung

Der Sunda Kontinentalrand bildet die östliche Begrenzung des Indischen Ozeans entlang des indonesischen Archipels, wo die Subduktion der Indo-Australischen Platte unter Eurasien statt findet. Die Konvergenzrichtung variiert von orthogonal im östlichen Bereich des Kontinentalrandes zu einer schrägen Konvergenzzone im Bereich vor Sumatra. Die Variation von Subduktionsszenarien entlang dieses Kontinentalrandes ermöglicht das Studieren von unterschiedlichen Subduktions-Parametern und deren Auswirkung auf die Dynamik der Subduktionszone.

Diese Dissertation integriert geophysikalische und tektonische Interpretationen von acht Seismik/Gravimetrie- und etlichen marinen Mehrkanalseismik - Profilen, die den Sunda Kontinentalrand erfassen. Die Daten umfassen Weitwinkelseismik, Mehrkanalseismik, und Gravimetriedaten. Die Modellierung einer refraktionsseismischen Tomographie inkludiert geologische Informationen aus Mehrkanalseismiken und ermöglicht die Erstellung von geophysikalischen Modellen entlang mehreren Lokalitäten des Subduktionskomplexes. Zusätzliche geophysikalische Daten aus Gravimetriemodellen und bathymetrische Datensätze erlauben eine Verbesserung des ursprünglichen geodynamischen Modells.

Durch die exzellente Datenqualität konnten hochauflösende strukturelle Modelle des Subduktionskomplexes im Streichen und quer zum Sunda Kontinentalrand erstellt werden. Diese Modelle zeigen signifikante Unterschiede im strukturellen Aufbau der Kruste und des oberen Erdmantels innerhalb des Subduktionskomplexes. Die Studie zeigt eine Zunahme der kristallinen Krustenmächtigkeit in der Savu See, aufgrund der Annäherung des Australischen

Schelfs in Richtung Tiefseerinne. Die ozeanische Kruste vor der Insel Lombok zeigt eine Mächtigkeit von 7 km, die durch starke tektonische Abschiebungsbrüche charakterisiert ist. Die Krustenstruktur des ozeanischen Roo Rise Plateaus wurde in dieser Arbeit erstmalig modelliert und weist eine Mächtigkeit von 15 km auf. Die Subduktion des Plateaus führt zur inhomogenen Deformation des Forearcs sowie zu einer komplexen Entwicklung des gesamten Subduktionsprozesses. Weiterhin wurden große Unterschiede in der Sedimentmächtigkeit auf der einfahrenden Platte beobachtet. Diese reichen von ~3 km in der Savu See bis nur geringfügiger Sedimentbedeckung in den Bereichen um Lombok und Ost-Java. Ein Vergleich verschiedener Krustenprofile vor Nord-Sumatra, entlang der Segmentgrenze der Erdbeben von 2004 und 2005, zeigt Unterschiede in der Struktur der ozeanischen Platte sowie Unterschiede in der Sedimentmächtigkeit in der Tiefseerinne. Dies resultiert in den unterschiedlich großen Akkretionskeilen und der Breite der seismogenen Zone.

Ein Vergleich der unterschiedlichen Profile des Subduktionskomplexes zeigt, dass strukturelle Variationen der subduzierten ozeanischen Platte dramatische Veränderungen in der Struktur und Entwicklung des Subduktionskomplexes hervorbringen. Unsere krustenmaßstäblichen geophysikalischen Modelle zeigen die geodynamischen Effekte, die durch den Übergang von ozeanischer Subduktion zu kontinentaler Schelfkollision, das anomale Relief der ozeanischen Platte, Veränderungen in der Morphologie der subduzierten ozeanischen Kruste, sowie die Präsenz von Segmentgrenzen hervorgerufen werden. Diese Modelle bilden eine solide Basis für geodynamische Interpretationen von Subduktionsprozessen und den damit verbundenen Naturgefahren und Georisiken.

1. Motivation

Subduction zones, as an important end-member in the dynamics of the Earth, continue to be of major interest to the Earth Science community. Convergent margins represent a significant stage in the oceanic crust recycling process; the associated magmatism and accretion are the key factors responsible for the formation of the continental crust. Processes occurring in subduction zones are responsible for the generation of a major part of the Earth's seismicity, volcanic activity and tsunamis, and are thus directly linked to geohazards. From long-term observations it is known that the distribution of large devastating earthquakes and tsunamis is not homogeneous along subduction zones. Furthermore, there are strong variations in the structure of the subduction complex along individual margins; such variability is partially linked to structural heterogeneity of the incoming oceanic plate and the overriding plate. However, factors controlling margin-scale dynamics of the subduction process are still not fully understood, to a certain extent due to a limited number of geophysical models of the marine forearc.

2. Factors controlling subduction dynamics: the Sunda margin

The Sunda margin subduction zone, running offshore Indonesia from India to Australia (*Fig. 1*), is a natural test-site to examine the role of different factors in controlling subduction dynamics on a regional (margin) scale, given the significant lateral variation in the convergence regime and the crustal structure along the different segments of the margin. Among the key factors that affect and control the dynamics of subduction along the margin

are the rate and the direction of plate convergence, the age of the oceanic plate, the amount of sediment in the trench, the presence of anomalous relief on the oceanic plate, and the nature and structure of the overriding plate.

2.1 Rate and direction of convergence

The convergence of the Indo-Australian plate and Eurasia is almost trench-perpendicular in the south-east (offshore Java, Lombok and Flores islands) (*Fig. 1, top*). It becomes more oblique towards the north-west offshore Sumatra, with the trench-parallel motion accommodated by the Sumatra fault system [*Sieh and Natawidjaja, 2000*]. The convergence rate varies from 51 mm/y offshore northern Sumatra [*Prawirodirdjo and Bock, 2004*] to 67 mm/y offshore eastern Java [*DeMets et al., 1994*] and drops to ~15 mm/y around the Timor trough [*Bock et al., 2003*]. The relative convergence vectors at different segments of the margin based on the GSRM1.2 model [*Kreemer et al., 2000; 2003; UNAVCO GEON¹*] are shown in *Figure 1 (top)*.

2.2 Sediment thickness and the seafloor age

Along the Sunda margin, the age of the oceanic Indo-Australian lithosphere increases towards Australia from ca. 45 My offshore Northern Sumatra to ca. 165 My offshore Sumba (*Fig. 2, top; Table 1*). The age of the ocean floor also increases northwards from offshore Northern Sumatra where the now extinct Wharton spreading center is located and reaches ca. 85 My near the Gulf of Bengal.

¹ http://geon.unavco.org/unavco/IDV_datasource_gsr.html

Sediment thickness in the trench along the Sunda margin is highly variable and has a complicated pattern with more sediment in the north-west (due to a large sediment deposit flux associated with the Bengal Fan) and a significant sediment decrease in the south-east towards offshore Sumba. In general, the Sunda margin is commonly ascribed to the “accretive” margin regime [Hamilton, 1988]. However, the global threshold value for the trench sediment of ~1 km [Clift and Vannucchi, 2004] is not valid for the entire margin, at least in its current state (**Table 1**). Furthermore, both accretive [Kopp and Kukowski, 2003] and erosive [Kopp et al., 2006] segments are recognized along the margin. Such variability of the margin regime is related to the amount of trench sediment and is thought to be one of the key factors affecting the overall behavior of a subduction system [Ruff, 1989]. Therefore, the Sunda margin provides an opportunity to study the effect of sediments on subduction dynamics in a wide range of environments as discussed in **Planert et al., 2010; Lueschen et al., 2011 and Shulgin et al., 2012²**.

2.3 Anomalous relief (geometry, topography) of the subducting plate

The presence of anomalous relief on the oceanic plate affects the behavior and the structure of the subduction complex just like any other inhomogeneity [Collot et al., 2004]. Subduction of seamounts, ridges, fracture zones, ocean plateaus, and other tectonic structures present on the ocean floor introduces drastic changes in the dynamics and structure of the shallow subduction complex. In particular, the presence of structural heterogeneity on the subducting plate causes frontal erosion, steepening of the frontal slope, uneven uplift of the

² References in bold refer to the papers (co)authored by the candidate

forearc high, and also has a crucial effect on the seismogenesis of the margin [Yamazaki and Okamura, 1989; Scholz & Small 1997, von Huene et al., 2000, Bangs et al., 2006]. All possible types of relief distortions are found in the Indian Ocean along the Sunda margin (*see Figs 1,4*):

- offshore Northern Sumatra, the Ninety East Ridge approaches the trench;
- further south-east along the margin, a number of fracture zones are subducting (**Shulgin et al., 2012**);
- offshore central Sumatra, the subduction zone is affected by the Investigator Ridge;
- offshore Java, the Christmas Island Igneous Seamount province (which is composed of numerous individual seamounts and the Roo Rise Plateau) is about to enter the subduction zone (**Shulgin et al., 2011**);
- east of Java, offshore Lombok, is the only place along the margin where the “normal” flat abyssal plain is present (**Planert et al., 2010; Lueschen et al., 2011**);
- at the transition from the Sunda arc to the Banda arc (between Sumba and Timor islands), the Australian shelf has approached the trench (**Shulgin et al., 2009**).

Each of these structural domains along the Sunda margin exhibits its own set of specific effects on the subduction process. Thus, the Sunda margin offers a possibility to examine a full range of subduction system responses to anomalous relief of the lower plate.

2.4 Forearc high

The formation and evolution of the forearc high are governed by a combination of factors, such as the convergence rate, the amount of trench sediment, and the structure of the

backstop [Dahlen, 1990]. Thus the structure of the forearc high along a subduction zone can provide additional information on the internal structure and processes in the subduction complex itself.

Along the Sunda margin, bathymetric studies [Krabbenhoeft *et al.*, 2010] show a significant topographic variability of the forearc high along the subduction zone (**Fig. 1**):

- in the northern segment of the margin, offshore Sumatra, the forearc high is manifested in a number of islands located parallel to the trench;
- offshore western Java, the forearc high deepens and lacks any islands, rather being manifested by a continuous underwater ridge-like structure;
- further east, offshore eastern Java, the continuous ridge-like structure is broken into a series of individual summits and troughs, which follow a linear trend parallel to the trench;
- offshore Bali and Lombok, the continuous ridge-like structure of the forearc is restored, but at a lower elevation as compared to the western segments;
- in the vicinity of Sumba, the forearc high as a bathymetric feature diminishes. There, the transition from the Sunda to the Banda arc takes place and the convergence regime changes from oceanic subduction to continent – island arc collision.

The observed variability of the forearc high does not correlate with the seismicity domains shown in **Figure 3** (see the subsection 2.6 for details). In contrast, it clearly reflects distinctive differences in the internal structure and subduction regime along the trench (**Fig. 4; Table 1**).

2.5 Structure of the overriding plate

The structure of the overriding plate (the Eurasian plate in case of the Sunda margin) exhibits an additional control on the dynamics and kinematics of the subduction zone. The part of the Eurasian plate adjacent to the Sunda margin is Sundaland - a continental core of southeastern Asia [Hamilton, 1988; Hall, 2002; Hall & Smyth, 2008]. The crust of Sumatra and western Java is thought to be of continental nature. However, further eastwards along the edge of the plate the nature of the crust is more dubious. Beneath eastern Java, the transition from continental crust to an island-arc type crust occurs, further complicated by the presence of Archaean crustal fragments [Smyth *et al.*, 2007]. The tectonic origin and the crustal structure of the islands east of Lombok is still an open question; existing hypotheses propose as their origin tectonically escaped fragments of Australia or remnants of a preexisting forearc [Rutherford *et al.* 2001; Hall & Smyth 2008]. Regardless of their origin, there are significant variations in the structure of the overriding plate along the entire margin. Numerous fault zones and possible trapped fossil crustal fragments in some parts of the margin further complicate the tectonic structure of the Sunda margin.

2.6 Seismicity along the Sunda margin

Subduction zones are known for generating the most devastating earthquakes. However, the distribution of seismicity along individual margins is not uniform; in a non-unique way it reflects the internal structure and dynamic regime of the subduction zone. The Sunda margin is not an exception; it exhibits significant variations in the seismicity pattern along the arc (*Fig. 3*):

-
- the segment offshore northern Sumatra generates a large number of mega large earthquakes, including one of the strongest ever documented, the Mw=9.3 Great Sumatra 2004 Earthquake;
 - offshore central Sumatra, the seismicity covers a full range of depths and magnitudes, with Mw not exceeding 8.5. Additionally, a study of historical seismicity at this segment of the margin reveals a consistent segmentation of the seismic ruptures [*Lay et al., 2005*] (the segmentation of the 2004/2005 earthquakes rupture areas is discussed in **Shulgin et al., 2012**);
 - further east along the arc, the segment offshore Java shows a completely different pattern of seismicity with a lower seismic activity as compared to the Sumatra segments. The maximum magnitudes documented for this sector of the margin do not exceed Mw=8.0 (for references see **Planert et al., 2010**; **Shulgin et al., 2010**). Besides, the major events here are shallow and concentrate closer to the trench with a little activity below the forearc;
 - the transition region from the Sunda to the Banda arc manifests another change in the seismicity pattern. No significant shallow seismicity is documented east of Sumba island, where the activity starts at a depth of ~70 km, thus suggesting a fundamental change in the style of subduction in that area (**Shulgin et al., 2009**).

Given that physical (rheological) properties of the seismogenic zone are essentially controlled by the thermal state [*Hyndman et al., 1997*], the seismicity pattern along the margin provides evidence that thermal evolution of the margin is not uniform, as also reflected in the plate age.

2.7 Summary

The diverse data on the structure, tectonic features, and physical properties of the crustal terranes along the Sunda trench are summarized in *Table 1* and *Figure 4*. The Indonesian subduction zone may be subdivided into six major large-scale domains based on the combined analysis of various parameters: the age of the oceanic lithosphere, the amount of trench sediment, the presence of anomalous relief on the oceanic plate, the rate and the direction of the convergence, and the seismicity regime. Such a subdivision of the margin into several domains, although subjective, simplifies the analysis of factors controlling dynamics and kinematics of subduction, under an assumption that within each domain lateral variations of controlling parameters along the margin are small, compared to their changes across the domains.

This brief summary shows that a wide range of subduction settings are present within the Sunda margin, making it a natural test-site to study the variability of the subduction process, as well as the cumulative effects in variations in the structure of the incoming or the overriding plates and the type and the rate of plate convergence on the evolution of active margins and the associated geohazards.

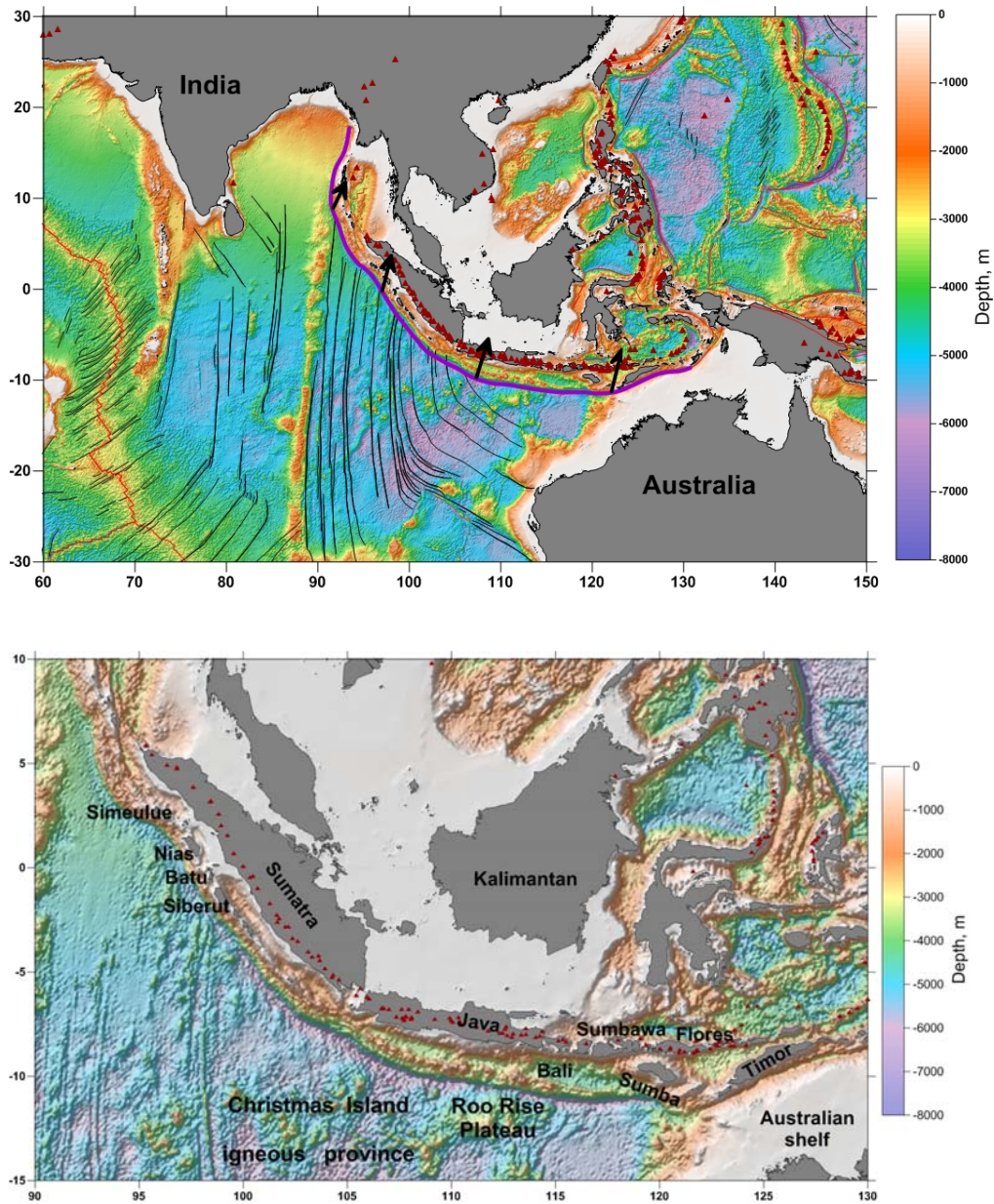


Figure 1. Top: Bathymetric map of the Indian Ocean and the western Pacific. Red lines - major plate boundary features (subduction zones, mid-ocean ridges); black lines – major fracture zones, red triangles - volcanoes. Black arrows show the relative motion of the Indo-Australian plate relative to Eurasia based on the GSRM1.2 model. The Sunda margin (purple line) runs along Indonesia, from the Gulf of Bengal in the north-west to Timor in the south-east, where the transition to the Banda arc occurs. Bottom: zoom-in on the central part of the Sunda margin showing the bathymetric map of the Indian Ocean and the western Pacific with major geographic names mentioned in the text.

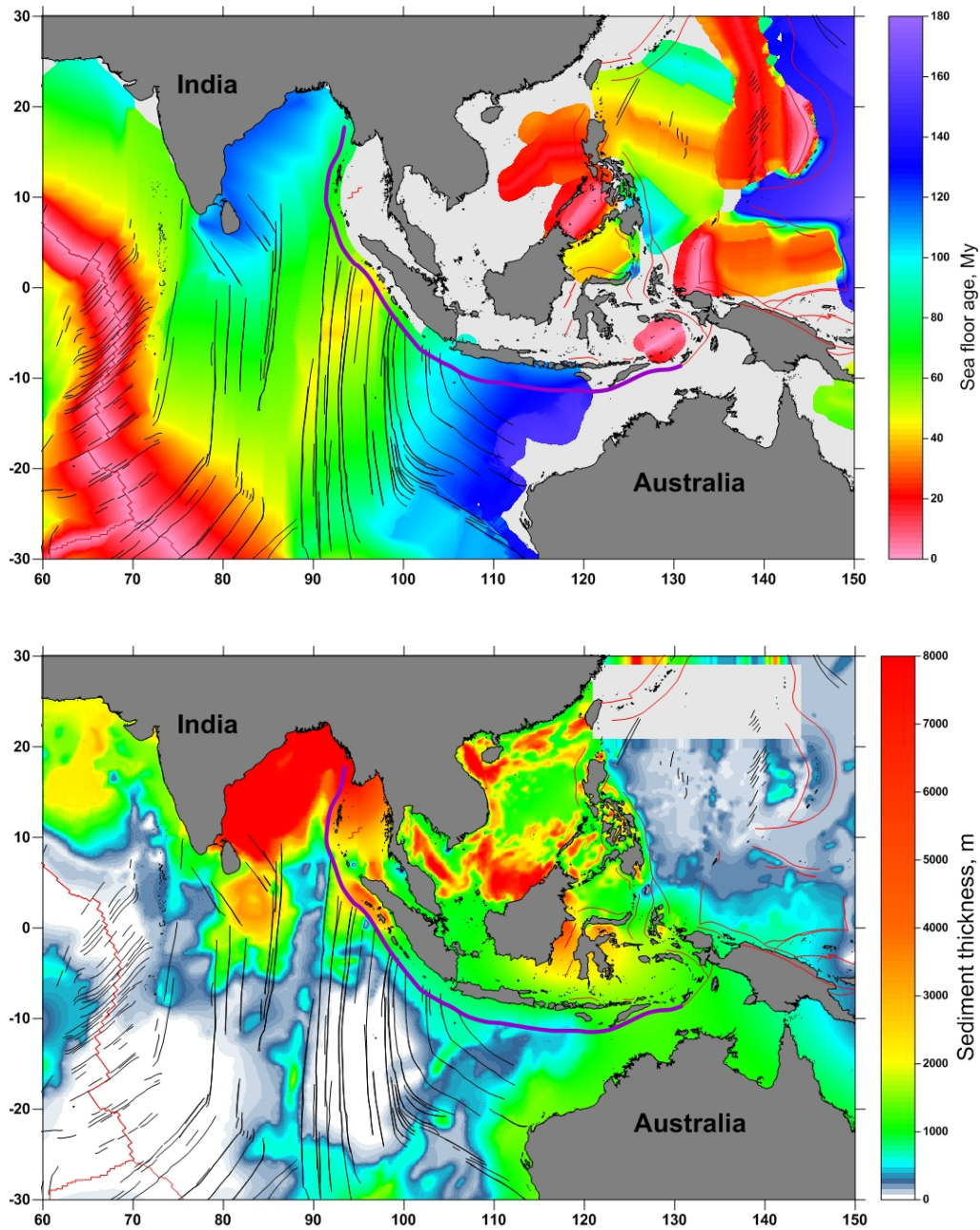


Figure 2. Top: Age of the oceanic crust [Mueller et al., 1997]. Bottom: Thickness of sediments on the oceanic plates [Divins, 2003; NGDC ³]. Red lines indicate the major plate boundary features (trenches, mid-ocean ridges); black lines – major fracture zones. The location of the Sunda subduction zone is shown by the magenta line.

³ <http://www.ngdc.noaa.gov/mgg/image/sedthickimages.html>

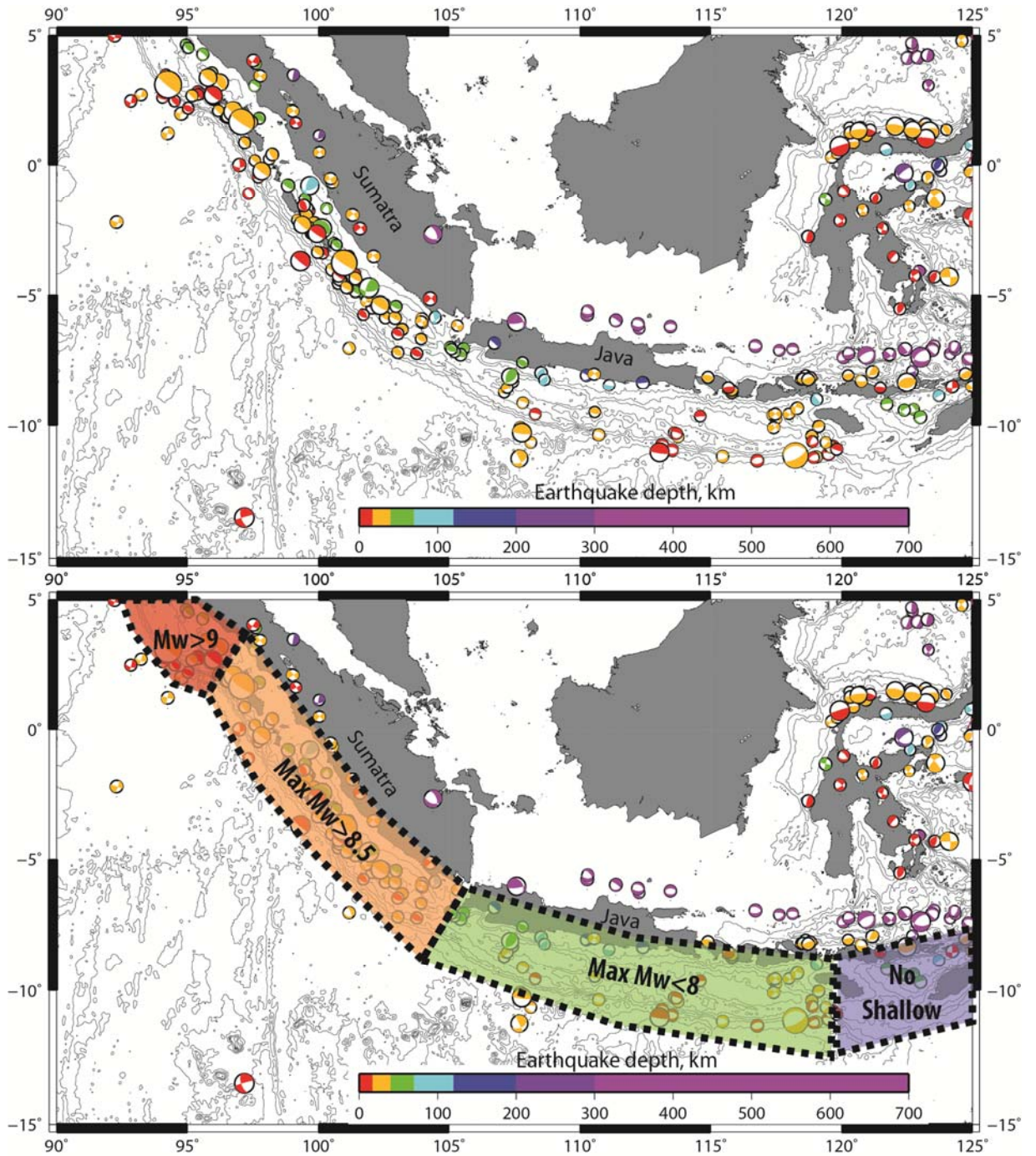


Figure 3. Top: historical seismicity along the Sunda margin, earthquake solutions are plotted for events with $M_w > 5.5$ (after Harvard CMT) and are color-coded according to the depth. Bottom: subdivision of the margin into domains based on the prevailing seismicity.

| Domain | Age of the oceanic lithosphere | Sediment thickness at the trench | Convergence type | Relief on the oceanic plate | Type of the overriding crust | Seismicity |
|------------------------|--------------------------------|----------------------------------|------------------|---|------------------------------|------------------------------------|
| Andaman Islands | 55-80 My | 3-5 km | oblique | no | continental | max Mw=9.3, entire segment rupture |
| Northern Sumatra | 55-80 My | 1.5-3 km | oblique | fracture zones & the Investigator Ridge | continental | max Mw=8.5, segmented ruptures |
| Southern Sumatra | 90-115 My | 1-1.5 km | direct | no | continental | max Mw<8.0, little seismicity |
| Western Java | 130-135 My | < 0.5 km | direct | seamounts & the Roo Rise plateau | island arc | max Mw<8.0, shallow seismicity |
| Eastern Java | 135-165 My | < 0.5 km | direct | no (abyssal plain) | island arc | max Mw<8.0, shallow seismicity |
| Lombok Is. - Sumba Is. | - (Australian shelf) | 2.5-3 km | direct collision | Australian shelf | island arc | no shallow seismicity |

Table 1. Subdivision of the Sunda margin into domains, based on the combination of tectonic and structural parameters and the seismicity regime.

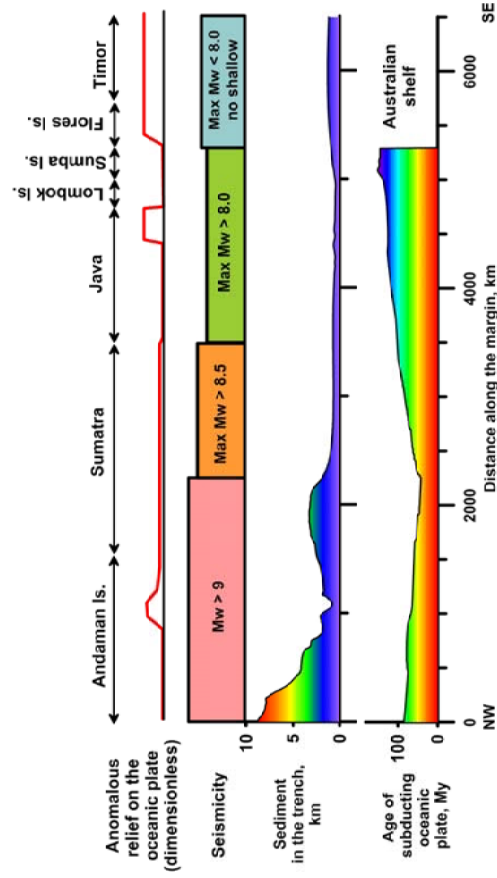


Figure 4. Distributions of anomalous relief, patterns of seismicity, the amount of sediment in the trench, and the age of the subducting oceanic crust along the Sunda margin.

3. The objectives of the study

The observed variability of geological and tectonic structures along the Sunda margin (*Table 1 and Fig. 4*) raises questions on how these changes affect the subduction complex and how they are linked to the observed seismicity patterns. The present study is based on new geophysical interpretation of high-resolution wide-angle seismic reflection/ refraction data, gravity data, MCS data, and bathymetry data acquired in 2006 in two segments of the Sunda margin (investigated by the Sindbad and the SeaCause marine experiments). The results that form the thesis augment earlier work on the Sunda margin in order to examine the entire Sunda Arc subduction zone. The areas of the previous and the current studies are shown in *Figure 5*.

Part 1: the Sindbad Project offshore eastern Java

The main focus of this part of the research project is to examine the effects of the lower plate variability on the subduction complex dynamics (**Shulgin et al., 2009; Planert et al., 2010; Lueschen et al., 2011; Shulgin et al., 2011**). The following main scientific questions are addressed:

- What is the geometry of the subduction complex and the plate interface?
- How does the transition from the oceanic to the continental lower plate affect the subduction complex structure and its dynamics?
- What is the crustal structure of the Roo Rise plateau/ the Christmas Island Igneous Seamount province? How does the subduction of these oceanic structures affect the convergent margin dynamics?

-
- What is the crustal-scale and the uppermost mantle structure of the subduction complex in the neighboring domains of the margin?
 - What causes changes in the forearc high pattern (offshore eastern Java and Lombok)?
 - How is the structure of the subduction complex linked to the seismicity pattern?

Part 2: the SeaCause project offshore northern Sumatra

The major focus of this part of the project is to examine possible causes of the observed seismicity at this segment of the margin (Shulgin et al., 2012). The study area is in the middle of the termination zones of the 2004 and 2005 Sumatra earthquakes ruptures, and is close to the proposed segment boundary that separates these events. The main research questions are:

- Can the segment boundary be identified from changes in the structure of the incoming plate, the overriding plate, or the accretionary complex across the segment boundary?
- Are the observed variations in the subduction complex sufficient to explain changes in the seismic behavior of the megathrust?
- What are likely to be the critical parameters controlling the variability of seismicity along the plate interface across the segment boundary?

4. Data and methodology

To address the set of scientific questions on the structure of the subduction system and the processes within it, the project study builds on geophysical modeling and tectonic interpretation of a unique seismic reflection/refraction data set. In addition, high-resolution bathymetry data were acquired in a number of cruises and several crustal-scale models of Vp

and density based on original interpretations of eight wide-angle collocated seismic/gravity profiles with a total length of ~2000 km and ~4900 km of multi-channel seismic (MCS) data were developed. In particular, within the Sindbad project, the data used in the study include seven wide-angle marine seismic profiles, 150 km to 350 km long, equipped with ocean bottom seismometers (OBS) with the collocated MCS and gravity transects. Additional MCS profiles were acquired inbetween the wide-angle corridors (*Fig. 5*). Within the SeaCause project, the data include the collocated wide-angle seismic profile, MCS and gravity data collected in 2006 .

Geophysical interpretation and modeling of the data was performed by a joint reflection/refraction seismic tomography inversion with incorporation of structural information obtained from the time and depth migrated MCS profiles. The results of the tomographic inversion are crustal-scale Vp seismic velocity models along the wide-angle marine seismic profiles, as well as models for the geometry of seismic reflectors, both controlled by a series of checker tests. The final velocity models are converted to densities, and forward gravity models are constructed to fit shipboard gravity data.

The next step included structural, tectonic, and geodynamic interpretations of the subduction complex along the Sunda margin based on integrated seismic and gravity modeling. Given the fundamental nature of the scientific questions, this work is not expected to give final and ultimate answers, but rather to extend our knowledge of the subduction processes in general by comparing and analyzing high-resolution regional models of the structure of the subduction complex along the convergent margin with highly variable tectonic and geological settings.

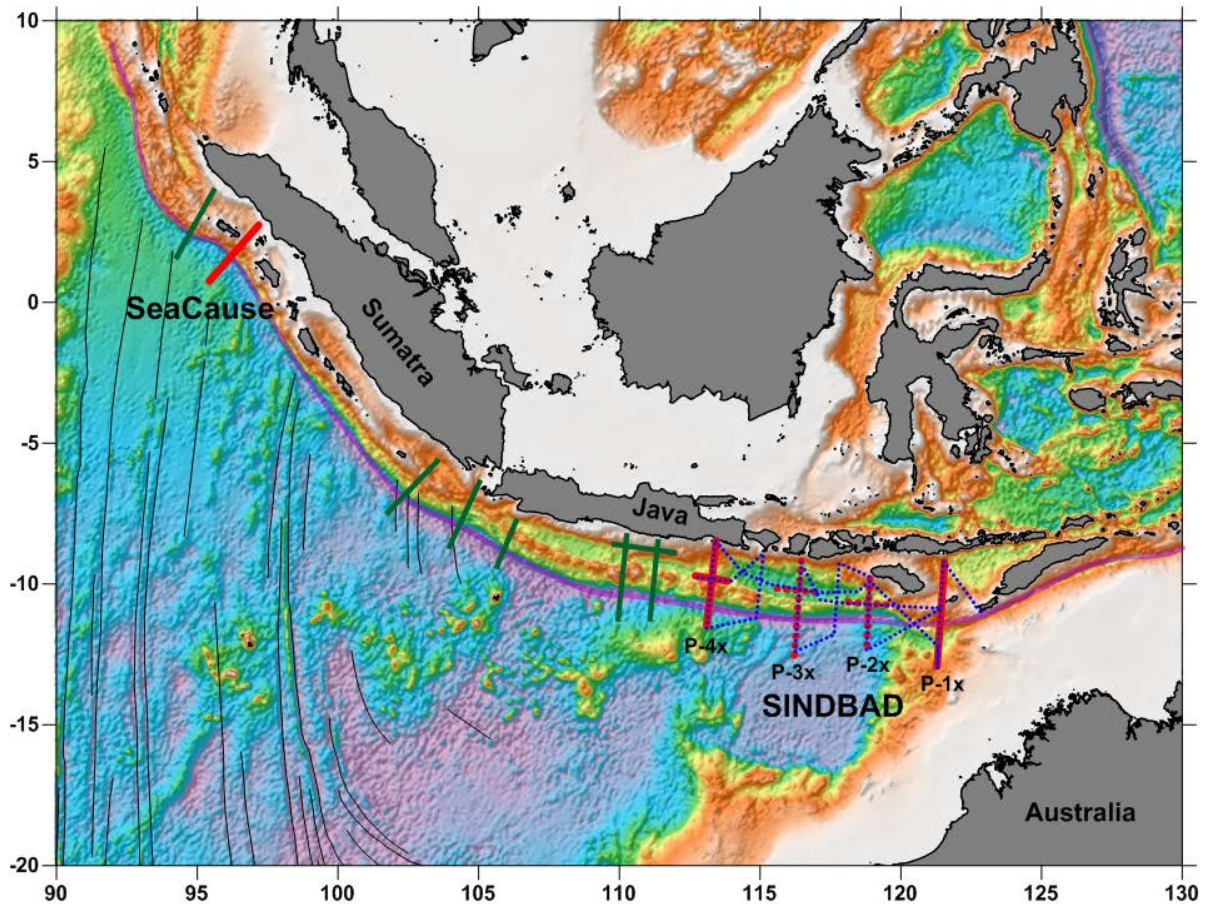


Figure 5. Bathymetric map of the Indian Ocean with the locations of the wide-angle seismic profiles and the multi-channel seismic (MCS) lines. Red – wide-angle seismic profiles interpreted and modeled in the thesis study; blue dotted – MCS profiles interpreted and modeled in the thesis study; green – previous studies in the area. Labels show the names of the marine projects on which this thesis is based.

5. Major Results and Novelty

Detailed crustal-scale seismic images have been obtained for the first time for the south-east portion of the Sunda margin (Shulgin et al., 2009; Planert et al., 2010; Shulgin et al., 2010; and Lueschen et al., 2011). The interpreted geophysical transects of the Sindbad project cover the full variety of the subduction system in the area: the subducting oceanic

crust and the continental shelf, the accretionary complexes, the outer arc highs, the forearc basins, and the slopes of the volcanic island arc. The deep sampling profile has also been interpreted in the vicinity of the 2004/2005 Sumatra earthquakes termination zones, as part of the SeaCause project (**Shulgin et al., 2012**). The combined analysis of seismic wide-angle refraction and reflection data, multichannel seismic data and shipboard gravity reveals the velocity and density structure across the entire subduction system in two key domains along the Sunda margin and results in the new geophysical models of the subduction complex in various tectonic environments. These geophysical models provide a solid basis for the geodynamic interpretations of the subduction processes. They also advance our understanding of the regional seismicity patterns and their links to the subduction settings. The major results related to newly developed geophysical models and their geodynamic interpretations, which are published in 5 peer-reviewed original research articles that compose the thesis:

1) The crustal structure of the incoming Indo-Australian plate has been revealed in detail along a set of adjacent profiles in the area of the Sunda-Banda arc transition (**Fig.5**). At this segment of the margin, the geophysical models show distinct changes in the structure of the incoming crust which ranges from the normal (7 km thick) oceanic crust offshore Lombok (**Planert et al., 2010**) to 12 km thick crystalline crust of the Australian continental shelf (**Shulgin et al., 2009**). The transition from the Sunda arc to the Banda arc is clearly attributed to the approach of the continental shelf to the subduction zone. According to the geophysical models, the subduction east of Sumba island has presently ceased, and the transition from the oceanic subduction to the continent collision regime is proposed (**Shulgin et al., 2009**). The present convergence state of the margin can be regarded as a precursor for the future thrust-

and-fold belt that may develop with time into a Himalayan-type orogeny. This interpretation explains the absence of shallow seismicity at this segment of the margin.

2) The sediment structure constrained by the geophysical models shows a significant variation across the transition zone between the Sunda and Banda arcs. The thickness of sediment along the entire Savu transect is at least 3 km (**Shulgin et al., 2009**), while westwards, offshore Lombok, the trench is almost devoid of sediments (**Planert et al., 2010**). Within the eastern end of the Sunda margin, the oceanic plate varies in its morphology from the “normal” oceanic crust of abyssal plain to sea plateau and continental shelf (**Shulgin et al., 2009; Shulgin et al., 2010; Planert et al., 2010**). The amount of sediment determines whether the segment of the margin is in the erosive or accretive state, as well as the overall size of the accretionary complex. The lower plate is further acting as a shaping tool, affecting the evolution and the deformation of the accretionary body and the forearc structure. Offshore Lombok, a well-developed forearc basin is recovered, and its size diminishes towards Sumba and Java.

3) The analysis of the MCS data from the Sindbad project shows that the oceanic crust offshore Lombok, Sumba, and eastern Java is heavily faulted and fractured into 5-10 km wide blocks (**Lueschen et al., 2011**). Such faulting pattern suggests that faults and fractures control the geometry of the duplexes at the plate interface. In addition, fracturing may facilitate transporting fluids to the base of the crust, thus providing an explanation for the low seismic velocities in the uppermost mantle which can be attributed to serpentinization.

4) The entire crustal-scale seismic velocity and density structure of the oceanic Roo Rise plateau is modeled for the first time as a part of the Sindbad project. The thickness of the

plateau crust is interpreted to be 15 km (**Shulgin et al., 2010**). The subduction of an anomalous relief, such as the Roo Rise or its edge features, results in local frontal erosion, frontal slope steepening, and inhomogeneous deformation of the forearc as evidenced by the high-resolution bathymetry studies (**Lueschen et al., 2011**). In addition, the effect of the anomalous relief subduction is manifested in the increased number of shallow earthquakes, localized around the plate entry point, which is clearly seen in the seismicity patterns. Two geodynamic scenarios are proposed to explain an uneven uplift of the forearc high when the anomalous relief is present in the subduction zone: (a) accretion of the fractured Roo Rise fragments above the static forearc backstop, or (b) basal accumulation of the Roo Rise edge fragments (**Shulgin et al., 2010**).

5) The model of the crustal structure of the subduction zone offshore northern Sumatra, in the rupture area of the 2005 Sumatra earthquake, has been developed as a part of SeaCause project (**Shulgin et al., 2012**). The oceanic plate carries a thin sedimentary cover (<1 km) on top of the 8 km thick oceanic crust. The accretionary complex is composed of a 35 km wide active frontal prism, bounded by a ca. 85 km wide accretionary prism (**Shulgin et al., 2012**), which is significantly larger as compared to the southeast part of the margin. The location of the profile south of the proposed segment boundary between the 2004 and 2005 Sumatra earthquakes provides an opportunity to link the changes in the seismicity patterns to the variations in the structure of the subduction complex across the boundary. The major difference is observed in the amount of sediment on the oceanic plate (3.5 km versus <1 km) and in the trench (5 km versus 3 km), which results in the distinct differences in the volumes of the accretionary complexes. The size of the accretionary prism controls the pore fluid pressure, which, in turn, defines the slip properties of the megathrust, thus controlling the

seismogenesis. The observed difference in the sediment amount suggests that the segment boundary (attributed to the subduction of the 96°E fracture zone) acts as the barrier in the trench-parallel sediment transport. Therefore, it is concluded that the seismicity pattern and the associated geohazards are, to the first-order, controlled by the amount and physical properties of the sediment in the trench.

6. Prospects in subduction system research

Geophysical models of convergent margins, mostly obtained by active seismic methods, provide static 2D snapshots of the current state of subduction zones at different locations. Installations of seismic networks in marine environments are still largely local, targeted, and temporal campaigns. As a result, the marine part of subduction zones is not as well known as their land-side. In order to enhance our knowledge and understanding of the subduction zone behavior, further efforts are required in several directions.

1) Recent technological advances allow for acquisition of new types of geophysical data. The ongoing Ocean Drilling Project in the Nankai Trough will provide direct data on in-situ characteristics of the seismogenic zone as well as rock samples from the outer and inner wedges. Similar new data will be collected at the erosive type of margin offshore Central America. Remote seismological and gravity “sampling” is efficient in gaining information on the internal and deep structure of the subduction zones. Such studies should be complemented by electromagnetic methods, which have different parameter sensitivity and resolution and thus expand the range of physical parameters available for joint interpretation. The transition from 2D to 3D data acquisition and modeling techniques is crucial for further advances in

subduction studies, given short-wavelength structural heterogeneity of convergent margins. 3D data are also required in numerical simulations of the Earth 3D dynamics and will lead to the change in the interpretations of diverse geophysical data from “profiles” to “areas” and “volumes”.

2) The transition from snapshots to time-dependent observations is also important. Presently, studies of earthquakes cycles are limited to seismic monitoring since this is almost the only available real-time instrument. Data on the stress field at the seafloor are either absent or limited to individual locations. During the last decade, the GPS and InSAR systems provided fundamental breakthrough in understanding of stress and strain regimes on land during coseismic and postseismic relaxations. Unfortunately, for the marine environment such systems are only at the early stage of development, but will definitely be highly beneficial when launched.

To conclude, the upcoming research of convergent margins should incorporate a complete multitude of geophysical methods within a solid framework routine, including active and passive seismics, electromagnetics, gravity, marine geodesy, ocean drilling programs etc., further enhanced by the shift from current 2D data acquisition setups to 3D+time schemes and from 2D data interpretations to 3D modeling. I am looking forward to continue my research in this exciting area.

7. Acknowledgements

First and foremost, I would like to thank Prof. Heidrun Kopp and Prof Ernst Flueh for their continued guidance and support throughout the study, as well as for their trust and patience when the work was going slower, than wanted. Their advice and critics (mostly constructive) are warmly acknowledged for been the best help and motivation in improving my understanding of geodynamics. Special thanks go for their efforts in providing financial support.

I specially thank Prof. Ernst Flueh for sparking my interest to the marine geophysics and showing the beauty of the marine expeditions.

The Geodynamics Department is warmly thanked for fruitful discussions and for sharing their expertise in various fields. I thank IT department and especially E. Mezhyrov for solving computer problems they believed could never exist.

Special thanks go to all Ph.D students and post-docs, for their nice company and continued lively discussions on all possible and impossible topics.

I would like to thank all people (participants and the crews) with who I had a chance to be together on the cruises, making it an unforgettable experience.

I sincerely thank Prof. Hans Thybo for his continued support, advice and help during last years.

Many thanks go to my family for their everyday support, constant help, and critics. Special thanks go to my grandfather M. Artemjev and my mother I. Artemieva for convincing me to continue family tradition in geophysics; and to my father A. Shulgin for teaching me how to handle experimental science.

8. References

- Bangs, N.L.B., Gulick, S., Shipley, T., 2006. Seamount subduction erosion in the Nankai Trough and its potential impact on the seismogenic zone. *Geology*, 34, doi:10.1130/G22451.1
- Bock, Y., L. Prawirodirdjo, J. F. Genrich, C. W. Stevens, R. McCaffrey, C. Subarya, S. S. O. Puntodewo, and E. Calais (2003), Crustal motion in Indonesia from Global Positioning System measurements, *J. Geophys. Res.*, 108(B8), 2367, doi:10.1029/2001JB000324.
- Clift, P.D. and Vannucchi, P., 2004. Controls on tectonic accretion versus erosion in subduction zones: Implications for the origin and recycling of continental crust. *Rev. Geophys.* 42, doi:10.1029/2003RG000127
- Collot, J.-Y., et al., 2004. Are rupture zone limits of great subduction earthquakes controlled by upper plate structures? Evidence from multichannel seismic reflection data acquired across the northern Ecuador - southwest Colombia margin. *J. Geophys. Res.*, 109, doi:10.1029/2004JB003060
- Dahlen, F.A., 1990. Critical taper model of fold-and-thrust belts and accretionary wedges. *Annu. Rev. Earth Planet. Sci.*, 18, 55-99
- DeMets, C., Gordon, R.G., Argus, D.F. & Stein, S., 1994. Effect of recent revisions to the geomagnetic reversal time-scale on estimates of current plate motions, *Geophys. Res. Lett.*, 21(20), 2191–2194.
- Divins, D.L., 2003. Total Sediment Thickness of the World's Oceans & Marginal Seas, NOAA National Geophysical Data Center, Boulder, CO.
- Hall, R., 2002. Cenozoic geological and plate tectonic evolution of SE Asia and the SW Pacific: computer-based reconstructions, model and animations, *J. Asian Earth Sci.*, 20, 353–434.
- Hall, R., and H. R. Smyth (2008), Cenozoic arc processes in Indonesia: Identification of the key influences on the stratigraphic record in active volcanic arcs, *Geol. Soc. Am. Spec. Pap.*, 436, 27– 54.
- Hamilton, W., 1988. Plate tectonics and island arcs, *Geol. Soc. Amer. Bull.*, 100, 1503–1527.
- Hyndman, R.D., Yamano, M., Oleshkevich, D.A., 1997. The seismogenic zone of subduction thrust belts. *Island Arc*, 6, 3, doi:10.1111/j.1440-1738.1997.tb00175.x
- Kopp, H., and Kukowski, N., 2003. Backstop geometry and accretionary mechanics of the Sunda margin. *Tectonics*, 6, doi:10.1029/2002TC001420
- Kopp, H., et al., 2006. The Java margin revisited: Evidence for subduction erosion off Java. *Earth Plan. Sci. Lett.*, 242, 130-142.
- Krabbenhoef, A., et al., 2010. Bathymetry of the Indonesian Sunda margin – relating morphological features of the upper plate slopes to the location and extent of the seismogenic zone. *Nat. Hazards Earth Syst. Sci.*, 10, 1899-1911, doi: 10.5194/nhess-10-1899-2010
- Kreemer, C., Haines, A.J., Holt, W.E., Blewitt, G., and Lavalée, D., 2000. On the determination of a global strain rate model, *Earth Planets Space*, 52, 765-770.
- Kreemer, C., Holt, W.E, and Haines, A.J., 2003. An integrated global model of present-day plate motions and plate boundary deformation, *Geophys. J. Int.*, 154, 8-34.

-
- Lay, T., et al. (2005), The Great Sumatra-Andaman earthquake of 26 December 2004, *Science*, 308, 1127 – 1133, doi:10.1126/science.
- Prawirodirdjo, L., and Bock, Y., 2004. Instantaneous global plate motion model for 12 years of continuous GPS observations. *J. Geophys. Res.* 109, B08405. doi:10.1029/2003JB002944.
- R.D.Müller, W.R. Roest, J. Royer, L.M. Gahagan, J. Sclater, Digital isochrons of the world's ocean floor, *J. Geophys. Res.* 102 (1997) 3211–3214.
- Ruff, L., 1989. Do trench sediments affect great earthquake occurrence in subduction zones? *Pageoph.* 129, 1-2, 262-282.
- Rutherford, E., K. Burke, and J. Lytwyn (2001), Tectonic history of Sumba Island, Indonesia, since the Late Cretaceous and its rapid escape into forearc in the Miocene, *J. Asian Earth Sci.*, 19, 453– 479.
- Scholz, C.H. & Small, C., 1997. The effect of seamount subduction on seismic coupling, *Geology*, 25, 487–490.
- Sieh, K. and Natawidjaja, D., 2000. Neotectonics of the Sumatran fault, Indonesia. *J. Geophys. Res.* 105 (B12), doi: 10.1029/2000JB900120
- Smyth, H.R., Hamilton, P.J., Hall, R. & Kinny, P.D., 2007. The deep crust beneath island arcs: inherited zircons reveal a Gondwana continental fragment beneath East Java, Indonesia, *Earth planet. Sci. Lett.*, 258, 269–282.
- von Huene, R., Ranero, C., Weinrebe, W., 2000. Quaternary convergent margin tectonics of Costa Rica, segmentation of the Cocos plate, and Central American volcanism. *Tectonics*, 19, 314-334
- Yamazaki, T. & Okamura, Y., 1989. Subducting seamounts and deformation of overriding forearc wedges around Japan, *Tectonophysics*, 160, 207– 229.

9. Peer-reviewed papers produced during the study

1. **Shulgin, A.**, Kopp, H., Mueller, C., Lueschen, E., Planert, L., Engels, M., Flueh, E. R., Krabbenhoeft, A., Djajadihardja, Y., 2009. Sunda-Banda arc transition: Incipient continent-island arc collision (northwest Australia). *Geophys. Res. Lett.*, 36, doi: 10.1029/2009GL037533; 6 pp.

This paper investigates the structure of the subduction complex at the early stage of the transition from subduction to collision at the Sunda-Banda arc transition. A. Shulgin was responsible for the wide-angle seismic data acquisition & processing, tomographic and gravity modeling, and writing the manuscript and figures preparation.

2. Planert, L., Kopp, H., Lueschen, E., Mueller, C., Flueh, E.R., **Shulgin, A.**, Djajadihardja, Y., Krabbenhoeft, A., 2010. Lower plate structure and upper plate deformational segmentation at the Sunda-Banda arc transition, Indonesia. *J. Geophys.Res.*, 115, doi: 10.1029/2009JB006713; 25 pp.

This study addresses the structure of Sunda margin offshore islands of Flores and Sumba. It links the variability of the deformation patterns of the accretionary complex and forearc to the variations in the structure of the incoming oceanic plate. A. Shulgin was responsible for the wide-angle seismic data acquisition & processing, and the discussion on the results.

3. **Shulgin, A.**, Kopp, H., Mueller, C., Planert, L., Lueschen, E., Flueh, E.R., Djajadihardja, Y., 2011. Structural architecture of oceanic plateau subduction offshore Eastern Java and the potential implications for geohazards. *Geophys. J. Int.*, 184(1), doi: 10.1111/j.1365-246X.2010.04834.x; 17 pp.

This paper investigates the influence of the oceanic plateau on the subduction regime. It is shown that the subducting plateau causes inhomogeneous deformation of the forearc, frontal erosion, and frontal slope over-steepening which has significant effect on the local seismogenesis. A. Shulgin was responsible for the wide-angle seismic data acquisition & processing, tomographic and gravity modeling, and writing the manuscript and figures preparation.

-
4. Luschen, E., Muller, C., Kopp, H., Engels, M., Lutz, R., Planert, L., **Shulgin, A.**, Djajadihardja, Y.S., 2011. Structure, evolution and tectonic activity of the eastern Sunda forearc, Indonesia, from marine seismic investigations. *Tectonophysics*, 508(1-4), doi: 10.1016/j.tecto.2010.06.008; 16 pp.

This study reveals the high-resolution details on the structure of the forearc of the Sunda arc mostly based on the MCS data. It documents the heavy normal faulting of the oceanic crust, and ongoing tectonic activity of the entire outer arc high, including out-of-sequence thrusting, tilting of the sedimentary sequences and vertical displacements of young seafloor sediments. A. Shulgin was responsible for the wide-angle seismic data acquisition & processing, and the discussion on the results.

5. **Shulgin, A.**, Kopp, H., Klaeschen, D., Papenberg, C., Tilmann, F., Flueh, E.R., Franke, D., Barckhausen, U., Krabbenhoft, A., 2012. Subduction system variability across the segment boundary of the 2004/2005 Sumatra megathrust earthquakes. *Earth and Planet. Sci. Lett.* (under revision). 30 pp.

This manuscript addresses the questions of the structural variations across the segment boundary of 2004 and 2005 Sumatra earthquakes. The high resolution tomography model for the 2005 earthquake area is presented and compared to the previously published models for the 2004 epicentral region. The paper provides evidence that one of the main factors controlling the seismogenic behavior of the megathrust offshore northern Sumatra is the amount of sediment present at the trench. A. Shulgin was responsible for the wide-angle seismic data processing, tomographic and gravity modeling, and writing the manuscript and figures preparation.



Sunda-Banda arc transition: Incipient continent-island arc collision (northwest Australia)

A. Shulgin,¹ H. Kopp,¹ C. Mueller,² E. Lueschen,² L. Planert,¹ M. Engels,² E. R. Flueh,¹ A. Krabbenhoef,¹ and Y. Djajidhardja³

Received 29 January 2009; revised 15 April 2009; accepted 17 April 2009; published 27 May 2009.

[1] The eastern Sunda arc represents one of the few regions globally where the early stages of continent-arc collision can be studied. We studied along the western limit of the collision zone at the Sunda-Banda arc transition, where the Australian margin collides with the Banda island arc, causing widespread back arc thrusting. We present integrated results of a refraction/wide-angle reflection tomography, gravity modeling, and multichannel reflection seismic imaging using data acquired in 2006 southeast of Sumba Island. The composite structural model reveals the previously unresolved deep geometry of the collision zone. Changes in crustal structure encompass the 10–12 km thick Australian basement in the south and the 22–24 km thick Sumba ridge in the north, where backthrusting of the 130 km wide accretionary prism is documented. The structural diversity along this transect could be characteristic of young collisional systems at the transition from oceanic subduction to continent-arc collision. **Citation:** Shulgin, A., H. Kopp, C. Mueller, E. Lueschen, L. Planert, M. Engels, E. R. Flueh, A. Krabbenhoef, and Y. Djajidhardja (2009), Sunda-Banda arc transition: Incipient continent-island arc collision (northwest Australia), *Geophys. Res. Lett.*, 36, L10304, doi:10.1029/2009GL037533.

1. Introduction

[2] The convergence of the Indo-Australian plates and Eurasia and resulted in the formation of the Sunda and Banda island arcs. The transitional zone between the arcs is located south of Flores Island and is characterized by the change in the tectonic regime along the boundary. This segment of the plate boundary was only little investigated previously. In the scope of this study we address the problem of constraining the entire crustal scale structure and current geodynamic regime at the transitional zone using seismic reflection and wide-angle investigations and gravity modeling.

2. Tectonic Setting

[3] The plate boundary south of Sumba Island, Indonesia, is marked by a change in the tectonic regime (Figure 1) from subduction of the Indo-Australian oceanic lithosphere along the Sunda margin in the west that began ~45 m.y. ago [Hall, 2002] to continent - island arc collision along the Banda arc in the east [Audley-Charles, 1975; Katili, 1989; Milsom, 2001;

Audley-Charles, 2004]. This margin experiences the early stages of continent-island arc collision as a result of the interaction between the Australian margin and the Banda island arc in the Pliocene [Hall and Smyth, 2008].

[4] Our goal is to constrain the deep crustal structure and tectonic evolution of the forearc using geophysical data collected during the RV Sonne SO-190 cruise in 2006. Our profile starts at ca. 12.5°S at the transition from the Late Jurassic oceanic lithosphere of the Argo Abyssal plain to the rifted Triassic continental crust of the Scott plateau [van der Werff, 1995] that is marked by the eastern termination of the Java trench at the transition to the Timor trough (Figure 1). Northwards, the oblique collision of the rifted continental crust of the Scott plateau with the forearc commenced 3–5 Ma ago [Harris, 1991] at a rate of ~7 cm/yr [Curry, 1989]. The current convergence rate at the Timor trough is ~15 mm/yr [Bock et al., 2003] and it is manifested in back arc thrusting [Silver and Reed, 1988]. The Sumba Block, farther north, is believed to be an isolated tectonic block trapped between the trench and the volcanic arc (see Rutherford et al. [2001] and Hall and Smyth [2008] for discussion). Ridge structures of the Sumba Ridge include the submarine basement high, extending from Sumba Island to Savu Island and then merging with outer high crest towards Timor Island (Figure 1) [Silver et al., 1983]. The basement of the ridge is dated from >80 to ~18 Ma, as inferred from the outcrops of intrusives and volcanic rocks together with sediments on Sumba and Savu Islands [Karig et al., 1987], which might have been a part of the Paleogene Sumba-Banda forearc [Hall and Smyth, 2008].

[5] The origin of the abnormal width of the forearc south of Flores Island is enigmatic (Figure 1). Seismicity deeper than 30 km is absent between the islands of Sumba and Timor, while further north common earthquakes deeper than 100 km [Engdahl and Villaseñor, 2002] suggest the presence of the subducting slab below the Banda island arc, further confirmed by geochemical data from Flores Island [Elburg et al., 2004]. However, most volcanic rocks of the Banda islands consist of primitive basalts typical of a volcanic arc built on oceanic lithosphere [Hamilton, 1988]. The complex basement thus reflects different periods of extension, subduction, and collision in Eastern Indonesia [Hall and Smyth, 2008].

3. Data Acquisition and Modeling

[6] Here we present a Vp seismic tomography model along the Sunda - Banda arc transition, further constrained by gravity modeling. Marine seismic investigations (Figure 1) were carried out by multichannel seismic reflection profiling (MCS), accompanied by gravity measurements, and seismic refraction profiling with ocean-bottom seismometers (OBS)

¹Leibniz Institute of Marine Sciences, IFM-GEOMAR, Kiel, Germany.

²Federal Institute for Geosciences and Natural Resources, Hannover, Germany.

³Agency for the Assessment and Application of Technology, Jakarta, Indonesia.

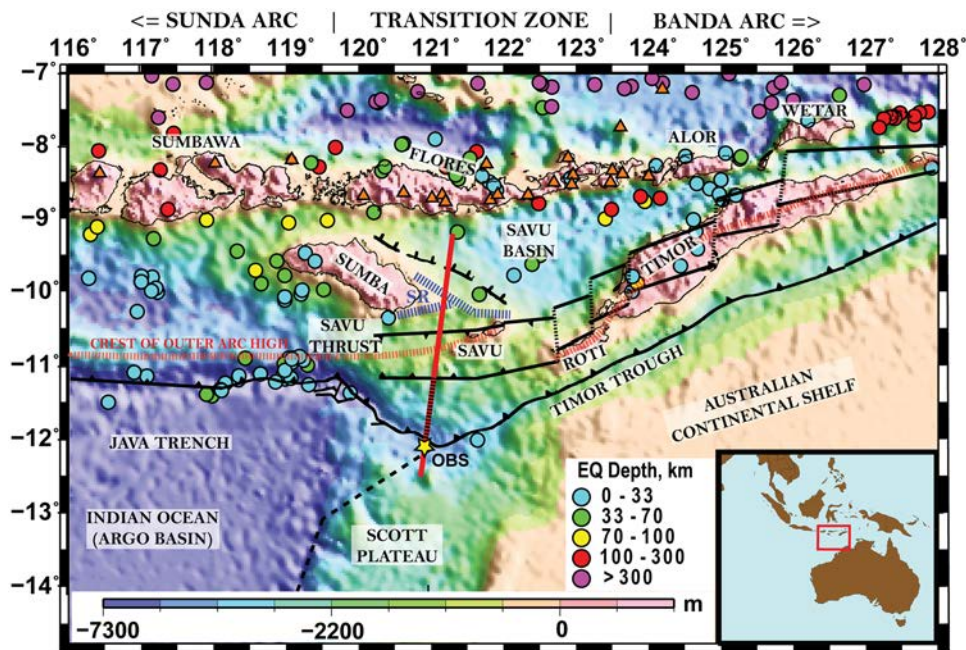


Figure 1. Simplified tectonic and bathymetric map of the Sunda-Banda Arc transition. Red line - seismic profile discussed in this study. Dashed red-black line - the MCS section shown in Figure 2. Yellow star - OBS location shown in Figure 2. Red triangles - active and Neogene volcanoes. Dashed blue line - a submarine Sumba Ridge (SR). Dashed red line - the crest of the outer forearc high. Black lines - faults [after *Rutherford et al.*, 2001; *Audley-Charles*, 2004]. Relocated earthquakes in the region are shown by filled circles, color-coded with depth [after *Engdahl and Villaseñor*, 2002].

and hydrophones (OBH) [Mueller *et al.*, 2008] (Text S1 of the auxiliary material).¹

[7] The seismic velocity model was constrained by joint refraction/reflection 2D tomographic inversion [Korenaga *et al.*, 2000]. Data from a total of 36 stations were used as input to the tomographic modeling. First, ~16,000 first arrival phases with offsets of up to 120 km were picked; subsequently, ~4,000 reflected phases were added to the dataset. We applied a “top to bottom” approach with a simple layered starting model, initially constraining the model only for the near offsets and then increasing the depth extent of the ray coverage to constrain the entire model space. The structure of the sediments and the upper crust was controlled by the MCS data (Figure 2), thus constraining the upper section of the profile in great detail. Calculated uncertainty of traveltimes for ~85% of the all picked phases lies within the picking error range of 50 ms.

[8] The resulting V_p seismic tomography model was extended 100 km to the north and south and to a depth of 75 km to be used in forward gravity modeling. Velocities were converted to densities [Christensen and Mooney, 1995; Carlson and Herrick, 1990] and the subducting slab extended to 75 km depth underneath the island arc, where the deep seismicity commences. A constant density of 3.35 g/cm^3 was assumed for the mantle (Figure 3c).

4. Results (South to North Along 121°E)

4.1. Scott Plateau: Australian Crust

[9] The 2 km thick sedimentary cover of the Java trench has average V_p seismic velocities of 2–3 km/s in the trench

section. A facies transition from deep marine fine grained carbonates to Upper Cretaceous shallow marine clastic deposits [Stagg and Exxon, 1979] recognized in the MCS data forms the décollement at ~5 km depth (Figure 2a). A mud diapir observed at CDP 12900 (Figure 2) may be related to high pore pressures in the lower unit, also a series of linear mud diapirs nearby have been reported by Breen *et al.* [1986]. At depths between 6 km and 10 km V_p below the reflection gradually change from 3.5 km/s to 5 km/s (Figure 3a). Upper crustal velocities are ~6.0 km/s and increase to 6.7–7.0 km/s in the lower crust (Figure 3a), as revealed by the Puc and Plc phases (Figure 2c). The transition from the upper to the lower crust is marked by a strong reflection well documented by Pic phases. The Moho is recovered by the PmP phases at a depth of 20 km and is apparently dipping northwards at an angle of ~1°. Thus, the thickness of the crystalline crust reaches 10 to 12 km only. Although a continental crust with an Australian affinity was proposed to exist further east [Kaneko *et al.*, 2007], these values are in contrast to the typical thickness of the continental crust in NW Australia [Collins *et al.*, 2003] and at other continental shelves [e.g., Ritzmann and Faleide, 2007].

4.2. Frontal Prism and the Neogene Accretionary Wedge

[10] Imbricate thrusting (Figure 2a) and relatively low seismic velocities of 2.5–3.5 km/s down to 6–7 km depth indicate the presence of a large, ~20 km wide, frontal prism arcward of the deformation front (51 km distance). The ~60 km wide Neogene accretionary prism, imaged in the MCS data and confirmed by V_p values <4.0 km/s, is located between 85–130 km profile distance and forms the middle prism, app. bounded by the 3 km/s isoline. It is characterized by a laterally inhomogeneous velocity field and thrust fault-

¹Auxiliary materials are available in the HTML. doi:10.1029/2009GL037533.

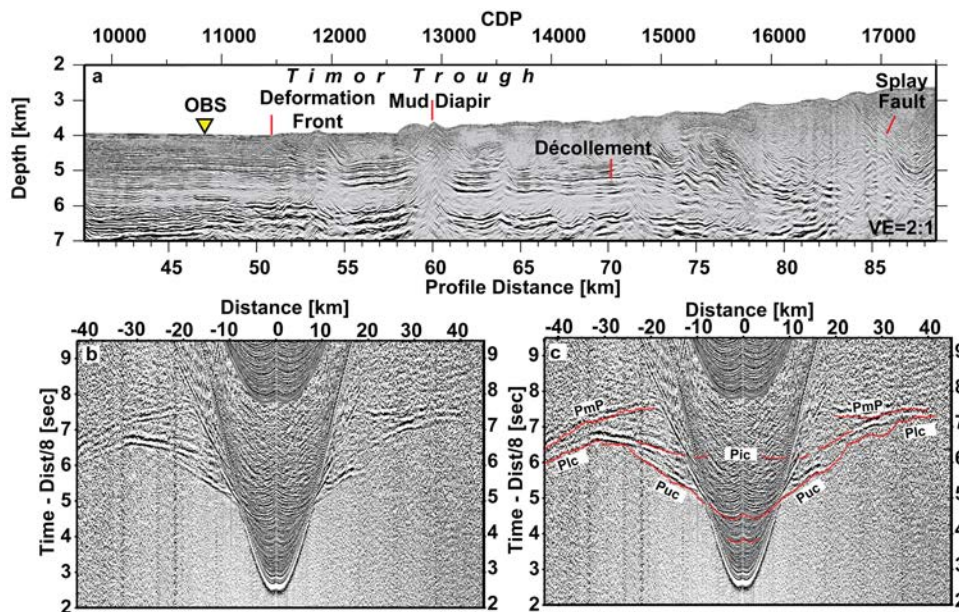


Figure 2. (a) MCS depth migrated section for the areas around Timor Trough (location shown in Figure 1). (b and c) example of the OBS data used in this study. Yellow triangle - the OBS position, shown in Figure 2b and 2c. Red dots show the computed travel-times of the seismic rays shot through the tomography model.

ing, observed in the MCS data. A system of splay faults that originate at the décollement and trend upwards at the angle of $\sim 20^\circ$ marks the transition to the middle prism (Figure 2a). The trench fill is composed of Mesozoic and Cenozoic sediments, eroded from the Australian continental shelf, with the lower part composed of clastic and volcano-clastic rocks, and the upper part composed of deep-water carbonates [Breen *et al.*, 1986]. The upper half of the sediments in the Timor trough is incorporated into the frontal prism. The lower 1000–1200 m of the clastic unit are currently bypassing the frontal prism (Figures 2a and 3a) and most likely underplate below the accretionary prism. The décollement is traced as a high-amplitude reflector for 30 km landward of the deformation front and extends to a depth of 6 km.

4.3. Paleo-accretionary Wedge

[11] The central section of the profile (140–210 km) suffers from limited energy penetration due to anomalous high attenuation and/or significant scattering. The opaque seismic character of the forearc high as observed both in the wide-angle and MCS data together with moderate V_p in the sedimentary cover (ranging from 2 km/s below the sea floor to 5 km/s at a depth of 10 km) (Figure 3a) suggests that the forearc high is composed of pre-Neogene accreted material that forms the paleo-accretionary complex. This material is probably derived from the stratigraphic units currently present on the Scott Plateau, which are composed of Jurassic sandstones overlain by Cretaceous marine shales [Breen *et al.*, 1986] and could have accumulated during the initial subduction of the passive Australian margin [van der Werff *et al.*, 1994] or during the subduction of Jurassic oceanic lithosphere of the Banda embayment (as shown by Hall and Smyth [2008]). Geologically the prism may be linked to the southern part of Timor, underlain by the outcropping Kolbano Complex, including Jurassic-Pliocene folded sediments of Australian origin, representing a segment of the accretionary complex [Karig *et al.*, 1987]. As suggested by numerical

modeling of collisional margin settings [Selzer *et al.*, 2008], the opaque seismic character of the deeper portion may be caused by basally stacked packages of highly scattering rock fabric thus inhibiting deep energy penetration.

4.4. Sumba Ridge

[12] The crest of the Sumba ridge [Silver *et al.*, 1983] is located at 250 km profile distance; the basement top (app. corresponding to the 4 km/s isoline) is at a depth of 3 km below sea level at the crest and slopes down to 9 km depth in the south and to 6 km depth in the north (Figure 3a). A sharp velocity change in the upper crust at ~ 200 km distance marks the southern limit of the Sumba ridge. A vertical displacement of the basement occurs at 260 km underneath a small sedimentary basin and again at the northern edge of the ridge (at 310 km). The ridge is covered by sediments (presumably eroded from the Sumba, Savu and Timor islands) with a thickness of 0.5 km increasing to more than 2 km in thickness at its flanks. A crustal reflection observed below the entire northern portion of the profile at depths of 15–17 km probably corresponds to the transition between the upper and the lower crust (Figure 3a). V_p velocities vary from 5.5 km/s to 6.4–6.5 km/s in the upper crust, and from 6.7–6.8 km/s to 7.1 km/s in the lower crust and are typical of a mature arc massif or possibly of a fragment of a continental crust, which can be linked to the existence of a volcanic arc in the eastern Indonesia during the Paleogene, traces of which may be found in the highest nappes of Timor and other Banda islands [Hall and Smyth, 2008]. The PmP phases indicate the slightly southwards dipping Moho at a depth of ~ 26 km below the Sumba ridge. Available Pn phases indicate $V_p \sim 8.0$ km/s in the forearc mantle.

4.5. Savu Basin

[13] The transition from the Sumba ridge to the Savu basin (at 310 km) is marked by sea floor deepening and an increase in sedimentary thickness. The sedimentary fill eroded from

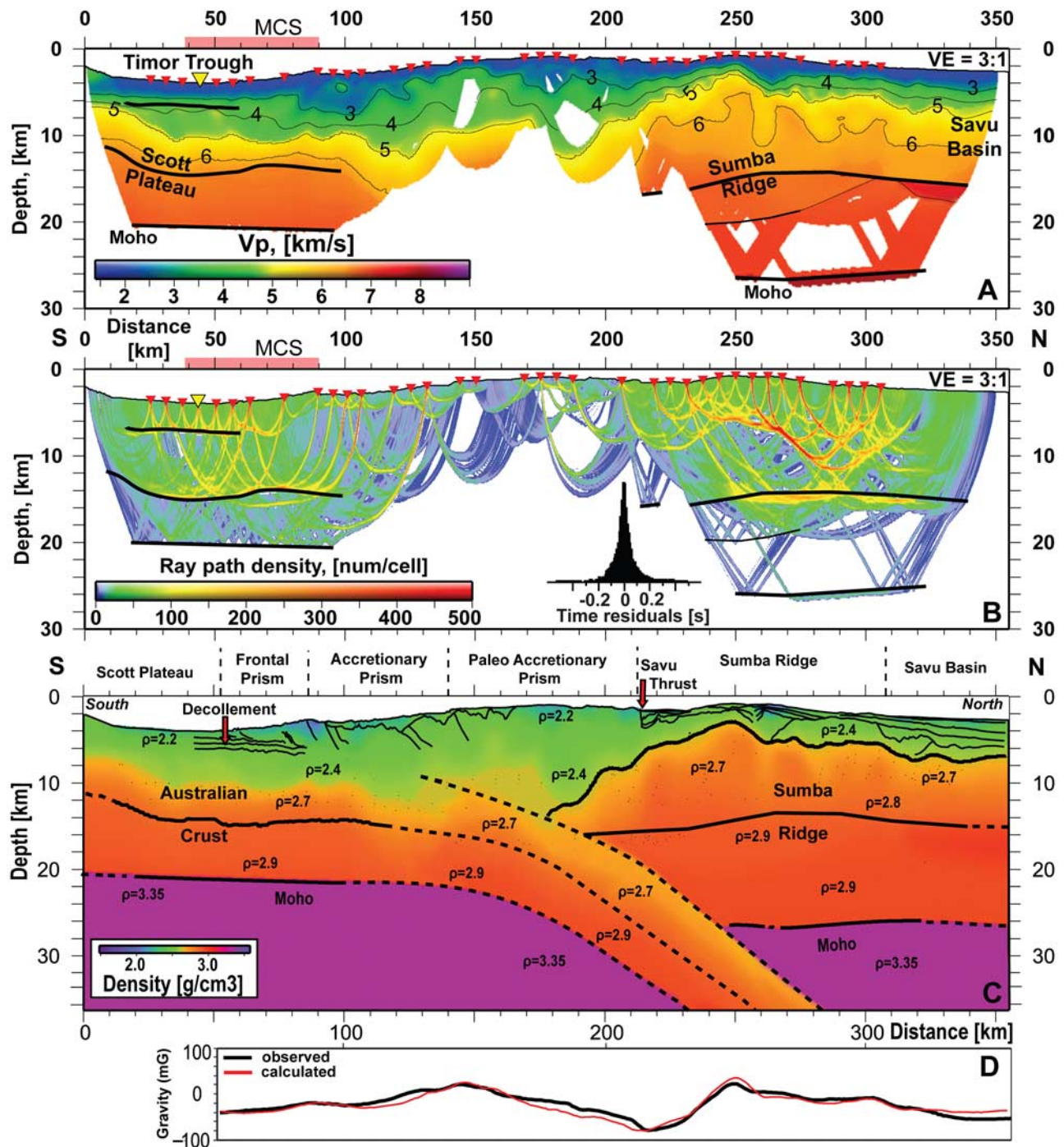


Figure 3. (a) Results of seismic tomography and gravity modeling a) Recovered tomography model, black lines - seismic reflectors. Red triangles - the OBS/OBH locations. Yellow triangle - OBS location (Figure 2). Pink line along the distance axis - MCS data shown in Figure 2. (b) Ray path coverage obtained during the tomographic inversion. Insert shows the time residuals distribution. (c) Combined model. Background color and numbers - density based the tomography and gravity results. Thin solid black lines - reflection horizons from the MCS data. Thick black lines - interfaces used in the gravity modeling. Interfaces not seismically resolved - dashed lines. (d) results of gravity modeling. Red line - observed data; black line - calculated gravity field.

the island arc [Audley-Charles, 2004] reaches a total thickness of 3 km with V_p velocities ranging from <2 km/s to 4 km/s (Figure 3a). The basement topography and sedimentary layering are consistent with earlier seismic reflection profiles

in the Savu basin [Karig *et al.*, 1987; Breen *et al.*, 1986; van der Werff *et al.*, 1994]. Our wide-angle data for the first time document the Moho at a depth of 26 km.

4.6. Crustal Structure From Seismic Inversion and Gravity Modeling

[14] Figure 3c shows the tectonic model based on the results of the reflection seismic imaging, the wide-angle tomography, and gravity modeling. In the south, the crust of Australian affinity is dipping arcward at an angle of $\sim 10\text{--}11^\circ$. The 10–12 km thick crystalline crust of the Scott plateau as a promontory of the Australian continent (described above) underthrusts the Banda forearc.

[15] Between the Sumba ridge and the trough, the accretionary complex shows thrusting and represents a nascent orogeny, forced by post-Pliocene convergence and buoyant uplift associated with the transition from active oceanic subduction to continent-island arc collision. The complex is composed of a frontal prism, where active frontal accretion is documented, juxtaposed against a 130 km wide accretionary prism. The central section of the profile (140–210 km distance) consists of the paleo-accretionary prism bounded northwards by the Sumba ridge, which acted as backstop to the paleo-prism during the time of accretion. Most likely the paleo-prism was added to the Sumba ridge, during the SSW tectonic escape of Sumba Island, caused by the initial contact of Australia and the Banda arc [Rutherford *et al.*, 2001]. The Savu thrust marks the tectonic transition from the accretionary wedge to the tectonic units of the Sumba ridge. Vertical growth of the prism facilitated backthrusting over the Sumba ridge along the Savu thrust [Silver and Reed, 1988], however, motion along the Savu thrust must primarily be driven by high basal friction due to the low relief difference between the prism and the ridge. The crustal thickness of the Sumba ridge is ~ 23 km with crustal densities ranging from 2.65 g/cm^3 to 2.90 g/cm^3 . Towards the island arc, the thickness of the crystalline crust is ~ 20 km below the Savu basin with the upper plate Moho at a depth of $\sim 26\text{--}27$ km, as also supported by gravity modeling. The crustal thickness is increased compared to the Lombok basin west of Sumba Island, which is underlain by 7 km thick crust (E. Lueschen *et al.*, Structure, evolution and tectonic activity at the Eastern Sunda forearc, Indonesia, from marine seismic investigations, submitted to *Tectonophysics*, 2009).

5. Discussion

[16] Newly acquired seismic reflection/refraction and gravity data east and south of Sumba Island resolve the deep crustal structure at the Sunda-Banda arc transition (Figure 3c). The current system can be regarded as a precursor of a fold-and-thrust belt, which may develop in the forearc as the collision progresses. The wide-angle seismic data resolve the full crustal structure of the Sumba ridge and the Savu basin and for the first time provide the geophysical background for geodynamic models of nascent collisional systems. The observed variations in crustal structure along the profile may be typical for tectonic settings with continental margins approaching island arcs. The observed variations in the crustal structure along the profile are similar to the present structure around Taiwan, formed by the transition from subduction to collision of Eurasia and the Philippine Sea plate [Huang *et al.*, 2006; Sibuet and Hsu, 2004].

[17] **Acknowledgments.** We would like to thank Captain Meyer and the crew of R/V Sonne and the SINDBAD Working group for their

enormous help in collecting and processing of the data. Authors express great gratitude to Jun Korenaga for the discussion on seismic tomography and Tomo2D code. We would like to thank the GRL editor Fabio Florindo and reviewers for their help in improving the manuscript. The SINDBAD project is funded by the German Federal Ministry of Education and Research (BMBF) (grants 03G0190A and 03G0190B).

References

- Audley-Charles, M. G. (1975), The Sumba fracture: A major discontinuity between eastern and western Indonesia, *Tectonophysics*, *26*, 213–228.
- Audley-Charles, M. G. (2004), Ocean trench blocked and obliterated by Banda forearc collision with Australian proximal continental slope, *Tectonophysics*, *389*, 65–79.
- Breen, N. A., E. A. Silver, and D. M. Hussong (1986), Structural styles of an accretionary wedge south of the island of Sumba, Indonesia, revealed by SeaMARC II side scan sonar, *Geol. Soc. Am. Bull.*, *97*, 1250–1261.
- Bock, Y., L. Prawirodirdjo, J. F. Genrich, C. W. Stevens, R. McCaffrey, C. Subarya, S. S. O. Puntodewo, and E. Calais (2003), Crustal motion in Indonesia from Global Positioning System measurements, *J. Geophys. Res.*, *108*(B8), 2367, doi:10.1029/2001JB000324.
- Carlson, R. L., and C. N. Herrick (1990), Densities and porosities in the oceanic crust and their variations with depth and age, *J. Geophys. Res.*, *95*, 9153–9170.
- Christensen, N. I., and W. D. Mooney (1995), Seismic velocity structure and composition of the continental crust: A global view, *J. Geophys. Res.*, *100*, 9761–9788.
- Collins, C. D. N., B. J. Drummond, and M. G. Nicoll (2003), Crustal thickness patterns in the Australian continent, *Geol. Soc. Am. Spec. Pap.*, *372*, 121–128.
- Curray, J. R. (1989), The Sunda arc: A model for oblique plate convergence, *Neth. J. Sea Res.*, *24*, 131–140.
- Elburg, M. A., M. J. van Bergen, and J. D. Foden (2004), Subducted upper and lower continental crust contributes to magmatism in the collision sector of the Sunda-Banda arc, Indonesia, *Geology*, *32*, 41–44.
- Engdahl, E. R., and A. Villaseñor (2002), Global seismicity: 1900–1999, in *International Handbook of Earthquake and Engineering Seismology*, pp. 665–690, Academic, San Diego, Calif.
- Hall, R. (2002), Cenozoic geological and plate tectonic evolution of SE Asia and the SW Pacific: Computer-based reconstructions, model and animations, *J. Asian Earth Sci.*, *20*, 353–434.
- Hall, R., and H. R. Smyth (2008), Cenozoic arc processes in Indonesia: Identification of the key influences on the stratigraphic record in active volcanic arcs, *Geol. Soc. Am. Spec. Pap.*, *436*, 27–54.
- Hamilton, W. B. (1988), Plate tectonics and island arcs, *Geol. Soc. Am. Bull.*, *100*, 1503–1527.
- Harris, R. A. (1991), Temporal distribution of strain in the active Banda orogen: A reconciliation of rival hypotheses, *J. Southeast Asian Earth Sci.*, *6*, 373–386.
- Huang, C.-Y., P. B. Yuan, and S.-J. Tsao (2006), Temporal and spatial records of active arc-continent collision in Taiwan: A syntaxis, *Geol. Soc. Am. Bull.*, *118*, 274–288.
- Kaneko, Y., S. Maruyama, A. Kadarusman, T. Ota, M. Ishikawa, T. Tsujimori, A. Ishikawa, and K. Okamoto (2007), On-going orogeny in the outer-arc of the Timor-Tanimbar region, eastern Indonesia, *Gondwana Res.*, *11*, 218–233.
- Karig, D., A. Barder, T. Charlton, S. Klempere, and D. Hussong (1987), Nature and distribution of deformation across the Banda Arc: Australia collision zone at Timor, *Geol. Soc. Am. Bull.*, *98*, 18–32.
- Katili, J. A. (1989), Review of past and present geotectonic concepts of eastern Indonesia, *Neth. J. Sea Res.*, *24*, 103–129.
- Korenaga, J., *et al.* (2000), Crustal structure of the southeast Greenland margin from joint refraction and reflection seismic tomography, *J. Geophys. Res.*, *105*, 21,591–21,614.
- Milsom, J. (2001), Subduction in eastern Indonesia: How many slabs?, *Tectonophysics*, *338*, 167–178.
- Mueller, C., *et al.* (2008), From subduction to collision: The Sumba-Banda Arc transition, *Eos Trans. AGU*, *89*, 49–50.
- Ritzmann, O., and J. I. Faleide (2007), Caledonian basement of the western Barents Sea, *Tectonics*, *26*, TC5014, doi:10.1029/2006TC002059.
- Rutherford, E., K. Burke, and J. Lytwyn (2001), Tectonic history of Sumba Island, Indonesia, since the Late Cretaceous and its rapid escape into forearc in the Miocene, *J. Asian Earth Sci.*, *19*, 453–479.
- Selzer, C., S. J. H. Buiters, and O. A. Pfiffner (2008), Numerical modeling of frontal and basal accretion at collisional margins, *Tectonics*, *27*, TC3001, doi:10.1029/2007TC002169.
- Sibuet, J.-C., and S.-K. Hsu (2004), How was Taiwan created?, *Tectonophysics*, *379*, 159–181.
- Silver, E. A., and D. L. Reed (1988), Backthrusting in accretionary wedges, *J. Geophys. Res.*, *93*, 3116–3126.

- Silver, E. A., D. L. Reed, and R. McCaffrey (1983), Back arc thrusting in the eastern Sunda arc, Indonesia: A consequence of arc-continent collision, *J. Geophys. Res.*, *88*, 7429–7448.
- Stagg, H. M. J., and N. F. Exon (1979), Western margin of Australia: Evolution of a rifted arch system—Discussion, *Geol. Soc. Am. Bull.*, *90*, 795–797.
- van der Werff, W. (1995), The evolution of the Savu Forearc Basin, Indonesia (Forearc response to arc/continent collision), *J. Mar. Petrol. Geol.*, *12*, 247–262.
- van der Werff, W., D. Kusnida, and H. Prasetyo (1994), On the origin of the Sumba forearc basement, *J. Mar. Petrol. Geol.*, *11*, 363–374.
-
- Y. Djajadihardja, Agency for the Assessment and Application of Technology, Jl.M.H. Thamrin No. 8, Jakarta 10340, Indonesia.
- M. Engels, E. Lueschen, and C. Mueller, Federal Institute for Geosciences and Natural Resources, Stilleweg 2, D-30655 Hannover, Germany.
- E. R. Flueh, H. Kopp, A. Krabbenhoef, L. Planert, and A. Shulgin, Leibniz Institute of Marine Sciences, IFM-GEOMAR, Wischhofstr. 1-3, D-24148 Kiel, Germany. (ashulgin@ifm-geomar.de)

Lower plate structure and upper plate deformational segmentation at the Sunda-Banda arc transition, Indonesia

L. Planert,¹ H. Kopp,¹ E. Lueschen,² C. Mueller,² E. R. Flueh,¹ A. Shulgin,¹ Y. Djajadihardja,³ and A. Krabbenhoef¹

Received 22 June 2009; revised 23 April 2010; accepted 29 April 2010; published 27 August 2010.

[1] The Sunda-Banda arc transition at the eastern termination of the Sunda margin (Indonesia) represents a unique natural laboratory to study the effects of lower plate variability on upper plate deformational segmentation. Neighboring margin segments display a high degree of structural diversity of the incoming plate (transition from an oceanic to a continental lower plate, presence/absence of an oceanic plateau, variability of subducting seafloor morphology) as well as a wide range of corresponding fore-arc structures, including a large sedimentary basin and an accretionary prism/outer arc high of variable size and shape. Here, we present results of a combined analysis of seismic wide-angle refraction, multichannel streamer and gravity data recorded in two trench normal corridors located offshore the islands of Lombok (116°E) and Sumba (119°E). On the incoming plate, the results reveal a 8.6–9.0 km thick oceanic crust, which is progressively faulted and altered when approaching the trench, where upper mantle velocities are reduced to ~7.5 km/s. The outer arc high, located between the trench and the fore-arc basin, is characterized by sedimentary-type velocities ($V_p < 5.5$ km/s) down to the top of the subducting slab (~13 km depth). The oceanic slab can be traced over 70–100 km distance beneath the fore arc. A shallow serpentinized mantle wedge at ~16 km depth offshore Lombok is absent offshore Sumba, where our models reveal the transition to the collisional regime farther to the east and to the Sumba block in the north. Our results allow a detailed view into the complex structure of both the deeper and shallower portions of the eastern Sunda margin.

Citation: Planert, L., H. Kopp, E. Lueschen, C. Mueller, E. R. Flueh, A. Shulgin, Y. Djajadihardja, and A. Krabbenhoef (2010), Lower plate structure and upper plate deformational segmentation at the Sunda-Banda arc transition, Indonesia, *J. Geophys. Res.*, 115, B08107, doi:10.1029/2009JB006713.

1. Introduction

[2] The Sunda-Banda arc transition comprises the portions of the Indonesian island arc where the tectonic regime changes from oceanic-island arc subduction along the eastern Sunda arc to continent-island arc collision along the Banda arc (Figure 1). Such a setting offers a broad spectrum of tectonic/geologic variation regarding the lower plate as well as the upper plate, which makes this plate boundary an ideal target to study detailed aspects of subduction zone processes.

[3] Scientific investigations at subduction zones conducted during recent years have increasingly put their focus on the physical interaction between the lower plate and the

fore arc and related aspects of material transfer and balancing. The physical and chemical properties of the lower plate, including its crustal and mantle structure/composition, fluid content, sedimentary cover, and thermal character (plate age), as well as the convergence rate are essential to processes of accretion, erosion and arc magmatism of the upper plate (see *Clift and Vannucchi* [2004] for a review). However, modern seismic and acoustic data are still rare for the eastern Sunda arc and the transition to the Banda arc and hence, this study aims at providing a clearer picture of the area's tectonic setting.

[4] Subduction zones may grow by frontal or basal accretion and may be classified as a compressive regime. Extension and large-scale subsidence on the contrary originate from erosive processes, which are often favored by a rough seafloor topography and a sediment-starved deep sea trench. Thus a change from an accretionary to a non-accretionary/erosive regime may be expected, concurrent with a change in the tectonic evolution of fore-arc structure. The eastern Sunda arc comprises a well-developed outer arc high and a major fore-arc basin (Lombok Basin). The deeper

¹IFM-GEOMAR, Leibniz Institute of Marine Sciences at the University of Kiel, Kiel, Germany.

²BGR, Federal Institute for Geosciences and Natural Resources, Hannover, Germany.

³BPPT, Agency for the Assessment and Application of Technology, Jakarta, Indonesia.

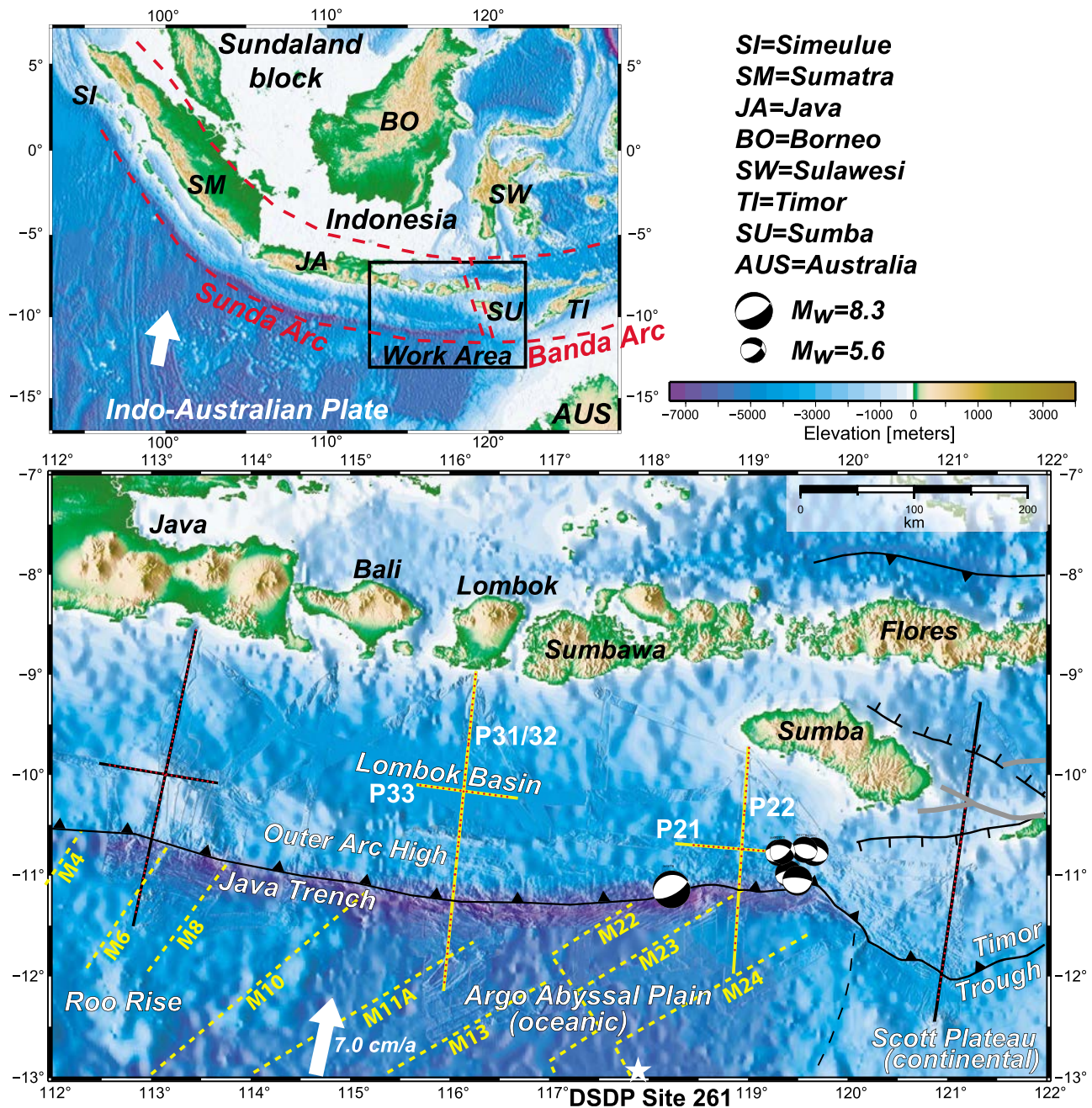


Figure 1. Regional map with features discussed in the text and close-up of work area with profile distribution of the SINDBAD seismic refraction experiment. Red points mark the locations of ocean bottom seismic recorders. In this study we present results for the corridors at 116°E and 119°E (yellow profiles) characterized by the subduction of oceanic crust of the Argo Abyssal Plain. The westernmost (113°E) as well as easternmost (121°E) corridors (black profiles) represent distinct tectonic regimes dominated by the subduction of thickened crust of the Roo Rise and Scott Plateau, respectively. The 121°E corridor is discussed in the work of *Shulgin et al.* [2009] and Shulgin et al (submitted manuscript, 2010). Focal mechanisms correspond to $M_w = 8.3$ main shock and 4 days aftershock series of the 1977 Sumba earthquake (<http://www.globalcmt.org>). Yellow dashed lines display magnetic anomalies from *Müller et al.* [2008]. Plate convergence is (white arrow) from *Simons et al.* [2007].

structure of these features is, however, not yet resolved and their origin is still not fully understood.

[5] Near the trench, the formation and reactivation of faults is related to the bending of the oceanic plate and often results in the hydratization of the oceanic crust and mantle

[e.g., *Ranero et al.*, 2003]. The 1977 Sumba earthquake, one of the largest normal-faulting earthquakes ($M_w = 8.3$) near an oceanic trench, occurred at the extreme eastern limb of the Java trench in our study area (Figure 1). Hence, it provides an opportunity to examine the amount and depth

extent of lower plate alteration as response to large bending stresses. Possible dewatering processes in the lower plate during subduction may also control the long-term tectonics of the fore arc, because these processes are pertinent to the functioning of seismogenic zones [e.g., *Peacock, 2001; Bostock et al., 2002; Ranero et al., 2008*]. At the eastern Sunda arc, there is a historical absence of large interface thrust earthquakes in a strip of 50–150 km between the along-trench seismicity and the onset of the Wadati-Benioff zone, which still requires further explanation [e.g., *Špičák et al., 2007*].

[6] The seismic and acoustic measurements, combined with gravimetric studies, conducted during R/V *Sonne* cruise SO190 allow a quantification of the “raw materials” (seafloor sediments, oceanic crust and mantle lithosphere), which are carried into the system at the deep sea trench, but also investigate the complex structure of the adjacent fore arc up to close to the volcanic arc. The results of this study may offer insights into the role of the lower plate, as the point of origin in the “subduction factory”, as well as into the reactions and consequences for the tectonic evolution of the overriding plate.

2. Tectonic Setting

[7] Convergence between the Indo-Australian Plate in the south and the Eurasian Plate in the north is active since the late Oligocene [*Hamilton, 1988; Hall and Smyth, 2008*] and currently occurs at a rate of ~70 mm/yr in N13°E direction offshore Bali [*Simons et al., 2007*]. Eastward from about 121°E, however, the relative motion at the Timor Trough has slowed down to ~15 mm/yr, and the development of back-arc thrusts appears to account for sustained northward motion of Australian lithosphere [*Bock et al., 2003*] (Figure 1). The seismic profile offshore Flores from *Shulgin et al.* [2009] shows a 12–15 km thick crust comprising the promontory of the Australian continental shelf, which currently underthrusts beneath the Banda fore arc, resulting into thickening and uplift of the outer arc ridge. Hence, conventional subduction cannot be occurring here.

[8] The transition from the Scott Plateau, which is marked by shallower seafloor depths and increased sedimentary coverage on the Australian continental shelf, to the oceanic lithosphere comprising the Argo Abyssal Plain occurs at ~120°E (Figure 1). The 1977 Sunda earthquake series [e.g., *Spence, 1986*] occurred at this transition region in the oceanic plate. Relocation of hypocenters and focal mechanisms are consistent with normal faulting throughout the upper 28 km of oceanic lithosphere (Figure 1). The earthquake produced a 10 m tsunami wave height on the island of Sumbawa, which suggests substantial deformation of the ocean bottom and associated fault displacement at very shallow depths. The aftershock area implies at least 200 km of fault rupture, with a concentration of aftershocks ~100 km northeast of the main shock close to the termination of the Java trench, where the underthrust Scott Plateau could have acted as a rupture barrier [*Spence, 1986; Lynnes and Lay, 1988*]. *Spence* [1986] attributes the origin of the large tensional stresses which caused the Sumba earthquake series to large bending stresses of slab-pull origin, facilitated by increased resistance to subduction of the adjacent Scott Plateau. Yet the resulting consequences of the inferred large

bending stresses on the structure of the subducting oceanic lithosphere in this area are unresolved.

[9] Seafloor age of the oceanic lithosphere increases toward the east from Early Cretaceous at 110°E to Late Jurassic close to 120°E [*Heine et al., 2004; Müller et al., 2008*]. The trend of magnetic seafloor anomalies is ~45–60° and thus oblique to the relative plate motion, which is almost perpendicular to the trench (Figure 1). The westernmost portions of our study area comprise the branches of an oceanic plateau, the Roo Rise, which is characterized by seafloor up to 1500 m shallower compared to the adjacent seafloor of the Argo Abyssal Plain.

[10] Fore-arc structures along this margin include a well-developed outer arc high (OAH) which is visible as a continuous bathymetric feature along the entire Indonesian fore arc, starting with Simeulue island offshore northern Sumatra as its subaerial expression and continuing as a submarine bathymetric elevation from offshore western Java to offshore the island of Sumba (Figure 1). The observed decrease in dimension and height of the OAH toward the east is related to the younger age of the eastern Sunda margin [e.g., *Van der Werff, 1995*] and to changes in trench sediment contribution and subducting seafloor morphology of the incoming Indo-Australian Plate. The related subduction processes at the plate boundary result in an accretionary regime offshore Sumatra and western Java [*Schlüter et al., 2002; Kopp and Kukowski, 2003*], whereas erosive processes dominate off central and eastern Java, where the subduction of the Roo Rise results in a northward retreat of the trench and the OAH [*Kopp et al., 2006*]. Farther east offshore Lombok and Sumbawa, however, the sediment input to the trench as well as the internal structure of the oceanic crust are largely unknown and as a consequence the processes governing the origin and evolution of the OAH are still unclear. A good indication of sediment origin and thickness farther south in the Argo Abyssal Plain can be gained from the results of DSDP site 261 (Figure 1), which drilled into a rugged oceanic basement of late Jurassic age at ~530 m below seafloor covered by Cretaceous claystones, Upper Miocene and Pliocene nannofossil oozes and Quaternary radiolarian clays [*Heirtzler et al., 1974*].

[11] The overriding plate is of continental nature off Sumatra [*Kopp et al., 2001*] and changes to an island arc type off Java/Lombok and farther east, although the internal structure of the islands and the adjacent fore arc is still largely unknown due to the lack of deep seismic data. The Lombok Basin forms a major fore-arc basin and is located between the OAH and the volcanic arc in the north (Figure 1). Its termination in the west is controlled by the subduction of the Roo Rise and related uplift of the adjacent fore arc [*Kopp et al., 2006*] and in the east by the collision of the Australian continental shelf with the crystalline basement comprising the island of Sumba [*Shulgin et al., 2009*]. The origin of Sumba is still enigmatic; it is not part of the modern Banda volcanic arc but according to a number of investigators [e.g., *Rutherford et al., 2001; Hall, 2002*] originated at a relict northern hemispheric arc system, situated south of West Sulawesi. The island migrated to its current position in the middle to late Miocene, as response to incipient collision with Australia, and now forms an integral part of the fore arc.

[12] In 2006, R/V *Sonne* cruise SO190 investigated the Sunda-Banda arc transition during two consecutive legs within the scope of the Seismic and Geoacoustic Investigations Along the Sunda-Banda Arc Transition (SINDBAD) project. During leg 1, almost 5000 km of multichannel streamer (MCS) seismic data and coincident shipboard gravity data were acquired between 112°E and 122°E. The MCS data are discussed in the work of *Lüschen et al.* [2010]. Leg 2 included the acquisition of more than 1700 km of wide-angle reflection and refraction seismic profiles in four different corridors of the margin (Figure 1), at 113°E (offshore eastern Java), 116°E (offshore Lombok), 119°E (offshore Sumba) and 121°E (offshore Flores). Additionally, seafloor swath mapping on both legs resulted in an almost complete coverage of the trench and the lower slope between 113°E and 121°E. The westernmost (113°E) as well as easternmost (121°E) corridors represent distinct tectonic regimes dominated by the subduction of thickened crust of the Roo Rise and Scott Plateau, respectively. The 121°E area is discussed in the work of *Shulgin et al.* [2009] and A. Shulgin et al. (Structural architecture of oceanic plateau subduction offshore Eastern Java and the potential implications for geohazards, submitted to *Geophysical Journal International*, 2010). In this study we present results from the analysis of deep penetrating seismic and shipboard gravity data to resolve the internal structure of the incoming and the overriding plates for the corridors at 116°E and 119°E.

3. Bathymetric Features

[13] At 116°E offshore Lombok, seafloor depths on the incoming oceanic plate are in the range of 5.0–5.5 km and reach up to 6.8 km in the trench. In the Argo Abyssal Plain, basement structures can be traced on the seafloor, aligned at angles of 45–60° and subparallel to the magnetic anomalies (Figure 1). Hence, these structures most likely correspond to original seafloor fabric imprinted during seafloor spreading. For distances less than ~40 km seaward of the trench, however, the prevailing strike of basement structures changes to a more trench parallel tectonic fabric (compare white-dashed lines in Figure 2), which may reflect recent activity and the onset of plate-bending related normal faulting in the oceanic plate.

[14] Where our seismic profile crosses the trench, the deformation front reveals a local indentation, indicating the erosion of the lowermost inner trench slope. Farther east, however, equivalent portions of the inner trench wall (>5 km depths) appear to be rather undisturbed. Here, more than three arrays of trench-parallel ridges and troughs suggest the presence of a frontal imbricate fan (Figure 2).

[15] Landward of the trench, the OAH seafloor rises up to water depths of 2.4 km (slope angle ~5°). Corresponding seafloor portions are characterized by a trench-parallel tectonic fabric including two pronounced ridges spaced ~25 km apart (Figure 2). On a MCS seismic profile located at ~114°E, *Müller et al.* [2008] identified recent vertical displacements of the seafloor and associated deformation at shallow depths as manifested in the uplift and tilting of small piggyback basins between the two tectonic ridges atop of the OAH. These structures are associated with landward dipping splay faults, which penetrate the entire crust and connect to the plate interface. The importance of such faults

for tsunami generation during great subduction zone earthquakes was recently demonstrated for Sumatra [*Sibuet et al.*, 2007], North Ecuador [*Collot et al.*, 2008] and Nankai [*Moore et al.*, 2007]. North of the OAH, the Lombok Basin exhibits a very smooth and virtually flat seafloor with water depths of 4.4 km.

[16] At 119°E offshore Sumba, water depths are slightly shallower for the oceanic plate and the trench (4.8–5.0 km and 6.5 km) and the corresponding seafloor is smoothed by a sediment blanket for distances >30 km seaward of the trench (Figure 2). Farther north, seafloor morphology changes abruptly, where a series of northward dipping normal faults induces intense fracturing and stepwise downflexure of the oceanic crust at the outer trench wall. In the trench, however, two faults, dipping to the south and striking at low angles relative to the trench, subduct beneath the inner trench wall, which results in pronounced indentations of the deformation front and the adjacent slope (Figure 2). The strike of these features is ~65°, i.e., subparallel to the magnetic anomalies. The 1977 Sumba earthquake epicenter [*Engdahl and Villaseñor*, 2002] is located roughly where the western fault subducts beneath the inner trench wall. The focal mechanism of the main shock (strike angle 61°; dip angle 67°; slip angle -98°; Global CMT Catalog, <http://www.globalcmt.org>) and the location of aftershocks with respect to the main shock (Figure 1) are consistent with a rupture zone striking at low angles relative to the trench. Hence, these data suggest a possible link between plate-bending related normal faulting, extending to perhaps 30–50 km depth [*Spence*, 1986; *Lynnes and Lay*, 1988], and the reactivation of inherited fault structures in the oceanic crust, as indicated by the observed trend oblique to the trench and subparallel to the magnetic anomalies. Fan-shaped slide deposits with a lateral dimension of ~25 km are visible ~30 km east of where our profile crosses the trench (Figure 2). We speculate that this slide was caused by slope failure due to the subduction of equivalent seafloor fabric.

[17] Offshore Sumba, the lateral and vertical dimensions of the outer arc high are smaller (~55 km compared to ~80 km offshore Lombok) and the transition in seafloor topography from the elevated segments toward the adjacent fore-arc portions in the north is much more subdued (Figure 2).

4. Seismic Data

[18] Offshore Lombok, profile 31/32 consists of two overlapping profiles and runs perpendicular to the trench reaching a full length of 354 km (Figure 2). A total of 46 IFM-GEOMAR ocean bottom hydrophones/seismometers (OBH/S) [*Bialas and Flueh*, 1999] were deployed on this line at ~6 km average instrument spacing. The profile extends from 100 km seaward of the trench to close to the island of Lombok, crossing the Lombok Basin and profile 33 at ~222 km profile distance. Profile 33 runs in a trench-parallel direction and covers a 113 km long portion of the Lombok Basin. On this line, 16 OBH/S were deployed at ~6 km instrument spacing.

[19] The 119°E corridor offshore Sumba comprises two additional seismic profiles: the 250 km long trench-perpendicular profile 22 and the 145 km long crossing profile 21, covered with 27 and 18 OBH/S at ~6 km

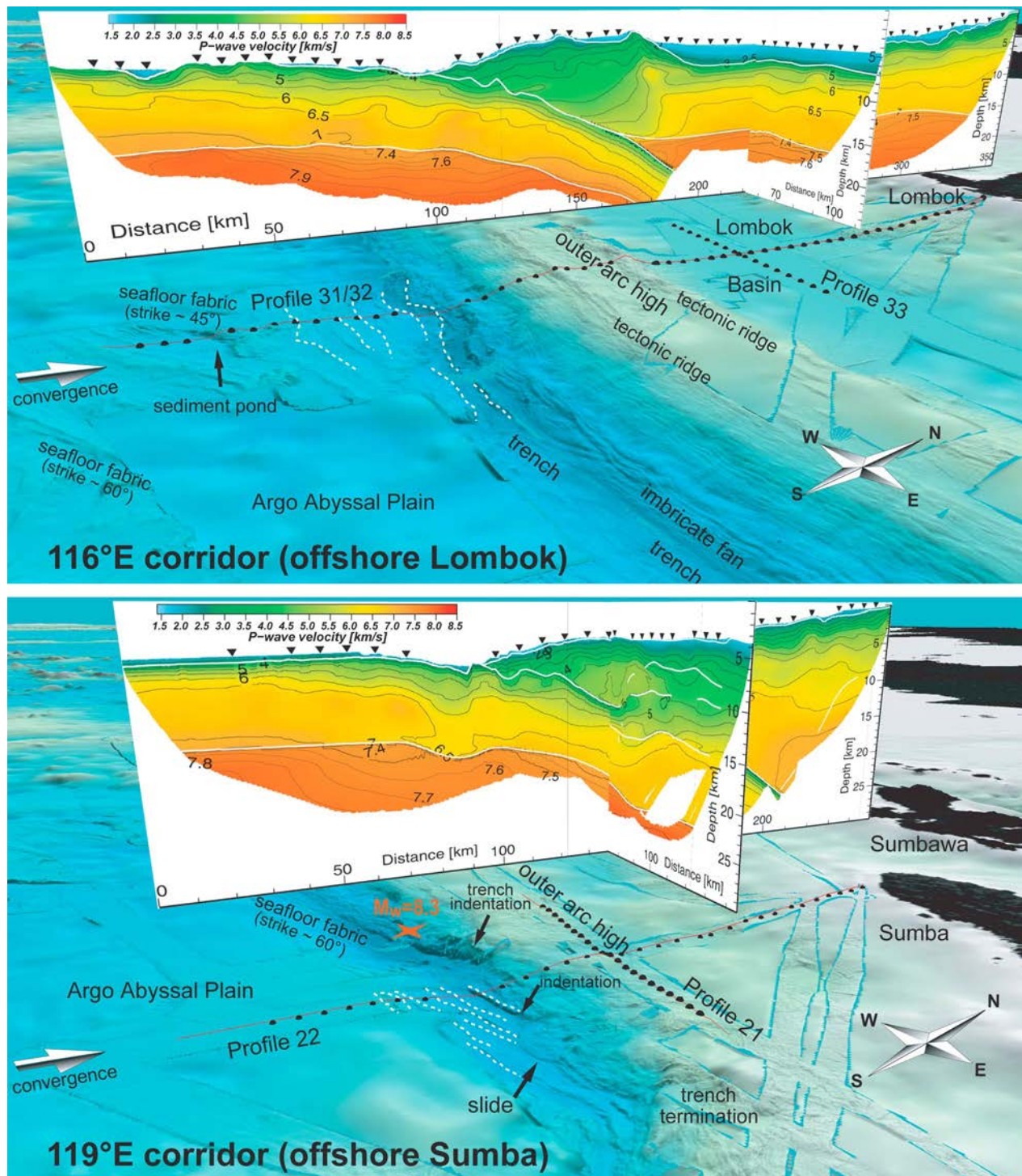


Figure 2. Perspective views of the (top) 116°E and (bottom) 119°E corridors including acquired seafloor bathymetry and seismic velocity profiles. The red lines are seafloor projections of the seismic shots; black spheres mark the instrument locations. Seafloor fabric locally crops out as basement structures on the oceanic plate. Offshore Lombok, inherited seafloor fabric strikes at angles of 45°–60°; plate-bending related normal faults trend more parallel to the trench (white dashed lines). The trench is largely devoid of sediment. A well-developed outer arc high comprises pronounced ridge structures. The Lombok Basin is characterized by a virtually flat seafloor. Offshore Sumba, inherited seafloor fabric strikes at angles of 60°–70° and seems to be reactivated as response to plate bending (red star marks epicenter of 1977 Sumba main shock). The subduction of basement structures locally results in the erosion of the lower slope and subsequent slope failure (note the coincidence of the eastern indentation and the slide). Annotated features are discussed in the text.

instrument spacing, respectively (Figure 2). Line 21 covers the OAH at its highest elevation.

[20] The seismic source used for wide-angle profiling was an eight element 64 l G-gun cluster fired at 3000 psi in constant time intervals, resulting in a nominal shot spacing of 130 m. Data processing included the localization of the ocean bottom instruments using the arrival time of the direct wave and the exact shot point geometry. In a second step, a time-gated deconvolution was applied to remove predictable bubble reverberations to produce a signal free of the disturbing interference of multiple and primary phases [Wiener, 1949]. Finally, a time and offset-variant Butterworth filter was applied in which the passband moves toward lower frequencies as record time and offset increases to account for frequency changes caused by signal attenuation.

[21] For the seismic velocity analysis we chose the tomographic method of *Korenaga et al.* [2000] (TOMO2D), which determines the 2-D velocity structure together with a floating reflector from the simultaneous inversion of refracted and reflected phases. The method employs a hybrid ray-tracing scheme combining the graph method with further refinements utilizing ray bending with the conjugate gradients method. Smoothing and damping constraints regularize the iterative inversion. The velocity model is defined as an irregular grid hung from below the seafloor. We used a horizontal node spacing of 250 m and a vertical node spacing, which linearly increases from 100 m at the seafloor to 250 m at 30 km depth below seafloor. Model regularization is accomplished by the use of correlation lengths, which control the size of those model areas affected by a velocity update of a grid cell [Korenaga et al., 2000]. We used a horizontal correlation length, which linearly increases from 1.5 km at the seafloor to 6 km at the model bottom, and a vertical correlation length with corresponding values of 0.2 km and 1.5 km, respectively. For reflector nodes, the appropriate regularization length scales are taken from the horizontal 2-D velocity correlation lengths at the corresponding depths.

[22] From the coincident MCS seismic profiles we incorporated the well resolved sedimentary portions as a priori structure into our starting models and fixed these areas during the iterations using spatially variable velocity damping. To make use of secondary arrivals and different reflections we utilized a “layer stripping” approach and subsequently built the velocity model from top to bottom. This approach further involves the use of spatially variable velocity damping for the upper layers, e.g., when restricting the picks to the lower layers, and the incorporation of velocity jumps into the input models at primary features such as the basement, plate boundary and the crust-mantle boundary (Moho). In practice, we used a 1-D velocity starting model and inverted first for the upper units (fore arc, outer arc high) down to the next major structural interface (fore-arc Moho, plate boundary). We then again used a 1-D velocity starting model for the inversion of the next deeper unit (fore-arc mantle, oceanic crust, oceanic mantle). RMS travel time misfits for the final velocity models shown here are in the range of 60 ms for a total of 9.000 (profile 21) to 26.000 (profile 31/32) arrivals, which were manually picked and assigned with individual pick uncertainties in the processed seismic sections (see Figures 3 and 4 for data examples of profile 31/32).

4.1. Profile 31/32

[23] Figure 5 shows the final tomographic solution of profile 31/32, the corresponding derivative weight sum (DWS), which is a measure of ray density in the neighborhood of a model node [Toomey and Foulger, 1989], and the coincident prestack depth-migrated (PSDM) MCS profile from *Lüschen et al.* [2010]. The incoming oceanic crust is on average 8.6 km thick and largely devoid of sediment, except for an isolated sediment pond at ~20 km profile distance (Figure 5a). This sediment accumulation occurs in a structural trap related to the original seafloor fabric imprinted during seafloor spreading (compare Figure 2). About 40–50 km seaward of the trench velocities start to decrease in the crust and in the underlying mantle, resulting in anomalously low mantle velocities of ~7.5 km/s directly beneath the Moho (Figure 5a; see Figure 3 for data examples). The area of reduced velocities coincides with the onset of plate-bending related normal faulting in the MCS seismic data (Figure 5c; compare white-dashed lines in Figure 2).

[24] The OAH reveals relatively low velocities of 2.5–5.5 km/s above the plate boundary. The plate boundary is constrained by reflections in both the wide-angle and MCS seismic data over a distance of at least 70 km beneath the OAH down to ~15 km depth (dip: 5–8°) (Figure 6). The plate interface is of irregular shape, suggesting in places several hundreds of meters vertical displacement.

[25] The Lombok Basin is characterized by up to 2.8 km of sediment infill comprising velocities of 1.6–2.8 km/s (Figures 5 and 6). The underlying crust is 9–10 km thick and reveals a pronounced model portion with velocities of 6–6.8 km/s (see Figure 4 for data example). The transition from the low velocity portions beneath the OAH to velocities >5.5 km/s beneath the Lombok Basin occurs abruptly over a distance of 10–30 km around profile km 180 (Figure 6). Velocities in the upper fore-arc mantle are in the range of 7.4–7.8 km/s and thus significantly lower compared to those expected for unaltered mantle peridotite [Carlson and Miller, 2003].

[26] In order to demonstrate the resolving power of the data in different parts of the model, a synthetic test was performed where a known model has to be resolved using the same profile geometry and data coverage as in the real experiment. A set of Gaussian velocity anomalies of ±3% velocity perturbation and dimensions of 25 km × 5 km was imposed in a checkerboard pattern on the final velocity solution of profile 31/32 (Figure 7). Synthetic traveltimes were computed through this model and Gaussian noise with a standard deviation equal to a quarter of the individual pick uncertainty was added to the synthetic traveltimes. The inversion was initialized using the underlying velocity model as a starting model. The aim of this approach is to test the algorithm’s capability of resolving small perturbations within the original tomographic output and whether anomalies are transferred into different areas during this process. Lower and upper plates were investigated separately, in order to incorporate reflections from the major interfaces and according to the tomographic approach chosen for these profiles. As displayed in the recovery panels of Figure 7, the incoming oceanic crust is well resolved, as is the oceanic uppermost mantle. Resolution of the upper plate

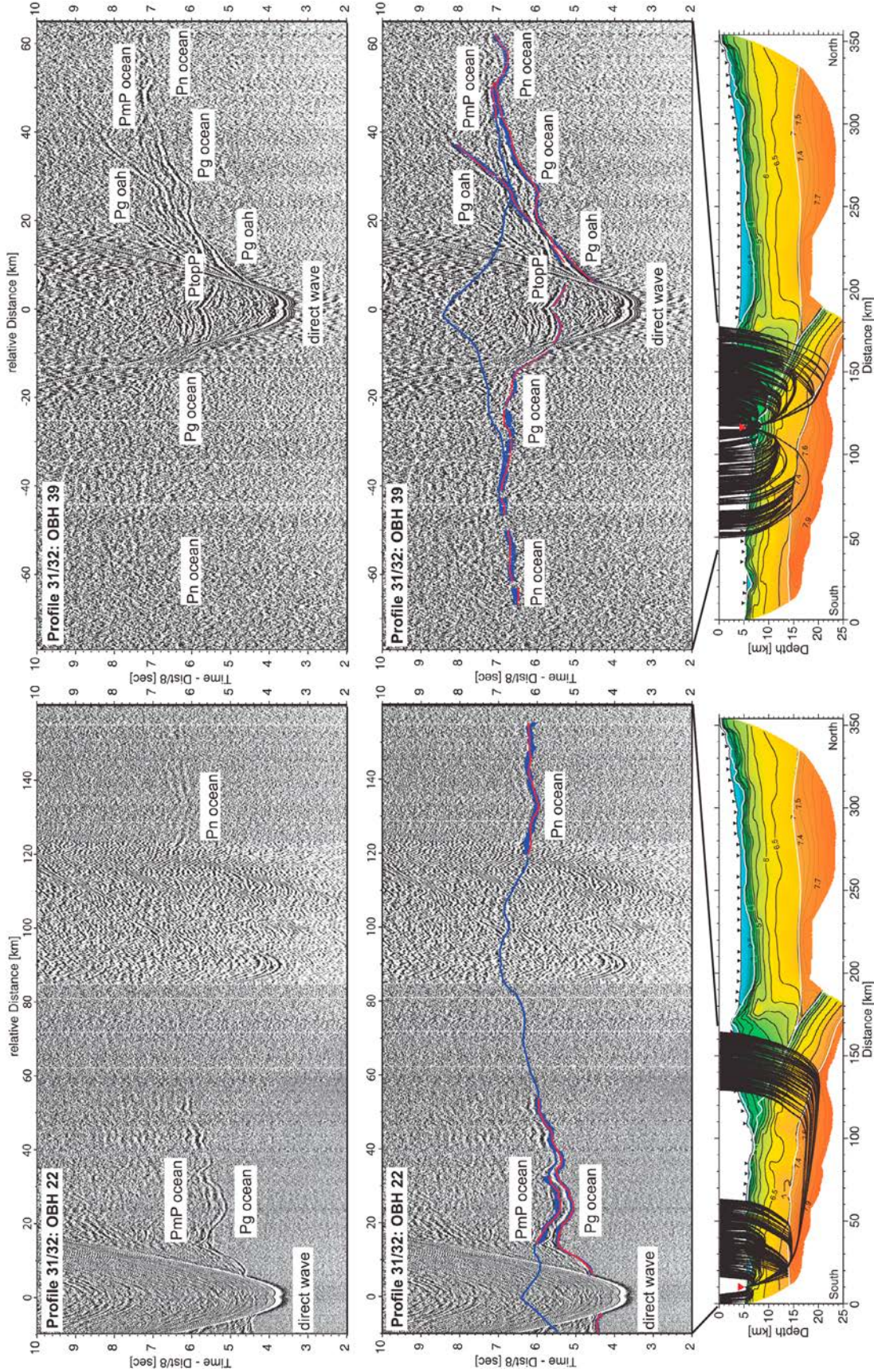


Figure 3. Seismic record sections (reduced to 8 km/s) of OBH 22 and OBH 39 on profile 31/32. (top) Interpreted seismic arrivals are labeled: Pg oah (turning rays within the outer arc high), Pg ocean (turning rays within the oceanic crust), Pn ocean (turning rays in the upper oceanic mantle), PtopP (reflected rays at the plate boundary), and PmP ocean (reflected rays at the oceanic Moho). (middle) Picks are shown as blue bars according to their pick uncertainty; computed traveltimes are shown as red dots. Blue lines represent traveltimes for offsets not constrained by picks. (bottom) Corresponding raypaths of the picked traveltimes through the final tomographic solution of profile 31/32.

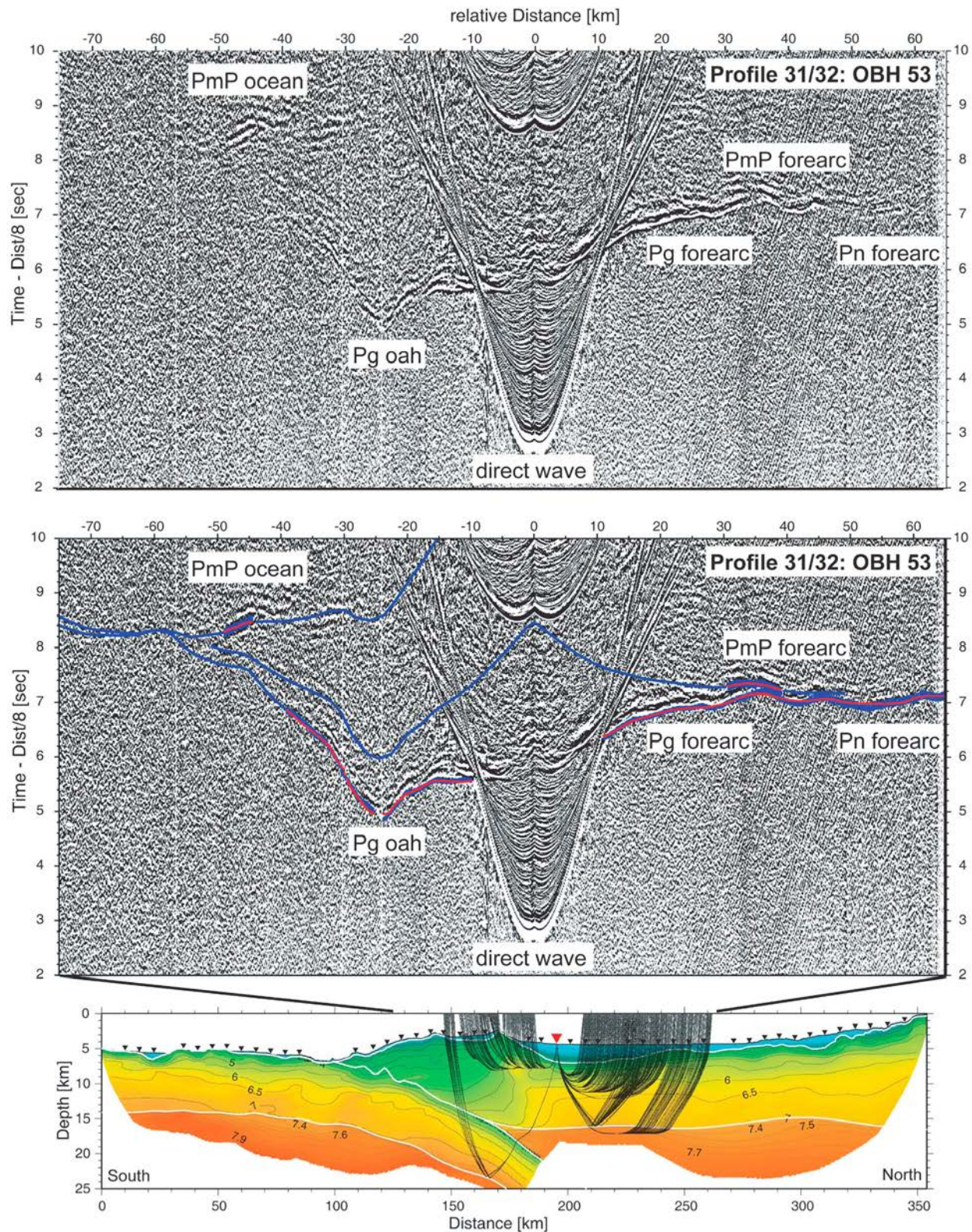


Figure 4. Seismic record section (reduced to 8 km/s) of OBH 53 on profile 31/32. (top) Interpreted seismic arrivals are labeled: Pg oah (turning rays within the outer arc high), Pg fore arc (turning rays within the fore-arc crust), Pn fore arc (turning rays in the upper fore-arc mantle), PmP fore arc (reflected rays at the fore-arc Moho), and PmP ocean (reflected rays at the oceanic Moho). (middle) Picks are shown as blue bars according to their pick uncertainty; computed traveltimes are shown as red dots. Blue lines represent traveltimes for offsets not constrained by picks. (bottom) Corresponding raypaths of the picked traveltimes through the final tomographic solution of profile 31/32.

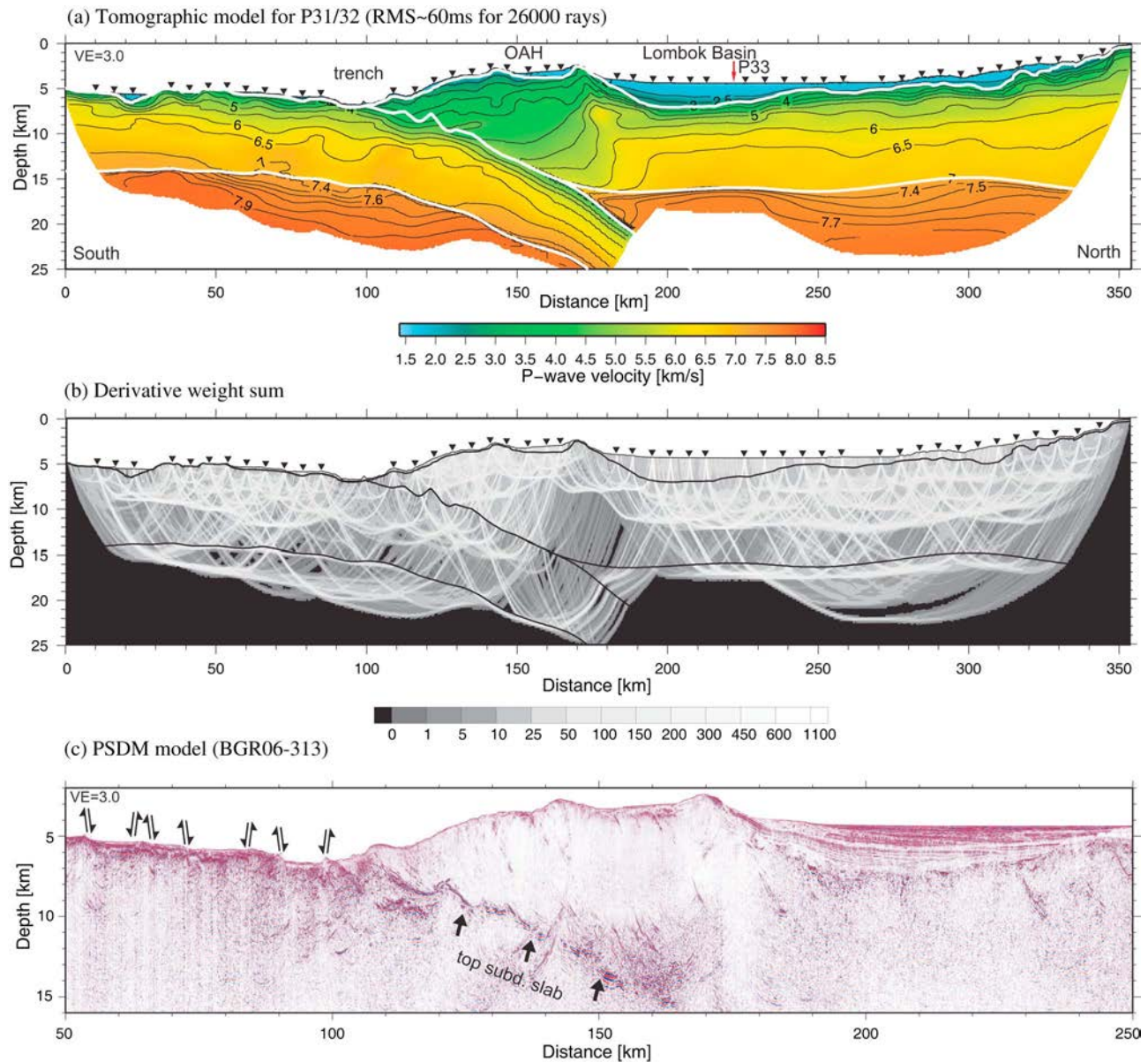


Figure 5. (a) Final tomographic velocity model of profile 31/32. Triangles indicate locations of ocean bottom seismographs. Red arrow displays line intersection with profile 33. White lines mark structural interfaces: sedimentary portions are derived from the analysis of high-resolution MCS seismic data; plate boundary, oceanic Moho and fore-arc Moho are obtained from the joint refraction and wide-angle reflection tomography. (b) Derivative weight sum for the final tomographic velocity model. (c) Prestack depth-migrated MCS line BGR06-313 from *Lüschen et al.* [2010]. All models are plotted at $3 \times$ vertical exaggeration. OAH, outer arc high.

diminishes at a depth of 18 km, but the entire crust and upper mantle wedge are resolved (please refer to Figures S1 and S2 of the auxiliary material for additional resolution tests with synthetic anomalies confined to the oceanic mantle underneath the trench and an evaluation of the impact of different mantle starting models on the tomographic solution of profile 31/32).¹

¹Auxiliary materials are available in the HTML. doi:10.1029/2009JB006713.

4.2. Profile 33

[27] On this line, the basement of the Lombok Basin is found in depths of 2.0 km to 3.7 km beneath the seafloor and resolved sediment velocities reach 2.8 km/s (Figure 8). Since no MCS seismic data are available for profile 33 also the sedimentary portions were modeled using refracted and wide-angle reflected seismic phases (see Figure 9 for data examples). The underlying crust shows some thickness variations around average values of 10 km and it includes a ~6 km thick portion of velocities of 6–6.8 km/s and relatively low velocity gradients. The velocities in the upper-

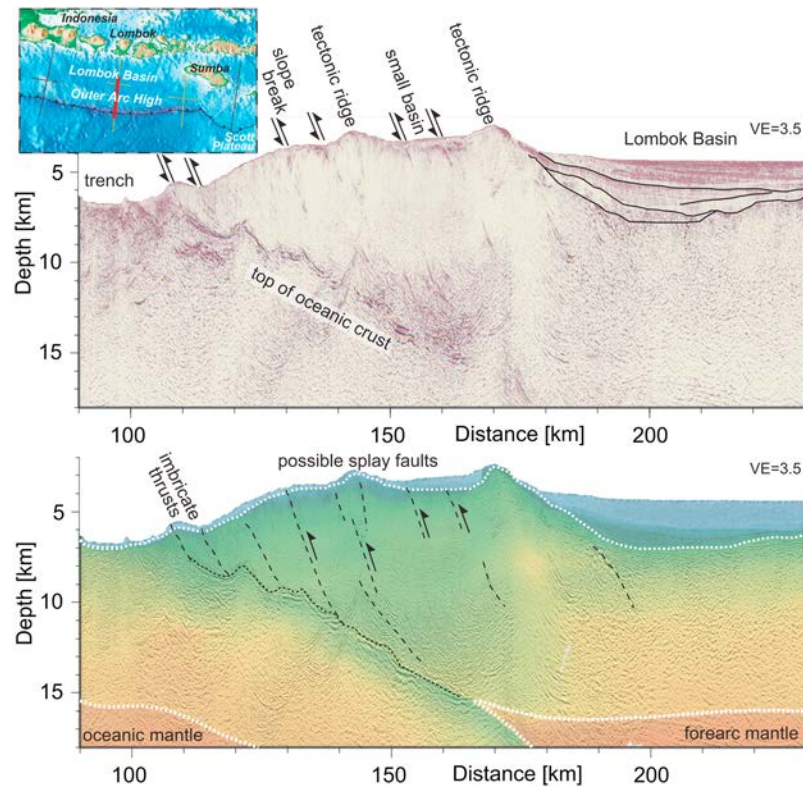


Figure 6. (top) Close-up of prestack depth-migrated MCS line BGR06-313 (modified from *Lüschen et al.* [2010]). The plate interface reveals a pronounced vertical relief. The outer arc high is characterized by landward dipping faults. (bottom) Final tomographic velocity model and line drawing overlain over PSDM image. Possible splay faults connect to the seafloor, where they are associated with changes in slope angle and tectonic ridges. Arrows indicate movement along faults. See text for discussion. Models are plotted at $3.5\times$ vertical exaggeration.

most mantle are in the range of 7.4 km/s, reaching 7.7 km/s in 21 km depth and thus are slightly lower compared to profile 31/32 at the line intersection.

4.3. Profile 22

[28] In the southernmost model portions the incoming oceanic plate reveals an up to 600 m thick and largely undisturbed sedimentary cover; approaching the trench, however, the sediments are entirely crosscut by plate-bending faults (Figure 10). The onset of basement structures at the seafloor ~ 30 km seaward of the trench coincides with a vigorous decrease of crustal and upper mantle velocities. Compared to those velocity portions located 60 km south of the trench, corresponding velocities at the trench are up to 1.2 km/s lower in the mid crust and 0.6 km/s in the lower crust directly above the Moho. The oceanic crustal thickness is 9.0 km on average and hence slightly thicker than on profile 31/32. The resolved upper mantle portions reveal velocities of 7.4–7.8 km/s (see Figure 11 for data examples), which is perhaps slightly lower than corresponding velocities on profile 31/32.

[29] The plate interface is constrained by wide-angle reflections up to distances of 100 km landward of the trench down to ~ 22 km depth (dip: $5\text{--}8^\circ$) (Figure 10a). The boundary is of irregular shape, at least in its shallower portions, with pronounced indentations suggesting vertical

displacements locally exceeding 1 km (Figure 10d). The pronounced asperity close to 105 km profile distance (Figure 10d) appears to lie in the trace of equivalent structure subducted at the western indentation of the lowermost inner-trench slope (compare Figure 2). Hence, the relief on the oceanic plate beneath the lower OAH slope may in places be associated with the subduction of inherited seafloor fabric, which is likely reactivated as response to plate bending.

[30] On this line, velocities beneath the OAH are <5.5 km/s down to ~ 11 km depth and thus only slightly lower than corresponding velocity portions farther north (Figure 10a). Different to the fore-arc setting observed offshore Lombok, there is only a thin sedimentary cover (no mature sedimentary basin) and crustal type velocities are observed down to ~ 25 km depth. Beneath the northern model edge, some steep seaward dipping reflections are observed in the wide-angle seismic data set (Figure 10b; see Figure 12 for data example). From the velocity information gained from the few rays penetrating those areas, however, it seems unlikely that this reflector is associated with a major velocity discontinuity such as the crust-mantle boundary.

4.4. Profile 21

[31] Compared to the previous lines data quality on profile 21 is only moderate, which is most likely related to the

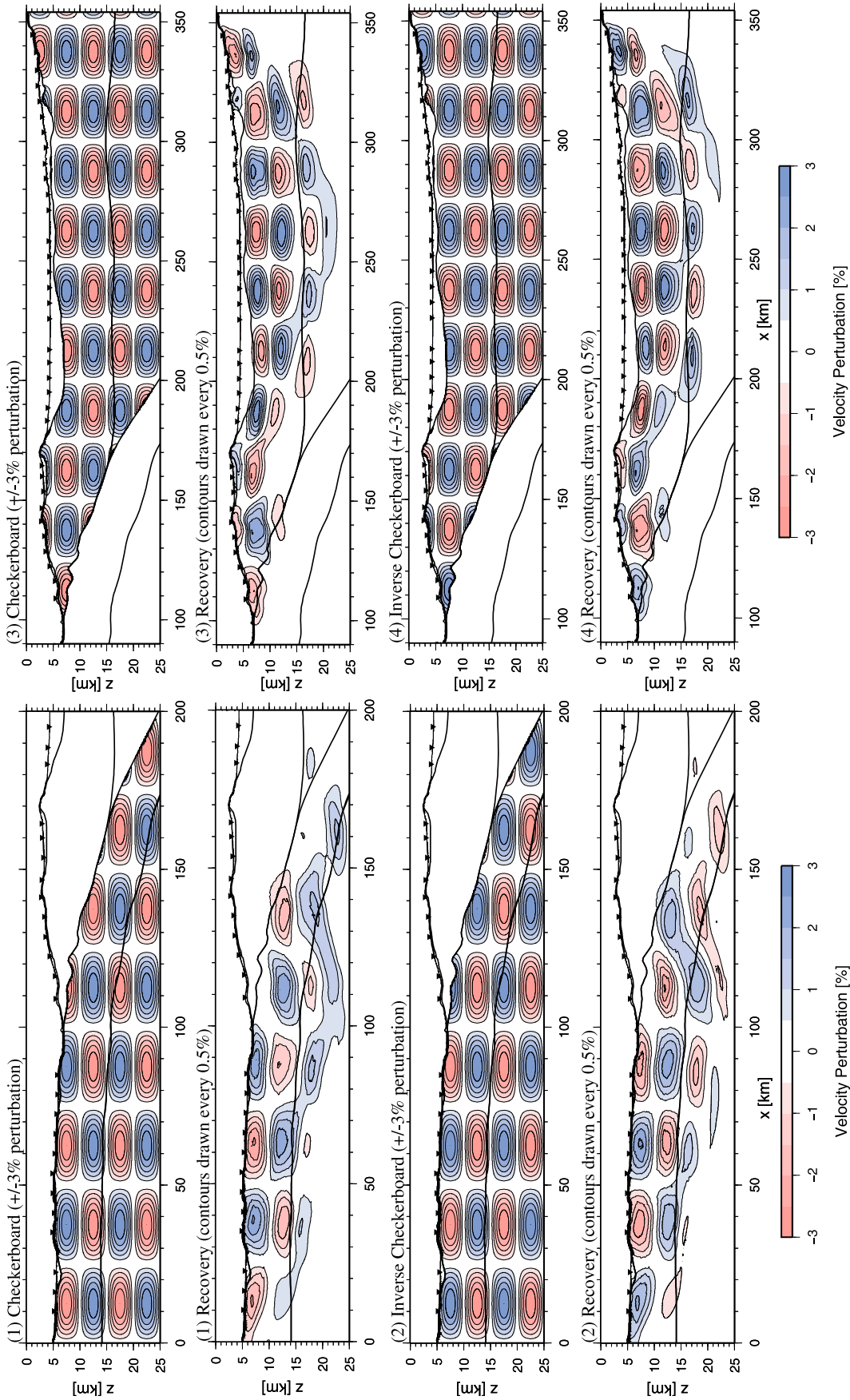


Figure 7. Resolution tests using a $\pm 3\%$, $25 \text{ km} \times 5 \text{ km}$ checkerboard pattern of synthetic velocity anomalies (left) within the oceanic model portions and (right) within the fore-arc model portions of profile 31/32. Tests show normal and inverse checkerboard patterns, original perturbation model and recovery after three iterations, respectively. The background model for the anomalies is the tomographic velocity model of Figure 5a. See text for discussion.

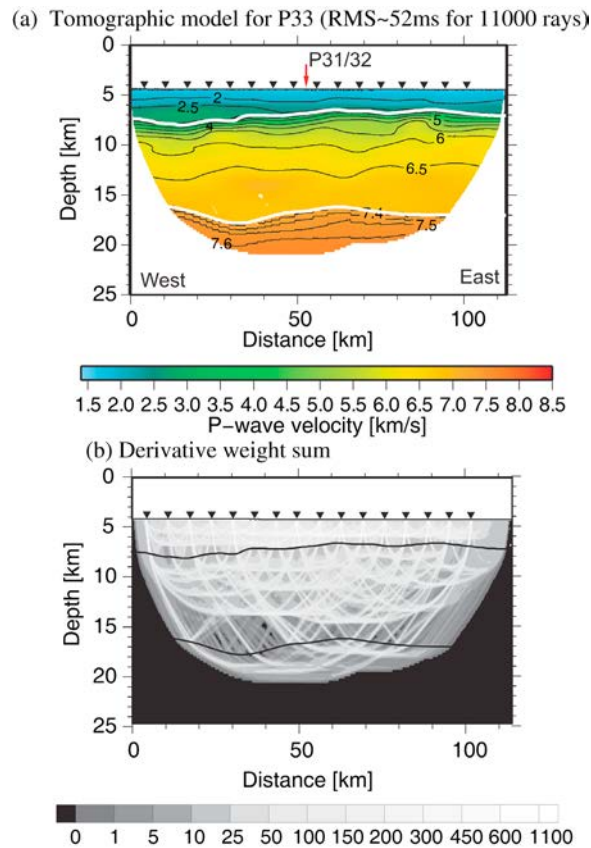


Figure 8. (a) Final tomographic velocity model of profile 33 (Lombok Basin). Triangles indicate locations of ocean bottom seismographs. Red arrow displays line intersection with profile 31/32. White lines mark structural interfaces: basement and fore-arc Moho are obtained from the joint refraction and wide-angle reflection tomography. (b) Derivative weight sum for the final tomographic velocity model.

rather complex morphology and internal structure of the OAH close to the transition to the collisional regime (see Figure 13 for data examples). The velocity model suggests significant structural changes between the western and the eastern model portions and a transition zone between ~ 60 km and ~ 100 km profile distance where the depth of the oceanic Moho increases from 19 km to 23 km (Figure 14). In the western model portions velocities reach 5.3 km/s above the plate boundary which can be traced as a continuous reflector in 11–12 km depth up to ~ 80 km profile distance (Figure 14b). Along the entire profile, the oceanic slab is characterized by an intracrustal reflector, which is associated with the 5.5–6.0 km/s iso-velocity line. In the eastern model portions, there is evidence for two shallower reflectors, although their continuation is sometimes unclear due to the lack of reflection coverage. If the lower reflector represents the eastern continuation of the plate boundary, this would imply a ~ 13 km thick subducting oceanic slab in the eastern model portions versus a 8–9 km thick slab in the western model portions (Figure 14). Accordingly, we interpret the observed change toward greater thickness of the

lower plate as the transition to the collisional setting comprising the promontory of the Australian continental shelf. Resolved mantle velocities are in the range of 7.7–8.0 km/s and thus, ~ 0.3 km/s higher compared to corresponding velocities on profile 22 at the line intersection.

5. Gravity Data

[32] Gravity data were acquired every second using the KSS31M sea gravimeter system built by Bodenseewerk Geosystem GmbH. Using the navigation information from the ship, the measured data were corrected for the Eötvös effect and for the instrumental drift by tying it to calibrated land stations after completion of the cruise. The Free-Air Anomaly (FAA) was then obtained by subtracting the WGS67 normal gravity.

[33] We used the TOMO2D code [Korenaga *et al.*, 2001], which adopts the method of Parker [1973] modified by topographic correction terms, to calculate the 2-D FAA gravity response to a velocity-derived density model. For sediment, as resolved from MCS seismic data, we used the empirical velocity-density relationship $\rho = 1 + 1.18(V_p - 1.5)^{0.22}$ [e.g., Korenaga *et al.*, 2000]. Carlson and Herrick's [1990] conversion formula for igneous crust, $\rho = 3.81 - 6.0/V_p$, was adopted for the upper oceanic crust ($V_p < 6.0$ km/s) and we used a constant density of 2.90 g/cm^3 for the lower oceanic crust. Beyond the depth of seismic penetration the thickness and velocity structure of the subducting slab were held constant and its geometry was inferred from the distribution of Wadati-Benioff hypocenters [Engdahl and Villaseñor, 2002]. For the upper oceanic mantle we used the V_p versus ρ relationship of Carlson and Miller [2003], which accounts for the dependence of V_p with the degree of serpentinization and we limited the density to maximal 3.23 g/cm^3 for the deeper mantle portions.

[34] According to thermal simulations, serpentine breaks down via dehydration reactions in the subducting oceanic mantle at depths greater ~ 50 km ($>600^\circ\text{C}$) and for old/cold slabs likely at much greater depths [Peacock, 2001; Rüpke *et al.*, 2004]. Hence, we expect that hydrated oceanic mantle will not recover its density by metamorphic deserpentinization reactions within the depth range of our models. We thus held constant the reduced mantle densities within the shallowmost oceanic mantle portions landward of the trench, even though V_p partly increases in our models by possible fracturing recover.

[35] For the subsequent gravity modeling we tested several models, keeping unchanged the density distribution in the oceanic crust and mantle, and changing only the densities in the overriding plates. The major aim of the applied approach is to test whether our seismically derived fore-arc geometries (mantle wedge offshore Lombok, crustal wedge offshore Sumba) can explain the gravity data reasonably well by using widely accepted velocity to density conversions.

5.1. Gravity Modeling of Profile 31/32

[36] For the overriding plate we used Hamilton's [1978] relation for shale, $\rho = 0.917 + 0.747V_p - 0.08V_p^2$, for

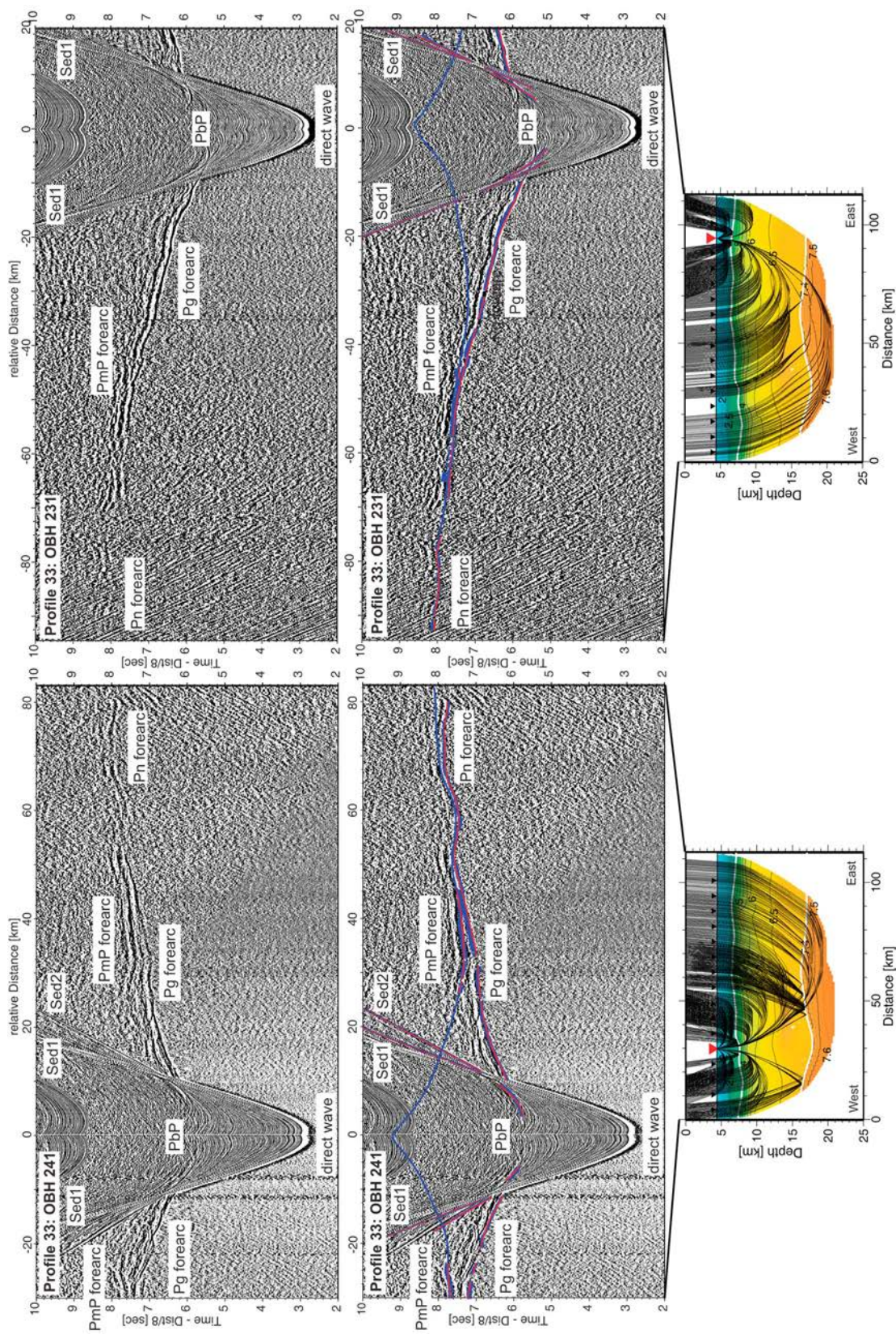


Figure 9. Seismic record sections (reduced to 8 km/s) of OBH 231 and OBH 241 on profile 33. (top) Interpreted seismic arrivals are labeled: Sed1, Sed2 (sedimentary phases), Pg fore arc (turning rays within the fore-arc crust), Pn fore arc (turning rays in the upper fore-arc mantle), PbP (reflected rays at the basement), and PmP fore arc (reflected rays at the fore-arc Moho). (middle) Picks are shown as blue bars according to their pick uncertainty, and PmP fore arc (reflected rays at the fore-arc Moho). (bottom) Corresponding raypaths of the picked traveltimes for offsets not constrained by picks. Blue lines represent traveltimes for offsets not constrained by the picked traveltimes through the final tomographic solution of profile 33.

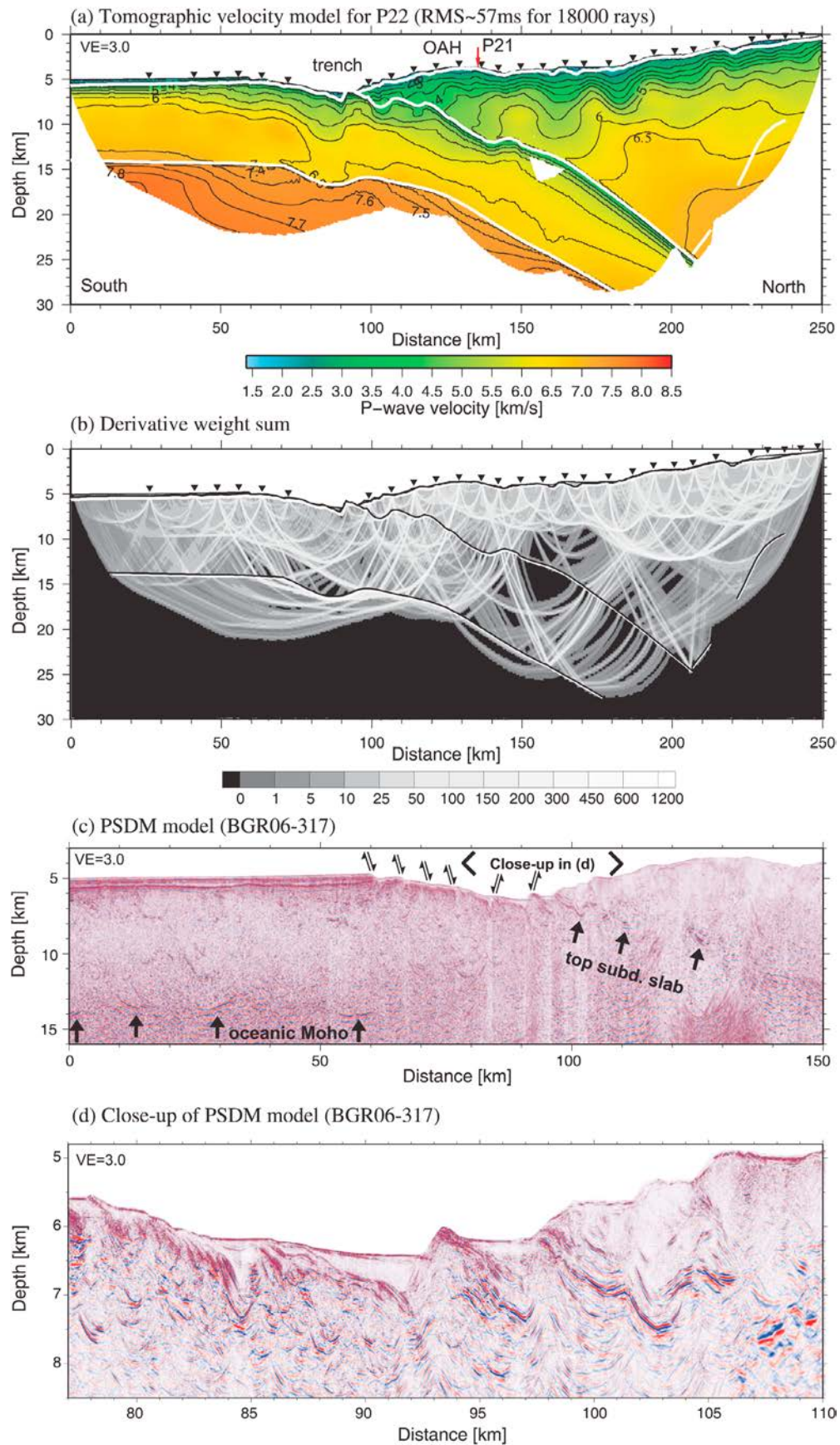


Figure 10

crustal portions characterized by $V_p < 5.7$ km/s. We then tested three different laws for the deeper crustal portions and the fore-arc mantle (Figure 15): (1) *Carlson and Herrick's* [1990] relation (igneous crust) and a constant mantle density of 3.20 g/cm³, (2) *Christensen and Mooney's* [1995] nonlinear regression for continental crustal rocks, $\rho = 5.055 - 14.094/V_p$, and a constant mantle density of 3.21 g/cm³, and (3) a constant density of 2.80 g/cm³ for the crust and the same V_p versus ρ relationship used for oceanic mantle.

[37] For the overriding plate, the relationships of *Carlson and Herrick* [1990] (igneous crust) and *Christensen and Mooney* [1995] (continental crust) yield a comparable fit by adjusting the fore-arc mantle density from 3.20 g/cm³ to 3.21 g/cm³ (Figure 15b). The fit is slightly improved for a model comprising a constant crustal density of 2.80 g/cm³ and a fore-arc mantle comprising the same V_p versus ρ relationship used for oceanic mantle (Figure 15c). Thus, the gravity data is consistent with mantle alteration and a shallow fore-arc mantle, as inferred from the analysis of seismic refraction data.

5.2. Gravity Modeling of Profile 22

[38] Similar to the above described scheme we tested four different scenarios for those fore-arc portions characterized by $V_p > 5.7$ km/s (Figure 16): (1) a constant density of 2.75 g/cm³ and *Birch's* [1961] conversion law for lower crustal rocks, $\rho = (V_p + 1.0)/2.67$, for model portions between the intracrustal reflector and the top of the subducting slab, (2) *Carlson and Herrick's* [1990] relationship (igneous crust) for the entire crust, (3) *Christensen and Mooney's* [1995] relationship (continental crust) for the entire crust, and (4) a constant density of 2.80 g/cm³ and a constant density of 2.95 g/cm³ for model portions between the intracrustal reflector and the top of the subducting slab.

[39] The results show that a model comprising a locally lightened mantle density yields a good match to the observed gravity anomaly, again implying that the oceanic mantle beneath the trench has been altered. For the overriding plate, the relationship of *Carlson and Herrick* [1990] yields a rather poor match to the observed gravity anomaly, at least up to ~ 200 km profile distance (Figure 16b). Applying *Christensen and Mooney's* [1995] conversion law (continental crust) provides a much better match to the observed data for these model portions but underpredicts the FAA anomaly for greater profile distances. Accounting for the dichotomy of the crust (upper fore arc and lower fore arc), either by using constant densities of 2.80 g/cm³ and 2.95 g/cm³ or by using 2.75 g/cm³ and *Birch's* [1961] conversion law, respectively, yield an altogether better RMS fit. However, assuming the presence of crustal-type densities beneath the steeply seaward-dipping reflector

yields a good fit of the gravity data. Hence, these results are in accordance with our seismically derived model, which lacks a shallow mantle wedge offshore Sumba.

6. Discussion

6.1. Oceanic Plate and Trench

[40] A thickened oceanic crust is observed on both trench-perpendicular profiles. In case of profile 31/32, average values of 8.6 km are interpreted as the transition to the easternmost extensions of the Roo Rise and another bathymetric high near the trench close to 114.5°E (Figure 1), which locally reveal crustal thicknesses >15 km [*Curray et al.*, 1977; *Shulgin et al.* (submitted manuscript, 2010)]. The refraction profile offshore Lombok Strait from *Curray et al.* [1977] runs ~ 50 km west of profile 31/32 and reveals velocities of 8.1 km/s at 23 km depth at the trench (compared to velocities of ~ 7.9 km/s at ~ 22 km depth at the trench on profile 31/32). Owing to the large shot spacing and related difficulties in following secondary arrivals from one record to another, their evaluation of layer thickness is mainly based on the recordings of refracted arrivals, which makes their interpretation of Moho depths from these early shot records ambiguous. Hence, their depth for the 8.1 km/s velocity layer may not mark the top of the mantle, which here is constrained at ~ 17 km depth, but may indicate the lower limit of the observed mantle alteration.

[41] On profile 22 the crustal thickness of 9.0 km is likely related to the transition to the Scott Plateau representing the promontory of the Australian continental shelf [*Shulgin et al.*, 2009]. This is confirmed by the trench-parallel profile 21 off Sumba which suggests structural changes of the subducting crust manifested in a thickness increase of ~ 5 km over a distance of 40 km to the east (Figure 14). Most of the observed crustal thickening is related to the thickening of the upper crustal layer. The profile of *Shulgin et al.* [2009] at 121°E (Figure 1) reveals a 15 km thick crust beneath the Scott Plateau which seems to thin out northward when subducting beneath the Sumba Ridge. The crust shows a pronounced intracrustal reflector at roughly mid-crustal depths and is interpreted to be of continental nature. Accordingly, we interpret the easternmost portions of profile 21 as the ocean-continent transition in the subducting plate (Figure 14).

[42] Both trench-perpendicular profiles show a reduction of crustal and upper mantle velocities at distances <30 – 50 km seaward of the trench (Figures 5a and 10a). Obtained uppermost mantle velocities (down to ~ 2 km beneath the Moho) in the trench are well resolved and independent of the mantle starting model; they represent a robust feature of the tomographic inversion (please refer to Figures S1 and S2 in the auxiliary material for additional resolution tests with

Figure 10. (a) Final tomographic velocity model of profile 22. Triangles indicate locations of ocean bottom seismographs. Red arrow displays line intersection with profile 21. White lines mark structural interfaces: sedimentary portions are derived from the analysis of high-resolution MCS seismic data; plate boundary, oceanic Moho and seaward dipping intra-fore-arc reflector are obtained from the joint refraction and wide-angle reflection tomography. (b) Derivative weight sum for the final tomographic velocity model. (c) Prestack depth-migrated MCS line BGR06-317 from *Lüschen et al.* [2010]. (d) Close-up of BGR06-317. Subduction of basement asperities, located near 95 km and 105 km profile distance, results in local indentations of the deformation front (compare Figure 2). All models are plotted at $3 \times$ vertical exaggeration. OAH, outer arc high.

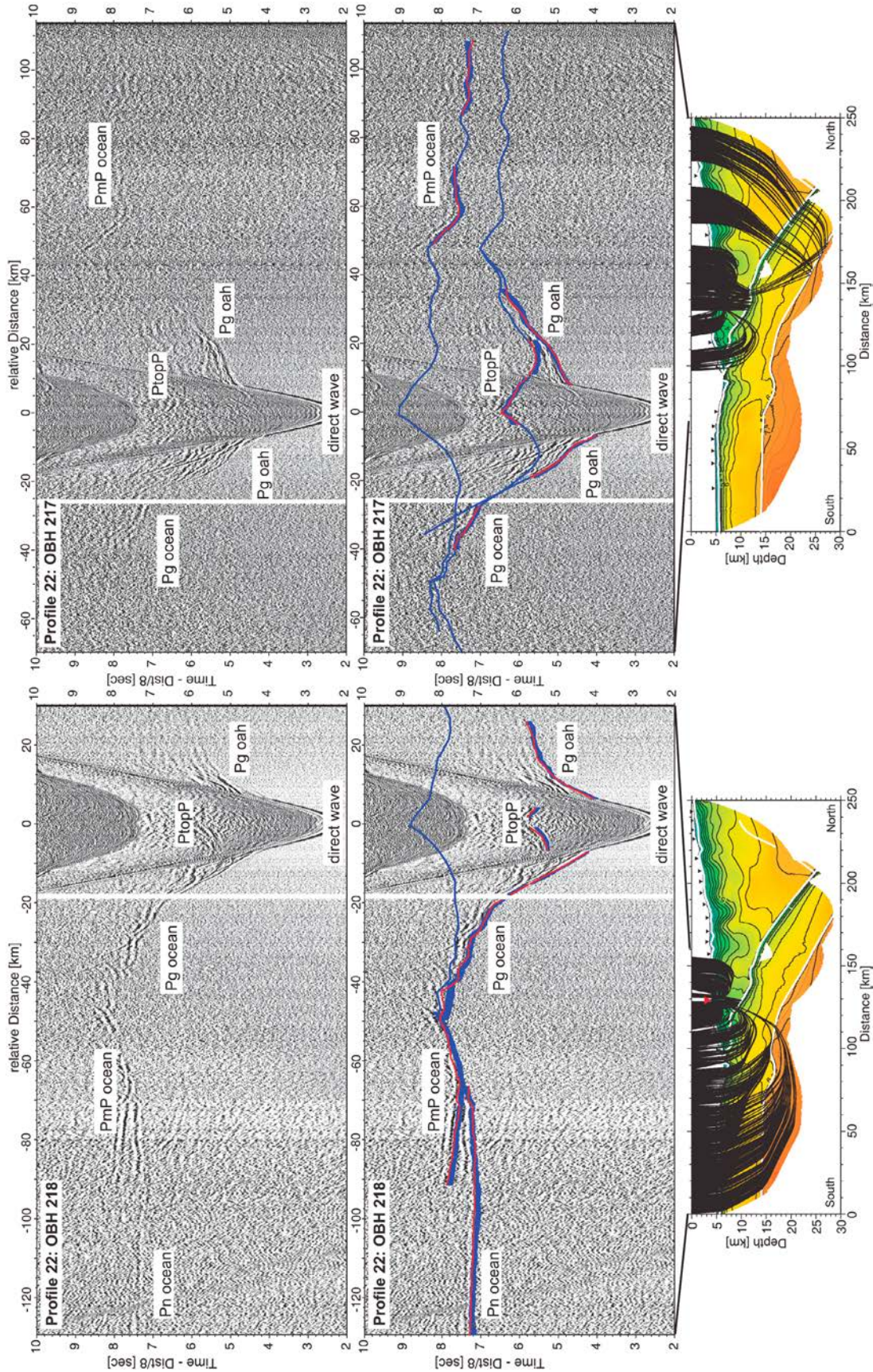


Figure 11. Seismic record sections (reduced to 8 km/s) of OBH 217 and OBH 218 on profile 22. (top) Interpreted seismic arrivals are labeled: Pg oah (turning rays within the outer arc high), Pg ocean (turning rays within oceanic crust), Pn ocean (turning rays in the upper oceanic mantle), PtopP (reflected rays at the plate interface), and PmP ocean (reflected rays at the oceanic Moho). (middle) Picks are shown as blue bars according to their pick uncertainty, computed traveltimes are shown as red dots. Blue lines represent traveltimes for offsets not constrained by picks. (bottom) Corresponding raypaths of the picked traveltimes through the final tomographic solution of profile 22.

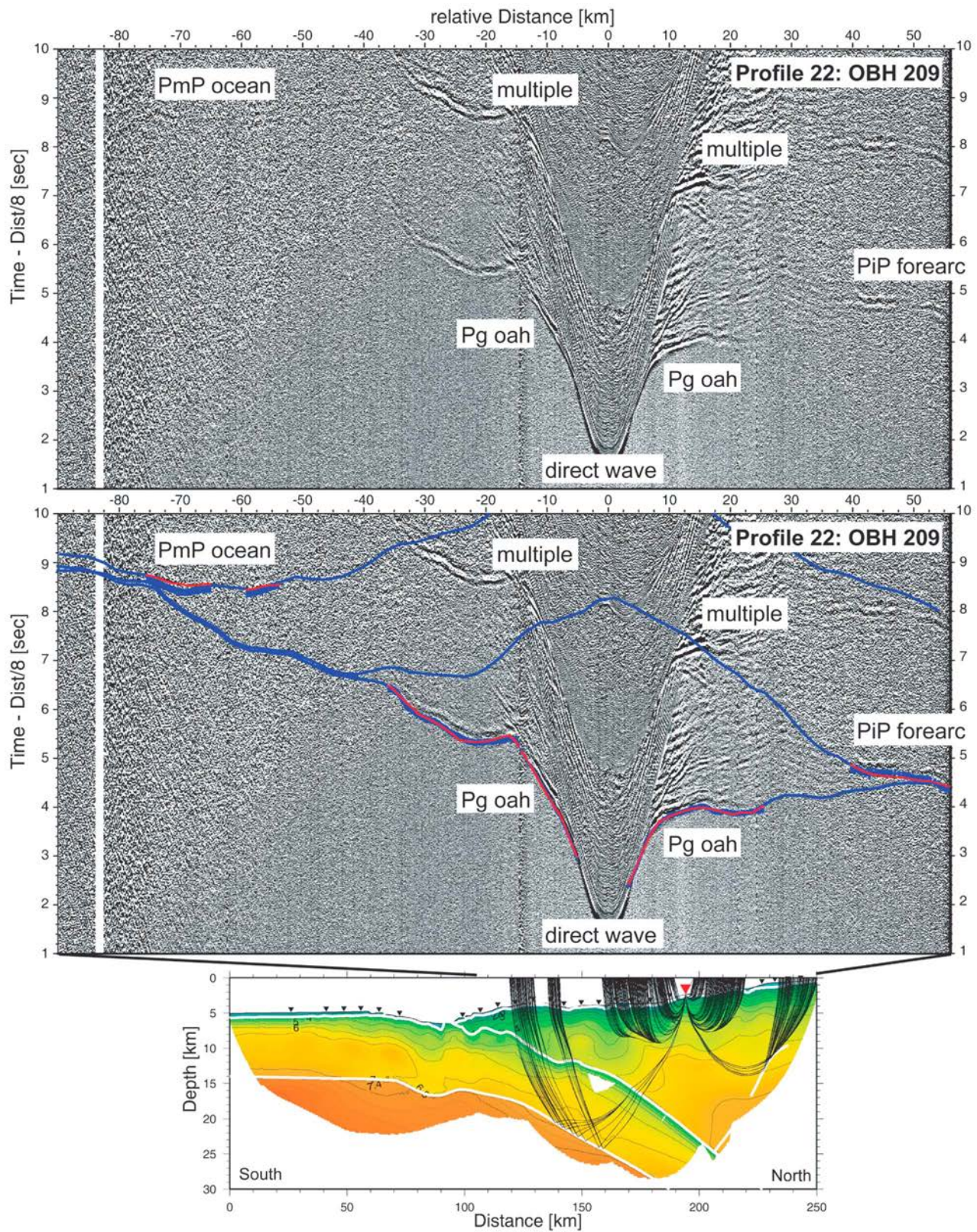


Figure 12. Seismic record section (reduced to 8 km/s) of OBH 209 on profile 22. (top) Interpreted seismic arrivals are labeled: Pg oah (turning rays within the outer arc high/fore arc), PiP fore arc (reflected rays at the intracrustal fore-arc reflector), and PmP ocean (reflected rays at the oceanic Moho). (middle) Picks are shown as blue bars according to their pick uncertainty, computed traveltimes are shown as red dots. Blue lines represent traveltimes for offsets not constrained by picks. (bottom) Corresponding ray-paths of the picked traveltimes through the final tomographic solution of profile 22.

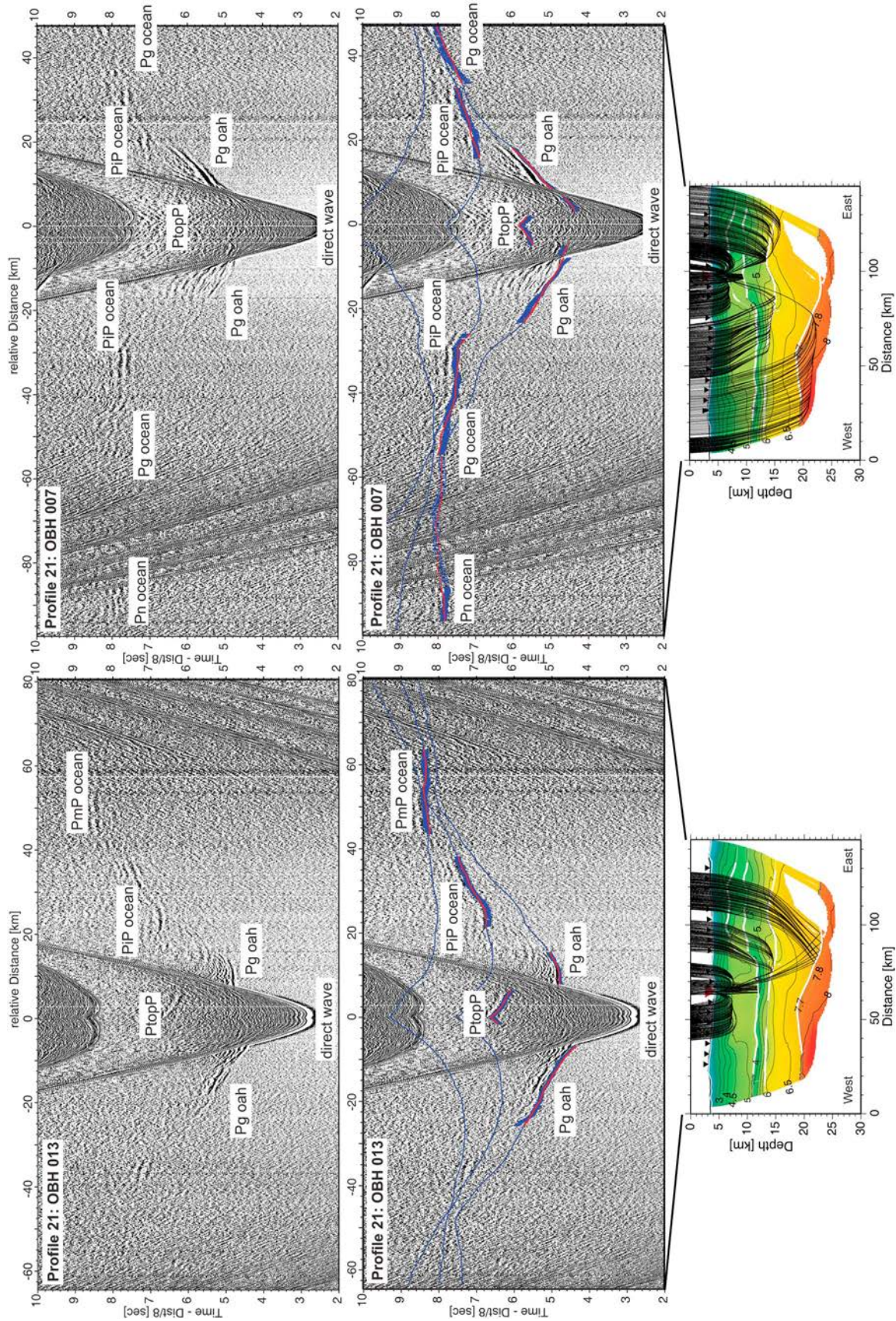


Figure 13

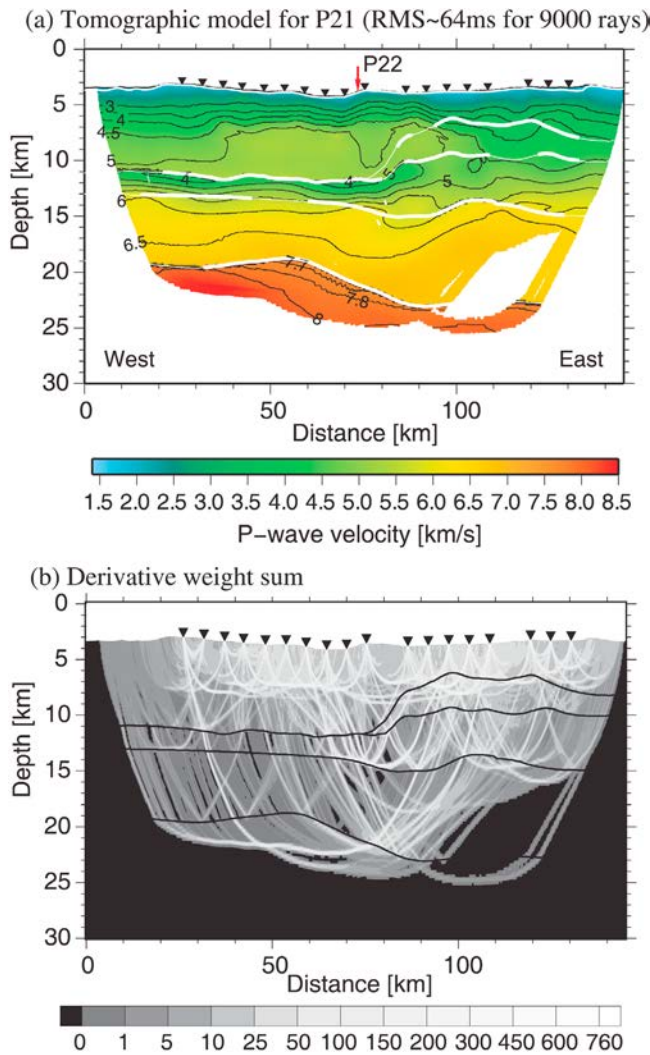


Figure 14. (a) Final tomographic velocity model of profile 21 (outer arc high). Triangles indicate locations of ocean bottom seismographs. Red arrow displays line intersection with profile 22. White lines mark structural interfaces obtained from the joint refraction and wide-angle reflection tomography (see text for details). (b) Derivative weight sum for the final tomographic velocity model.

synthetic anomalies confined to the oceanic mantle underneath the trench and an evaluation of the impact of different mantle starting models on the tomographic solution of profile 31/32). The apparent coincidence of the velocity decrease with the onset of faulting can be interpreted as the result of fracturing and subsequent alteration of the oceanic crust and serpentinization of the underlying upper mantle. Reduced upper mantle velocities within a similar range close to the trench and associated with the bending of the oceanic

plate prior to subduction are found, e.g., at the Middle America trench [Grevenmeyer *et al.*, 2007; Ivandic *et al.*, 2008] and offshore Chile [Contreras-Reyes *et al.*, 2007].

[43] Assuming that the velocity reduction in the upper mantle is exclusively caused by serpentinization, velocities of 7.9–7.4 km/s would imply a 0.6–2.4% increase in water content resulting in 5–19% serpentinization of mantle peridotite as a maximum estimate [Carlson and Miller, 2003]. However, the velocity model of profile 31/32 shows that upper mantle velocities recover to some extent from ~7.5 km/s at the trench to ~7.7 km/s beneath the lower slope of the OAH (Figure 5a; please also refer to Figure S2 of the auxiliary material). The partial recovery of mantle velocities at depths of ~20 km may indicate compressive sealing of cracks by slab-refolding and fracture-filling precipitation, because metamorphic de-serpentinization reactions occur at much greater depth during subduction of old (cold) oceanic lithosphere [Peacock, 2001; Rüpke *et al.*, 2004; Faccenda *et al.*, 2009]. Hence, the presence of mantle-penetrating cracks and faults likely controls the extent of the low velocity anomaly at the trench and reduces the possible degree of mantle serpentinization to probably less than 15%.

[44] On profile 22, the amplitude and intensity of the crustal low-velocity anomaly is larger and occurs more tightly confined to the trench, respectively. This is likely related to the stronger fragmentation of the oceanic crust as indicated by the greater basement relief with vertical throws of sometimes >1 km (Figure 10d). Moreover, upper mantle velocities in the uppermost 2–3 km depth beneath the Moho do not recover within the resolved model portions downdip of the trench. These observations may indicate increased tensional tectonic forces in the subducting plate.

[45] Spence [1986] inferred from the absence of large interface thrust earthquakes in the Sumba region, that gravitational pull of the old (dense) sinking oceanic lithosphere might have partially decoupled the subducted plate from the overriding plate. The juxtaposition of old (Late Jurassic) oceanic crust and continental crust close to ~120°E provides one of the most dramatic lateral gradients in interplate seismic coupling in the world. The combination of slab-pull on an uncoupled slab in the Java trench and the strong resistive force of the buoyant crust of the Scott Plateau to the east appears to store a tremendous amount of elastic tensile strain energy in the lithosphere at the junction of the two zones [Spence, 1986]. The inferred stress in the oceanic slab is transferred updip to the bending-region at the trench, leading to the 1977 Sumba earthquake, and to intense fracturing and alteration of the subducting oceanic crust and the underlying upper mantle.

6.2. Fore-Arc Offshore Lombok

[46] The most striking feature of the OAH offshore Lombok is the portion of low seismic velocities ($V_p < 5.5$ km/s)

Figure 13. Seismic record sections (reduced to 8 km/s) of OBH 007 and OBH 013 on profile 21. (top) Interpreted seismic arrivals are labeled: Pg oah (turning rays within the outer arc high), Pg ocean (turning rays within oceanic crust), Pn ocean (turning rays in the upper oceanic mantle), PtopP (reflected rays at the plate interface), PiP ocean (reflected rays at an intracrustal oceanic reflector), and PmP ocean (reflected rays at the oceanic Moho). (middle) Picks are shown as blue bars according to their pick uncertainty; computed traveltimes are shown as red dots. Blue lines represent traveltimes for offsets not constrained by picks. (bottom) Corresponding raypaths of the picked traveltimes through the final tomographic solution of profile 21.

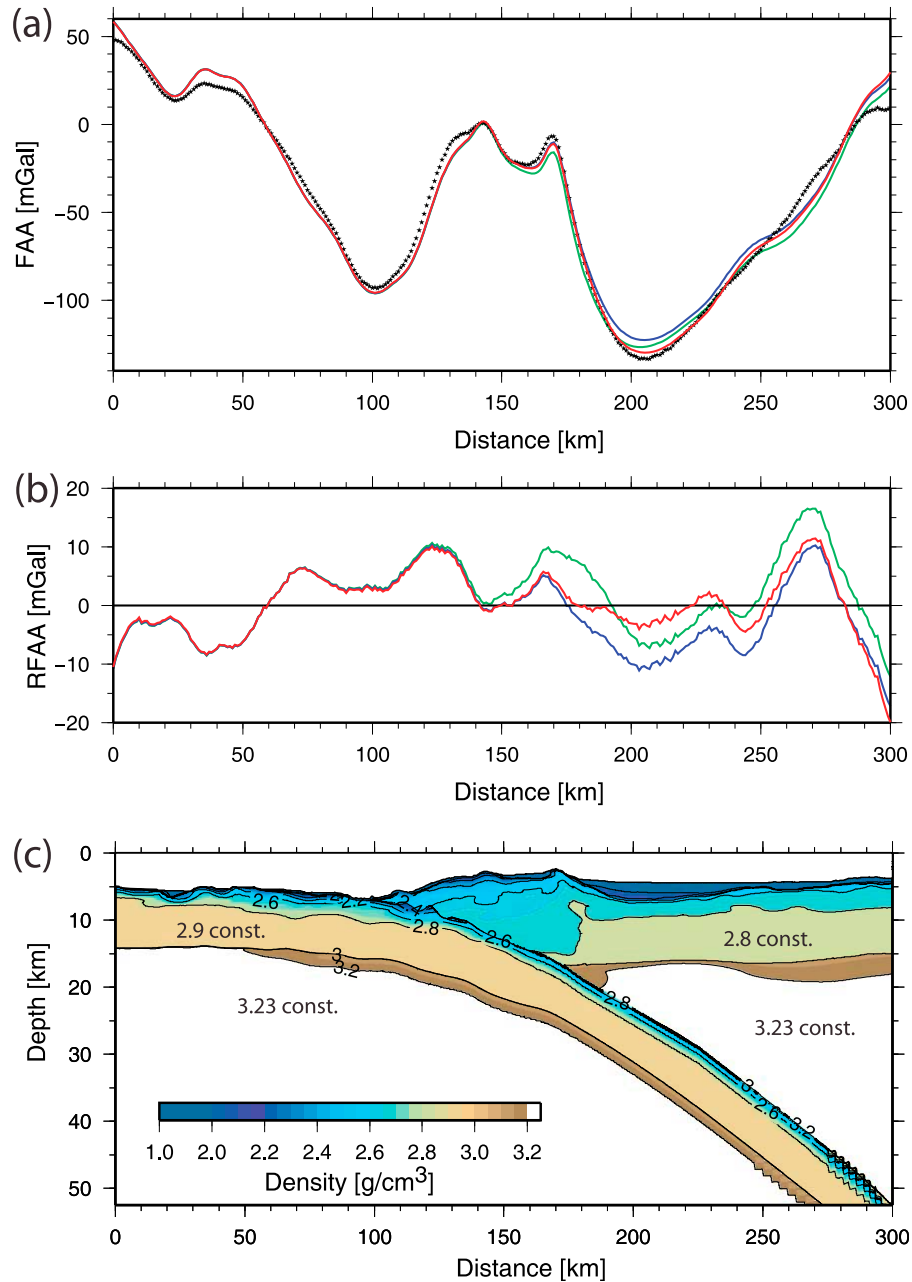


Figure 15. Gravity modeling of profile 31/32. (a) Observed free-air gravity anomaly (black points). Solid lines are from models obtained by changing overriding plate densities and keeping the same structure for oceanic crust and mantle (see text). For all calculations, *Hamilton's* [1978] conversion law for shale is used for fore-arc portions characterized by $V_p < 5.7$ km/s. Blue line is for using *Carlson and Herrick's* [1990] conversion law (igneous crust) for fore-arc crust ($V_p > 5.7$ km/s) and a constant fore-arc mantle density of 3.20 g/cm³. Green line is for using *Christensen and Mooney's* [1995] conversion law (continental crust) for fore-arc crust ($V_p > 5.7$ km/s) and a constant fore-arc mantle density of 3.21 g/cm³. Red line is preferred model shown in Figure 15c. (b) Residual free-air gravity anomaly (RFAA) obtained by subtracting calculated from observed anomaly. Model with *Carlson and Herrick's* [1990] conversion law has RMS of 6.5 mGal (blue line). Model with *Christensen and Mooney's* [1995] conversion law has RMS of 6.2 mGal (green line). Preferred model has RMS of 5.7 mGal (red line). (c) Preferred density model using a constant density of 2.8 g/cm³ for fore-arc crust ($V_p > 5.7$ km/s) and *Carlson and Miller's* [2003] conversion law for both the oceanic and fore-arc mantle (restricted to maximal 3.23 g/cm³).

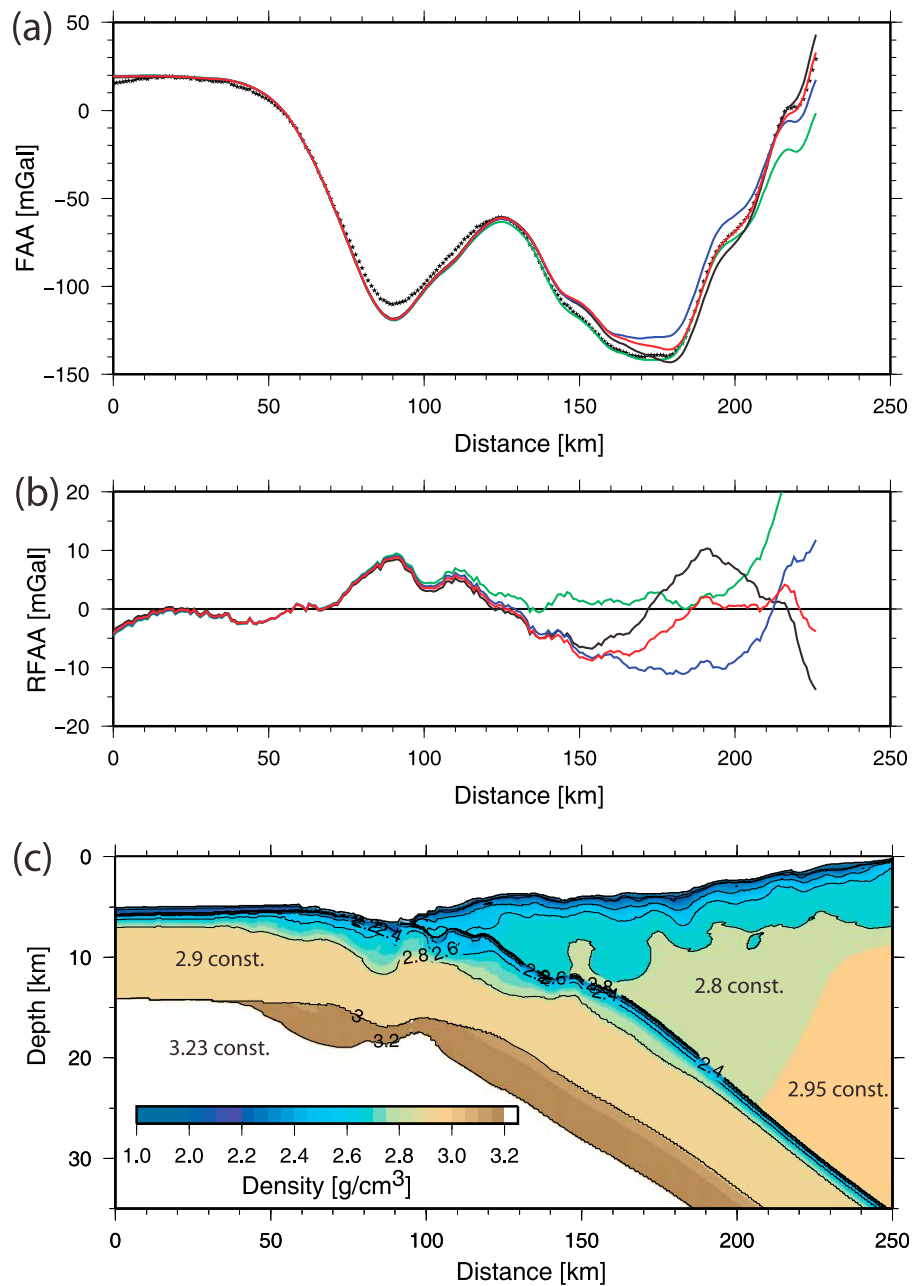


Figure 16. Gravity modeling of profile 22. (a) Observed free-air gravity anomaly (black points). Solid lines are from models obtained by changing overriding plate densities and keeping the same structure for oceanic crust and mantle (see text). For all calculations, *Hamilton's* [1978] conversion law for shale is used for fore-arc portions characterized by $V_p < 5.7$ km/s. Black line is for using a constant density of 2.75 g/cm³ for the upper fore arc ($V_p > 5.7$ km/s) and *Birch's* [1961] conversion law (lower crust) for the lower fore arc between intracrustal reflector and top of subducting slab. Blue line is for using *Carlson and Herrick's* [1990] conversion law (oceanic crust), restricted to maximal 2.9 g/cm³, for the entire fore arc ($V_p > 5.7$ km/s). Green line is for using *Christensen and Mooney's* [1995] conversion law (continental crust), restricted to maximal 2.9 g/cm³, for the entire fore arc ($V_p > 5.7$ km/s). Red line is preferred model shown in Figure 16c. (b) Residual free-air gravity anomaly (RFAA) obtained by subtracting calculated from observed anomaly. Model with *Carlson and Herrick's* [1990] conversion law has RMS of 6.4 mGal (blue line). Model with *Christensen and Mooney's* [1995] conversion law has RMS of 5.8 mGal (green line). Model with *Birch's* [1961] conversion law for the lower fore arc has RMS of 4.5 mGal (black line). Preferred model has RMS of 4.0 mGal (red line). (c) Preferred density model using a constant density of 2.8 g/cm³ for the upper fore arc ($V_p > 5.7$ km/s) and 2.95 g/cm³ for the lower fore arc between intracrustal reflector and top of subducting slab.

down to the plate interface (down to ~13 km depth), which points toward a sedimentary rock origin of this feature (Figure 5). On the lowermost inner trench slope (>5 km depth) profile 31/32 suggests the presence of a frontal prism, which displays low seismic velocities ($V_p \sim 3$ km/s) and originates from frontal accretion of trench sediments. The MCS profile draws only one imbricate thrust sheet (Figure 6), probably due to local indentations of the trench, but more than three arrays of thrust ridges appear at the seafloor farther to the east (Figure 2).

[47] Currently, only moderate sedimentary portions are involved in the formation of the OAH, comprising mainly the thin (<600 m) predominantly pelagic sedimentary cover visible atop the oceanic plate and some turbidites and slump deposits from the inner trench slope [Lüschen *et al.*, 2010]. A possible sediment supply from the fore arc is blocked due to the higher elevation of the OAH representing an effective barrier from the depocenters of the Lombok Basin. However, taking into account the ~25 Ma long period of subduction at the eastern Sunda Arc [e.g., Hall and Smyth, 2008], continuous accretion of sediment could have formed major portions of the OAH although involved sedimentary volumes are moderate [Van der Werff, 1995].

[48] Sediment supply may have been more abundant before the approach of the Roo Rise to the trench. Off eastern Java, the onset of subduction of the Roo Rise resulted in an uplift of the trench and subsequent truncation of sediment supply from the Bengal Fan. At present, however, only ~1.5 km sediment thickness are trapped west of this barrier in the trench off western Java [Kopp *et al.*, 2002], which suggests little effects on trench sediment contribution off Lombok and farther east.

[49] Beneath the higher elevated OAH portions the MCS seismic profile of Lüschen *et al.* [2010] displays a number of landward dipping faults associated with a prominent slope break and with the system of tectonic ridges and the small basin in between (Figure 6). This morphological array of ridges and piggyback basins in between correlates with similar structures farther west, where these features are associated with landward dipping splay faults [Müller *et al.*, 2008; Lüschen *et al.*, 2010]. Offshore Lombok, at least two faults seem to penetrate the entire OAH and connect to the plate interface (Figure 6). The higher-elevated OAH portions display only minimal reflectivity. Hence, from the available data it is difficult to judge whether these faults are “out of sequence” splay faults or reactivated imbricate thrust faults which are shortened and steepened due to compression.

[50] Profile 31/32 reveals a sharp lateral increase of crustal velocities beneath the landward slope break of the OAH suggesting distinct lithological changes associated with the transition from the northern ridge to those fore-arc portions capped by the sedimentary strata comprising the Lombok Basin (Figure 5). Crustal velocities beneath the basin rapidly increase to 5.5–6.0 km/s and then rise somewhat more gentle to ~6.8 km/s above the upper plate Moho. A similar lateral velocity change from 4.0 km/s to 5.5 km/s is observed offshore Chile at the transition from the outer rise to the Valparaiso Basin and is interpreted as a lithological transition from accreted sediment to continental margin framework [Flueh *et al.*, 1998]. On profile 31/32, there is a portion of high velocities, located at 7–10 km depth and ~180 km profile distance, which are bounded by landward

dipping reflections (Figure 6). The observed structure could be interpreted as the tip of the basement of the Lombok Basin, which was tilted and lifted up by underthrusting along with the thickening of sediments during OAH generation. Such architectures are common in ancient accretionary terranes exposed on land [Dickinson and Seely, 1979]. The uplift and northward tilt of the basement beneath the northern ridge and the seismic facies of the Lombok Basin crust distinct from the OAH may be suggestive for an arcward dipping backstop located beneath the landward slope break of the OAH. On a magnetic profile crossing the OAH this transition is marked by a sharp negative anomaly (~40 km wide, -300 nT amplitude), which might result from a package of steeply inclined tectonically accreted volcanic sills [Mueller and Neben, 2006]. Results from the analysis of MCS data show an irregular topography of the Lombok fore-arc basement reminiscent of horst and graben structures at rifted continental margins or stacked ophiolite sheets and nappes, which could be formed by underthrusting of younger oceanic blocks and subsequent steepening due to continuous compression [Lüschen *et al.*, 2010].

[51] The thickness of the fore-arc crust on profile 31/32 ranges from 9 km beneath the portions of highest sedimentary infill to 11 km at ~250 km profile distance (Figure 5). There is no distinct lateral change in crustal velocities in the northernmost model portions, but crustal thickness likely increases to >14 km here. A high velocity lower crust (6.8–7.2 km/s), which represents about 30% of the total crust of the subducting oceanic plate, is lacking in the fore-arc crust, resulting in an average crustal velocity (considering crustal velocity portions characterized by $V_p > 6.0$ km/s) of 6.51 ± 0.07 km/s compared to 6.71 ± 0.09 km/s for the subducting plate. From the distribution of zircon ages in sedimentary and igneous rocks from southeast Java, Smyth *et al.* [2007] infer the presence of a Gondwana continental fragment from northwest Australia, which was accreted offshore East Java in the Late Cretaceous; the eastern extent of this fragment is unknown but the oceanic type velocity structure beneath the Lombok Basin rather precludes a possible continuation into this area.

[52] The fore-arc crust in our models could be interpreted as an altered, heavily fractured piece of an older oceanic terrane, perhaps formed during the opening of the Indian Ocean during Cretaceous to middle Eocene times, which was hindered from subduction due to its increased buoyancy; a similar scenario was previously invoked to explain the origin of the fore arc offshore Lombok Strait [Curry *et al.*, 1977] and western Java [Kopp *et al.*, 2002]. The relatively constant crustal velocity of the fore-arc basement may imply a distinct change in lithological composition toward the volcanic arc, unless the arc massif is composed mainly of oceanic crust or ophiolite as the fore-arc basement. The base of the fore-arc basement marks the crust mantle boundary, as the seismic and gravity data strongly support the presence of shallow mantle material here.

[53] The uppermost mantle offshore Lombok exhibits rather low velocities (7.4–7.8 km/s). Similar velocity structures are observed beneath the Izu-Bonin intraoceanic arc and are interpreted as “Moho transition zone” comprising mafic restite and cumulatives resulting from processes of anatexis and magmatic differentiation of the mafic and ultramafic crustal components [Tatsumi *et al.*, 2008; Kodaira *et al.*, 2008]. In order to invoke analogous processes beneath the

fore arc offshore Lombok, this scenario would imply the presence of a paleoarc ~100 km south of the present volcanic front near 250–300 km profile distance on line 31/32, where the velocity reduction in the upper mantle appears to be enhanced. In East Java a paleoarc, which was active from Eocene to early Miocene times, is located ~50 km south of the current volcanic front [Smyth *et al.*, 2008; Hall and Smyth, 2008]. The coincident magnetic profile of line 31/32 shows a generally smooth magnetic field across the Lombok Basin, but beginning with ~265 km profile distance displays magnetic anomalies of ± 100 nT [Mueller and Neben, 2006], which would correspond to the location of enhanced velocity reduction in the upper mantle and thus to the inferred origin of this structure from a possible paleovolcanic arc.

[54] However, the strong Moho reflection associated with the top of the 7.4–7.8 km/s layer beneath the Lombok Basin (see Figures 4 and 9) argues for a distinct lithological boundary rather than a “chemically transparent” Moho located within the mafic restite/cumulate layer. In this alternative scenario, sub-fore-arc water release from subducted sediment and crust facilitates a significant degree of mantle serpentinization (up to 19% according to the V_p relationship of Carlson and Miller [2003]) [Bostock *et al.*, 2002; Hyndman and Peacock, 2003; Rüpke *et al.*, 2004].

[55] The presence of a shallow mantle wedge off Java was already proposed by Kopp *et al.* [2002, 2009] based on seismic wide-angle and refraction data, and a possible continuation farther east of this feature was suggested by Grevemeyer and Tiwari [2006] on the basis of gravity modeling. The profile of Curray *et al.* [1977] conducted ~50 km west of profile 31/32 shows a fore-arc Moho at ~18 km depth and upper mantle velocities of 7.8–8.4 km/s in the fore arc off the Lombok Strait. Hence, their Moho depths are ~2 km deeper and observed mantle velocities are 0.4–0.6 km/s higher than the results of this study (compare discussion of the results of Curray *et al.* [1977] in section 6.1).

[56] Oleskevich *et al.* [1999] suggest that the downdip limit and thus the width of the seismogenic coupling zone, which controls the potential magnitude of large megathrust earthquakes, is governed by the depth of the intersection of the thrust with the fore-arc mantle and the presence of weak hydrous minerals in the mantle wedge, which do not support seismogenic stick-slip behavior. Offshore Java a shallow serpentinized mantle wedge underlying the fore-arc basin would limit the width of the coupling zone to only 30–40 km, compared to >120 km offshore Sumatra [Grevemeyer and Tiwari, 2006]. Thermal modeling shows that the updip limit of the seismogenic zone (~100°C isotherm [Hyndman and Wang, 1993]) offshore Java is located ~80 km landward from the trench [Grevemeyer and Tiwari, 2006]. Offshore Lombok, the similar trench-normal convergence rate and dip but the older age of the subducting plate suggest a thermally defined updip limit that reaches farther landward from the trench and thus, the width of the seismogenic coupling zone is likely to be even narrower here. The distribution of earthquake hypocenters off Lombok and Sumbawa shows a band of extensional mechanisms closely confined to the trench and some events revealing compressional mechanisms beneath the fore-arc basin and the volcanic arc [Špičák *et al.*, 2007]. The OAH belongs to a >100 km wide zone in between characterized by virtually no teleseismically recorded earthquakes related to the plate

boundary (down to a regional threshold magnitude of ~5.5) [e.g., Engdahl and Villaseñor, 2002]. These observations strongly contrast with the adjacent Sumatra-Andaman margin segment where the recent and historic earthquake record suggests a much larger potential for destructive subduction zone megathrust earthquakes than for Java and Lombok [Lay *et al.*, 2005; Newcomb and McCann, 1987]. Thus, the shallow serpentinized mantle wedge, which is absent offshore Sumatra [Kieckhefer *et al.*, 1980; Kopp *et al.*, 2002], might be the major factor limiting the magnitude of rupture offshore Java and Lombok. The system of possible splay faults in the outer arc high, however, demonstrates that potential movements can be transmitted to shallow seafloor portions and thus, this margin is nevertheless prone to a serious tsunami hazard [Müller *et al.*, 2008; Kopp *et al.*, 2009; Lüschen *et al.*, 2010] (Figure 6).

6.3. Fore-Arc Offshore Sumba

[57] The strong relief of the plate boundary imaged in both the wide-angle and MCS seismic data suggests significant vertical steps between dissected oceanic blocks, probably further increased due to plate bending during subduction (Figure 10d). Where these asperities subduct beneath the trench they entrain lower slope material and cause slope failure in their wake (see slide in Figure 2) and thus, may unbalance the mass budget along this margin segment toward local erosion of the frontal prism.

[58] Contrary to the geometry offshore Lombok, the similar velocity structure of the OAH and the adjacent fore-arc portions farther north may imply similar constituents (Figure 10). Velocities in the northern fore-arc portions suggest a greater heterogeneity and related vertical velocity gradients are lower (velocities do not reach 6 km/s within the uppermost 6–10 km beneath the basement, compared to ~5 km on profile 31/32). In our models the base of this unit is marked by the steep seaward dipping reflector identified in the wide-angle seismic data. The seismic refraction data, however, do not support the presence of mantle velocities directly below this reflector and the gravity data go conform with the presence of crustal-type densities between the reflector and the plate interface (Figure 16). We interpret this deeper unit as the westward extension of the crystalline basement beneath the Sumba Ridge in the seismic profile of Shulgin *et al.* [2009] at 121°E and eventually as the onset of the “Sumba block” [e.g., Rutherford *et al.*, 2001]. In the structural interpretation of Shulgin *et al.* [2009], the seaward dipping interface separates the paleoaccretionary prism from the Sumba Ridge crust, which extends down to the crust-mantle boundary at 26–28 km depth. Hence, these models do not support the presence of a shallow mantle wedge south and east of the island of Sumba.

7. Conclusions

[59] The combined analysis of seismic wide-angle reflection and refraction data, multichannel streamer data and shipboard gravity data, reveals the velocity and density structure of the incoming oceanic plate and the overriding plate offshore Lombok and offshore Sumba at the transition to the collisional regime farther east.

[60] 1. Offshore Lombok, the incoming oceanic crust is on average 8.6 km thick and largely devoid of sediment.

Seismic velocities in the crust and in the uppermost mantle are reduced within 40 km seaward of the trench, which coincides with the onset of normal faulting in the bathymetry and MCS seismic data. Velocities of 7.4–7.9 km/s in the uppermost ~2 km beneath the Moho suggest the presence of mantle-penetrating cracks and faults as well as significant degrees of mantle serpentinization.

[61] 2. Velocities in the outer arc high rarely exceed 5.5 km/s down to the top of the subducting slab, which is traced over at least 70 km beneath the fore arc down to ~15 km depth. These bulk velocities are characteristic of an accretionary origin, with highly compacted sediments (possibly partially metamorphosed) at depth. The complex shape of the plate boundary in our models indicates a highly fractured oceanic crust.

[62] 3. In the Lombok Basin up to 3.7 km of sedimentary strata overlies a 9–11 km thick crust which is characterized by an oceanic type velocity structure. Velocities of 7.4–7.8 km/s beneath a distinct Moho reflector suggest a hydrated mantle wedge at ~16 km depth beneath the Lombok Basin, which is also supported by the gravity modeling for this corridor. Because serpentinites are expected at shallow depths in the mantle wedge, they may control, at least partially, the seismological stick-slip behavior of the megathrust; in particular, they may reduce the width of the seismic coupling zone and thus limit the potential magnitude of large subduction megathrust earthquakes offshore Lombok. The system of possible splay faults in the outer arc high, however, demonstrates that potential movements can be transmitted to shallow seafloor portions and thus poses a serious tsunami threat for this margin.

[63] 4. Offshore Sumba, the oceanic crust is on average 9.0 km thick and at greater distance from the trench comprises a thin (<600 m) largely undisturbed sedimentary cover. Within 30 km seawards of the trench, intense fracturing of the crust coincides with a vigorous decrease of crustal velocities. Here, upper mantle velocities reach 7.4–7.8 km/s. If the adjacent Scott Plateau resists to be subducted, pervasive rupture of the oceanic crust and subsequent serpentinization of the underlying mantle may be the effect of increased tensional tectonic forces due to sustained slab-pull.

[64] 5. Slope indentations and the presence of fan-shaped slide deposits in the trench suggest that subduction of pronounced seafloor asperities, including reactivated seafloor fabric and plate-bending faults, locally contribute to the frontal erosion of the lower slope.

[65] 6. From west to east the subducting slab thickens from ~9 km to ~13 km beneath the outer arc high, which we interpret as the transition from the oceanic crust of the Argo Abyssal Plain to the promontory of the Australian continental shelf comprising the Scott Plateau.

[66] 7. Our seismic and gravity models do not support the presence of a shallow mantle wedge beneath the fore arc. A steep seaward dipping reflector in the northernmost model portions of profile 22 may be related to the transition to the “Sumba block” farther north.

[67] **Acknowledgments.** This paper benefited from the constructive reviews by H. Ueda and an anonymous reviewer. The SINDBAD project was funded by the German Federal Ministry of Education and Research

(BMBF) under grants 03G0190A and 03G0190B. We would like to thank the master and crew of R/V *Sonne* for their professional assistance during cruise SO190 and the SINDBAD scientific party for their enormous help during data acquisition.

References

- Bialas, J., and E. R. Flueh (1999), Ocean bottom seismometers, *Sea Technol.*, 40(4), 41–46.
- Birch, F. (1961), The velocity of compressional waves in rocks to 10 kilobars, *J. Geophys. Res.*, 66, 2199–2224, doi:10.1029/JZ066i007p02199.
- Bock, Y., L. Prawirodirdjo, J. F. Genrich, C. W. Stevens, R. McCaffrey, C. Subarya, S. S. O. Puntodewo, and E. Calais (2003), Crustal motion in Indonesia from Global Positioning System measurements, *J. Geophys. Res.*, 108(B8), 2367, doi:10.1029/2001JB000324.
- Bostock, M. G., R. D. Hyndman, S. Rondenay, and S. M. Peacock (2002), An inverted continental Moho and the serpentinization of the forearc mantle, *Nature*, 417, 536–538, doi:10.1038/417536a.
- Carlson, R. L., and C. N. Herrick (1990), Densities and porosities in the oceanic crust and their variations with depth and age, *J. Geophys. Res.*, 95(B6), 9153–9170, doi:10.1029/JB095iB06p09153.
- Carlson, R. L., and D. J. Miller (2003), Mantle wedge water contents estimated from seismic velocities in partially serpentinized peridotites, *Geophys. Res. Lett.*, 30(5), 1250, doi:10.1029/2002GL016600.
- Christensen, N. I., and W. D. Mooney (1995), Seismic velocity structure and composition of the continental crust: A global view, *J. Geophys. Res.*, 100(B6), 9761–9788, doi:10.1029/95JB00259.
- Clift, P., and P. Vannucchi (2004), Controls on tectonic accretion versus erosion in subduction zones: Implications for the origin and recycling of the continental crust, *Rev. Geophys.*, 42, RG2001, doi:10.1029/2003RG000127.
- Curry, J. R., G. S. Shor, R. W. Raitt, and M. Henry (1977), Seismic refraction and reflection studies of crustal structure of the eastern Sunda and western Banda arcs, *J. Geophys. Res.*, 82, 2479–2489, doi:10.1029/JB082i017p02479.
- Collot, J.-Y., W. Agudelo, A. Ribodetti, and B. Marcaillou (2008), Origin of a crustal splay fault and its relation to the seismogenic zone and underplating at the erosional north Ecuador–south Colombia oceanic margin, *J. Geophys. Res.*, 113, B12102, doi:10.1029/2008JB005691.
- Conrteras-Reyes, E., I. Grevemeyer, E. R. Flueh, M. Scherwath, and M. Heesemann (2007), Alteration of the subducting oceanic lithosphere at the southern central Chile trench–outer rise, *Geochem. Geophys. Geosyst.*, 8, Q07003, doi:10.1029/2007GC001632.
- Dickinson, W. R., and D. R. Seeley (1979), Structure and stratigraphy of forearc regions, *AAPG Bull.*, 63, 2–31.
- Engdahl, E. R., and A. Villaseñor (2002), Global seismicity: 1900–1999, in *International Handbook of Earthquake and Engineering Seismology*, edited by W. H. K. Lee et al., pp. 665–690, doi:10.1016/S0074-6142(02)80244-3, Academic, Amsterdam.
- Faccenda, M., T. V. Taras, and L. Burlini (2009), Deep slab hydration induced by bending-related variations in tectonic pressure, *Nat. Geosci.*, 2, 790–793, doi:10.1038/ngeo656.
- Flueh, E. R., N. Vidal, C. R. Ranero, A. Hoijska, R. von Huene, J. Bialas, K. Hinz, D. Cordoba, J. J. Danobeitia, and C. Zelt (1998), Seismic investigations of the continental margin off- and onshore Valparaiso, Chile, *Tectonophysics*, 288, 251–263, doi:10.1016/S0040-1951(97)00299-0.
- Grevemeyer, I., and V. M. Tiwari (2006), Overriding plate controls spatial distribution of megathrust earthquakes in the Sunda–Andaman subduction zone, *Earth Planet. Sci. Lett.*, 251(3–4), 199–208, doi:10.1016/j.epsl.2006.08.021.
- Grevemeyer, I., C. R. Ranero, E. R. Flueh, D. Klaeschen, and J. Bialas (2007), Passive and active seismological study of bending-related faulting and mantle serpentinization at the Middle America trench, *Earth Planet. Sci. Lett.*, 258, 528–542, doi:10.1016/j.epsl.2007.04.013.
- Hall, R. (2002), Cenozoic geological and plate tectonic evolution of SE Asia and the SW Pacific: Computer-based reconstructions, model and animations, *J. Asian Earth Sci.*, 20, 353–431, doi:10.1016/S1367-9120(01)00069-4.
- Hall, R., and H. R. Smyth (2008), Cenozoic arc processes in Indonesia: Identification of the key influences on the stratigraphic record in active volcanic arcs, in *Formation and Applications of the Sedimentary Record in Arc Collision Zones*, edited by A. E. Draut, P. D. Clift, and D. W. Scholl, *Spec. Pap. Geol. Soc. Am.*, 436, 27–54, doi:10.1130/2008.2436(03).
- Hamilton, E. L. (1978), Sound velocity–density relations in sea-floor sediment and rocks, *J. Acoust. Soc. Am.*, 63(2), 366–377, doi:10.1121/1.381747.
- Hamilton, W. B. (1988), Plate tectonics and island arcs, *Geol. Soc. Am. Bull.*, 100, 1503–1527, doi:10.1130/0016-7606(1988)100<1503:PTAIA>2.3.CO;2.

- Heine, C., R. D. Mueller, and C. Gaina (2004), Reconstructing the lost Tethys Ocean basin: Convergence history of the SE Asian margin and marine gateways, in *Continent-Ocean Interactions Within East Asian Marginal Seas*, *Geophys. Monogr. Ser.*, vol. 149, edited by P. Clift et al., pp. 37–54, AGU, Washington, D. C.
- Heirtzler, J. R., et al. (1974), Site 261, *Initial Rep. Deep Sea Drill. Proj.*, 27, 129–192.
- Hyndman, R. D., and S. M. Peacock (2003), Serpentinization of the forearc mantle, *Earth Planet. Sci. Lett.*, 212, 417–432, doi:10.1016/S0012-821X(03)00263-2.
- Hyndman, R. D., and K. Wang (1993), Thermal constraints on the zone of major thrust earthquake failure: The Cascadia subduction zone, *J. Geophys. Res.*, 98, 2039–2060, doi:10.1029/92JB02279.
- Ivandić, M., I. Grevenmeyer, A. Berhorst, E. R. Flueh, and K. McIntosh (2008), Impact of bending related faulting on the seismic properties of the incoming oceanic plate offshore of Nicaragua, *J. Geophys. Res.*, 113, B05410, doi:10.1029/2007JB005291.
- Kieckhefer, R. M., G. G. Shor Jr., J. R. Curran, W. Sugiarta, and F. Hehuwat (1980), Seismic refraction studies of the Sunda Trench and forearc basin, *J. Geophys. Res.*, 85, 863–889, doi:10.1029/JB085iB02p00863.
- Kodaira, S., T. Sato, N. Takahashi, M. Yamashita, T. No, and Y. Kaneda (2008), Seismic imaging of a possible paleoarc in the Izu-Bonin intraoceanic arc and its implications for arc evolution processes, *Geochem. Geophys. Geosyst.*, 9, Q10X01, doi:10.1029/2008GC002073.
- Kopp, H., and N. Kukowski (2003), Backstop geometry and accretionary mechanics of the Sunda margin, *Tectonics*, 22(6), 1072, doi:10.1029/2002TC001420.
- Kopp, H., E. R. Flueh, D. Klaeschen, J. Bialas, and C. Reichert (2001), Crustal structure of the central Sunda margin at the onset of oblique subduction, *Geophys. J. Int.*, 147, 449–474, doi:10.1046/j.0956-540x.2001.01547.x.
- Kopp, H., D. Klaeschen, E. R. Flueh, J. Bialas, and C. Reichert (2002), Crustal structure of the Java margin from seismic wide-angle and multi-channel reflection data, *J. Geophys. Res.*, 107(B2), 2034, doi:10.1029/2000JB000095.
- Kopp, H., E. R. Flueh, C. J. Petersen, W. Weinrebe, A. Wittwer, and Meramex Scientists (2006), The Java margin revisited: Evidence for subduction erosion off Java, *Earth Planet. Sci. Lett.*, 242, 130–142, doi:10.1016/j.epsl.2005.11.036.
- Kopp, H., D. Hindle, D. Klaeschen, O. Oncken, C. Reichert, and D. Scholl (2009), Anatomy of the western Java plate interface from depth-migrated seismic images, *Earth Planet. Sci. Lett.*, 288, 399–407, doi:10.1016/j.epsl.2009.09.043.
- Korenaga, J., W. Holbrook, G. Kent, P. Kelemen, R. Detrick, H.-C. Larsen, J. Hopper, and T. Dahl-Jensen (2000), Crustal structure of the southeast Greenland margin from joint refraction and reflection seismic tomography, *J. Geophys. Res.*, 105(B9), 21,591–21,614, doi:10.1029/2000JB900188.
- Korenaga, J., W. S. Holbrook, R. S. Detrick, and P. B. Kelemen (2001), Gravity anomalies and crustal structure across the southeast Greenland margin, *J. Geophys. Res.*, 106, 8853–8870, doi:10.1029/2000JB900416.
- Lay, T., et al. (2005), The Great Sumatra-Andaman earthquake of 26 December 2004, *Science*, 308(5725), 1127–1133, doi:10.1126/science.1112250.
- Lüschen, E., C. Mueller, H. Kopp, M. Engels, R. Lutz, L. Planert, A. Shulgin, and Y. Djajadihardja (2010), Structure, evolution and tectonic activity at the eastern Sunda forearc, Indonesia, from marine seismic investigations, *Tectonophysics*, doi:10.1016/j.tecto.2010.06.008, in press.
- Lynnes, C. S., and T. Lay (1988), Source process of the great 1977 Sumba earthquake, *J. Geophys. Res.*, 93(B11), 13,407–13,420, doi:10.1029/JB093iB11p13407.
- Moore, G. F., N. L. Bangs, A. Taira, S. Kuramoto, E. Pangborn, and H. J. Tobin (2007), Three-dimensional splay fault geometry and implications for tsunami generation, *Science*, 318, 1128–1131, doi:10.1126/science.1147195.
- Mueller, C., and S. Neben (Eds.) (2006), *Cruise report: SO190 Leg I: Seismic and geoacoustic investigations along the Sunda-Banda Arc transition*, 142 pp., Bundesanstalt für Geowiss. und Rohstoffe, Hannover, Germany.
- Müller, C., et al. (2008), From subduction to collision: The Sunda-Banda arc transition, *Eos Trans. AGU*, 89(6), 49–60, doi:10.1029/2008EO060001.
- Newcomb, K. R., and W. R. McCann (1987), Seismic history and seismotectonics of the Sunda arc, *J. Geophys. Res.*, 92, 421–439, doi:10.1029/JB092iB01p00421.
- Oleskevich, D. A., R. D. Hyndman, and K. Wang (1999), The updip and downdip limits to great subduction earthquakes: Thermal and structural models of Cascadia, south Alaska, SW Japan, and Chile, *J. Geophys. Res.*, 104(B7), 14,965–14,991, doi:10.1029/1999JB900060.
- Parker, R. L. (1973), The rapid calculation of potential anomalies, *Geophys. J. R. Astron. Soc.*, 31, 447–455, doi:10.1111/j.1365-246X.1973.tb06513.x.
- Peacock, S. M. (2001), Are the lower planes of double seismic zones caused by serpentine dehydration in subducting oceanic mantle, *Geology*, 29(4), 299–302, doi:10.1130/0091-7613(2001)029<0299:ATLPOD>2.0.CO;2.
- Ranero, C. R., J. Phipps-Morgan, K. McIntosh, and C. Reichert (2003), Bending-related faulting and serpentinization at the Middle America trench, *Nature*, 425, 367–373, doi:10.1038/nature01961.
- Ranero, C. R., I. Grevenmeyer, H. Sahling, U. Barckhausen, C. Hensen, K. Wallmann, W. Weinrebe, P. Vannucchi, R. von Huene, and K. McIntosh (2008), Hydrogeological system of erosional convergent margins and its influence on tectonics and interplate seismogenesis, *Geochem. Geophys. Geosyst.*, 9, Q03S04, doi:10.1029/2007GC001679.
- Rutherford, E., K. Burke, and J. Lytwyn (2001), Tectonic history of Sumba Island, Indonesia, since the Late Cretaceous and its rapid escape into forearc in the Miocene, *J. Asian Earth Sci.*, 19, 453–479, doi:10.1016/S1367-9120(00)00032-8.
- Rüpke, L. H., J. P. Morgan, M. Hort, and J. A. D. Conolly (2004), Serpentine and the subduction zone water cycle, *Earth Planet. Sci. Lett.*, 223, 17–34, doi:10.1016/j.epsl.2004.04.018.
- Schlüter, H. U., C. Gaedicke, H. A. Roeser, B. Schreckenberger, H. Meyer, C. Reichert, Y. Djajadihardja, and A. Prexl (2002), Tectonic features of the southern Sumatra-western Java forearc of Indonesia, *Tectonics*, 21(5), 1047, doi:10.1029/2001TC901048.
- Shulgin, A., H. Kopp, C. Mueller, E. Lüschen, L. Planert, M. Engels, E. R. Flueh, A. Krabbenhoef, and Y. Djajadihardja (2009), Sunda-Banda arc transition: Incipient continent-island arc collision (northwest Australia), *Geophys. Res. Lett.*, 36, L10304, doi:10.1029/2009GL037533.
- Sibuet, J.-C., et al. (2007), 26th December 2004 great Sumatra-Andaman earthquake: Co-seismic and postseismic motions in northern Sumatra, *Earth Planet. Sci. Lett.*, 263, 88–103, doi:10.1016/j.epsl.2007.09.005.
- Simons, W. J. F., et al. (2007), A decade of GPS in Southeast Asia: Resolving Sundaland motion and boundaries, *J. Geophys. Res.*, 112, B06420, doi:10.1029/2005JB003868.
- Smyth, H. R., P. J. Hamilton, R. Hall, and P. D. Kinny (2007), The deep crust beneath island arcs: Inherited zircons reveal a Gondwana continental fragment beneath East Java, Indonesia, *Earth Planet. Sci. Lett.*, 258, 269–282, doi:10.1016/j.epsl.2007.03.044.
- Smyth, H. R., R. Hall, and G. J. Nichols (2008), Cenozoic volcanic arc history of East Java, Indonesia: The stratigraphic record of eruptions on an active continental margin, in *Lessons From the Stratigraphic Record in Arc Collision Zones*, edited by A. E. Draut, P. D. Clift, and D. W. Scholl, *Spec. Pap. Geol. Soc. Am.*, 436, 27–54, doi:10.1130/2008.2436(10).
- Spence, W. (1986), The 1977 Sumba earthquake series: Evidence for slab pull force acting at a subduction zone, *J. Geophys. Res.*, 91(B7), 7225–7239, doi:10.1029/JB091iB07p07225.
- Špičák, A., V. Hanuš, and J. Vaněk (2007), Earthquake occurrence along the Java trench in front of the onset of the Wadati-Benioff zone: Beginning of a new subduction cycle?, *Tectonics*, 26, TC1005, doi:10.1029/2005TC001867.
- Tatsumi, Y., H. Shukuno, K. Tani, N. Takahashi, S. Kodaira, and T. Kogiso (2008), Structure and growth of the Izu-Bonin-Mariana arc crust: 2. Role of crust-mantle transformation and the transparent Moho in arc crust evolution, *J. Geophys. Res.*, 113, B02203, doi:10.1029/2007JB005121.
- Toomey, D. R., and G. R. Foulger (1989), Tomographic inversion of local earthquake data from the Hengill-Grensdalur central volcano complex, Iceland, *J. Geophys. Res.*, 94, 17,497–17,510, doi:10.1029/JB094iB12p17497.
- Van der Werff, W. (1995), Structure and morphotectonics of the accretionary prism along the eastern Sunda-western Banda Arc, *J. Southeast Asian Earth Sci.*, 11, 309–322, doi:10.1016/0743-9547(94)00038-G.
- Wiener, N. (1949), *Extrapolation, Interpolation, and Smoothing of Stationary Time Series*, John Wiley, New York.
- E. R. Flueh, H. Kopp, A. Krabbenhoef, L. Planert, and A. Shulgin, IFM-GEOMAR, Leibniz Institute of Marine Sciences at the University of Kiel, Wischhofstr. 1-3, D-24148, Germany. (lplanert@ifm-geomar.de)
- E. Lueschen and C. Mueller, BGR, Federal Institute for Geosciences and Natural Resources, Stillweg 2, D-30655 Hannover, Germany.
- Y. Djajadihardja, BPPT, Agency for the Assessment and Application of Technology, Jl. M.H. Thamrin No. 8, Jakarta 10340, Indonesia.

Structural architecture of oceanic plateau subduction offshore Eastern Java and the potential implications for geohazards

A. Shulgin,¹ H. Kopp,¹ C. Mueller,² L. Planert,¹ E. Lueschen,² E. R. Flueh¹ and Y. Djajadihardja³

¹IFM-GEOMAR, Leibniz Institute of Marine Sciences, Wischhofstr. 1-3, 24148 Kiel, Germany. E-mail: ashulgin@ifm-geomar.de

²Federal Institute for Geosciences and Natural Resources (BGR), Stilleweg 2, 30655 Hannover, Germany

³Agency for the Assessment and Application of Technology (BPPT), Jl.M.H. Thamrin No. 8, Jakarta 10340, Indonesia

Accepted 2010 September 29. Received 2010 September 27; in original form 2010 April 26

SUMMARY

The region offshore Eastern Java represents one of the few places where the early stage of oceanic plateau subduction is occurring. We study the little investigated Roo Rise oceanic plateau on the Indian plate, subducting beneath Eurasia. The presence of the abnormal bathymetric features entering the trench has a strong effect on the evolution of the subduction system, and causes additional challenges on the assessment of geohazard risks. We present integrated results of a refraction/wide-angle reflection tomography, gravity modelling, and multichannel reflection seismic imaging using data acquired in 2006 south of Java near 113°E. The composite structural model reveals the previously unresolved deep geometry of the oceanic plateau and the subduction zone. The oceanic plateau crust is on average 15 km thick and covers an area of about 100 000 km². Within our profile the Roo Rise crustal thickness ranges between 18 and 12 km. The upper oceanic crust shows high degree of fracturing, suggesting heavy faulting. The forearc crust has an average thickness of 14 km, with a sharp increase to 33 km towards Java, as revealed by gravity modelling. The complex geometry of the backstop suggests two possible models for the structural formation within this segment of the margin: either accumulation of the Roo Rise crustal fragments above the backstop or alternatively uplift of the backstop caused by basal accumulation of crustal fragments. The subducting plateau is affecting the stress field within the accretionary complex and the backstop edge, which favours the initiation of large, potentially tsunamogenic earthquakes such as the 1994 $M_w = 7.8$ tsunamogenic event.

Keywords: Tomography; Subduction zone processes; Oceanic plateaus and microcontinents; Crustal structure; Asia.

1 INTRODUCTION

The converging margins around the world are major areas for generating the most devastating earthquakes and tsunamis. Any variations in the subduction systems are of extreme importance due to the changes in the geohazards situation. In this work we investigate the subduction of a previously little investigated oceanic plateau—the Roo Rise, its structure and its interaction with the Java margin at around 113°E. We focus on the recovery of the structural architecture in the region and its tectonic interpretation. We provide insights on the following questions for this particular region: (1) what are the effects of an oceanic plateau subduction, (2) what consequences does the subducting plateau have on the forearc deformation, (3) what is the structure of the forearc in such settings and (4) what are the effects that the subducting plateau have on the earthquake and tsunami generation?

The Sunda arc forms a part of more than 5000-km-long continuous subduction system, spanning from Flores and Sumba islands in the east to Burma in the northwest. The transition from the Sunda arc to the Banda arc is located at around 121°E, where the Australian continental shelf is approaching the trench (Shulgin *et al.* 2009). Both arcs are active since the Eocene collision of India and the Sundaland (the continental core of the southeast Asia (Hamilton 1988; Hall 2002; Hall & Smyth 2008) and are formed by the subduction of the Indo-Australian Plate underneath Eurasia (Hamilton 1979). The basement underneath Eastern Java is formed by arc and ophiolitic rocks accreted during the Mesozoic (Hall & Smyth 2008). Based on zircon dating, Smyth *et al.* (2007) propose an Archean continental fragment of Australian origin to be trapped between the forearc and the present volcanic arc in Eastern Java. The current convergence rate offshore Western Java is estimated to be 6.7 ± 0.7 cm yr⁻¹ in the direction 11°N that is almost perpendicular to the trench (DeMets

et al. 1994; Tregoning *et al.* 1994). A northward shift of the volcanic arc is recognized in Eastern Java with the present-day arc located *ca.* 50 km to the north of an older currently inactive volcanic arc (Hall & Smyth 2008); the shift is associated with changes in the subduction setting and interaction with the proposed Gondwana remnant (Smyth *et al.* 2007).

The Roo Rise oceanic plateau is located offshore Eastern Java. Oceanic plateaus are defined as a large, relatively flat submarine region that rises well above the level of the ambient seabed [*Encyclopedia Britannica*]. Oceanic plateaus can be formed from the remnants of continental crust or be a part of marine large igneous provinces. Currently there are no definitions based on the crustal structure. Their presence at the subduction zones is crucial in the evolution and dynamics of convergent margins. The subduction of the oceanic plateau triggers qualitatively different processes in the subduction system as compared to the subduction of 'normal' oceanic crust (White *et al.* 1992). The major differences caused by the approach of elevated rough bathymetric features (sea plateau, seamounts) to the trench include active frontal erosion of the margin, uneven uplift and deformation of the forearc, and a principally different regime of seismicity (Yamazaki and Okamura, 1989; Scholz & Small 1997). The migration of the trench is also in a good agreement with the numerical modelling of oceanic plateau subduction, comparable to the subduction of the Roo Rise (Gerya *et al.* 2009; Mason *et al.* 2010).

A 135-Ma-old Indian oceanic crust is currently subducting offshore Central–Eastern Java (Moore *et al.* 1980; Masson 1991) in the vicinity of the Roo Rise oceanic plateau. The Roo Rise is a broad smooth bathymetric feature with a number of isolated summits with an average elevation of about 2000 m above the adjacent oceanic floor (Fig. 1). It forms the eastern extension of the Christmas Island Seamount Province (Fig. 1). Planert *et al.* (2010) determine a crustal thickness of 10 km and show that earlier estimates by Curray *et al.* (1977) may be regarded as a lower limit. Rock samples taken across the entire Christmas Island Seamount Province do not show any clear formation time trend across the region (Werner *et al.* 2009). Based on dredged samples (dredging location closest to the study area is shown in Fig. 1), the Roo Rise is composed of strongly altered olivine phyric lava fragments with Mn-crusts and sediment. The formation of the plateau is associated with a series of large magmatic events as no formation time trend is observed. The increased crustal thickness should be accommodated by thickening of the gabbroic or basaltic layer (van Hunen *et al.* 2002). In order to explain the absence of a correlated gravity anomaly, the presence of a low density compensating crustal root was suggested (Newcomb & McCann 1987). Currently, the northern flank of the Roo Rise enters the trench (Fig. 1). Based on the bathymetry the edge of the plateau, which already subducted could be located as far as 70 km north from the trench, implying that it started to subduct 1.1–1.3 Ma. However, there is no direct evidence.

Offshore Central–Eastern Java, where the northern portion of the Roo Rise has already started to subduct, a northward displacement of the trench by 40 km on average is observed; the subduction of the individual seamounts causes an additional landward retreat of the deformation front by up to 10 km (Kopp *et al.* 2006). The bathymetric data collected in the trench area around 113°E (Fig. 1) show the trench is mostly devoid of sediments, except for local ponded accumulations associated with original seafloor fabric (Planert *et al.* 2010). Similar observations have been reported for the trench segment in between 108°E and 114°E (Curray *et al.* 1977; Masson *et al.* 1990). This study is a part of a large scale effort where data along the margin from Java to Lombok have been collected and analysed,

for details on the adjacent profiles please see Planert *et al.* (2010), Shulgin *et al.* (2009) and Lueschen *et al.* (2010). These profiles augment earlier work on the Sumatra and Sunda Strait and Western Java (Kopp *et al.* 2002), so that we are able to describe the entire Sunda Arc subduction zone.

The forearc high, characterized in this area by a number of isolated well-defined peaks, shows an average elevation of *ca.* 800–1200 m, contrasting with the deeper forearc high ridges to the west (Kopp *et al.* 2001, 2002) and to the east offshore Lombok (Planert *et al.* 2010) (Fig. 1). The location of the forearc high peaks correlates with the proposed locations of completely subducted seamounts; however, the estimated subducted volume is smaller than the observed uplift of the forearc (Masson *et al.* 1990).

A number of tsunamogenic earthquakes have been recorded in the areas of seamount subduction offshore Java, which brings these locations into special focus in terms of geohazards. In 1994 and 2006, magnitude 7.8 earthquakes struck offshore Java causing more than 1000 deaths due to the triggered tsunamis. Abercrombie *et al.* (2001) showed that the highest slip was collocated with the proposed location of a subducted seamount. More recently, Bilek & Engdahl (2007) and Kopp *et al.* (2009a) enhanced the idea of the correlation of structural forearc highs and associated subducted structures with the maximum slip of tsunami-generating earthquakes. The distribution of shallow earthquakes shows a pronounced spatial clustering, associated with the rough oceanic seafloor (Fig. 1).

2 DATA ACQUISITION AND MODELLING

We present V_p seismic tomography models of the Java forearc (Fig. 2, discussed below) (located offshore Eastern Java at 113°E), which are further constrained by gravity modelling. The SINDBAD marine seismic experiment onboard R/V 'Sonne' in 2006 (Fig. 1) included multichannel seismic reflection profiling (MCS) accompanied by gravity measurements, seismic refraction profiling with ocean-bottom seismometers (OBS) and hydrophones (OBH) (Mueller *et al.* 2008) and high-resolution multi-beam bathymetry.

2.1 Acquisition

The corridor near 113°E consists of three wide-angle seismic refraction/reflection profiles with collocated MCS data and gravity measurements. Two profiles (P-42 and P-43) run north–south and are joint to one continuous transect, trending approximately perpendicular to the trench (Fig. 1). A total of 46 ocean bottom stations (Bialas & Flueh 1999) were deployed along these profiles. The profiles P-42/P-43 have an overlap of about 75 km, and we will refer to this joint profile as P4–23. P-41 is a shorter, east–west trending, trench parallel line located on the top of the forearc high (Fig. 1). During OBS recording, four G-gun clusters with a total volume of 64 l shot at 210 bar were used as seismic source. The average spacing between the shots is around 150 m; the average instrument spacing is 7 km. For the MCS reflection profiling, shots of ten G-gun clusters fired at 135 bar with the total volume of 56 l at a shot spacing of 50 m were recorded on a 3000 m long 240-channel streamer (Lueschen *et al.* 2010).

2.2 Processing

The processing of the ocean bottom data included the localization of the ocean bottom instruments using the arrival time of the direct

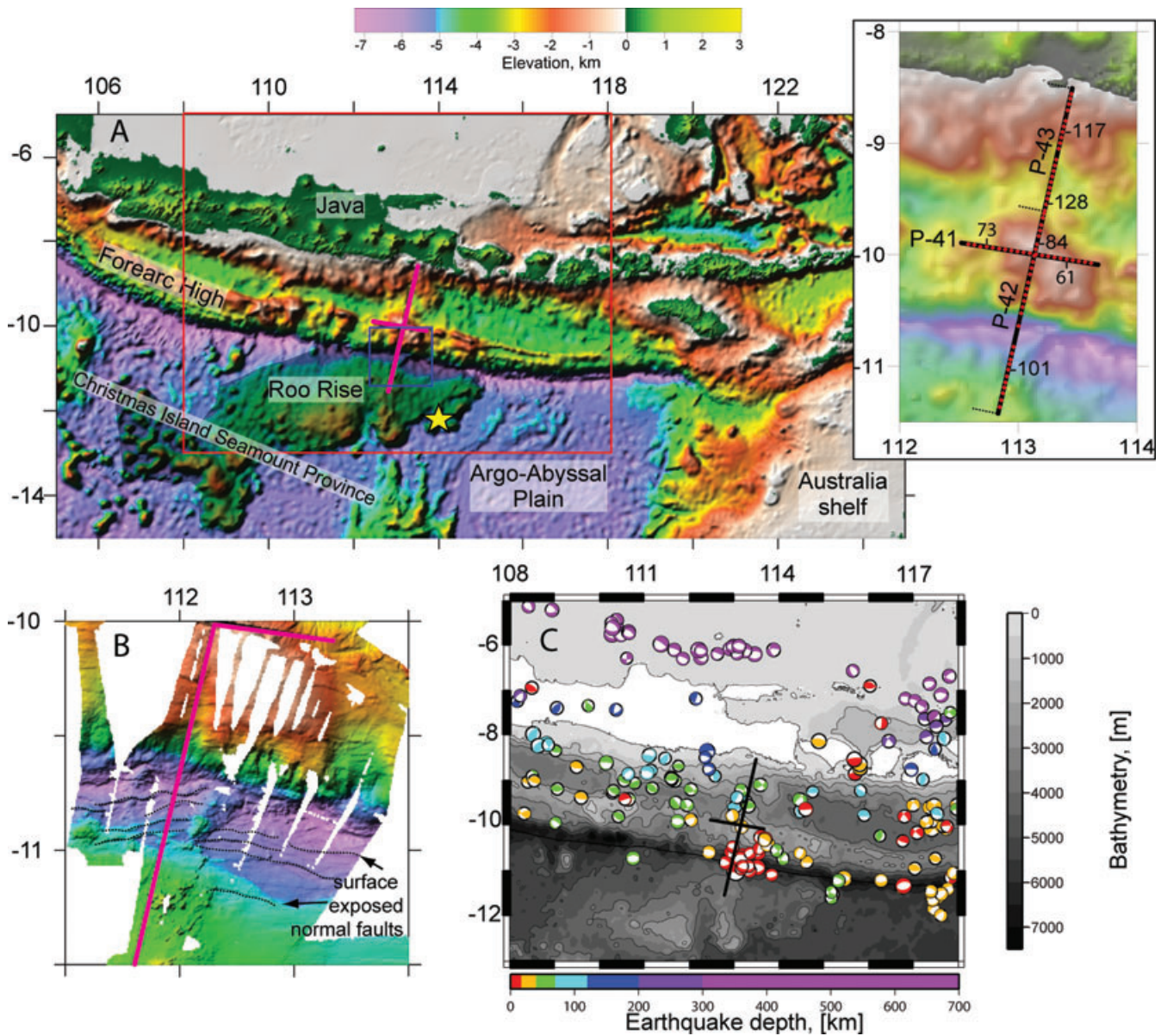


Figure 1. Topographic map of the study area. Seismic profiles examined in this study are shown by magenta lines in panel A and B and with black lines on C plot. Panel (a) shows the global bathymetry/elevation for the area around the Java trench. The insert map at the right shows the detailed geometry of the profiles and the location of ocean bottom stations shown in Figs 3 and 4, overlain on the bathymetry map. The spatial extent of the Roo Rise oceanic plateau is shown with dark shading. Yellow star marks the dredging samples location on Roo Rise (Werner *et al.* 2009). Panel (b) is a close up of the area marked by blue box in A. The multibeam bathymetry data collected during the cruise (the colourscale is identical to A) reveals seamounts and normal faults. Panel (c) shows the earthquake spatial and depth distribution and the focal mechanisms for the area marked by the red box in A (data are taken from the *Harvard Centroid Moment Tensor* catalogue).

water wave and the exact shot point geometry. A time-gated deconvolution was applied to remove predictable bubble reverberations to produce a signal free of the disturbing interference of multiple and primary phases (Wiener 1949). Finally, a time and offset-variant Butterworth filter, in which the pass-band moves towards lower frequencies as record time and offset increase, was applied to consider frequency changes caused by signal attenuation. The processing of the MCS data is described in detail by Lueschen *et al.* (2010).

Data examples are shown in Figs 3 and 4 for profiles P4–23 and P-41, respectively. For line P4–23, the stations located on the oceanic plate south of the trench (instruments 97–107) show clear records of the refracted phases together with clear oceanic Moho reflections

(PmP) (Fig. 3a). These stations recorded Pn oceanic mantle phases reaching offsets up to 180 km (Figs 3a and b). The stations placed on top of the accretionary prism and forearc high (instruments 83–96) recorded refracted arrivals within shorter offsets compared to stations deployed on the oceanic crust. Reflections from the top of the oceanic crust (P_{toc}P) were recorded as well as the oceanic Moho reflections (P_mP) (Fig. 3b). Clear records of the forearc Moho reflections (P_mfP) and the forearc P_nf phases with offsets up to 150 km are seen on the stations deployed along the northern part of the profile (instruments 108–128) (Figs 3c and d). For the trench-parallel profile P-41, the first arrival phases are clearly identified within 50 km offset, together with the reflections from the top of the

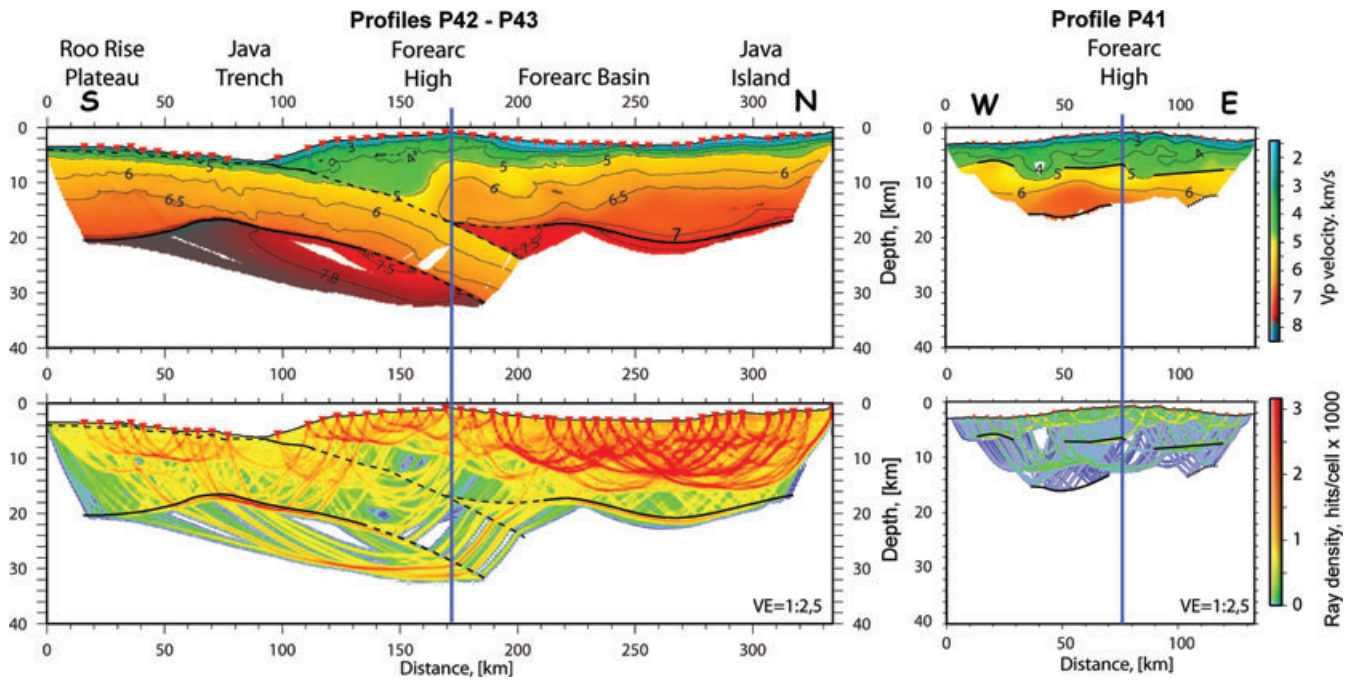


Figure 2. The results of the joint tomographic inversion for the profiles P4–23 and P-41. Top plots show the modelled V_p velocity distribution together with the recovered deep reflector geometry. Bottom plots show the seismic ray path density distributions. Both of the profiles are plotted with the identical scales and colourcodes. The solid black lines are the actually recovered positions of the reflectors and the dashed lines are the extrapolated positions based on the velocity distribution, MCS, and gravity models. Vertical blue line shows the cross points of the profiles.

basement (PtfP) (Fig. 4). Several stations (instruments 58–59, 61 and 72–74) on this profile have recorded plate interface reflections (PpintP) (Fig. 4).

2.3 Tomographic inversion

The seismic velocity distribution was modelled by joint refraction/reflection 2-D tomographic inversion (Korenaga *et al.* 2000). We applied a ‘top to bottom’ approach with a simple layered starting model. The grid spacing was defined by 250 m in the horizontal direction and with vertical spacing increasing with depth from 50 m at the top to 330 m at 40 km depth. The correlation length parameters were chosen to be 1 km \times 0.2 km (horizontal \times vertical) at the top and linearly increasing with depth to 8 km \times 4 km at 40 km depth. Initially, the model was constrained only for the near offsets; then the depth extent of the ray coverage was increased to include the entire model space, with a simultaneous inversion for the reflector positions based on the available reflection phases. 46 stations were available for profile P4–23 with a length of 334 km, resulting in \sim 36 500 first arrival traveltimes picks and \sim 7000 reflected picks. The shorter (135 km long) profile P-41 was covered by 21 stations, summing up to \sim 9300 first arrival traveltimes and \sim 1200 reflected picks. Data examples are shown in Figs 3 and 4. All available picked traveltimes and the fit of the corresponding computed traveltimes are shown on Fig. S1. The structure of the sediment and the basement topography were adopted from the MCS data (Lueschen *et al.* 2010), thus constraining the upper section of the profiles in great detail. Additionally, the top of the oceanic crust as identified in the depth-migrated MCS data was incorporated into the tomography model. The generalized routing during the inversion was as follows: constraining the interface geometry based on the corresponding MCS depth sections where available; inverting the near offset refracted phases to verify the consistency between data sets; fixing the upper section of the model with a weight of

1000 compared to the deeper sections. Then, we ran the simultaneous inversion for the velocity and reflector geometry for the next depth layer. Subsequently, we fixed the obtained layer structure and repeated the previous step for the following deeper layer. Finally, we kept the entire crustal structure fixed and inverted for the velocity in the upper mantle. The final models for all of the profiles are shown in Fig. 2.

2.4 Resolution tests

Several tests were performed to check the resolution of the obtained models. Initially, we used a forward ray shooting method to compute the synthetic traveltimes for the first arrival and reflected phases through our final models. The comparison of the seismic sections and the synthetic calculated traveltimes for several stations on both of the profiles is shown in Figs 3 and 4. The calculated traveltimes, as predicted by the tomographic V_p velocity models, are in a good agreement with the recorded seismic sections. All the refracted phases, including Pg and Pn, are fitted to the observed arrivals. The reflection phases (PmP, PmfP and PtocP) also match the recorded data; however, pre-critical reflections are not clearly identified in the seismic record sections.

Checkerboard resolution tests have been computed for both of the profiles to gain information on the spatial and amplitude resolution, which is dependent on the given ray geometry and the velocity distribution. The final V_p velocity model is perturbed by a small (compared to the real) value using a checkerboard pattern (for P4–23 additionally an isolated Gaussian anomaly pattern was used). Synthetic traveltimes are computed through the perturbed medium for the same source–receiver geometry as in the tomographic inversion. Subsequently, the tomography is computed based on the synthetic traveltimes in order to recover the initial perturbation pattern. The results of a test for P4–23 are shown in Figs 5(a)–(c). Three different anomaly sizes were used in the tests: 5 \times 2.5 km,

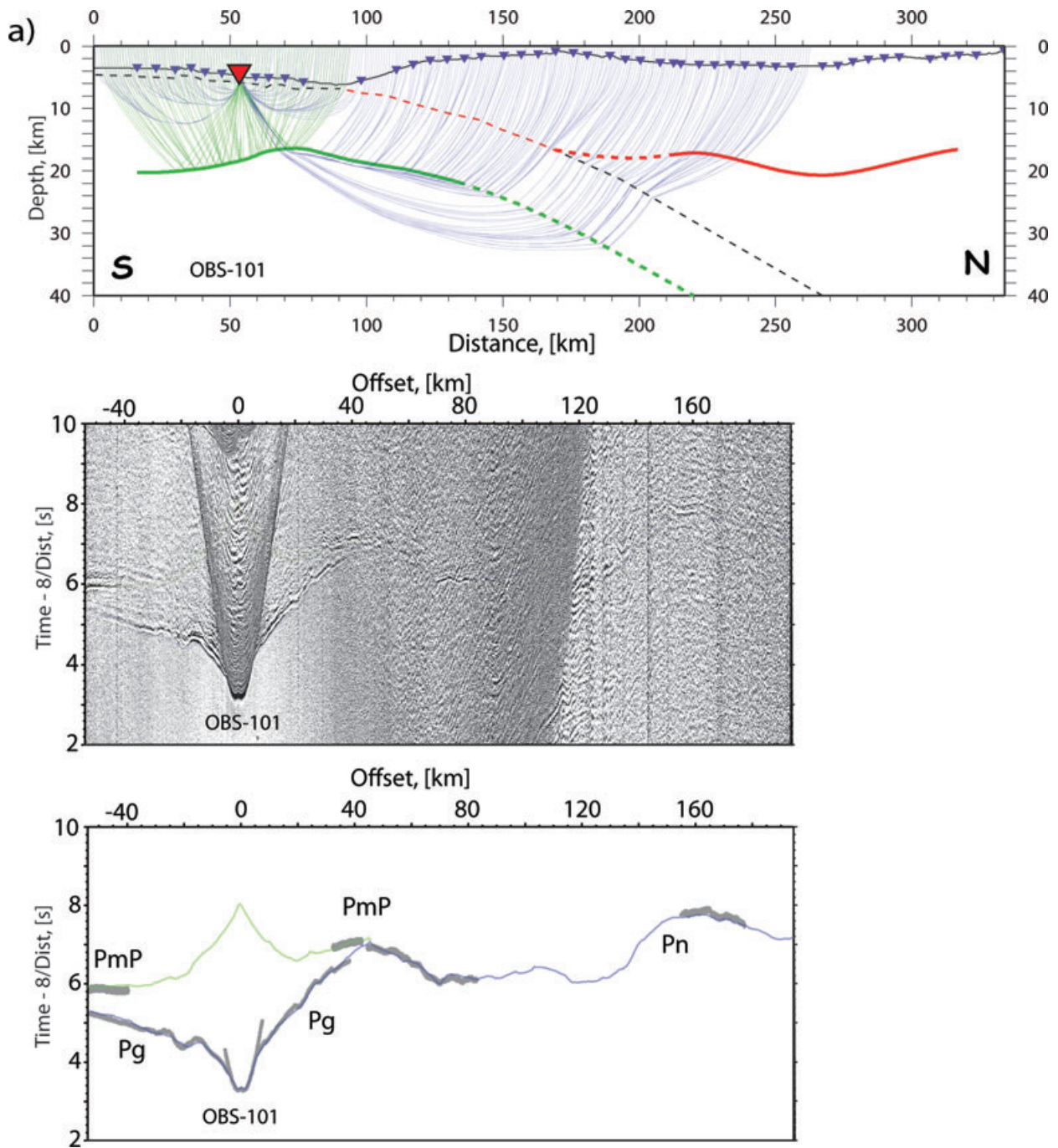


Figure 3. A forward ray shooting test for the selected stations on profile P4–23. For each station the first arriving and reflected traveltimes through the final model were computed and plotted on top of the actual seismic records. Bottom plots show with grey lines the picked phases, with width of the line representing the picking uncertainty. The computed traveltimes through the final model show good fit to the picked phases. Blue line – first arriving phases, green – reflections from the oceanic crust Moho, red – reflections from the forearc crust Moho. Top sections in each of the subplots show the schematic model of the profile. Solid lines correspond to well-defined reflectors constrained by wide-angle seismic data; dashed lines – structural interfaces constrained from MCS and/or gravity data, but purely resolved by the OBS data set. The corresponding ray paths, colour-coded as described above, are shown above each station in the model window.

10 × 5 km and 20 × 10 km (horizontal × vertical size). For all of them the starting model was perturbed using ±5 per cent values. For the small scale perturbation, the model is recovered down to a depth of 12 km, which roughly corresponds to the top of the forearc basement that we define to be around 5 km s⁻¹ isocontour (Fig. 5a). The 20 × 10 km size perturbation was adequately recovered down to a 20 km depth, which correlates with the location of the horizontal

segments of the oceanic and forearc crust (Fig. 5c). The middle size pattern showed, as expected, an intermediate resolution down to a 16 km depth (Fig. 5b). Portions of the model deeper than ~20 km failed to be recovered even with the biggest size pattern. To check the model validity for these areas, a resolution test using a single isolated Gaussian anomaly was performed. The anomaly was centred at 130 km offset and at 25 km depth. The tests were performed

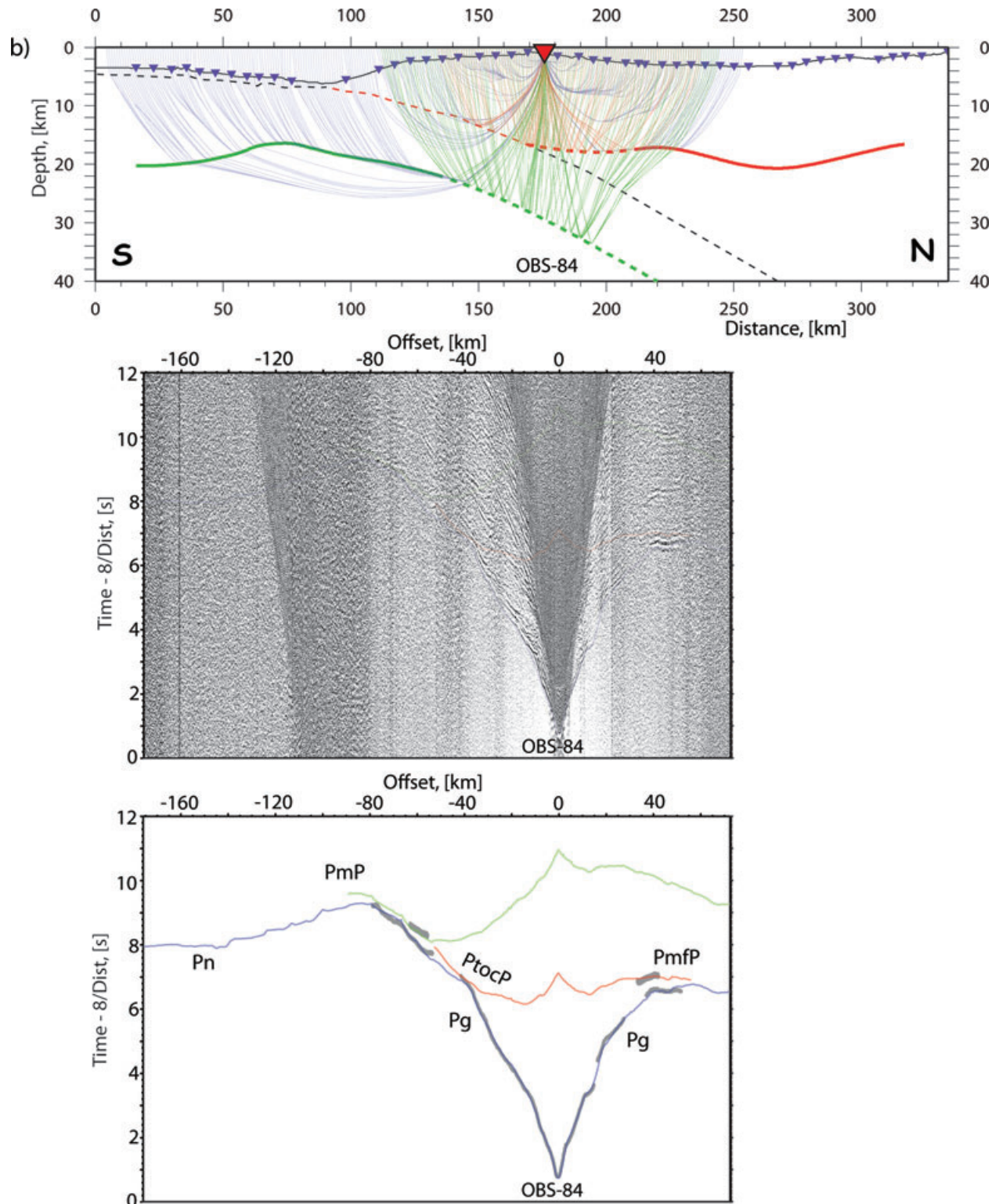


Figure 3. (Continued.)

for +10 and -10 per cent anomalies. As displayed in Figs 5(f) and (h), for the negative anomaly it was not possible to recover neither the shape nor the real amplitude of the anomaly due to the geometry of the seismic rays in this area, which are mostly non-crossing. For the positive anomaly test, the amplitudes were recovered; however, the location is smeared along the ray paths. In tomographic inver-

sions with similar geometries (i.e. a small number of crossing rays), it is normal to observe the effect of averaging of the anomaly along the whole ray path between the crossing points. This is the case with the P4-23 profile. Additionally, the structure was checked by fitting the position of the critical distances for PmP reflections, this supports the obtained depth and velocity contrast at Moho (Fig. 6).

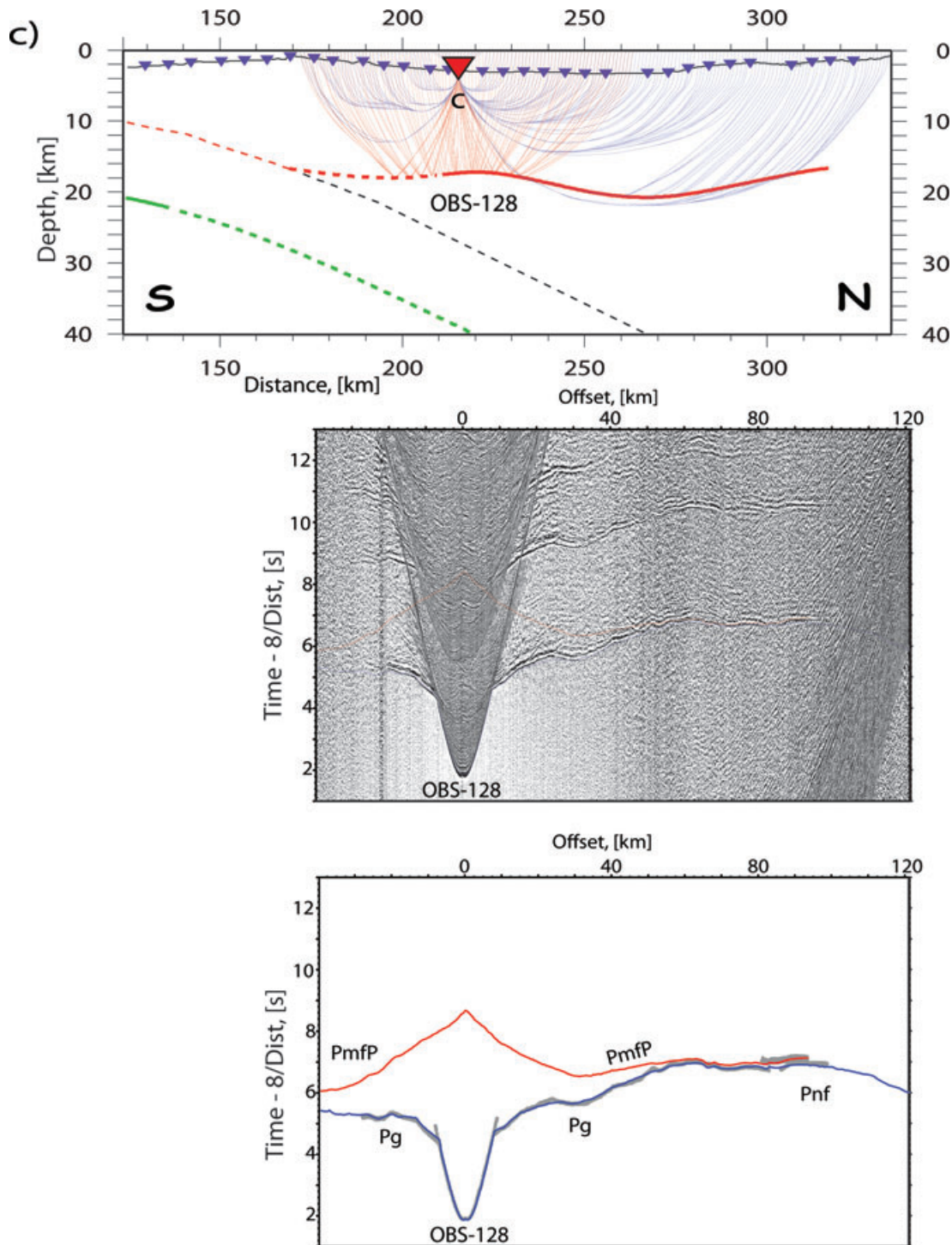


Figure 3. (Continued.)

Based on the resolution tests, it is likely that during the tomographic inversion the actual V_p velocity values tend to be overestimated and can be in the range of -7 to $+3$ per cent from the ones recovered for depths greater than 20 km.

Similar to P4-23, checkerboard tests were conducted for profile P-41. The results are shown in Figs 5(d) and (e). Two different pattern sizes were tested: 5×2.5 km and 10×5 km, both with a ± 5 per cent amplitude perturbation. The smaller size anomalies are recovered down to 6 km depth, while the larger ones are recovered down to 12 km depth.

2.5 Gravity modelling

The resulting V_p velocity seismic tomography model for profile P4-23 was extended by 100 km both to the north and to the south and down to a depth of 75 km, to be used in forward gravity modelling. Seismic velocities were converted to densities using empirical and experimental relationships (Christensen & Mooney 1995; Carlson & Herrick 1990) and the subducting slab was extended down to 75 km depth, where the deep seismicity is observed. A constant density of 3.30 g cm^{-3} was assumed for the forearc mantle, with

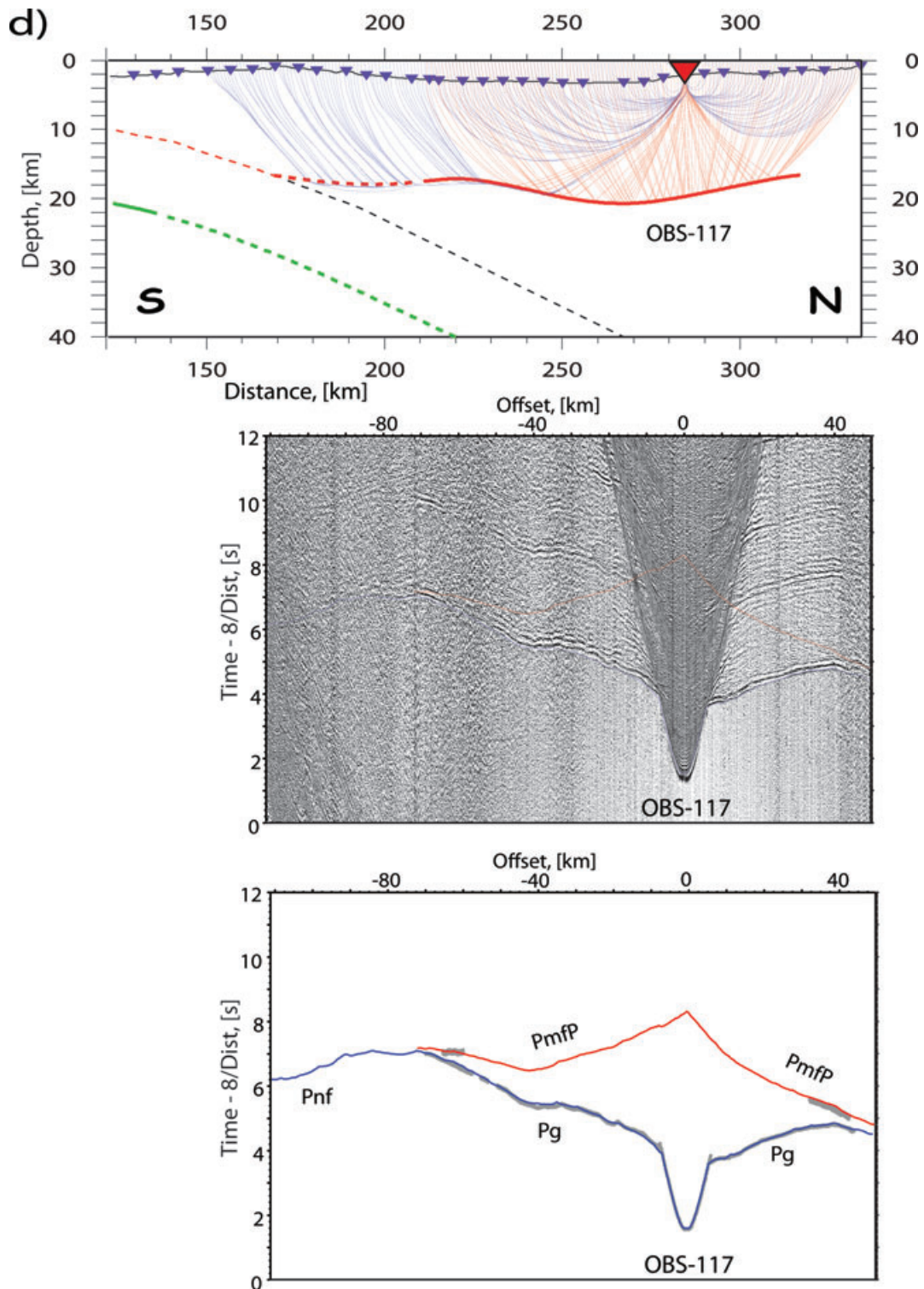


Figure 3. (Continued.)

the exception of the 30-km-long innermost mantle wedge where a density of 3.27 g cm^{-3} was used (Fig. 7). The calculated gravity response of the model is in a good agreement with the observed data. The maximum misfit of 15–20 mGal is observed at the edge of the profile.

The area around the profile P4–23 shows a high degree of bathymetric changes in the east–west direction, associated with isolated

forearc highs and the extended shelf zone offshore Java to the west of the northern termination of the profile. There is also a possibility for lateral variations of forearc crust offline the profile. Although these features should produce measurable 3-D effects on the gravity field along the profile, their effects were ignored in the gravity modelling. Despite the above mentioned simplifications, the gravity modelling confirms the features resolved by the tomographic

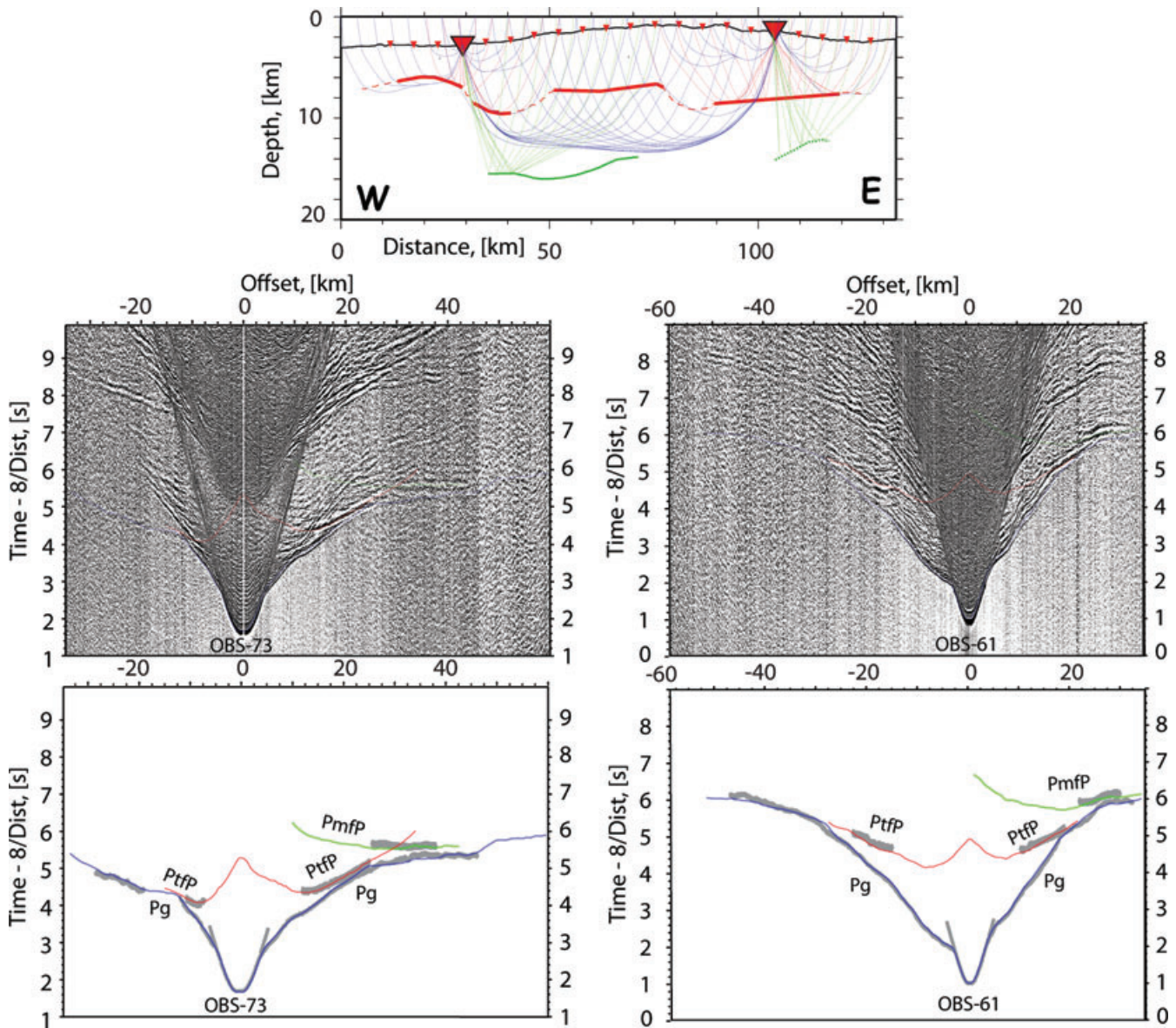


Figure 4. The forward ray shooting test for the selected stations on profile P-41. For each station the first arriving traveltimes (blue lines) through the final model were computed and plotted on top of the actual seismic records. Red and green lines are the synthetic reflection traveltimes from the top of the basement and plate interface, correspondingly. Bottom plots show with grey lines the picked phases, with width of the line representing the picking uncertainty. The top plot shows the locations of the corresponding stations and the ray paths for both stations, colour-coded as described above. Solid lines correspond to the well-defined portions of the reflectors. Dashed lines are reflectors that are purely resolved, or where the strong 3D propagation effects are assumed.

inversion (Fig. 7). The increased crustal thickness of the Roo Rise is required to fit the gravity field. The low mantle velocities, recovered in-between offsets of 60 and 160 km, correlate with the zone of a decreased mantle density of 3.29 g cm^{-3} . Such geometry of the forearc crust and the decreased density in the forearc mantle, associated with a relatively slow velocity in the forearc mantle, are required to fit the gravity data. Additionally, the possibility for the near vertical backstop, as seen offshore Lombok (Planert *et al.* 2010) has been tested (Fig. 7). The larger misfit with the observed gravity, compared to dipping backstop, further supports that the study area is transitional from Lombok domain to Java domain.

3 RESULTS AND DISCUSSION

The results are discussed from south to north of the region, starting from the southern segment of profile P4–23 towards Java. They are based on the joint interpretation of the wide-angle reflection/refraction tomography models, MCS data, and gravity model shown in Figs 2, 7, 8 and 9.

3.1 Roo Rise crustal structure

The southernmost section from 0 to 65 km offset on the north-south striking profile (P4–23) is the area where the Roo Rise oceanic

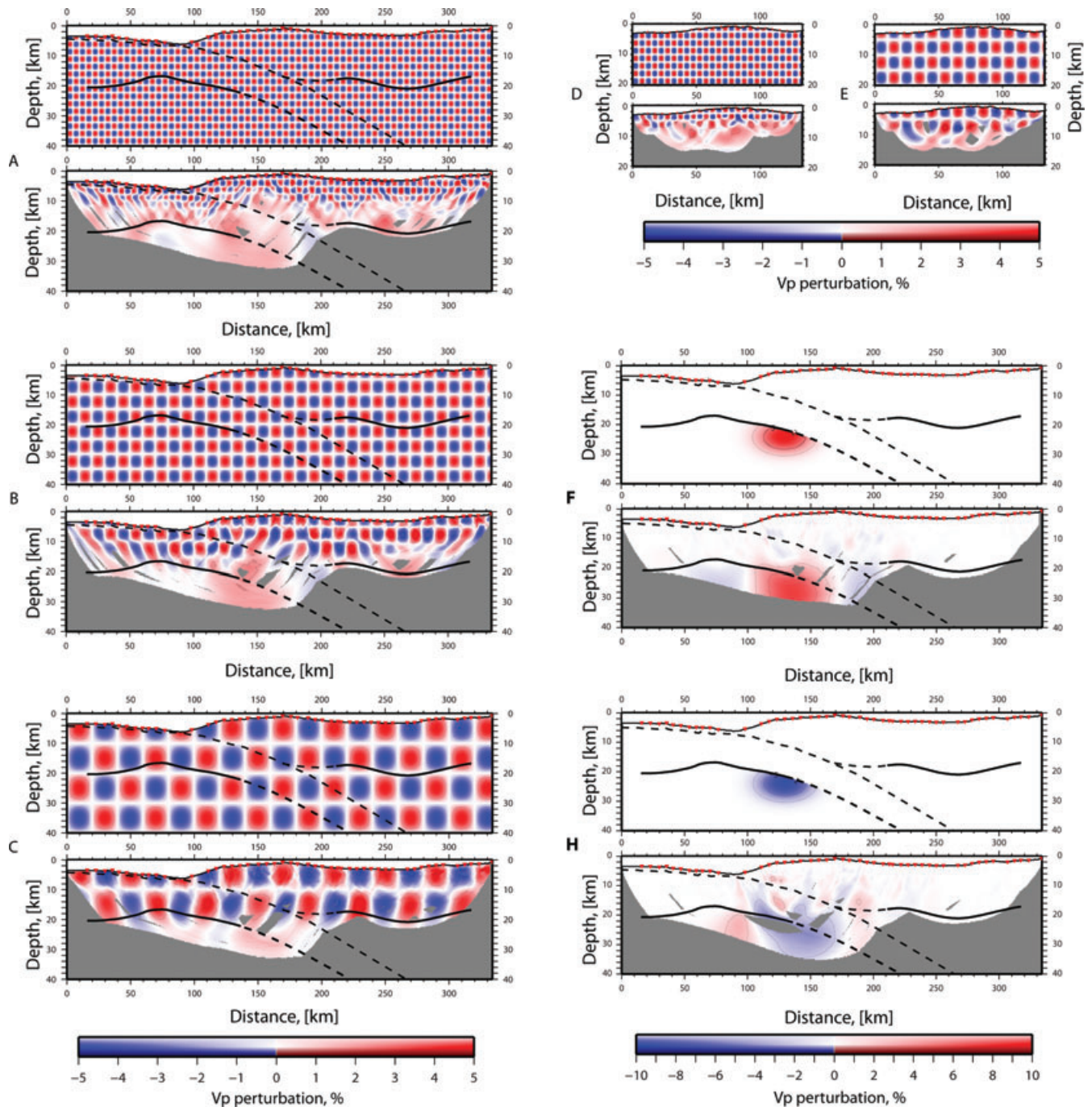


Figure 5. The results of the resolution tests. For each of the subplots the top figure is the synthetic resolution pattern and the bottom one is the recovery. A, B and C are the ± 5 per cent V_p anomaly tests for profile P4–23. The sizes of the anomalies are: (A) 5×2.5 km; (B) 10×5 km; (C) 20×10 km (first number – horizontal extend, second – vertical). (D) and (E) are the ± 5 per cent V_p anomaly tests for profile P41. The sizes of the anomalies are: (D): 5×2.5 km; (E) 10×5 km; (first number – horizontal extend, second – vertical). F and H are the resolution tests for profile P4–23 with a single isolated anomaly (F: +10 per cent; H: –10 per cent). Black solid and dashed lines are structural elements, the same as in Fig. 2.

plateau enters the trench (Fig. 2). The water depth is increasing here from 3 km at the southern end of the profile in the oceanic domain to 6 km depth at the trench. The V_p velocity structure of the upper portion of the oceanic plate is laterally homogeneous: velocities increase from about 2.7 to 3.0 km s^{-1} below the seafloor (bsf) to 5 km s^{-1} at about 2 km depth bsf (Fig. 8). At greater depth, the velocity gradient decreases and the velocities rise to 6.5 – 6.8 km s^{-1} at the Moho which is located at 20–16 km depth (Fig. 2). Thus, the crustal thickness of the plateau varies from 18 km to 11 km (Fig. 2);

these values are significantly greater than predicted earlier (Curry *et al.* 1977). The position of the critical distance for the PmP reflections (Fig. 6) fits the data, confirming the velocity model and the oceanic Moho topography. As is seen in the velocity model (Fig. 2), the major increase of the crustal thickness is accommodated by thickening of the lower oceanic crust. The gravity modelling of this crustal block yields a reasonable fit to the observed gravity field, which confirms the thickened (up to 20 km) crust underneath the oceanic plateau (Fig. 7). This result confirms the suggestion of

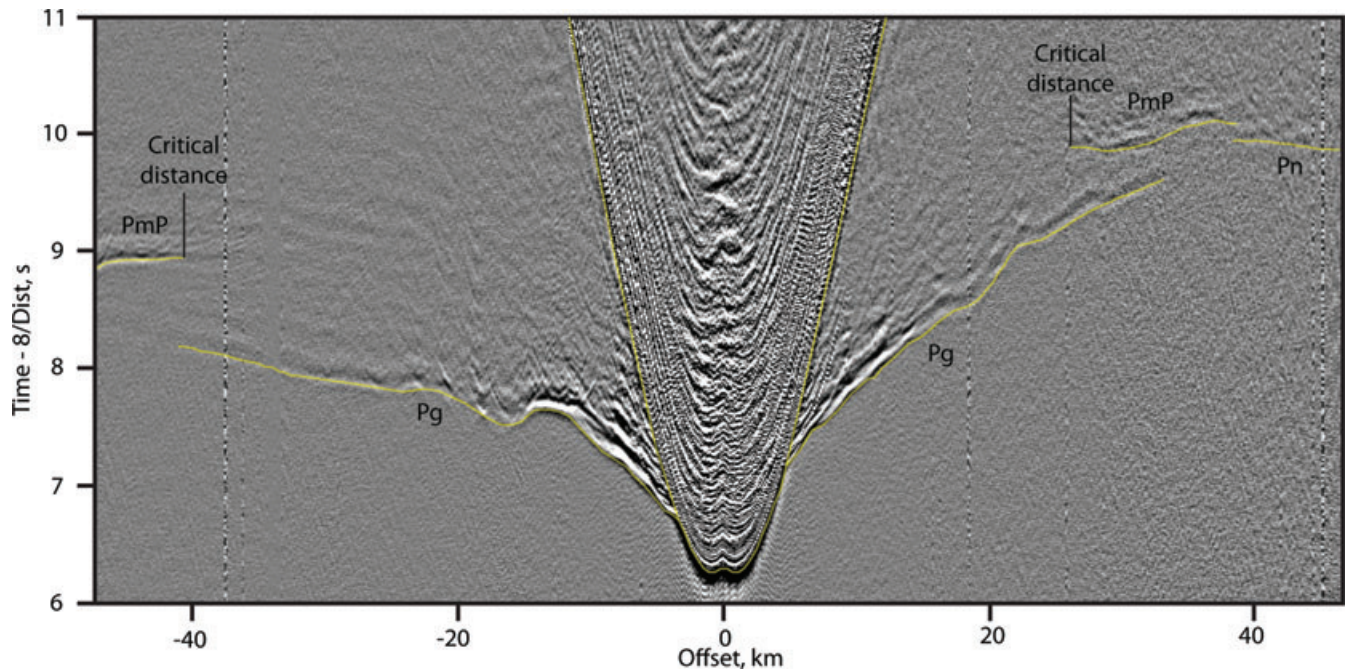


Figure 6. Record section of the vertical component of the OBH-101 located on the P4–23 profile around 51 km offset. Yellow lines show some selected phases. The forward ray shooting method nicely fits the observed critical points for the PmP.

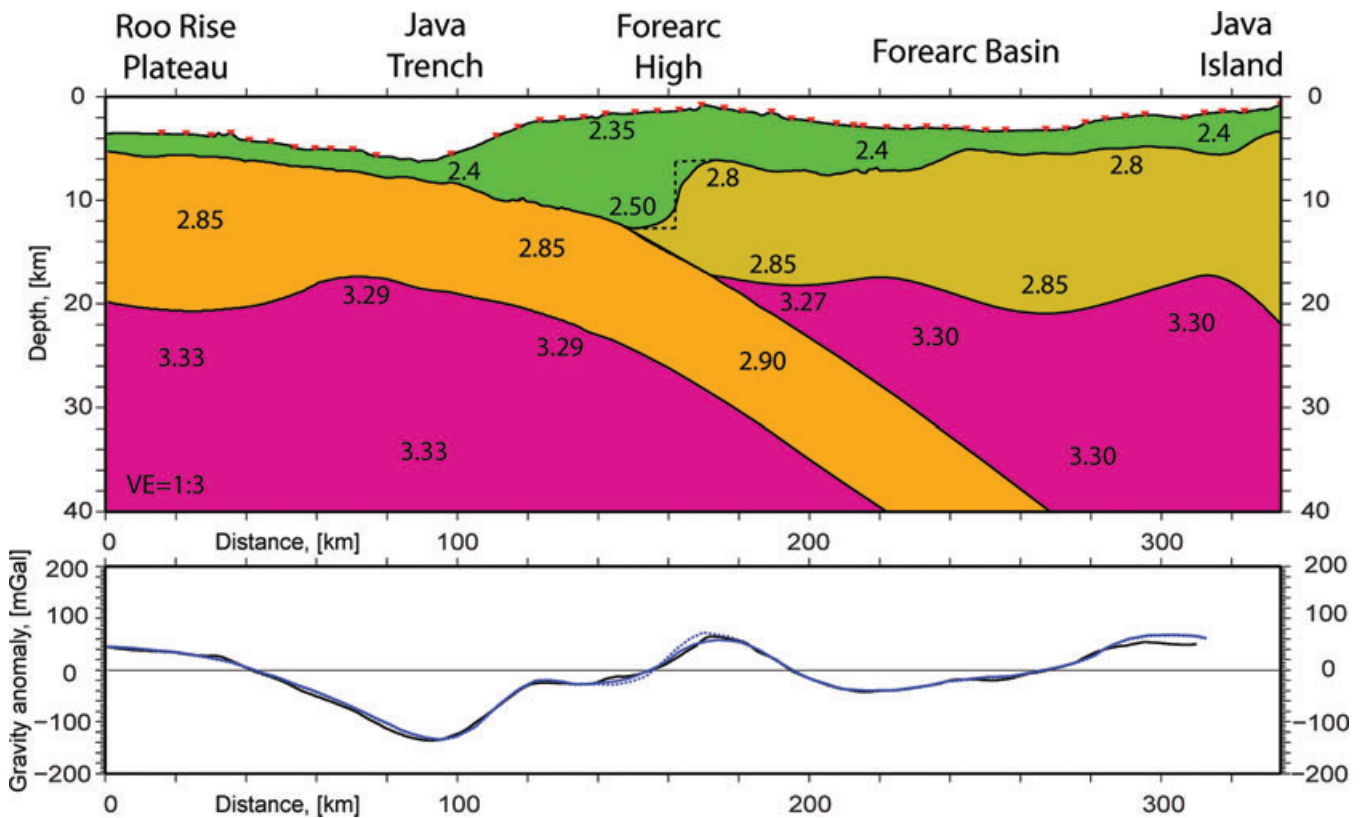


Figure 7. The gravity model for the profile P4–23. Top plot shows the density distribution in the model. Numbers correspond to the density values in units of g cm^{-3} . Densities below the shown depth are kept constant. The bottom plot shows the observed (black) and calculated (blue) free-air gravity anomalies along the profile. The dashed line on top plot corresponds to the gravity model where the backstop is assumed to be pure vertical; the computed gravity anomaly is shown on the bottom plot by dashed blue line.

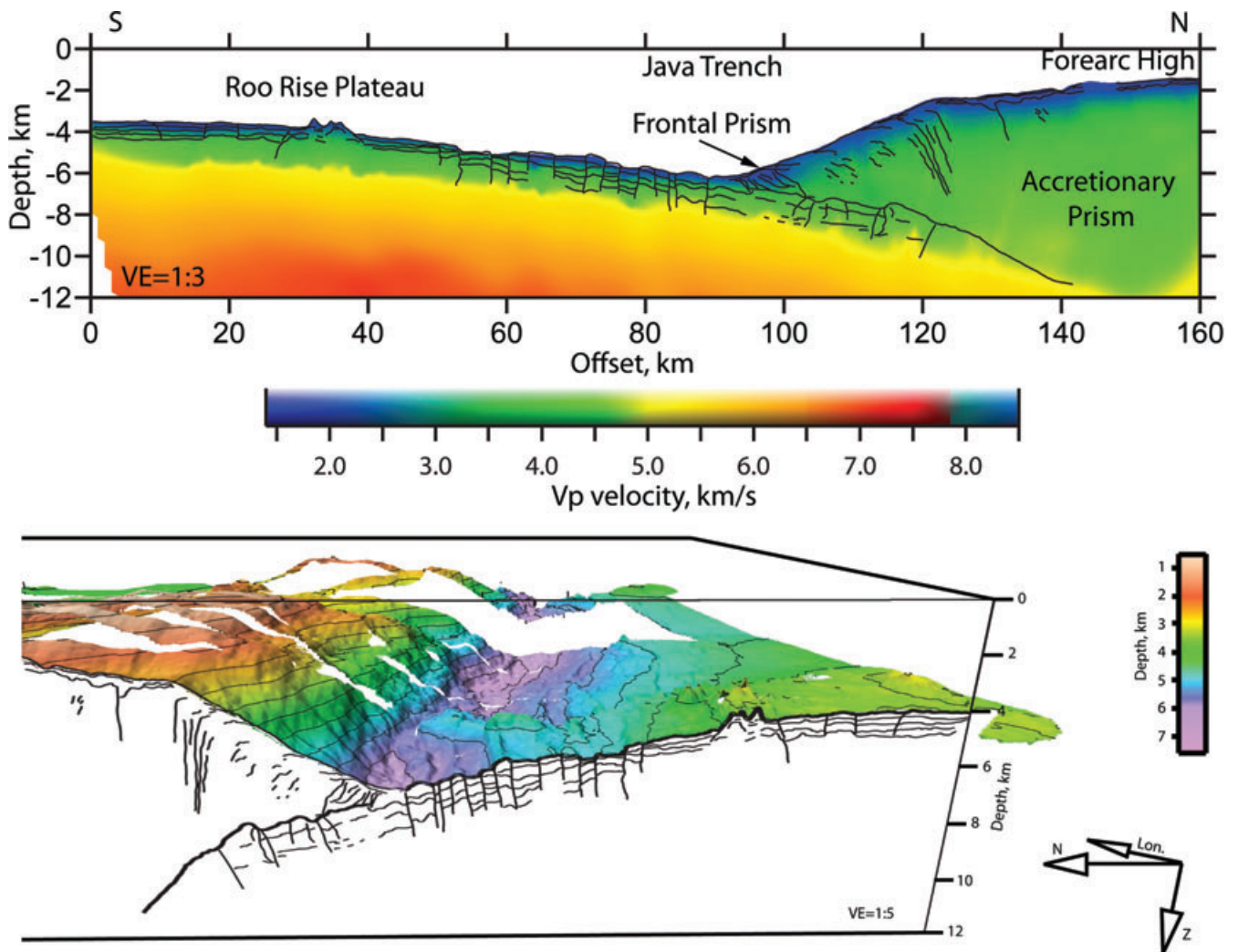


Figure 8. Top panel: A close look on the V_p distribution model around the Java trench. The black lines are the line-drawing interpretation of the collocated MCS profile. Bottom panel: 3-D view of the high-resolution bathymetry, centred at the trench location. The view is from west to east. Vertical slice is the linedrawing interpretation of the MCS line collocated with the P4–23 profile. Highly fractured upper oceanic crust is clear visible in both data sets.

Newcomb & McCann (1987) for the presence of a deep crustal root. The observed northward thinning of the Roo Rise crust (Fig. 2) may have several explanations. The most straightforward explanation is to interpret the region with the thinnest crust as the edge of the plateau and its transition to the conventional oceanic crust. Alternatively, this region may represent localized crustal thinning still within the Roo Rise that extends further north. Variations in crustal thickness of up to several kilometres are common for magmatically overprinted oceanic crust and may be associated with past, now inactive, phases of localized increased magmatic activity (Kopp *et al.* 2004). The interpretation of seismicity by Abercrombie *et al.* (2001) suggests the presence of subducted seamounts and thus implies a northward extension of the Roo Rise into the subduction complex. However, as it was shown by the numerical modelling, the presence of a buoyant oceanic plateau subducted below ~ 30 km should lead to the formation of a flat subduction and ceasing of magmatism in the volcanic arc (van Hunen *et al.* 2002; Gerya *et al.* 2009; Mason *et al.* 2010). Since it is not the case in this area, we conclude that the main block of the Roo Rise is currently only approaching the trench and the anomalous crustal features present below the forearc are the isolated edge structures of the plateau (i.e. individual seamounts).

Starting from an offset of 60 km further northwards, the oceanic crust is highly fractured and is cut by a number of normal faults clearly visible in the MCS data (Lueschen *et al.* 2010) (Fig. 8) and in the multibeam bathymetry data at the surface (Fig. 1a and b). The observation of the faults and fractures is in an agreement with the results of Masson *et al.* (1990) which show that the subducted oceanic crust is fractured by normal faults due to the tension in its upper part caused by plate bending. Below the trench, the oceanic crust thins to about 10 km and maintains this thickness upon subduction (Fig. 2). The velocities at the top are about $3.5\text{--}4.0\text{ km s}^{-1}$ increasing to 5 km s^{-1} at a 2 km depth below sea floor, and gradually increasing to $6.5\text{--}6.6\text{ km s}^{-1}$ at the Moho. The modelled low velocities are presumably caused by the highly fractured, altered fluid-filled crust which causes the decrease of effective velocities. In addition, velocity smoothing implemented in the tomographic inversion is also likely to contribute to this effect. The lateral variations of the V_p velocity structure within the oceanic crust are small (Figs 2 and 8).

Comparison of the obtained structure of the Roo Rise with similar terrains in other regions shows similarities both in the velocity distribution and the crustal thickness. The Hikurangi plateau, offshore New Zealand, which is similar in structure but much larger, is

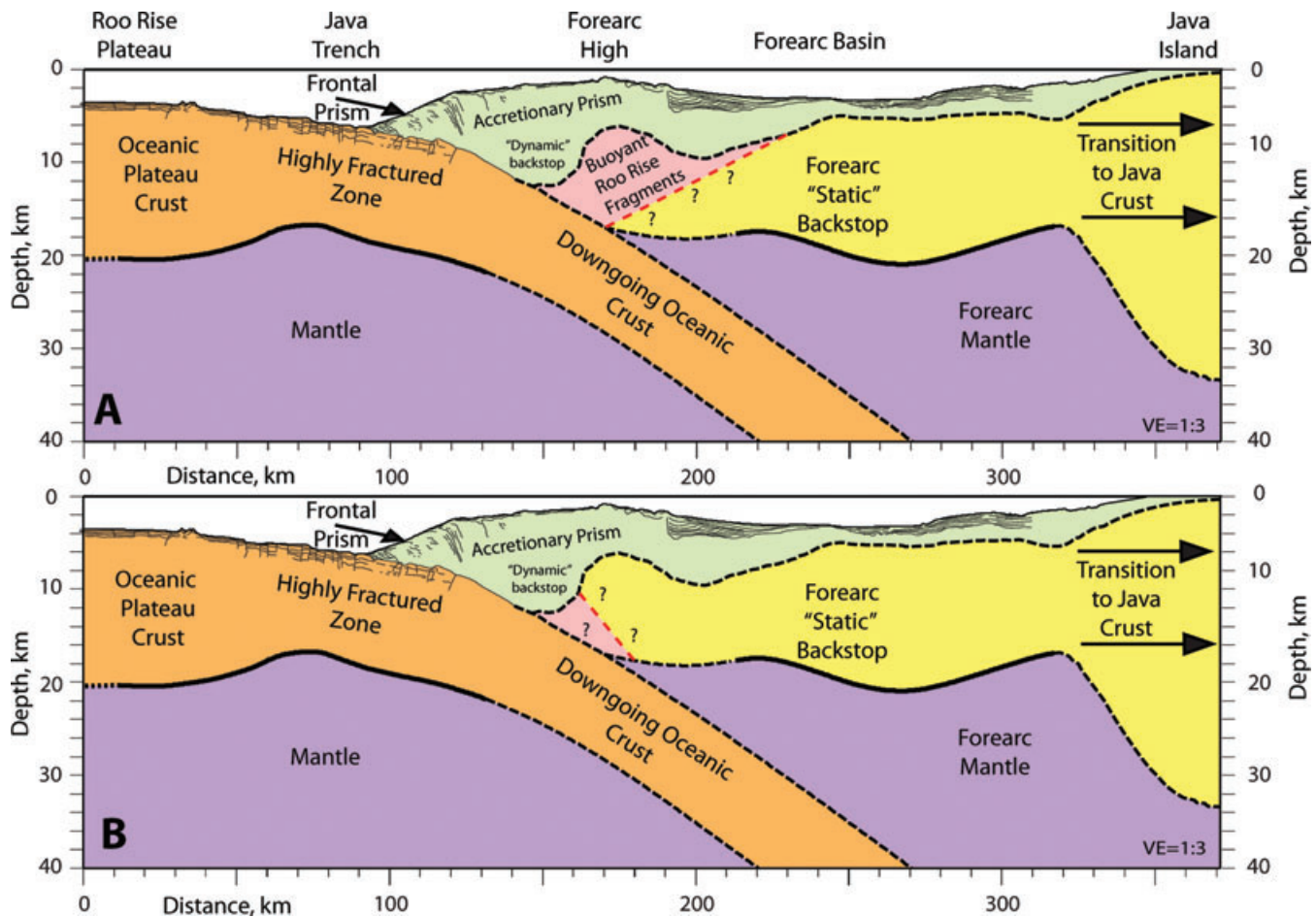


Figure 9. Joint interpretation models for profile P4–23 based on combined results of seismic tomography, MCS and gravity modelling. Thick solid lines are the reflectors constrained by the joint refraction/reflection inversion. Thick dashed lines are structural elements based on the results of gravity modelling. Thin lines are the line-drawing interpretation of the collocated MCS profile. Plots A and B show two variants for the structure of the backstop. (a) Interpretation based on the geometry of the forearc backstop observed to the west from our profile. (b) Interpretation based on the backstop geometry to the east of our profile and the ideas of Bangs *et al.* (2003).

reported to have 10–23-km-thick crust, and V_p values ranging from 4.9 to 7.2 km s⁻¹ (Davy *et al.* 2008; Scherwath *et al.* 2010). Similar to the Roo Rise, much of the crustal thickening is accommodated by the increase of the lower crust. However, comparing to other Large Igneous Provinces, with common thicknesses of 20–40 km (Coffin & Eldholm 1994), the Roo Rise is at the lower end of these values. This could be due to seismically resolving only the edge of the plateau, but not its centre, where the crust could be thicker. Another comparison could be done with the Nazca ridge offshore Peru, which is more comparable with the size of the Roo Rise, sampled in the study. The crustal thickness of the Nazca ridge reaches 16 km, with V_p values ranging from 4.5 to 6.6 km s⁻¹ in the upper crust and 6.7 to 7.5 km s⁻¹ in the lower crust (Hampel *et al.* 2004). Similar to the Roo Rise and Hikurangi plateaus most of the crustal thickening is accommodated by the lower crust. However, the velocities in the lower crust are much higher compared to the Roo Rise.

3.2 Accretionary prism structure

Starting from the trench (90 km offset) and further north, an active frontal prism is observed, characterized by thrust faults and fronting the accretionary prism (Fig. 8). The frontal prism extends laterally for about 12–15 km. Due to the minor sediment input into the system, the frontal slope of the accretionary prism (from 95 to 125 km

offsets) is about 8°–10° with only about 2°–3° in its upper portion, so that the mean slope of ~5.2° is at the high end of the slope angle range within the neighboring segments (Kopp *et al.* 2006). The frontal prism is characterized by low V_p velocity values ranging from 2 to 2.8 km s⁻¹. Further north, in the accretionary prism which extends from 105 to 185 km offsets, velocities increase from 2 km s⁻¹ below the sea floor to about 3.5 km s⁻¹ at a depth of 3–4 km bsf; the V_p velocity in the consolidated sediments in the deeper part of the accretionary prism (6 to 10 km depth) ranges from 3.5 to 5.0 km s⁻¹ at the top of the basement.

The accreted sediments forming the forearc high are resolved on both profiles, allowing for a 2.5-D interpretation of this area at the profiles crossing (Fig. 2). The velocity–depth distribution in the sediments is similar for both of the profiles, with V_p velocities starting at 2 km s⁻¹ and reaching 5 km s⁻¹ at the top of the basement at 8 km depth (for the forearc region, we assume the top of the basement to correspond to approximately 5 km s⁻¹ isocontour). However, the north–south striking profile suggests a semi-horizontal basement interface extending laterally for, at least, 40 km. This is in contrast to the observations along the east–west profile which reveals a rather undulating topography of the top of the basement, varying from 6 to 10 km depth. This observation can be explained in several ways. It is possible that the forearc crust is composed of several small-scale independent crustal fragments, and thus displays a blocky style of

basement. Another explanation would be to consider the subduction of the basement topographic relief located off profile P4–23, and thus unresolved on it. The presence of such features in the incoming oceanic crust would perturb and dynamically deform not only the overlying sedimentary packages, but also affect the crustal edge of the backstop.

3.3 Forearc crustal structure

The forearc crust carrying a number of sedimentary basins is located further north, from ~ 185 km offset and to the northern termination of the profile (Fig. 2). The depth of the basins ranges from ~ 1200 to 1500 m, which is less than in the well-developed forearc basins to the east and to the west where the sediment infill reaches 3 km (Kopp *et al.* 2009a; Planert *et al.* 2010). The V_p velocity of the sediment in the basins ranges from 1.7 to 3.0 km s $^{-1}$ in the upper 1 – 1.5 km (Fig. 2). The velocities in the consolidated sediments above the basement increase from 3.5 to 5.0 km s $^{-1}$. The crystalline crust of the forearc displays V_p velocities ranging from 5.0 km s $^{-1}$ at the top (~ 5 km depth) to 6.5 – 7.0 km s $^{-1}$ at the Moho. The northern segment of the profile (from ~ 220 km offset) shows higher velocities in the lower crust, while in between 160 and 220 km offset the velocities in the lower crust do not exceed 6.5 km s $^{-1}$ (Fig. 2). For the same location (~ 180 km offset) on the trench-parallel profile, lateral velocity variations in the lower forearc crust are even higher, reaching values up to 7.1 km s $^{-1}$ at 60 km offset of profile P-41 (unfortunately, the low signal-to-noise ratio and a complex 3-D ray propagation for most of the stations on this profile made reflection modelling debatable, especially for the plates interface). The forearc Moho shows minor undulations, as revealed by the tomography model. In the northern section, the Moho is located at a 18 km depth, deepening to ~ 20 km at around 270 km offset, and then shallowing again to about 17 km at ~ 320 km offset. It indicates that the thickness of the crystalline crust is in the range of 12 – 16 km. The results from the neighboring segments (111°E and 115°E) image the forearc Moho in a depth range of 14 – 18 km (Kopp *et al.* 2009b; Planert *et al.* 2010), in agreement with our results. Further to the north, the gravity modelling (Fig. 8) requires a sharp deepening of the Moho to a depth of at least 30 km underneath Java. Crustal deepening can be associated either with the transition to the island arc-like crustal block below Java, or with the presence of the Gondwana revenue as suggested by Smyth *et al.* (2007). Unfortunately, this section is not covered by the seismic data and, due to the non-uniqueness of the gravity modelling, cannot be reliably interpreted.

3.4 Oceanic mantle

The deep structure (below ~ 20 km depth) of the profile was resolved mostly in the southern-central portion of the study area (Fig. 2). However, the model resolution is limited for the deep part (Fig. 5). The calculated V_p velocity values have an uncertainty of about $-7 + 3$ per cent due to the velocity averaging along the ray paths (Fig. 5). In the uppermost oceanic mantle, the velocities are estimated to be in the range from 7.5 to 7.9 km s $^{-1}$. The area of the lower seismic velocities is located between 85 and 170 km offset: it starts approximately below the trench and extends to a depth of at least 30 km where the resolution of our model diminishes. The velocities in the forearc mantle are lower as compared to the oceanic mantle; we observe the values of around 7.5 – 7.6 km s $^{-1}$ under the forearc Moho (Fig. 2). The calculated velocity structure of the forearc and the underlying mantle is in a good agreement with the results calcu-

lated for the adjacent segments offshore Lombok and Central Java around 110°E (Kopp *et al.* 2009b; Planert *et al.* 2010).

3.5 Backstop geometry and structure

The backstop edge is located at ~ 160 km offset; it represents a near-vertical feature bounding the accretionary prism at depth. The forearc high pattern caused by the Roo Rise approach is unusual, as for the ‘normal’ oceanic subduction a continuous ridge-like forearc high structure is expected. This should be an effect caused by the oceanic plateau subduction. We speculate on possible scenarios for the structure of the forearc backstop which would explain the observed bathymetry (Fig. 1). Possible options are shown in Fig. 9.

Variant A is based on the geometry of the forearc backstop observed on the profiles to the west from this study, where the backstop gently dips towards the trench (Kopp & Kukowski 2003). The term backstop defines a region within a forearc that is characterized by an increased yield strength compared to the region trenchward of it and thus by its ability to support larger deviatoric stresses. The kinematic discontinuities which form a backstop may be ‘static’, as would be the case for the continental arc basement, or ‘dynamic’ and thus still deforming, though at a slow rate, as may be expected for compacted accreted material resulting from an earlier phase of accretion (Kopp & Kukowski 2003). In the latter case, the material located southward of the ‘static’ backstop would represent buoyant fragments of the oceanic plate, of the Roo Rise nature, which were detached from the plate and stacked over the static backstop (i.e. little-deforming continental arc basement, following Kopp & Kukowski (2003)). This scenario is valid under conditions that the oceanic crust, currently subducted below the accretionary complex, was as fractured as the segment currently observed at around trench, and that there were some elevated relief features that would have detached from the plate. In this case, the observed forearc high would correspond to the area of maximum stacking of such relief revenues against the static forearc backstop. This correlates with the location of the forearc highs and also explains the relatively shallow forearc basins, as they would experience uplift together with a lateral compression.

Variant B is based on the similarities of our study region to the Lesser Antilles subduction zone. The subduction of the large aseismic Tiburon ridge might be comparable by size and scale to the subduction of the Roo Rise. Following this analogy and the ideas of Bangs *et al.* (2003) and Christeson *et al.* (2003), we speculate on the other option for the backstop structure (Fig. 9b). In this case, the static forearc backstop geometry is similar to the one observed on the profile located eastwards from the study area, offshore Lombok (Planert *et al.* 2010). The observed forearc high then would be linked to the bending-related uplift of the forearc edge, caused by the presence of stacked fragments of the oceanic origin below it. The same conditions should be valid for this scenario as in option A. For this case, the location of the forearc high and its uplift are correlated with the uplift of the crystalline forearc edge.

The choice of any particular variant is governed by the geometry of the static forearc backstop at its exact location, which is not resolved in the study. However, both of the options would influence the geohazard potential for the area, including tsunami and earthquakes. The detailed assessment of the geohazards is outside of the scope of this study. Following, will provide some insight on the earthquake and tsunami potential of the region. In order to trigger a tsunami, a sufficient vertical movement of the seafloor is required. This can be achieved either by crustal movements on the

trust faults as a result of earthquake slip, or as a result of a submarine landslide, possibly triggered by an earthquake. The 2004 Sumatra earthquake and tsunami is an example of the large megathrust event where the major slip was accommodated on the trust faults, resulting in ~ 14 m uplift (Sibuet *et al.* 2007). Similar settings are expected for the Chili and the Cascadia margins. The submarine landslides are the explanation for the tsunamis in the Atlantic region and other regions such as Papua New Guinea and Puerto Rico (ten Brink *et al.* 2009), which puts them into a special class of geohazard as the initiating earthquakes can be much smaller than in mega-thrust events. Offshore Java, where the frontal erosion causes the oversteepening of the frontal slope, any changes in the seismicity regime are of high importance. Both proposed crustal interpretations invoke local deformation of the backstop and the overlying sediments and can lead to the formation of large laterally inhomogeneous stress gradients in the area, thus increasing the probability of rupture on the normal faults in the oceanic crust due to load as well as on thrust faults within the accretionary prism and within the seismogenic zone. It explains the observed increased level of the shallow seismicity clustered around 113°E (Fig. 1) and the dynamically caused perturbations of the basement top and associated forearc high. A similar seismicity pattern is observed in the Lesser Antilles subduction zone where the clustering of shallow seismicity is spatially correlated with the collision of the subducting aseismic ridge with the backstop (Christeson *et al.* 2003). Unfortunately, the lack of deep penetrating seismic reflection data imaging the internal structure of the observed crustal edge and the absence of local relocated seismicity leaves this question open for further research.

The northward shift of the active volcanic arc observed on Java (Fig. 1) can be correlated to the northward trench r advancing in the vicinity of the Roo Rise, approaching the trench. The presence of elevated bathymetric features associated with sea plateau subduction can cause the frontal erosion of the accretionary complex and thus the landward migration on the trench. Numerical modelling shows that it can be considered as an initial stage of the formation of a flat shallow subduction and ceasing of melt production (van Hunen *et al.* 2002; Gerya *et al.* 2009). Furthermore, a proposed Gondwana revenue (Smyth *et al.*, 2007), located in between the trench and Southern Java, can be also responsible for producing complex interaction processes within the subduction system, resulting in the northward volcanic arc propagation. The structure of this lithospheric block and the processes that it triggers are unclear and should be studied in order to understand the entire dynamics of this subduction margin.

Summarizing, we observe the complex subduction of abnormally thick oceanic crust under the rigid forearc crust. The accretionary complex is experiencing an inhomogeneous current uplift due to one of the proposed scenarios. The approach of the buoyant oceanic plateau to the trench causes active frontal erosion as well as internal deformation of the accreted sediments which, in turn, dynamically affects the tip of the forearc crust and the structure of the forearc basins. This complex deformation pattern has a strong effect on local seismicity and increases the geohazard risk for tsunamogenic seismic events.

4 CONCLUSION

The summary of our results is shown in Fig. 9. In the 113°E segment of the Java trench, we observe the approach of the oceanic

plateau Roo Rise to the trench, and the effects it causes on the local subduction regime.

The Roo Rise is characterized by variable crustal thickness ranging from 18 to 12 km and shallowing towards Java. It extends laterally for at least 70 km within our profile (Fig. 2). Based on the bathymetric data and its link to the presence of a deep compensating crustal root, the thickened oceanic plateau crust with an average thickness of about 15 km is expected to cover an area of approximately $100\,000\text{ km}^2$ ($200\text{ km} \times 500\text{ km}$) offshore Central-Eastern Java. The transition to normal oceanic crust is not well defined, but the plateau can extend into the subduction system up to 60 km northward from the trench.

The structure of the upper crust of the incoming oceanic plate shows a high degree of fracturing in its top section. This fracturing is clearly visible in the high-resolution bathymetry and MCS transect down to 2 km below the top of the crust (Fig. 8). It is possible that the crust is cut by faults even to a greater depth, as indicated by the low mantle velocities that require fluid percolation (Carlson & Miller 2003), and by an increased level of shallow crustal seismicity (Abercrombie *et al.* 2001; Bilek & Engdahl 2007).

Within our profiles, we do not recover any direct evidence for the presence of the bathymetric features on the oceanic plate currently present below the accretionary prism. Depth variations of the basement observed on the trench-parallel profile, may serve as evidence for bathymetric features associated to the RooRise.

Gravity modelling requires a sharp crustal thickness increase below Java. As the region is not covered with seismic data, we can only speculate on the origin of this crustal structure. The thick crust can be a part of the Gondwana revenue as suggested by Smyth *et al.* (2007).

The approach of the Roo Rise to the trench has strong effects on the local seismicity setting. The geohazard risks should be reconsidered as this segment of the margin has an increased probability for tsunamogenic earthquakes.

ACKNOWLEDGMENTS

We would like to thank Cpt. Meyer and the crew of R/V Sonne and the SINDBAD Working group for their enormous help in collecting and processing of the data. We express great gratitude to Jun Korenaga for the discussion of seismic tomography and the Tomo2D code. We highly appreciate the reviews and comments from Saskia Goes and Gail Christeson, which improved the paper. We would like to extend special thanks to Greg Houseman and Alessandro Forte for fruitful discussions. The SINDBAD project is funded by the German Federal Ministry of Education and Research (BMBF) (grants 03G0190A and 03G0190B). Special thanks to Petersen-Stiftung foundation for their funding to complete this study.

REFERENCES

- Abercrombie, R., Antolik, M., Felzer, K. & Ekström, G., 2001. The 1994 Java tsunami earthquake: slip over a subducting seamount, *J. geophys. Res.*, **106**, 6595–6607.
- Bangs, N.L., Christeson, G.L. & Shipley, T.H., 2003. Structure of the Lesser Antilles subduction zone backstop and its role in a large accretionary system, *J. geophys. Res.*, **108**(B7), doi:10.1029/2002JB002040.
- Bialas, J. & Flueh, E.R., 1999. Ocean bottom seismometers, *Sea Technol.*, **40**(4), 41–46.
- Bilek, S.L. & Engdahl, E.R., 2007. Rupture characterization and aftershock relocations for the 1994 and 2006 tsunami earthquakes in the Java subduction zone, *Geophys. Res. Lett.*, **34**, L20311.

- Carlson, R.L. & Herrick, C.N., 1990. Densities and porosities in the oceanic crust and their variations with depth and age, *J. geophys. Res.*, **95**, 9153–9170.
- Carlson, R.L. & Miller, D.J., 2003. Mantle wedge water contents estimated from seismic velocities in partially serpentinized peridotites, *Geophys. Res. Lett.*, **30**(5), 1250, doi:10.1029/2002GL016600.
- Christensen, N.I. & Mooney, W.D., 1995. Seismic velocity structure and composition of the continental crust: a global view, *J. geophys. Res.*, **100**, 9761–9788.
- Christeson, G.L., Bangs, N.L. & Shipley, T.H., 2003. Deep structure of an island arc backstop, Lesser Antilles subduction zone, *J. geophys. Res.*, **108**(B7), doi:10.1029/2002JB002243.
- Coffin, M.F. & Eldholm, O., 1994. Large igneous provinces: crustal structure, dimensions, and external consequences, *Rev. Geophys.*, **32**(1), 1–36, doi:10.1029/93RG02508.
- Curry, J.R., Shor, G.G., Rait, R.W. & Henry, W., 1977. Seismic refraction and reflection studies of crustal structure of the eastern Sunda and western Banda Arcs, *J. geophys. Res.*, **82**, 2479–2493.
- Davy, B., Hoernle, K. & Werner, R., 2008. Hikurangi Plateau: crustal structure, rifted formation, and Gondwana subduction history, *Geochem. Geophys. Geosyst.*, **9**, Q07004, doi:10.1029/2007GC001855.
- DeMets, C., Gordon, R.G., Argus, D.F. & Stein, S., 1994. Effect of recent revisions to the geomagnetic reversal time-scale on estimates of current plate motions, *Geophys. Res. Lett.*, **21**(20), 2191–2194.
- Gerya, T.V., Fossati, D., Cantieni, C. & Seward, D., 2009. Dynamic effects of the aseismic ridge subduction: numerical modeling, *Eur. J. Mineral.*, **21**(3), 649–661.
- Hall, R., 2002. Cenozoic geological and plate tectonic evolution of SE Asia and the SW Pacific: computer-based reconstructions, model and animations, *J. Asian Earth Sci.*, **20**, 353–434.
- Hall, R. & Smyth, H.R., 2008. Cenozoic arc processes in Indonesia: identification of the key influences on the stratigraphic record in active volcanic arcs, *Geol. Soc. Am. Spec. Pap.*, **436**, 27–54.
- Hamilton, W., 1979. Tectonics of the Indonesian region. *U. S. Geol. Surv. Prof. Pap.*, **1078**, 308–335.
- Hamilton, W., 1988. Plate tectonics and island arcs, *Geol. Soc. Amer. Bull.*, **100**, 1503–1527.
- Hampel, A., Kukowski, N., Bialas, J., Hebscher, C. & Heinbockel, R., 2004. Ridge subduction at an erosive margin: the collision zone of the Nazca Ridge in southern Peru, *J. geophys. Res.*, **109**, B02101, doi:10.1029/2003JB002593
- Kopp, H. & Kukowski, N., 2003. Backstop geometry and accretionary mechanics of the Sunda Margin, *Tectonics*, **22**(6), 1072, doi:10.1029/2002TC001420.
- Kopp, H. *et al.* 2009b. *Convergent Margin Structure and Tectonics of the Java Subduction Zone (105°E–122°E)*, EOS, Vol. 90, Number 52, 29 December 2009, Fall Meet. Suppl. Abstract T33B-1916.
- Kopp, H., Flueh, E.R., Klaeschen, D., Bialas, J. & Reichert, C., 2001. Crustal structure of the central Sunda margin at the onset of oblique subduction, *Geophys. J. Int.*, **147**, 449–474.
- Kopp, H., Flueh, E.R., Papenberg, C. & Klaeschen, D., 2004. Seismic investigations of the O'Higgins Seamount Group and Juan Fernandez Ridge: aseismic ridge emplacement and lithosphere hydration, *Tectonics*, **23**, TC2009, doi:10.1029/2003TC001590.
- Kopp, H., Flueh, E.R., Petersen, C.J., Weinrebe, W., Wittwer, A. & Meramex Scientists., 2006. The Java margin revisited: evidence for subduction erosion off Java, *Earth planet. Sci. Lett.*, **242**, 130–142.
- Kopp, H., Hindle, D., Klaeschen, D., Oncken, O. & Scholl, D., 2009a. Anatomy of the western Java plate interface from depth-migrated seismic images, *Earth planet. Sci. Lett.*, doi:10.1016/j.epsl.2009.09.043.
- Kopp, H., Klaeschen, D., Flueh, E.R. & Bialas, J., 2002. Crustal structure of the Java margin from seismic wide-angle and multichannel reflection data, *J. geophys. Res.*, **107**(B2), doi:10.1029/2000JB000095.
- Korenaga, J., Holbrook, S., Kent, G., Kelemen, P., Detrick, R.S., Larsen, H.-C., Hopper, J.R. & Dahl-Jensen, T., 2000. Crustal structure of the southeast Greenland margin from joint refraction and reflection seismic tomography, *J. geophys. Res.*, **105**, doi:10.1029/2000JB900188.
- Lueschen, E., Mueller, C., Kopp, H., Engels, M., Lutz, R., Planert, L., Shulgin, A. & Djajadihardja Y., 2010. Structure, evolution and tectonic activity at the Eastern Sunda forearc, Indonesia, from marine seismic investigations, *Tectonophysics*, in press, doi:10.1016/j.tecto.2010.06.008.
- Mason, W.G., Moresi, L., Betts, P.G. & Miller, M.S., 2010. Three-dimensional numerical models of the influence of a buoyant oceanic plateau on the subduction zones, *Tectonophysics*, **483**, doi:10.1016/j.tecto.2009.08.021.
- Masson, D.G., 1991. Fault patterns at outer trench walls, *Mar. geophys. Res.*, **13**, 209–225.
- Masson, D.G., Parson, L.M., Milsom, J., Nichols, G., Sikumbang, N., Dwiyanto, B. & Kallagher, H., 1990. Subduction of seamounts at the Java Trench: a view with long-range sidescan sonar, *Tectonophysics*, **185**, 51–65.
- Moore, G.F., Curray, J.R., Moore, D.G. & Karig, D.E., 1980. Variations in geologic structure along the Sunda Fore Arc, northeastern Indian Ocean, in *The Tectonic and Geologic Evolution of Southeast Asian Seas and Islands*, Vol. **23**, pp. 145–160, eds Hays, D.E., Geoph. Mon.
- Mueller, C. *et al.* 2008. From subduction to collision: the Sumba-Banda Arc transition, *EOS, Trans. Am. geophys. Un.*, **89**, 49–50.
- Newcomb, K.R. & McCann, W.R., 1987. Seismic history and seismotectonics of the Sunda Arc, *J. geophys. Res.*, **92**(B1), 421–439.
- Planert, L., Kopp, H., Lueschen, E., Mueller, C., Flueh, E.R., Shulgin, A., Djajadiharja, Y. & Krabbenhoef, A., 2010. Lower plate structure and upper plate deformational segmentation at the Sunda-Banda arc transition, *J. geophys. Res.*, **115**, B08107, doi:10.1029/2009JB006713.
- Scherwath, M. *et al.* 2010. Fore-arc deformation and underplating at the northern Hikurangi margin, New Zealand, *J. Geol. Res.*, **115**, B06408, doi:10.1029/2009JB006645.
- Scholz, C.H. & Small, C., 1997. The effect of seamount subduction on seismic coupling, *Geology*, **25**, 487–490.
- Shulgin, A. *et al.* 2009. Sunda-Banda arc transition: incipient continent-island arc collision (northwest Australia), *Geophys. Res. Lett.*, **36**, L10304, doi:10.1029/2009GL037533.
- Sibuet, J.-C. *et al.* 2007. 26th December 2004 great Sumatra-Adamant earthquake: co-seismic and post-seismic motions in northern Sumatra, *Earth planet. Sci. Lett.*, **263**, doi:10.1016/j.epsl.2007.09.005.
- Smyth, H.R., Hamilton, P.J., Hall, R. & Kinny, P.D., 2007. The deep crust beneath island arcs: inherited zircons reveal a Gondwana continental fragment beneath East Java, Indonesia, *Earth planet. Sci. Lett.*, **258**, 269–282.
- ten Brink, U.S., Lee, H.J., Geist, E.L. & Twichell, D., 2009. Assessment of tsunami hazard to the U.S. East Coast using relationships between submarine landslides and earthquakes, *Mar. Geol.*, **264**, doi:10.1016/j.margeo.2008.05.011.
- Tregoning, P. *et al.* 1994. First geodetic measurement of convergence across the Java Trench, *Geophys. Res. Lett.*, **21**(19), 2135–2138.
- van Hunen, J., van den Berg, A.P. & Vlaar, N.J., 2002. On the role of subducting oceanic plateaus in the development of shallow flat subduction, *Tectonophysics*, **352**, 317–333.
- Werner, R., Hauff, F. & Hoernle, K., 2009. RV Sonne. Cruise report SO-199 CHRISP. Christmas Island Seamount Province and the Investigator Ridge: age and causes of intraplate volcanism and geodynamic evolution of the south-eastern Indian ocean, **25**, 1614–6298.
- White, R.S., McKenzie, D. & O'Nions, R.K., 1992. Oceanic crustal thickness from seismic measurements and rare earth element inversions, *J. geophys. Res.*, **97**, 19 681–19 715.
- Wiener, N., 1949. *Extrapolation, Interpolation, and Smoothing of Stationary Time Series*, John Wiley and Sons, New York.
- Yamazaki, T. & Okamura, Y., 1989. Subducting seamounts and deformation of overriding forearc wedges around Japan, *Tectonophysics*, **160**, 207–229.

SUPPORTING INFORMATION

Additional Supporting Information may be found in the online version of this article:

Figure S1. The comparison of all the picked traveltimes available for the tomographic inversion for the two profiles. The picked traveltimes are shown by black dots for the refracted phases and green dots for the reflected phases. Corresponding computed traveltimes through our final models are shown by red and blue dots, for the refracted and reflected phases, respectively. Top plot is the

fit comparison for the N–S profile, bottom—for the E–W profile. Note, the identical distance and timescale for both plots.

Please note: Wiley-Blackwell are not responsible for the content or functionality of any supporting materials supplied by the authors. Any queries (other than missing material) should be directed to the corresponding author for the article.



Structure, evolution and tectonic activity of the eastern Sunda forearc, Indonesia, from marine seismic investigations

E. Lüschen^{a,*}, C. Müller^a, H. Kopp^b, M. Engels^a, R. Lutz^a, L. Planert^b, A. Shulgin^b, Y.S. Djajadihardja^c

^a Federal Institute for Geosciences and Natural Resources (BGR), Stilleweg 2, 30655 Hannover, Germany

^b Leibniz Institute of Marine Sciences (IFM-GEOMAR), Wischhofstr. 1-3, 24148 Kiel, Germany

^c Agency for the Assessment and Application of Technology (BPPT), J.L.M.H. Thamrin No. 8, Jakarta 10340, Indonesia

ARTICLE INFO

Article history:

Received 15 January 2009

Received in revised form 27 May 2010

Accepted 17 June 2010

Available online 26 June 2010

Keywords:

Sunda Arc

Indonesia

Accretionary prism

Outer arc high

Forearc basin

Multichannel seismic profiling

ABSTRACT

Forearc structures of the eastern Sunda Arc are studied by new multichannel reflection seismic profiling. We image a high along-strike variability of the subducting oceanic plate, the interface between subducting and overriding plate, the accretionary wedge, the outer arc high and forearc basins. We highlight ongoing tectonic activity of the entire outer arc high: active out-of-sequence thrust faults connecting the plate interface with the seafloor, slope basins showing tilted sedimentary sequences on the outer arc high, vertical displacement of young seafloor sediments, and tilted sedimentary sequences in the Lombok forearc basin. While frontal accretion plays a minor role, the growth of the outer arc high is mainly attributed to oceanic sediments and crustal fragments, which are attached to the base of the upper plate and recycled within the forearc. We image ongoing large-scale duplex formation of the oceanic crust. The incoming oceanic crust is dissected by normal faulting into 5–10 km wide blocks within a 50–70 km wide belt seaward of the deep sea trench. These blocks determine the geometry and evolution of duplexes attached to the base of the overriding plate landward of the trench. Long-lasting and ongoing subsidence of the Lombok Basin is documented by distinct seismic sequences. In the Lombok Basin we image mud diapirs, fed from deeply buried sediments which may have been mobilized by rising fluids. We propose a wrench fault system in the eastern Lombok forearc basin that decouples the subduction regime of the Sunda Arc from the continent–island arc collision regime of the western Banda Arc. The observed tectonic activity of the entire forearc system reflects a high earthquake and tsunami hazard, similar to the western part of the Sunda Arc.

© 2010 Elsevier B.V. All rights reserved.

1. Introduction

The 7000 km long Sunda Arc has long been considered as a classical accretionary margin system where the Indo-Australian oceanic plate is underthrust beneath the South-East Asian continent, active since the Upper Oligocene (Hamilton, 1979, 1988). The accretionary margin has produced an accretionary wedge and a pronounced outer arc high forming the subduction complex landward of the deep sea trench, deep forearc sedimentary basins and a volcanic arc (Dickinson, 1977). These structures evolve in response to a number of key parameters, such as age, composition and structure of the subducting plate, convergence rate and direction, and the thickness and origin of the incoming sediments (e.g. Van der Werff, 1996; and references therein). Mass transfer, backstop and accretionary mechanics of this ‘subduction factory’ offshore Sumatra and Java, ranging from accretionary to erosive styles, have recently been studied by Kopp and Kukowski (2003) and Kopp et al. (2001, 2006).

At the eastern end of the Sunda Arc the convergent system changes from oceanic subduction to continent–island arc collision of the Scott Plateau, part of the Australian continent, colliding with the Banda island arc and Sumba Island in between. The origin of Sumba Island is still debated (Rutherford et al., 2001; and references therein).

The Sunda Arc is known as an active convergence zone producing tremendous earthquakes, tsunamis and volcanic hazards. The M_w 9.3 Indian Ocean earthquake and tsunami of December 26, 2004 killed more than 250,000 people. Numerous investigations have been commissioned near the epicentre offshore northern Sumatra to evaluate the earthquake and tsunami hazards. These projects have mapped seafloor morphology and imaged deep structures and faults in order to better understand the origin of megathrust earthquakes and tsunamis in the western portion of the Sunda Arc subduction system (e.g. Henstock et al., 2006; Ladage et al., 2006; Singh et al., 2008; Franke et al., 2008). Little attention concerning tectonics, structural geology and risk analysis has been paid recently to the eastern part of the Sunda Arc, south of eastern Java, the islands of Bali, Lombok, Sumbawa and Flores, so far. This area is the focus of the SINDBAD project (Seismic and Geoacoustic Investigations Along the Sunda–Banda Arc Transition), a joint German–Indonesian project that

* Corresponding author. Leibniz Institute for Applied Geophysics (LIAG), Stilleweg 2, 30655 Hannover, Germany.

E-mail address: Ewald.Lueschen@liag-hannover.de (E. Lüschen).

carried out cruise SO190 with R/V SONNE end of 2006 in two consecutive legs (Fig. 1).

In this paper we present an overview on new seismic images with the main goals (i) to image and characterise the interaction between the subducting and the overriding plate, (ii) to investigate the structure and evolution of the subduction complex and the Lombok forearc basin in response to the variation in age and structure of the incoming oceanic plate (Roo Rise and Argo Abyssal Plain) and (iii) to characterise the transition from ocean–island arc subduction in the eastern Sunda Arc to continent–island arc collision at the western Banda arc. The data comprise 4933 km of multichannel reflection seismic (MCS) profiling, combined with magnetic and gravimetric measurements, sediment echo sounding and swath bathymetry, as well as refraction/wide-angle seismic measurements with ocean bottom seismometers (OBS) for velocity modelling on four corridors coincident with N–S running MCS profiles (Fig. 1). Preliminary interpretations were presented by Müller et al. (2008).

2. Regional tectonic setting

The subduction of the Indo-Australian plate along the Java Trench is active since the late Oligocene (e.g. Hamilton, 1979). The overriding plate is continental including Sumatra and western Java (Kopp et al., 2001) and the basement below the forearc basin offshore Bali and Lombok is probably rifted crust of continental character in transition to oceanic character at Sumbawa and further east (Banda Sea) (Van der Werff, 1996). The convergence rate increased from 5 cm/a to 7 cm/a during the last 10 Ma (7.3 cm/a today according to the global velocity model MORVEL, DeMets et al., 2010) and is almost perpendicular to the Java Trench, in contrast to oblique convergence

offshore Sumatra, where plate motion is partitioned into thrust and strike-slip movements. The volcanism of the island arc was initiated during the Pliocene and changes from an intermediate composition on East Java to a mafic composition on Sumbawa, which documents a transition from a continental to an oceanic overriding upper plate (Hamilton, 1988). The present-day configuration of plate boundaries in South-East Asia shows a quite complex history of interaction of the Pacific, the Indo-Australian and the Eurasian plate. Reconstructions and modelling by Hall (2002, with a comprehensive literature list) and Hall and Smyth (2008) suggest major plate reorganizations at 45, 25 and 5 Ma. Seismological mantle tomography indicates seismic velocity anomalies to a depth of 1500 km attributed to the subducted lithospheric slab, which is probably continuous below Java but discontinuous and detached from the seismogenic slab below Sumatra (Widiyantoro and Van der Hilst, 1997). Seismicity is present in clusters tracing the Wadati–Benioff zone from the outer-trench bulge of the subducting oceanic plate to maximum 300 km depth beneath Sumatra and even 600 km depth beneath the eastern Sunda Arc (e.g. Widiyantoro and Van der Hilst, 1997; Spicák et al., 2007).

The subducting oceanic Indo-Australian plate in the study area (Fig. 1) can be subdivided into three distinct provinces: Roo Rise, Argo Abyssal Plain and Scott Plateau. The Roo Rise offshore Java is characterized by a rough morphology more than 1500 m above the surrounding seafloor level. The subduction of seamounts with their irregular relief contributes to subduction erosion and to the block structure of the outer arc high (Kopp et al., 2006). The trench here is less deep in comparison to adjacent regions, 5600 m to 6000 m versus 7000 m, respectively (Masson et al., 1990). The Argo Abyssal Plain offshore Lombok and Sumbawa (Fig. 1) is smooth at water depths of 5000–5500 m and has a pelagic sediment cover of about 600 m, which

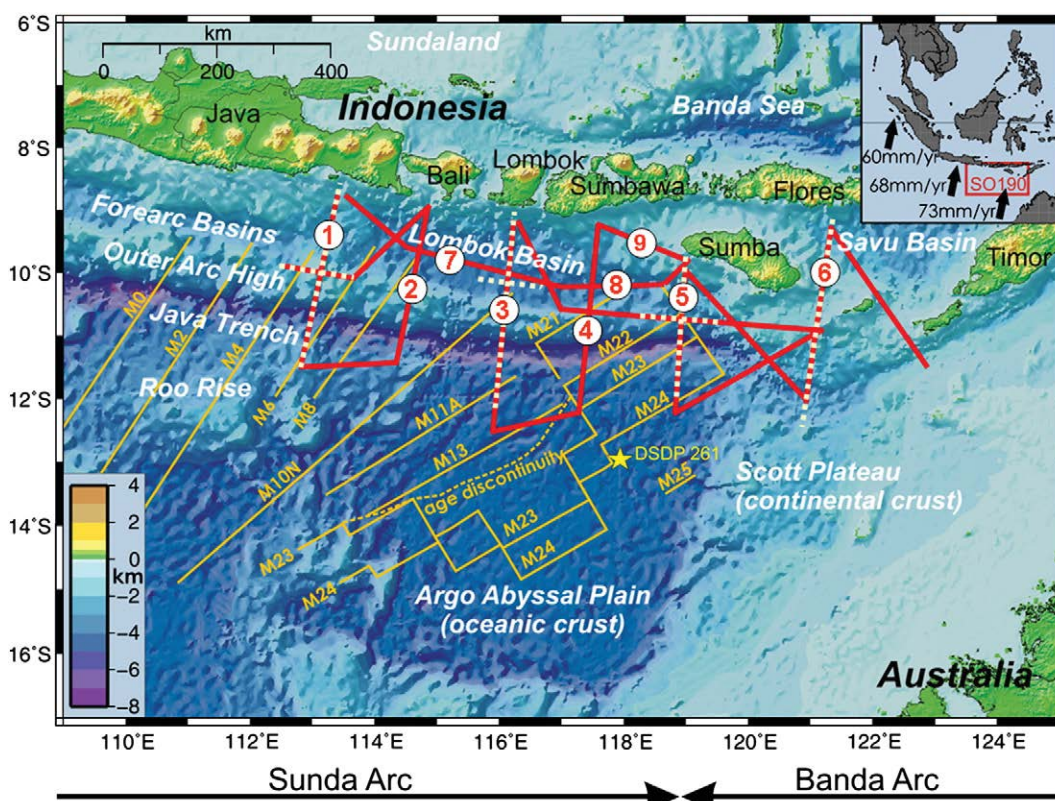


Fig. 1. Location map and inset (upper right) of the SINDBAD survey SO190 with 4933 km of multichannel reflection seismic (MCS) profiling (red lines) and 4 corridors of wide-angle/refraction seismic measurements with ocean bottom seismometers (OBS, red/white dotted lines). Yellow lines are magnetic lineations of reinterpreted anomalies based on studies of Heine et al. (2004) and SO190 measurements. Age of the oceanic plate ranges from early Cretaceous (M0) to late Jurassic (M25). Convergence rates (inset, upper right) of 73 mm/yr in the study area are according to the global velocity model MORVEL (DeMets et al., 2010). Bathymetry from Sandwell and Smith (1997) is based mainly on satellite gravity data. Lines discussed in the text: North–South: 1 = BGR06-305, 2 = BGR06-303, 3 = BGR06-313, 4 = BGR06-311, 5 = BGR06-317, 6 = BGR06-319; East–west: 7 = BGR06-307, 8 = BGR06-308, 9 = BGR06-310.

was sampled at DSDP site 261 (e.g. Heirtzler et al., 1974; Van der Werff, 1995). The oceanic crust including the Roo Rise and the Argo Abyssal Plain dates from late Jurassic (M25 = 155 Ma) to early Cretaceous (M0 = 125 Ma, Fig. 1) and is (particularly the Argo Abyssal Plain) regarded as a remnant of the Tethys ocean (e.g. Heine et al., 2004). In contrast, the Scott Plateau at the eastern part of the Indo-Australian plate in the study area is of continental character and has been colliding with Eurasia since Late Miocene (e.g. Harris, 1991; Van der Werff, 1995). This collision controls the uplift of the Sumba Ridge and the development of the Savu Basin. The origin of Sumba Island is still debated. It could be part of Australia, alternatively of Sundaland or part of an island arc which rifted to its present position during Miocene times (Rutherford et al., 2001, and references therein).

The structure of the subduction complex (accretionary wedge, outer arc high) and the forearc basins have been studied by Hamilton (e.g., 1979, 1988), Van der Werff (1995, 1996) and Van der Werff et al. (1994) using single-channel seismic recordings of relatively low resolution and depth penetration, and, in parts, using multi-channel seismic profiling provided by industrial companies and other institutions in the 1980s. These data have shown that the accretionary wedge consists of imbricated thrust sheets consisting of a melange of sediments/rocks offscraped from the subducting plate. Forearc basins are fed from the growing volcanic arc and the outer arc high as the oldest part of the accretionary prism. In the context of large megathrust earthquakes and ruptures, the subduction complex offshore Sumatra shows abrupt uplift of several meters, the forearc basin subsidence is in the same order of magnitude (Briggs et al., 2006). The youngest thrust faults in the accretionary wedge sole out at a pronounced décollement between upper and lower plate. The structure and stratigraphy of forearc subduction systems with subduction complexes (accretionary wedge, outer arc ridge) and forearc basins have been described in general terms by Dickinson and Seely (1979) and Dickinson (1995). Thickness and width of the subduction complex decrease from the western Sunda Arc towards the eastern Sunda Arc in response to the decreasing thickness of seafloor sediments on the incoming plate (4 km offshore Sumatra, 1.3 km offshore western Java, less than 1 km in our study area). The sediment thickness reflects the southward progradation of immense submarine fans from the Bay of Bengal sourced from the Himalayan collision belt (Dickinson, 1995). Modern MCS data of the western and central Sunda Arc are presented by Schlüter et al. (2002), Kopp and Kukowski (2003), Franke et al. (2008), Singh et al. (2008) and Berglar et al. (2010). Material accretion from the lower to the upper plate dominates in the western and central Sunda Arc, whereas erosional processes at the base of the upper plate are facilitated by seafloor roughness of the Roo Rise, low sediment supply and higher convergence rate further east (Kopp et al., 2006).

The Lombok Basin is one of the largest (600 × 120 km) and deepest (4 km water depth) of the forearc basins located between the outer arc high and the magmatic arc (Fig. 1). The forearc basins are separated by transverse ridges with elevations of 1000–1500 m above the basin seafloor and a thin sediment cover. To the East, the Lombok Basin is controlled by the collision of the Scott Plateau with Sumba Island and the Banda arc, resulting in an uplift of the eastern part of the basin. The basement of the Lombok Basin is of unknown nature, but has been interpreted variously as anomalously thick oceanic crust, rifted continental crust or as metamorphosed accretionary prism (Dickinson, 1995). Five almost undeformed seismostratigraphic units have been interpreted in the Lombok Basin based on early seismic measurements until the 1980s and analogies to well data from the Bali Basin in the backarc area north of Bali (Van der Werff et al., 1994). Horst and graben structures in the basement have also been recognized, suggesting that the basement is of continental origin. The maximum sediment thickness amounts to around 4.5 km. Carbonate platforms developed during the Eocene. This implies that the basement subsided from the sea surface by nearly 10 km (Van der Werff et al., 1994).

3. Methods, data acquisition, and processing

During Leg 1 of cruise SO190 with research vessel SONNE from 9th October to 9th November 2006, twenty profiles of multichannel seismic reflection (MCS) data were acquired (Fig. 1). A tuned G-gun array comprising 16 airguns with a total volume of 50.8 l, working pressure of 145 bar, array length of 15.5 m and a towing depth of 6 m served as seismic source. The shot interval of 18 s corresponds to 50 m at a speed of about 5 kn. Data were acquired with a 240 channel streamer of 3 km length (group interval: 12.5 m). Record length was 14 s at a sampling interval of 2 ms. Nominal coverage was 30-fold.

Conventional common midpoint (CMP) processing of the twenty MCS lines produced Kirchhoff poststack time and depth sections as a standard, mainly for a first quality control. Kirchhoff prestack depth migrations (PreSDM) on the six North–South running lines and most of the intersecting lines (Fig. 1) were then used for velocity building and enhanced imaging. Major issues in seismic processing were identified in multiple rejection and velocity model building. For seabottom multiple attenuation various approaches were tested, among them parabolic Radon filter with inner trace mutes, f–k-filter and wave equation based prediction. However, because of varying results within individual seismic lines, the filter attenuated successfully the multiples, but often also deep reflections, e.g. from the interface between upper and lower plate, we decided to use consistently a prestack time-variant bandpass filter (passband 4–26 Hz in the lower part of the recordings where higher-frequency multiples prevail) permitting residuals of the multiples in some parts of the sections. A frequency range of 4–120 Hz proved to be profitable in the upper sedimentary part of the sections. After conversion of smoothed stacking velocities to interval-depth velocities, these models served as initial models for the migration velocity analysis (MVA) using PreSDM of common offset sections. The upper, sedimentary part of the velocity models was iteratively improved from top to bottom using the focussing technique. Because of the limited offset range, this approach was not sensitive enough for the deeper parts of the profiles. Therefore, the upper, sedimentary part was fixed and then extended towards greater depth using the tomography approach of the refraction/wide-angle modelling (see below). Because of computing time considerations, the frequency range was limited to 4–60 Hz for prestack depth migration. The resulting velocity–depth model was additionally used for poststack time and depth migrations with the full frequency and resolution range. Therefore, for interpretational and quality control purposes poststack time and depth migrations as well as prestack depth migrations were considered.

Leg 2 of cruise SO190 from 11th November to 22nd December 2006 was dedicated to refraction/wide-angle seismic observations with ocean-bottom-seismometers (OBS). A cluster of 8 G-guns with a total volume of 64 l was used as seismic source. Average spacing between shots was 100/150 m and average OBS spacing was 6 km. 28 instruments were used on 239 sites. Four corridors were covered, including some cross-lines (Fig. 1), resulting in approximately 1900 line-km. Seismic tomography inversion for the Vp velocity distribution was performed by running a joint refraction/reflection inversion (Korenaga et al., 2000), complemented by forward seismic modelling and gravity modelling. Individual corridors are described and interpreted by Shulgin et al. (2009) and Planert et al. (2010).

Swath bathymetry was acquired by the shipboard 12-kHz SIMRAD EM 120 system. The data from the two legs were edited (for outliers) and merged to provide a consistent map over the area, extending the maps compiled by Ladage et al. (2006) and Franke et al. (2008) towards the East.

Echosounding was performed by the shipboard PARASOUND system which works as a low-frequency sediment echosounder and as a high-frequency narrow beam sounder to determine the water depth with a hull-mounted transducer array. It utilizes the parametric

effect which produces additional frequencies through non-linear interactions of acoustic waves of similar frequencies, 18 kHz and 22 kHz, which produce a resulting frequency of 4 kHz. Depth penetration in flat sedimentary sections is often of the order of 100–150 m. The analogue traces of 250 ms around the seafloor are digitized onboard and transformed into the seismic SEG-Y format with the time delay and GPS-based coordinates saved to their headers, and were thus suited to seismic processing.

We also recorded magnetic data using a towed magnetometer array consisting of two total field sensors (Overhauser type) operating in gradiometer mode and one oriented vector magnetometer (fluxgate type). Gravity data were obtained by the gyro-stabilized

Askania type sea gravimeter KSS31M. Details of potential field data acquisition and processing are described in the cruise report (BGR, 2006).

4. Major structural units

Fig. 2 shows a compilation of the six N–S running 250–380 km long profiles, consistently processed with the PreSDM approach. They extend from the Indo-Australian plate over the deep sea trench, the accretionary prism, the outer arc high, the forearc basin to the slope of the island arc. The most striking observation concerns the imaging of the subducting upper/lower plate interface over 70 km and related

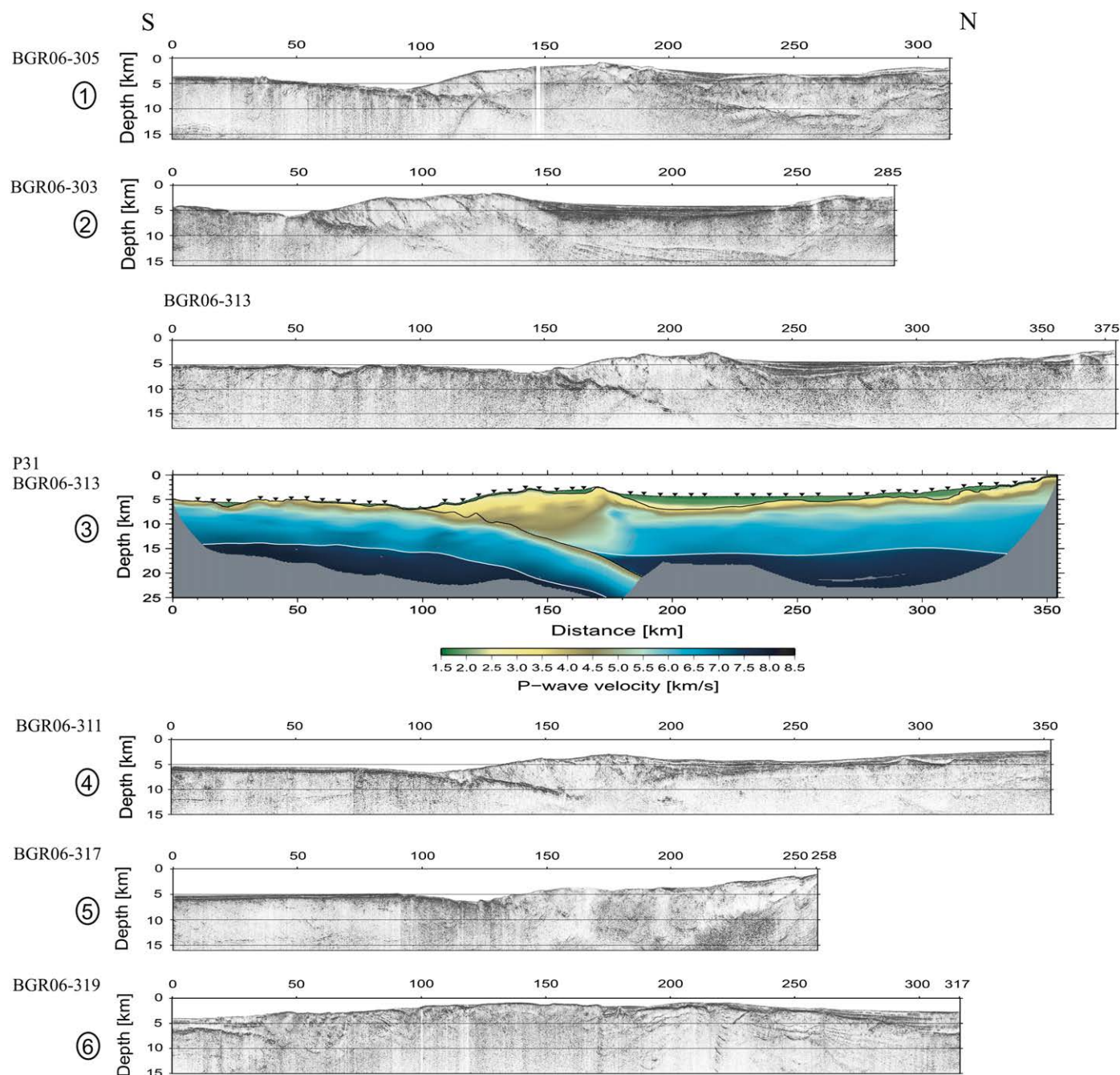


Fig. 2. Compilation of six North–South running profiles from West (top) to East (bottom) traversing oceanic crust, deep sea trench, accretionary prism, outer arc high and forearc basin (see Fig. 1 for location) derived from Kirchhoff prestack depth migration (PreSDM) with a frequency range of 4–60 Hz. Profile BGR06-313 shows exemplarily a velocity–depth model according to refraction/wide-angle seismic tomography on coincident profile P31. Triangles indicate positions of ocean-bottom seismographs. Vertical exaggeration of all sections is 2:1.

splay faults within the accretionary prism and outer arc high. Comparable seismic imaging results are known from the Nankai Trough offshore Japan (Park et al., 2002). Velocity control is shown exemplarily for line P31 (coincident with the longest MCS line BGR06-313). In the following we discuss the individual sections from South to North based on Fig. 2, then in chapter 5 in more detail from West to East in Figs. 3–14.

4.1. Indo-Australian crust

The subducting oceanic crust is characterized by only a few hundred meters thick sedimentary cover. The sediment thickness on the continental Australian crust (Scott Plateau) just south of the main deformation front reaches 2 km (Fig. 2, easternmost section BGR06-319). The water depth seaward of the trench changes from about 3500 m in the westernmost profile (Roo Rise) to 5000 m (Argo Abyssal Plain) and again to 3500 m at the Scott Plateau on the easternmost profile. A pronounced bulge seaward of the trench is not observed even on the longest profile BGR06-313. Instead, a stepwise downbuckling over a distance ranging between 30 km and 70 km, decreasing from West to East, is observed before reaching the deep sea trench and the deformation front. This is an indication of an old non-elastic lithosphere under rigid deformation. The steps or vertical displacements are related to normal faulting within the oceanic crust as response to the downbending. Crustal and mantle velocities are remarkably decreasing when approaching the deep sea trench, probably caused by intruding seawater (normal faults as pathways) and subsequent serpentinization. On profiles BGR06-311 and -317, where the sea floor is particularly smooth, continuous reflections from the crust–mantle boundary are observed, indicating a 7–9 km thick crystalline oceanic crust.

4.2. Subduction complex

In the deep sea trench only little sediments accumulated due to the thin sediment cover of the oceanic crust. Landward of the deep sea trench, a pronounced interface of complex shape between upper and lower plate is observed over a distance of 50–70 km on most of the profiles. Further imaging of the plate interface is prevented most likely due to the increasing subduction angle or due to a loss of reflectivity because of dewatering. The 70–120 km wide (widest opposite to the Roo Rise) subduction complex on top is up to 12 km thick with sediment-type velocities. Van der Werff (1995) postulated that the decreasing width of the complex towards the East may be due to the younger age of the subduction system. The accretionary wedge and its older part, the outer arc high, has long been suggested as being trench-fill turbidites, pelagic sediments and oceanic crust scraped from the descending oceanic plate by the leading edge of the overriding plate to which they become accreted (e.g. Karig and Sharman, 1975; Schlüter et al., 2002). Our sections show that the entire subduction complex is characterized by a northward dipping system of imbricate thrust sheets with major thrust faults of listric shape connecting seafloor and plate interface. These faults are associated with pronounced breaks in morphology at the seafloor. Small piggy-back sedimentary basins are observed between the morphologic kinks, particularly seaward of the Lombok forearc basin.

4.3. Forearc basin

The Lombok forearc basin located between the outer arc high and the volcanic island arc is up to 120 km wide with up to 4500 m of sediment thickness and water depth of about 4000 m (Fig. 2, lines BGR06-303, -313 and -311). The basement is characterized by a central high or horst. Several unconformities are visible within the sedimentary succession. The basin is underlain by anomalously low mantle velocities at relatively shallow depths of about 15 km, which

might be due to an alteration from dehydration processes by rising fluids within the subducting oceanic plate. Seismostratigraphic analysis of the basin fill based upon early seismic profiling in the context of hydrocarbon exploration has been carried out by Van der Werff et al. (1994). On the westernmost profile BGR06-305 a basement high or ridge without sediments divides the basin into two parts with 1–1.5 km sediment thickness. The easternmost profiles BGR06-317 and -319 are characterized by the collision of the oceanic/continental Indo-Australian plate with the block of Sumba Island. Underthrusting of the Scott Plateau beneath a large accretionary prism and the Sumba block is observed, which produces uplift and a large bivergent structure. The Savu basin with up to 4 km sediment thickness is shown at the northern end of the easternmost profile.

5. Results and discussion

In the following Sections 5.1–5.4 we discuss the main structural units, the Roo Rise (Section 5.1) and the Argo Abyssal Plain (Section 5.2) with their influence on the overriding plate, the Lombok forearc basin (Section 5.3) and the transition zone between the subduction regime in the West and the collision regime in the East (Section 5.4) in further detail. All figures with few exceptions are based on the PreSDM approach.

5.1. Roo Rise and forearc

On profile BGR06-305, in the west of the study area (Fig. 3), we zoom into the coupling zone of upper and lower plate with the accretionary wedge on top. Landward of the Roo Rise the seabottom is about 1–2 km higher than on the other profiles. The downbending oceanic crust is segmented by steep normal faults which appear to become reversed due to compression when approaching the deep sea trench. Exceptionally, sediments gradually accumulate over a distance of 30 km in front of the trench up to 2 km thickness within the trench. This is probably due to reverse backthrusting and folding induced by the toe of the accretionary wedge. Turbiditic slumps from the inner-trench slope (3–4°) may contribute to this thickness. There are signs of buried seamounts beneath the accretionary prism (Fig. 3) similar to those interpreted by Collot et al. (2008) at the erosional North Ecuador–South Colombia oceanic margin. Correspondingly, the bathymetry exhibits signs of subcircular indentation at the inner trench slope. The boundary between upper and lower plate, which is imaged over 70 km length, is of irregular shape with km-wide vertical displacements obviously imprinted by the complex shape of the subducting oceanic basement. This may be interpreted as duplex building with most of the oceanic sediments beneath and in front of the accretionary wedge. Landward dipping reflections at the toe of the accretionary wedge indicate that sediment sheets are attached to the base of the wedge. The wedge is fairly transparent over a distance of about 20 km. However, at the pronounced slope break, a series of steep landward dipping reflections, obviously thrust sheets, connect to the plate interface at about 9 km depth. Here, the interface changes its dip and shape abruptly. We speculate that a major block of the Roo Rise or perhaps even the onset of the Roo Rise, has arrived here and produced compression-related uplift during the last 500,000 years (at a convergence rate of 7.3 cm/a). The splay faults of the thrust sheets, which originate here, and the pronounced slope break indicate recent movements which produce the ridge between adjacent forearc basins. This uplift is also confirmed by pronounced unconformities of a sedimentary wedge with steeply dipping reflections at the western part of the Lombok forearc basin.

The deformation pattern within the subduction zone and forearc is imaged on all N–S running profiles, however, most prominently, on profile BGR06-303 (Fig. 4). Normal faulting dissecting the oceanic crust with vertical offsets of 0.5 km and block widths of 5–10 km is observed on the outer-trench slope. Most of the oceanic sediments are

subducted and underplated beneath the accretionary wedge to form a several kilometer thick reflection pattern including duplex structures. A single décollement is not observed. Instead, a zone of ~2–3 km thickness showing high amplitude reflections characterizes the interface between subducting and overriding plate. Thrusts are observed across the whole subduction system and form an imbricate fan system. The thrusts branch from the duplex zone and generate pronounced breaks in seafloor morphology at their upper end. The length of the duplexes seems to be controlled by the length of the dissected blocks of the incoming oceanic crust. In the case of a sudden major slip between upper and lower plate, perhaps causing also a greater earthquake, it will appear that this slip is partitioned into several branches (see arrows in Fig. 4). The slip may be deviated at the edges of the dissected oceanic blocks, which might act as bulldozers against the bottom of the upper plate, towards the seabottom where they cause horses with breaks in the morphology. From there the sediments are partly transferred towards the trench where they are recycled, and/or fill the piggy-back basins at the slope. At the toe of the accretionary wedge slump activity can be recognized by the echosounder recordings (Fig. 4b). Therefore, the subducted sediments may be partly incorporated into a cycle, first being underplated beneath the outer arc high, then thrust upward and slumped down into the trench again. This cycle is ongoing, and first of all, recently active over the entire subduction complex along out-of-sequence splay faults, not only at the accretionary wedge. This is convincingly demonstrated by the structure of several small piggy-back basins (Fig. 5). Their sediment infill is entirely seaward tilted in the two southernmost piggy-back basins by thrust activity of the outer arc

high basement sheets. In the middle piggy-back basin, a vertical displacement of about 100 m, particularly seen in the echosounder recordings, indicates recently active movements. In the northernmost basin the reflectors are almost horizontal, but thrusting along splay faults may tilt these sediments in the future, similar to the two southerly located basins, thus indicating out-of-sequence thrusts.

5.2. Argo Abyssal Plain and forearc

The piggy-back basins on the outer arc high are located between major breaks in seafloor morphology. These breaks and corresponding basins can be correlated in E–W direction over more than 300 km (Fig. 6). This segment length at a water depth of 1–2 km gives a tremendous tsunami hazard in case of a sudden displacement of several meters related to a megathrust earthquake. The E–W extension of the piggy-back basins and their confining breaks in the seabottom morphology correlate with the extension of the Lombok forearc basin, and furthermore, roughly with the E–W extension of the Argo Abyssal Plain. Therefore, a genetic relationship between these major structural units of the subduction system can be assumed. The high perpendicular convergence rate of 73 mm/yr in combination with old oceanic crust, which is relatively cold and brittle, may be responsible for growth and deformation of the entire forearc system, despite of relatively low sedimentary input as compared to the arc further west. Because of the general segmentation of the oceanic crust in E–W as well as in N–S direction, slip in case of large earthquakes originating at the megathrust within the seismogenic zone (beneath the forearc basin) will not proceed along a single décollement towards

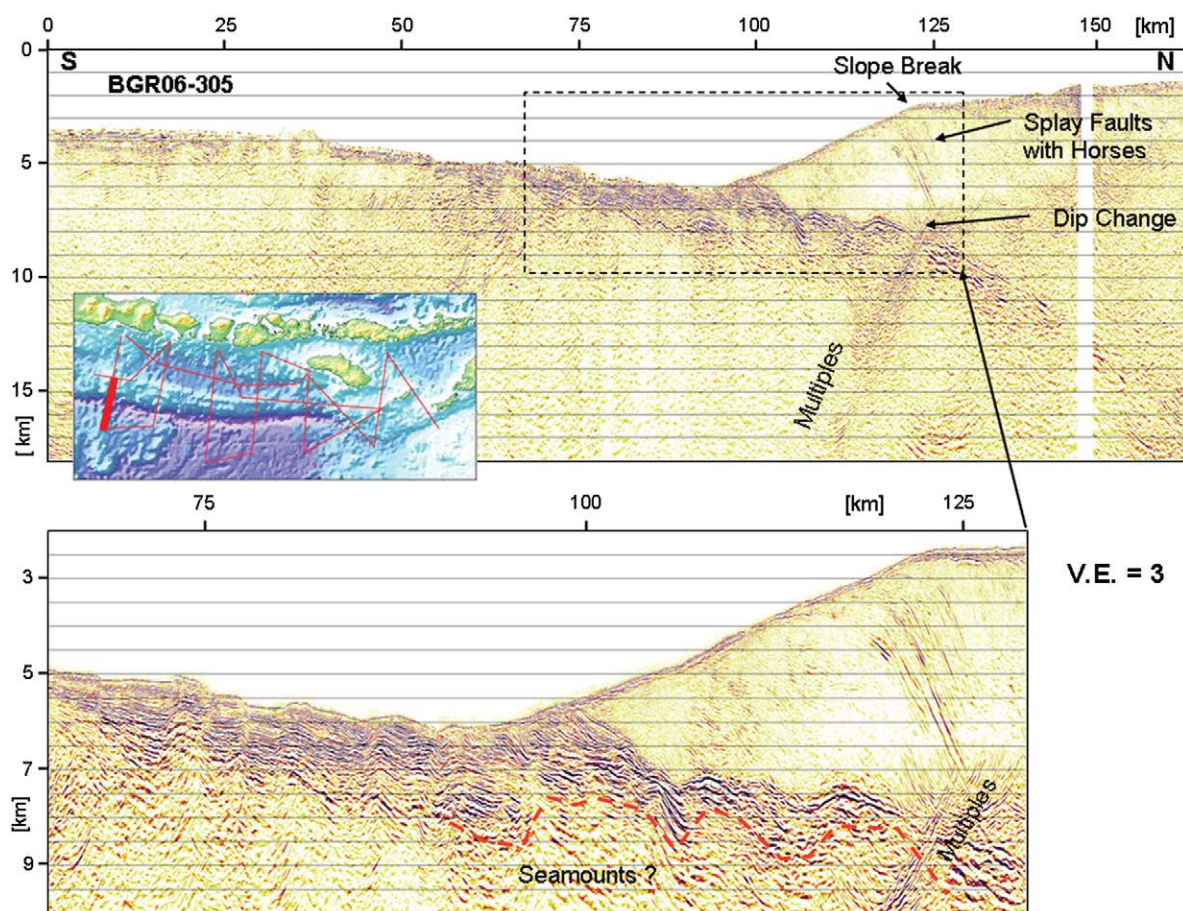


Fig. 3. Details of profile BGR06-305 (PreSDM). For location see inset. Note the prominent interface between lower (oceanic, Roo Rise) and upper plate, and thrust sheets and splay faults within the subduction complex. The bottom of the highly reflective sediments is offset by about 1 km beneath the toe of the accretionary wedge, which might be caused by subducting seamounts.

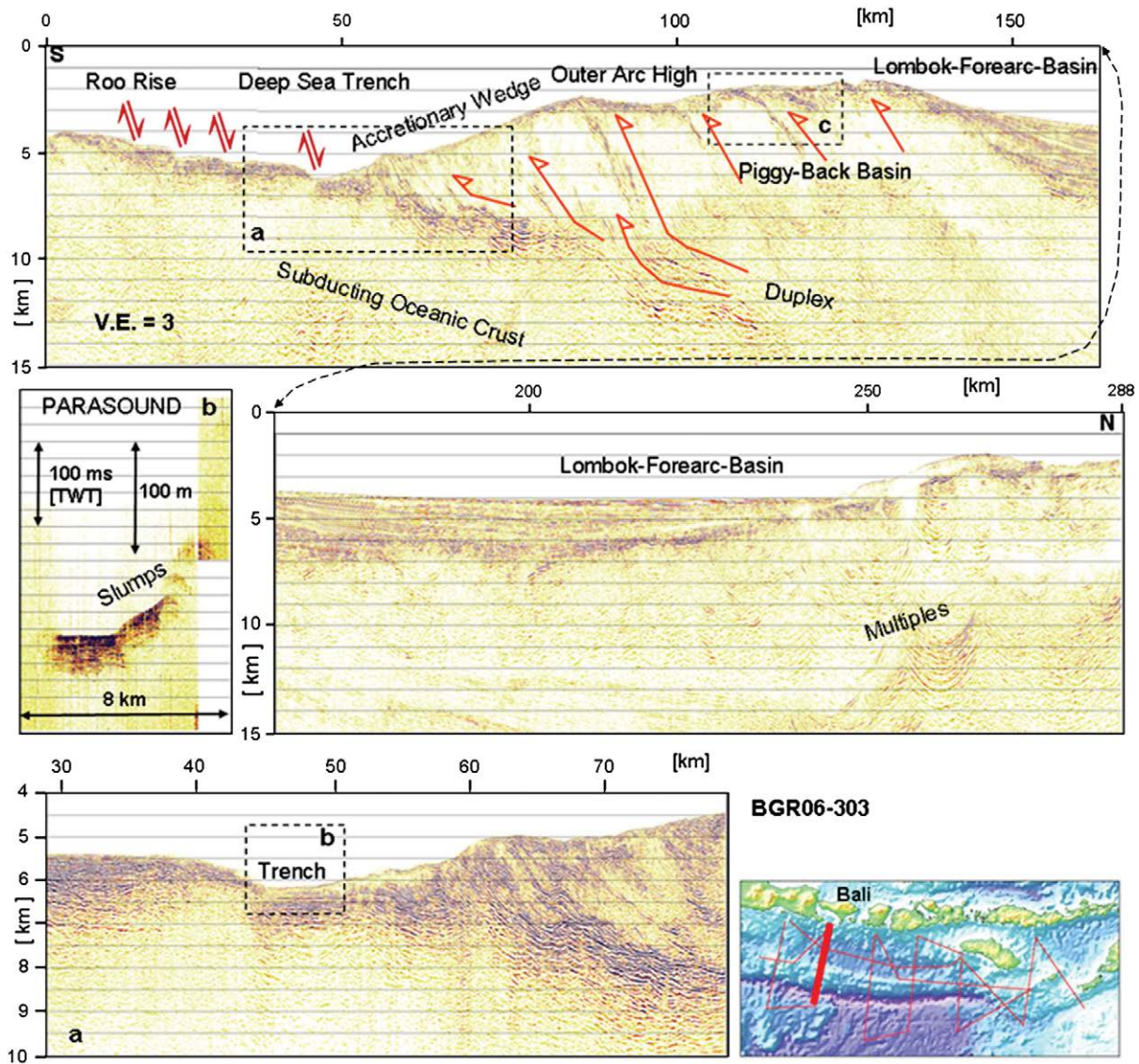


Fig. 4. Details of profile BGR06-303 (PreSDM). See inset for location. Arrows mark relative movements, normal faulting in the outer trench, thrust faulting within the subduction complex. Note that arrows for opposite relative movements are omitted for clarity. Frame (a) marks position of lower left section. Echosounder (b) detail shows slump activity from the inner trench slope. Frame (c) in the upper right corner points to Fig. 5.

the trench, but will be transferred and partitioned into several splay faults as outlined before. Reduced friction due to high water content within the duplexes and the splay faults will facilitate this process. We interpret the high reflectivity of the interface duplexes and the splay faults as due to high porosity with a high fluid content. Seismicity is not observed along the 50–70 km imaged upper/lower plate transition zone (e.g. Spicák et al., 2007). From seismological, bathymetric and echosounding evidence from the great 2004 Sumatra earthquake area Sibuet et al. (2007, and references therein) concluded that the main slip was partitioned into three splay faults distributed over the outer arc high with co-seismic motion (destructive tsunami) of maximum slip at the Upper Thrust Fault. A tsunami catalog of Indonesia (1600–1999) from Hamzah et al. (2000) lists about 10 destructive tsunamis in the East Sunda Arc.

Duplex formation at different scales and modes is the prevailing process at the plate interface upper/lower plate instead of a single décollement. A 1–2 km thick duplex structure is visible beneath the toe of the accretionary wedge on profile BGR06-313 (Fig. 7). The upper/lower plate transition consists of a series of branching thrusts building multiple imbricates. These imbricate sheets are composed of a melange of oceanic sediments and crystalline crust as well as

sediments of the upper plate wedge. The geometry of the glide planes is concave upward and continues generally into landward dipping thrusts of the outer arc high. The preexisting oceanic spreading structures and blocks, where fracturing of the oceanic crust is initiated, strike obliquely to the profile direction, thus causing possible offsets between splay faults and duplexes (Fig. 7). Crosscutting features in the upper/lower plate interface are also indicative of this 3-D effect. In principle, younger parts of the oceanic plate underthrust the already subducted parts, which are continuously compressed and steepened. Since about 1500 km of oceanic plate have been subducted already, a continued process as described may have formed the basement of the outer arc high, the forearc basin as well as the basement of the island arc east of Java, composed of ophiolite sheets and napes as described e.g. by Nicolcas (1989). Stratigraphic studies of the Sumatran forearc islands revealed an inhomogeneous basement with large intact sections of ophiolitic material on some islands and evidence for both oceanic and continental basement elsewhere (Samuel et al., 1997) which might indicate similar characteristics of the forearc basement in our study area. At this point we predict that the basement of the forearc basin exhibits a heavily broken geometry because of steeply dipping ophiolitic sheets (compare Fig. 12). Seismic

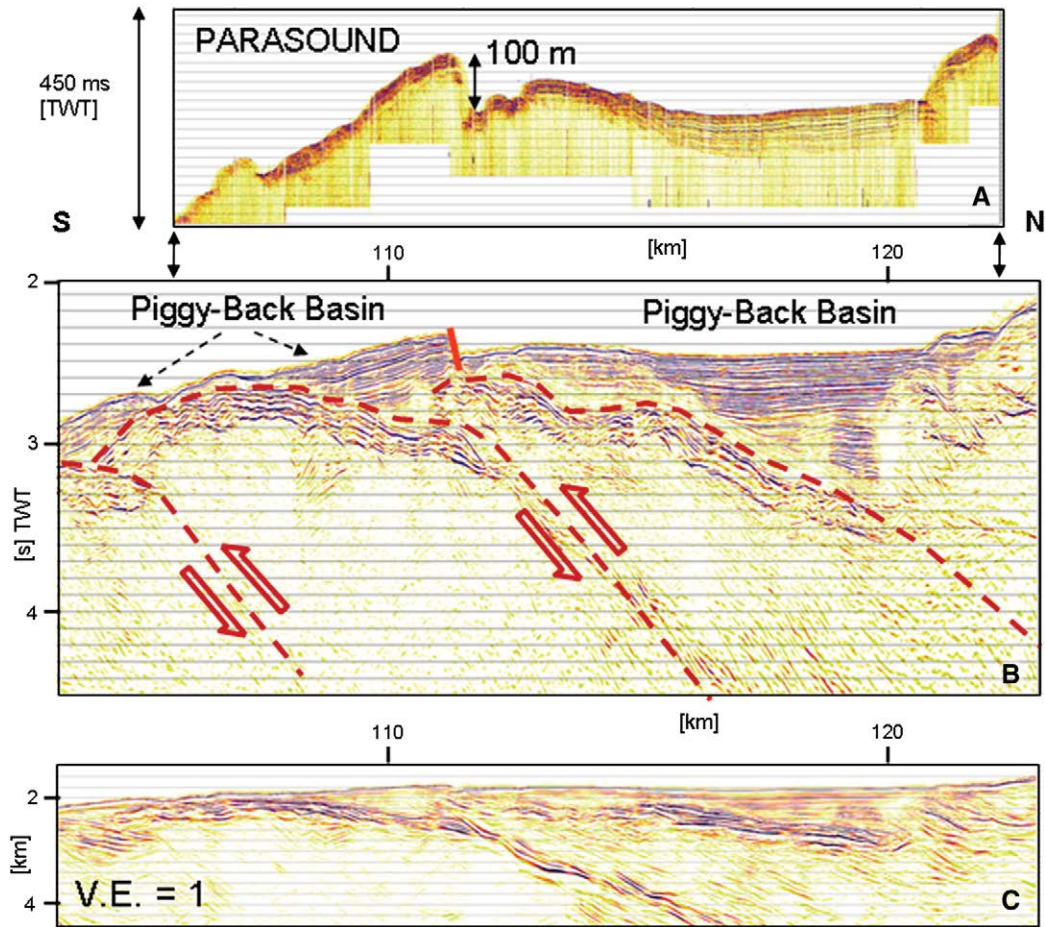


Fig. 5. Pattern of three piggy-back basins on top of the outer arc high. Arrows indicate proposed thrust activity within the outer arc high basement, which is responsible for tilting of small basins. A: Echosounder image. B: Post-stack time-migrated (4–120 Hz) section corresponding to frame (c) in Fig. 4. The vertical displacement of 100 m in the centre of the section marks recent activity. C: Coincident pre-stack depth migrated (PreSDM, 4–60 Hz) section without vertical exaggeration. The thrust sheet of the outer arc high basement in the centre of the image is interpreted to have uplifted and extended the overlying piggy-back basin. Its southernmost wedge-shaped part then becomes rotated anticlockwise.

velocities are sedimentary-type in the outer arc high, however they are locally increased at the transition to the forearc basin (Fig. 2) which has been pictured by Hamilton (1979) as a buttress formed by the outer edge of the overriding lithosphere. Hamilton (1979) already presented a profound picture of the mechanism of offscraping masses

of oceanic crust and mantle and their transport together with sediments via imbrication into the wedge.

An even more drastic situation concerning the upper/lower plate interface is observed on profile BGR06-311 (Fig. 8). Normal faulting affects the oceanic sediments and their basement over a distance of 40 km seaward of the trench. The bathymetry shows that this corresponds to a belt of ripples striking obliquely to the trench and parallel to magnetic lineations. In contrast to the previously described N–S running profiles, the plate interface is relatively smooth over long distances. The great difference occurs beneath the toe of the accretionary wedge, where a prominent break is visible. A similar offset of the plate interface has been observed by Hamilton (1979, his Fig. 9) with similar implications. This break seems to be present at the base of the oceanic crust, too. The crust–mantle boundary is imaged on this profile nearly continuously as a discrete reflection band at 7–8 km beneath the seafloor. The crystalline part of the oceanic crust is relatively transparent or shows scattered events. The displacements in the plate interface and crust–mantle boundary may be interpreted as the initial stage of underthrusting of the seaward part of the entire oceanic crust beneath the subducted crust, or in other words, the initial stage of a large duplex formation. Such duplexes with horses dipping to the Hinterland (island arc) may form the basement of the forearc basin. Duplexes or imbricate thrust structures at the upper/lower plate interface occur in our study area at different sequences and dimensions and may have a mixed character: imbricate thrust structures in which the faults develop from Hinterland (forearc) to Foreland (ocean) or imbricate thrust structure in which the faults

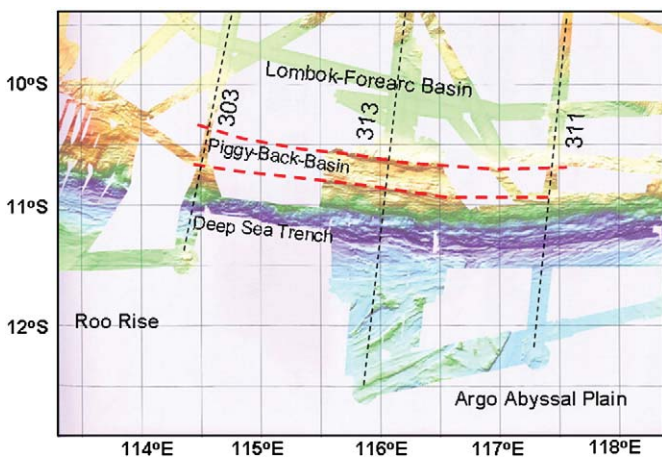


Fig. 6. Bathymetry showing seafloor morphology in the area of the three profiles BGR06-303, -313 and -311 as map view. Note that pronounced breaks (dashed lines) in seafloor morphology of the outer arc high and related piggy-back basins correlate over more than 300 km in E–W direction.

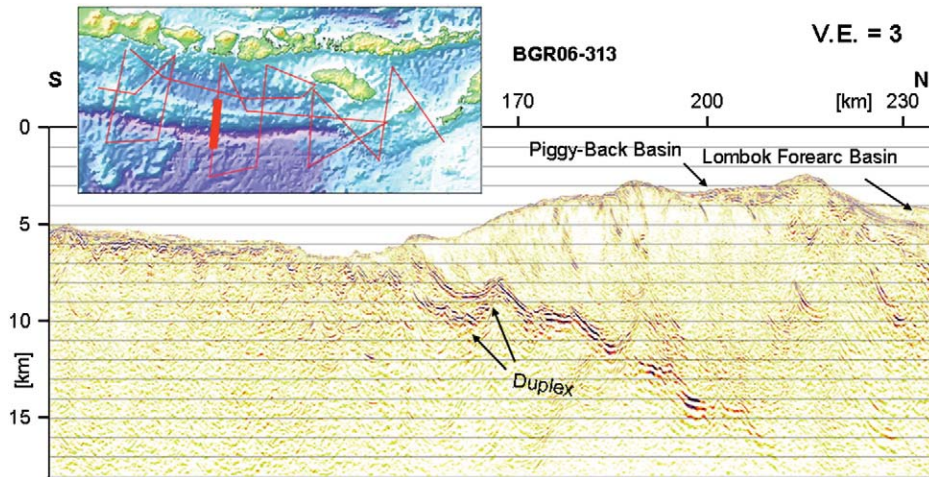


Fig. 7. Details of profile BGR06-313 (PreSDM) in the Argo Abyssal Plain area. See inset for location. Note the wavy interface upper/lower plate. Morphologic highs on the outer arc high with the piggy-back basin in between correlate with similar features of the profile further west.

develop from Foreland to Hinterland. The dimension of the imbricate slices is determined by the length of oceanic blocks after fracturing and normal faulting in the outer trench zone. We argue that this duplex formation may be the principal cause for the evolution of the basement of the outer arc high and the forearc basin. From a seismic line acquired offshore Sumatra across the 2004 Sumatra earthquake epicentral region Singh et al. (2008) reported on broken oceanic crust and interpreted a pair of reflections beneath the forearc basin and above the inferred oceanic slab as a detached piece of the slab produced by oceanic crust underplating. We interpret the crustal thrust at the toe of the accretionary wedge in profile BGR06-311 (Fig. 8) as the onset of such underplating. The crustal thickening

beneath the continental shelf of Vancouver Island, revealed by seismic reflection profiling and velocity models, has been interpreted by Calvert et al. (2006) also through duplex formation at the subduction décollement.

Earthquake focal mechanisms confirm the mechanism described above (Fig. 9). A belt of extensional mechanism of relatively shallow earthquakes is located in front of the trench. Compressional mechanism of deeper earthquakes may correspond to the seismogenic zone beneath the forearc basins and the volcanic arc. Magnetic lineations correlate roughly with elongated ripples in the oceanic seafloor indicating that extensional faulting occurs at preexisting oceanic structures produced at the former seafloor spreading centre.

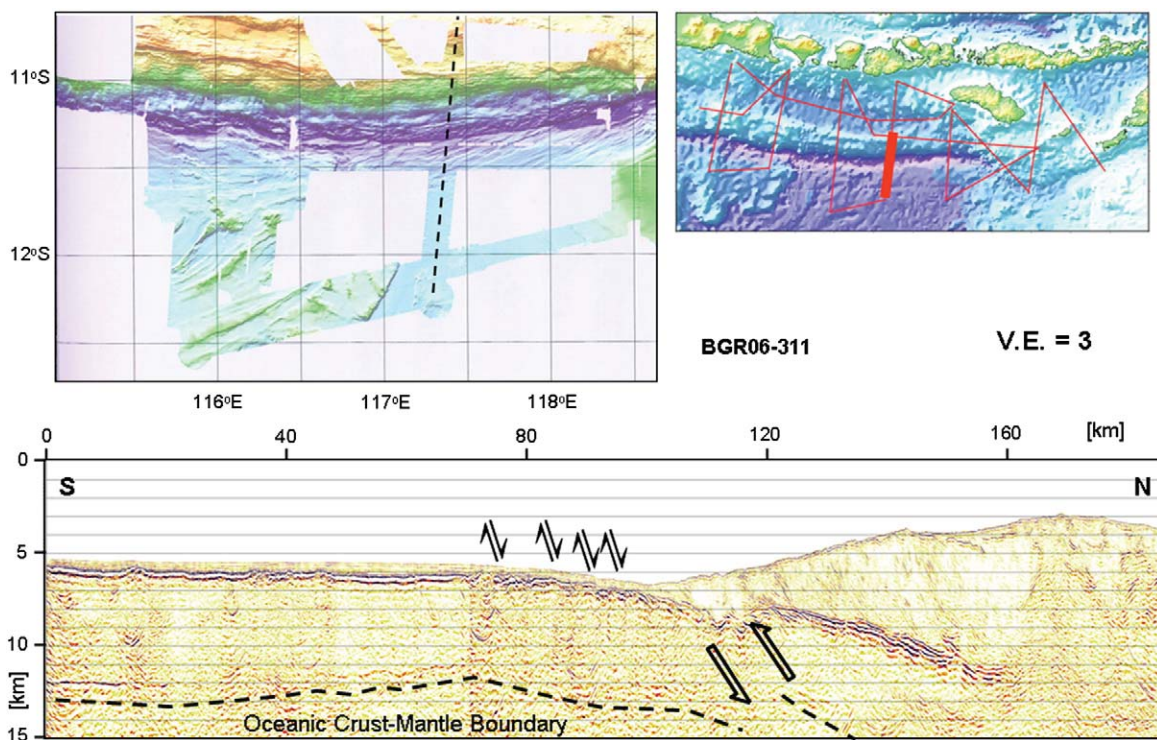


Fig. 8. Details of profile BGR06-311 (PreSDM) in the Argo Abyssal Plain area. Arrows mark relative movements with normal faulting in the outer trench slope. The upper/lower plate interface beneath the outer arc high is relatively smooth, in contrast to other profiles. However, beneath the toe of the accretionary wedge a prominent break is visible, which is mirrored also at the base of the oceanic crust (Moho). Large arrows indicate interpreted thrust movements affecting the entire oceanic crust. Note that the dashed line indicating the oceanic crust–mantle boundary has been shifted a little to greater depth in order to not obscure the boundary. Bathymetry (upper left) shows rippled seafloor south of the trench, corresponding to the belt of normal faulting.

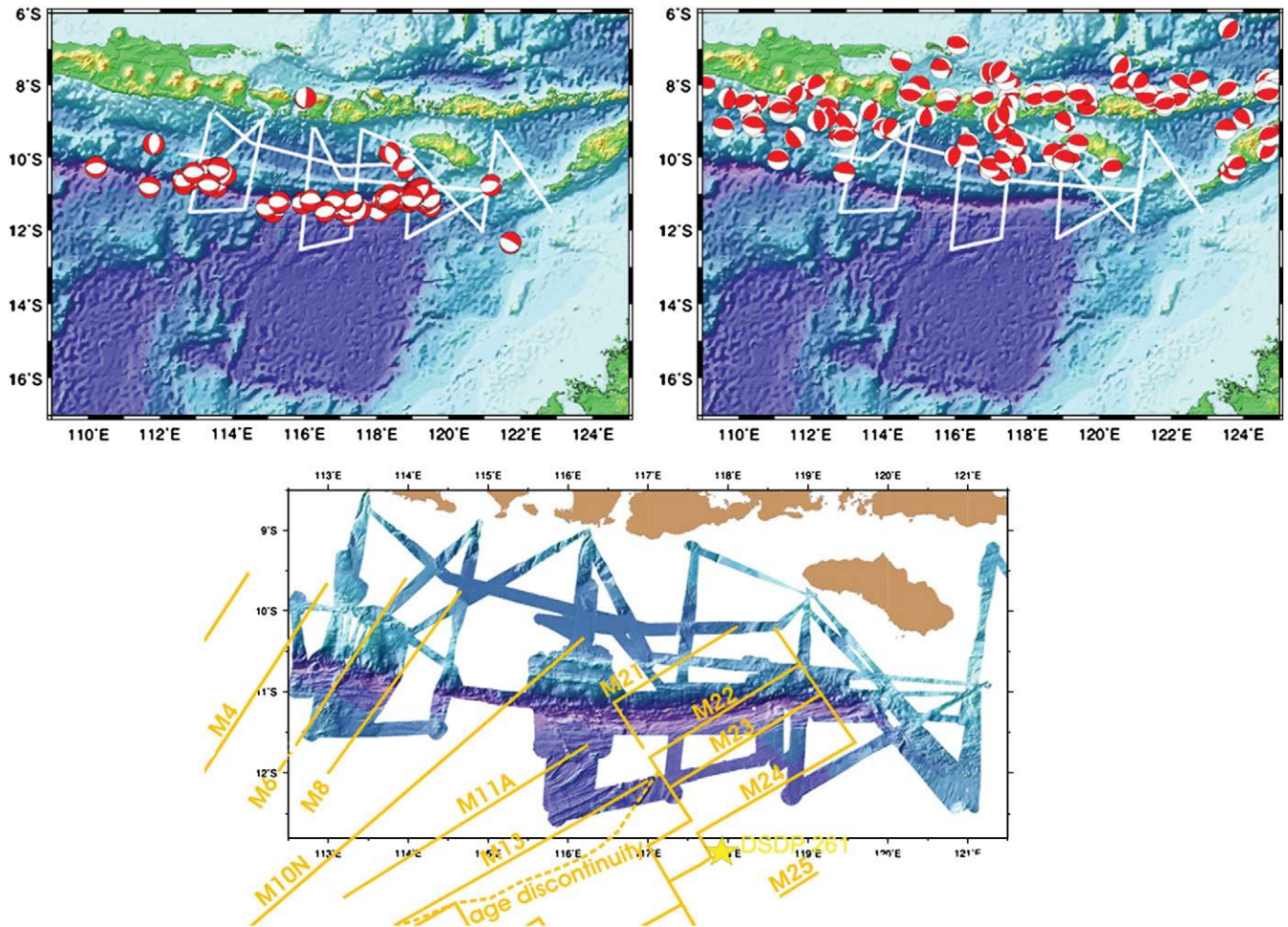


Fig. 9. Focal mechanism of shallow earthquakes (Engdahl, pers. comm., 2008; Engdahl et al., 2007) selected for focal depth lower than 30 km (10 km depth resolution) of normal faulting type (upper left) and all earthquakes (10 km depth resolution) of thrust type (upper right) in the study area. Normal faulting southward of the trench is characterized by an extensional regime (upper left). Compressional mechanism (upper right) may correspond to the seismogenic zone beneath the forearc basins and the volcanic arc. Note that beneath the outer arc high there is no earthquake activity. Bathymetry and interpreted magnetic lineations are shown at bottom. Plate convergence is in North–South direction. Age of subducting oceanic plate increases from West to East from Cretaceous (Roo Rise) to Jurassic (Argo Abyssal Plain).

These pre-existing oceanic spreading structures, since they strike at an oblique angle to the trench, together with transform faults, may be responsible for segmentation of the subducting plate leading to the variety of plate interface geometries from West to East. A dramatic segmentation in North–South direction is visible on profile BGR06–317 (Fig. 10). The oceanic crust is segmented into 5–7 km wide blocks which show vertical displacements of about 1 km against each other. The blocks are rotated as they approach the main deformation front.

Thick sediment wedges have been formed between the basement blocks. We speculate that there is also a block rotation in E–W direction. These structures may be seen as ramps where imbricate thrust sheets develop, obviously driven by the enhanced compression between the oceanic plate and the upper plate, which is thickened here because of the collision of the continental Scott Plateau and Sumba Island little further east. Hamilton (2007) presented the idea of subduction-hinge rollback and subduction driven plate movements,

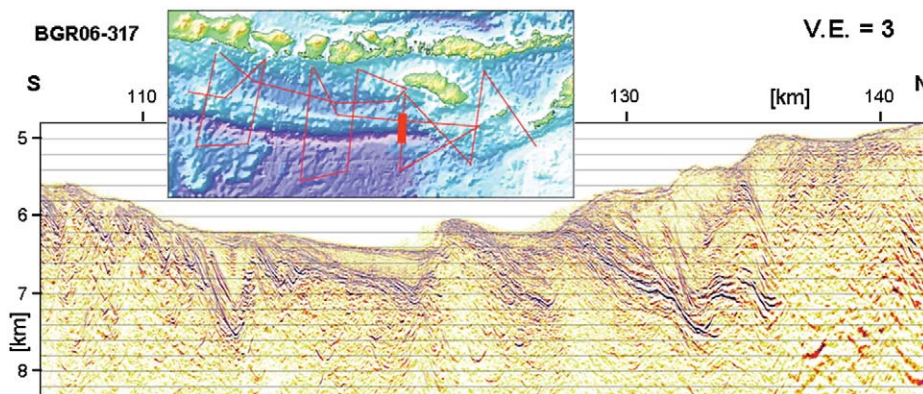
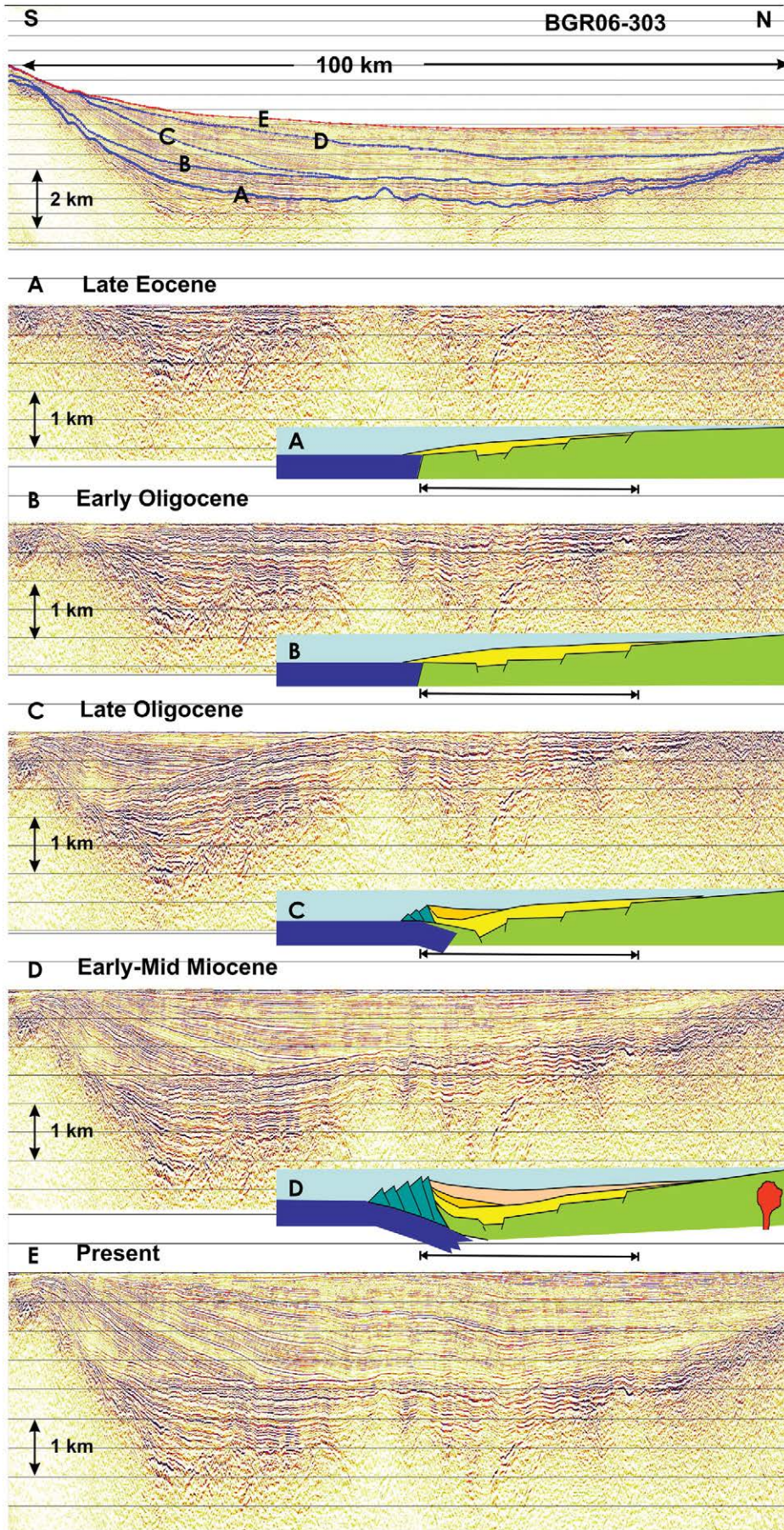


Fig. 10. Details of profile BGR06–317 (PreSDM). See inset for location. Note the heavily broken oceanic crust while subducting beneath the upper plate.



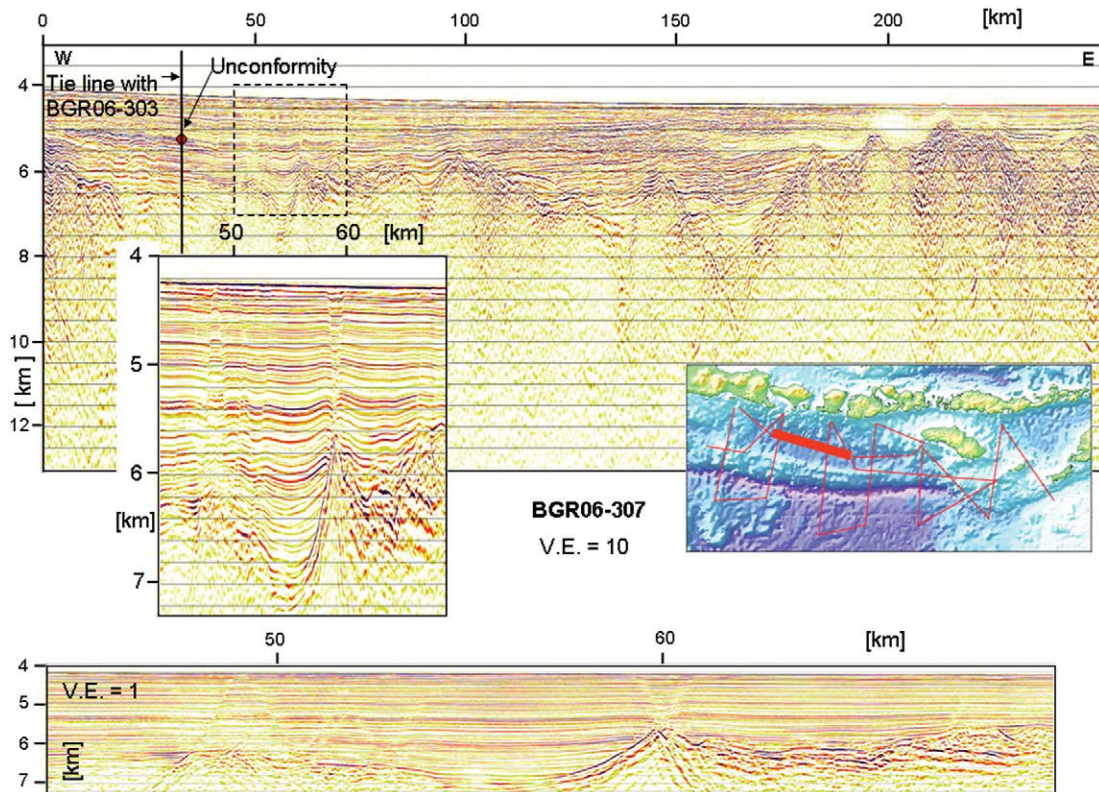


Fig. 12. Profile BGR06-307 (PreSDM) at full length (top). Zoom (middle) corresponds to frame above. Same zoom without vertical exaggeration at bottom. See inset for location. Note the irregular geometry of the basement of the Lombok forearc basin. Several 60° dipping faults in the basin are probably caused by differential compaction.

provoking also conceptual shifts in global dynamics, in major parts based on observations at the Sunda Arc. This implicates forces through slab pull of the old and dense oceanic plate. We see a possible conflict with our interpretation that the oceanic crust is fragmented entirely or dissected into major blocks that behave individually. In this case crustal stresses may not be transmitted over long distances. An overall compressional regime seems to be dominant instead of an extensional regime related to slab pull. However, the 1977 Sumba earthquake, located beneath the eastern Sunda trench, provided evidence for normal faulting throughout the upper 28 km of the oceanic lithosphere and thus for slab pull forces (Spence, 1986). Further complication is provided by the embedment of the anomalous Roo Rise and the Scott Plateau, which might resist further subduction and produce compression and collision structures such as duplex building.

5.3. Lombok forearc basin

Recent deformation with prominent vertical components is not only confined to the accretionary wedge nor to the outer arc high as demonstrated by out-of-sequence splay faults and tilted and disrupted piggy-back basins (Figs. 4 and 5) but also affect the formation of the Lombok forearc basin. A major unconformity (Fig. 11 top, horizon B) and a shift of the depocentre towards the North are expressions of vertical movements during basin development. This can be demonstrated by a simple restoration through flattening of selected horizons. As there are no severe time constraints, we adopted our time scaling to that of a seismic stratigraphy presented by Van der

Werff et al. (1994, and references therein) based on early single-channel and multi-channel reflection profiles obtained until the end of the 1980s. Until Late Eocene a passive margin existed with a continuously thickening sedimentary shelf basin (Fig. 11A). The basement shows signs of a rifted continental margin by horst and graben structures. However, as discussed earlier, the basement could also consist of stacked ophiolitic nappes. The nature of the basement has long been in debate (e.g. Dickinson, 1995). We speculate, that the basement is gradually changing from continental character beneath Sumatra and Java (Sundaland) to intermediate or mixed character further east below the present island arc.

The insets in Fig. 11 show the development of the forearc basin schematically in response to the initiation of subduction which influences the sedimentation pattern in the forearc basin. At about Late Oligocene the onset of oceanic subduction occurs pushing or pulling the southern part of the basin downward. The Early Oligocene horizon (Fig. 11B) is observed as unconformity where sediment wedges onlap until Late Oligocene (Fig. 11C) derived from a raising accretionary wedge at the southern margin of the basin. While the accretionary wedge grows towards the ocean, rebound forces lift the southern part of the basin upward, now showing downlapping strata on the unconformity (Fig. 11D). The depocentre of sedimentation moves to the centre of the basin which is fed by sediments from North and South. The outer arc high grows by stacking and the forearc basin continuously thickens while its depocentre moves slightly northward (Fig. 11E). The individual strata show different wedge shapes, indicating that the depocentre moves back- and forward.

Fig. 11. Simplified restoration of the Lombok forearc basin development on profile BGR06-303 (PreSDM). Present situation is shown on top with marked horizons A, B, C, D and E. Note the angular unconformity at horizon B. Vertical restoration is done by flattening the marked horizons step by step. Situation E shows the present seafloor flattened. Age assignment from Eocene (A) to Early-Mid Miocene is adopted from Van der Werff et al. (1994). Insets show cartoons of the basin development according to seismic sections A to D. Initial stage (A) is that of a passive margin before subduction commenced, including a shelf basin with sediments derived from the continent (or a fossil island arc). Continued sediment loading depresses the shelf (B) until subduction creates first accretionary wedges and seaward moving of the depocentre of the basin (C). Further subduction leads to landward shift of the depocentre and, when the oceanic plate has reached a depth of the order of 100 km, to island arc magmatism (D). Horizontal bars denote the length of the seismic sections. Sections are highly vertically exaggerated, compare with Figs. 2 and 4 for V.E. = 2 or 3.

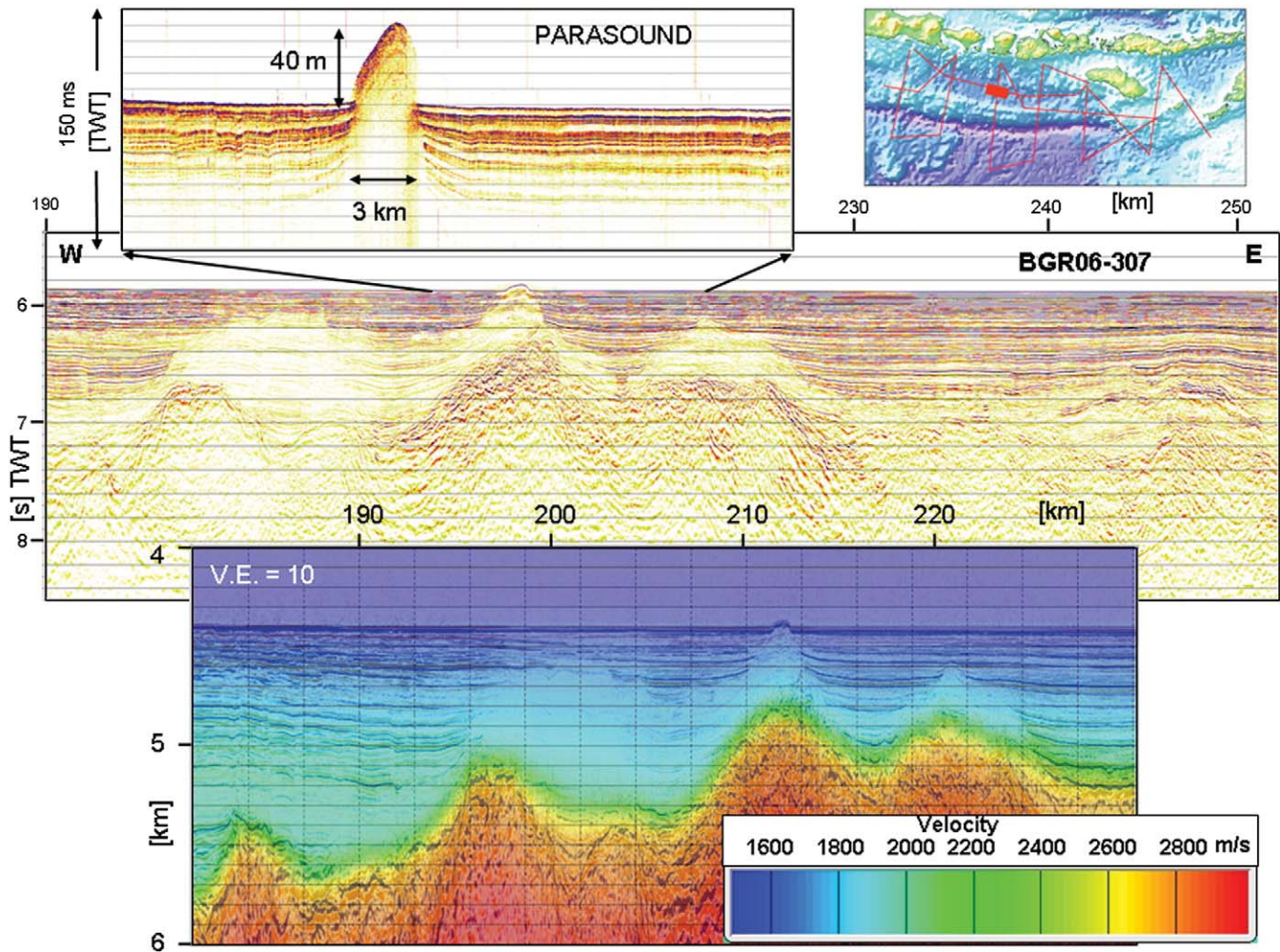


Fig. 13. Detail of profile BGR06-307, eastern end. Middle: Post-stack Kirchhoff time migration, 8–120 Hz (compare Fig. 12). Note the relatively transparent zone above the basement. High-resolution echosounder section is shown on top of the profile. Clear evidence for diapirism of a mud volcano is discernable as well as a small ramp at the bottom of the mud volcano. Bottom: Velocity–depth section superposed on PreSDM section of part of the profile (bottom) indicates that there is no sharp velocity contrast between the transparent zone and the surrounding sediments.

Sedimentation until the Early Oligocene unconformity differs in reflection strength from the younger strata. This might be due to a change from terrestrial input to clay-rich marine input. Most of the characteristic features observed on profile BGR06-303 can be correlated along the E–W axis of the Lombok forearc basin. The ridge-like western termination of the basin is very likely due to the incorporation of seamounts of the Roo Rise into the forearc as argued by Kopp et al. (2006). The eastern termination is characterized by elevated compressional structures in transition from subduction to collision tectonics (compare Fig. 14).

The basement of the Lombok forearc basin exhibits a rather irregular geometry, as mentioned earlier (Fig. 12). This is obvious particularly in E–W direction, but also in N–S direction, where a mid-basin ridge is seen on most of the N–S profiles (Fig. 2). The reason might be that it is formed by a stretched continental margin with horsts and grabens in the West and/or a melange or stack of ophiolitic nappes. Local magnetic anomalies of several hundred nT may be attributed to these structures. Sediment thickness varies strongly between 500 m and 4000 m in E–W direction along the axis of the basin (Fig. 12). Only smooth signs of deformation inside the sediments are visible, mostly attributable to differential compaction. A particular feature of interest is a relatively blank zone above the basement (Fig. 13). Such zones are often interpreted as carbonate buildups, which have certain implications for hydrocarbon exploration because of their porosity. However, when searching for typical

seismic signatures (Vail et al., 1977), no roof reflections nor velocity anomalies against surrounding layers are found here (Fig. 13). Instead, a pinnacle-like feature penetrates the seafloor, particularly seen in the echosounding profile (Fig. 13, top) and deforms the adjoining layers upward. This is clear evidence for diapirism of a mud volcano, driven by a density contrast within the blank zone (lower density) against the adjoining sediments. The density contrast is probably caused by an enhanced fluid content which also lowers the viscosity of the involved sedimentary layers, probably clay-rich, and mobilizes the stratified sediments driven by overpressure at depth. Their strata are still visible by weak reflections. These blank zones just above the basement are a widespread phenomenon in our study area. The involved fluids may originate from dewatering of subducted oceanic sediments pervading the basin basement. In this case it seems to be a continuing process, instead of a cyclic one as observed frequently in the Barbados accretionary prism (Deville et al., 2006). A similar situation is known as the catastrophic East Java mud volcano (Davies et al., 2008). Since most of the oceanic sediments of the Argo Abyssal Plain are subducted (and partly recycled within the outer arc high), the amount of subducted seawater must be relatively high.

So far the forearc basins between an outer arc high and the volcanic arc are seldom considered as important petroleum province, despite of some industrial seismic surveying. The sediment thickness of the Lombok forearc basin is with about 3 s TWT much less than in other forearc basins further west. The Simulue Basin with a sediment

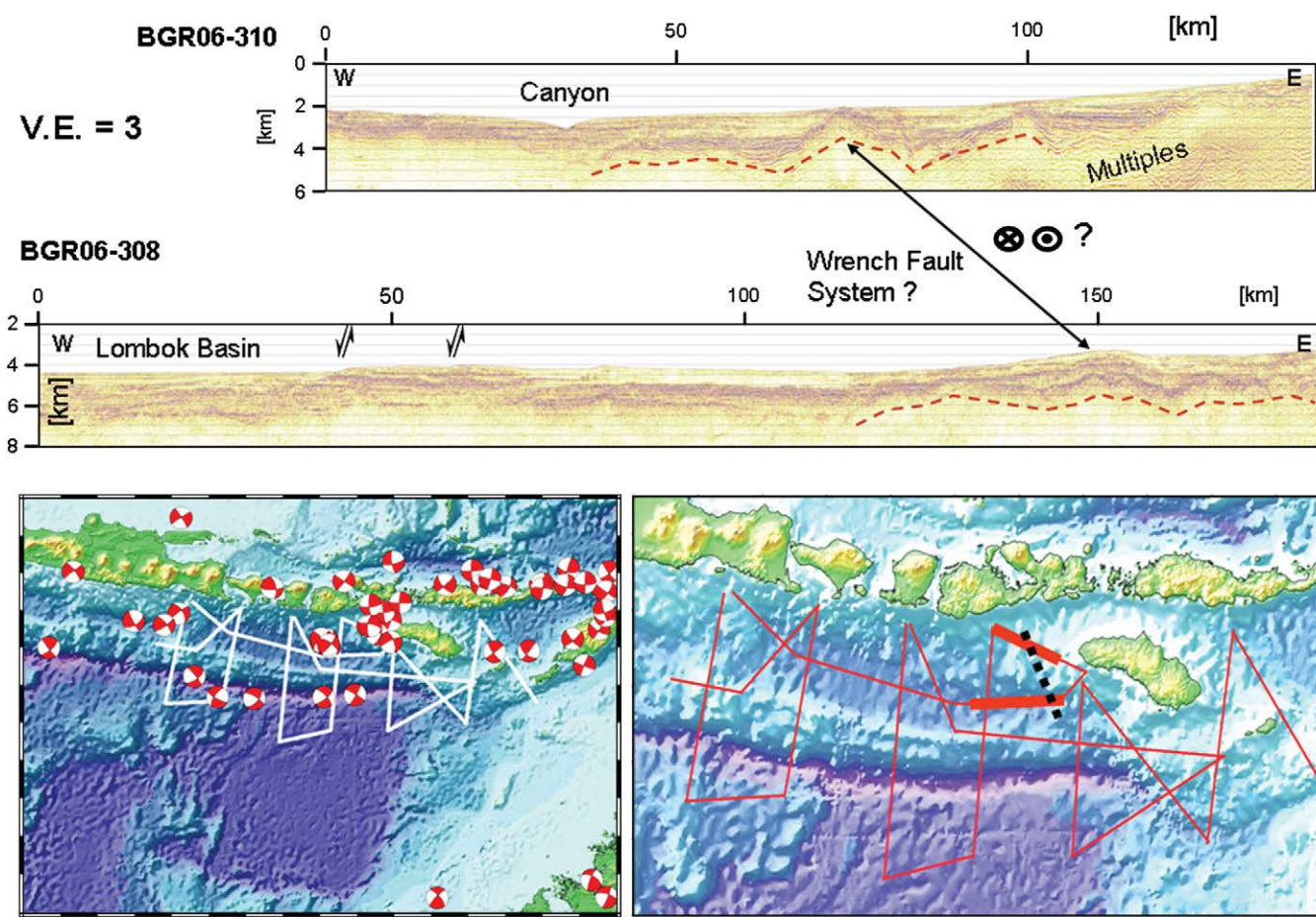


Fig. 14. Details of PreSDM-profiles BGR06-310 (top), BGR06-308 (middle) in the transition zone between the subduction regime in the West and the collision regime in the East. See inset (lower right) for location. Arrows in the middle section mark an abrupt vertical movement and thus a termination of the Lombok forearc basin, with relative uplift in the East and subsidence in the basin. Basement highs between the upper two sections correlate and may be interpreted as a wrench fault system (dashed line in location map). Focal mechanisms selected for strike-slip type (depth lower than 50 km, 10 km depth resolution) (Engdahl, pers. comm., 2008; Engdahl et al., 2007; lower left) show focal planes almost parallel and perpendicular to the dominant direction of the magnetic lineation (compare Fig. 9).

thickness of 5 s TWT offshore NW Sumatra has been shown by 3-D basin modelling to bear enough hydrocarbon potential in its depocentre, if the heatflow is high enough (Lutz et al., submitted for publication). Heatflow values between 40 and 60 mW/m² have been deduced from the depth of BSRs (bottom simulating reflectors) which indicate the base of the gas hydrate stability zone. Gas hydrates require relatively low temperatures. BSRs are a widespread phenomenon in the western and central Sunda Arc (Kopp, 2002; Lutz et al., submitted for publication). However, in the present study area neither bright spots nor BSRs are observed. The reason might be that sufficient organic rich sediment input is missing or that the heatflow is considerably higher than in the western forearc basins. Further indication for higher temperatures is the observation of a submarine volcano offshore Bali at the western boundary of the Lombok Basin, shown as a 500 m high cone-like edifice with a crater on top in bathymetry and by free-air gravity and magnetic anomalies. Echo-sounding signals reveal a very hard sea bottom in the western Lombok Basin, probably caused by an ash layer. Therefore, in spite of relatively low sediment thickness, the hydrocarbon potential might be enhanced due to higher temperatures.

5.4. Transition from subduction to collision

The block rotation of oceanic crust (Fig. 10) is probably related to the transition between the subduction regime in the West to the collision regime in the East of our study area. We might expect related structures further north–northwest, located at the eastern boundary

of the Lombok forearc basin. In the profiles BGR06-308 and BGR06-310 (Fig. 14) prominent basement highs of similar geometry can be correlated in north–northwestern direction showing signs of positive flower structures due to compression and uplift. We interpret these features as belonging to a broad complex system of wrench faults which decouple the subduction regime in the West from the collision regime in the East. The long E–W profile BGR06-315 (not shown here), which is located on top of the outer arc high, is difficult to interpret in this respect, however it shows a very rough topography with horsts and sediment-filled grabens. There is some indication in the pattern of interpreted magnetic anomalies (Fig. 9). A possibly reactivated Cretaceous transform or fracture zone at the transition from the Argo Abyssal Plain to the Scott Plateau shows a strike direction, which may support our interpretation. However, its precise location cannot be resolved and is thus estimated only.

Further east, the profile BGR06-319 has been interpreted by Shulgin et al. (2009) using the MCS data and OBS wide-angle seismic tomography. The Scott Plateau as a promontory of the Australian continent is underthrust beneath the Banda forearc. The system is regarded as a precursor of a fold-and-thrust belt in front of a paleo-accretionary prism bounded northwards by the Sumba ridge, which acted as backstop to the prism during the time of accretion.

6. Conclusions

Seismic images of unprecedented resolution and depth penetration have been collected during cruise SO190 in the eastern Sunda

forearc at the transition from an oceanic-island arc subduction regime to a continental-island arc collision regime in the western Banda arc. Six long N–S traverses cover the entire subduction system, from the oceanic crust, accretionary wedges, outer arc high, forearc basin to the slope of the volcanic island arc. The interface between the subducting oceanic plate and the forearc structures of the upper plate is imaged in great detail and variability in terms of dip, segmentation, subducted sediments, tectonic melange and duplex structures. The interface is continuously imaged over a length of 50–70 km from the trench landward. Its high reflection amplitudes are attributed to material of high porosity with high fluid content enabling low friction. Therefore, megathrust earthquake foci are unlikely to be located within the imaged plate interface.

We draw the following additional conclusions:

- 1) The subducting oceanic crust is dissected by downbending of the oceanic crust and associated normal faulting into 5–10 km wide blocks within a 50–70 km wide belt seaward of the deep sea trench. These blocks determine geometry and evolution of duplexes at the base of the upper plate.
- 2) Duplexes of various modes and geometries are observed at the interface between upper and lower plate. These duplexes are connected to landward dipping splay faults which penetrate the entire outer arc high. Here, these thrust faults cause prominent breaks in seabottom morphology as well as rotation and vertical displacements of associated piggy-back basins.
- 3) Major volumes of oceanic sediments are subducted and incorporated into a thrust and erosion cycle within the outer arc high. The outer arc high is characterized by deep-reaching, recently active thrust faults and vertical displacements, which constitute a considerable tsunami hazard.
- 4) The growth of the outer arc high is mainly due to attachment of oceanic sediment and crustal material to the base of the wedge and duplex formation. Magnetic anomalies may be attributed to melange zones and ophiolites within the forearc.
- 5) The 3.5–4 km sediment thickness of the Lombok forearc basin is less than in other forearc basins along the Sunda Arc and contains therefore less favourable conditions for hydrocarbon generation, depending on the thermal regime. Bottom simulating reflectors and bright spots are not observed, in contrast to the Sunda Arc further west.
- 6) Vertical movements during the evolution of the Lombok forearc basin until recent times are documented in the sedimentary succession as prominent unconformities and shifting depocenters.
- 7) Mud diapirs of deep sediments mobilized by fluids at the bottom of the forearc basins are observed.
- 8) The western termination of the Lombok forearc basin is determined by an inter-basin ridge which is caused by increased compression by the arrival of elevated features of the Roo Rise.
- 9) A wrench fault system at the eastern boundary of the Lombok forearc basin decouples the subduction regime of the Sunda Arc in the West from the continent-island arc collision regime of the Banda arc in the East.

Acknowledgements

Cruise SO190 and the SINDBAD project are funded by the Federal Ministry of Education and Research (BMBF) under grants 03G0190A and 03G0190B. We thank Captain Oliver Meyer and his crew from RV SONNE for their professional assistance. Special thanks go to the SINDBAD scientific crew members and working group. We thank E.R. Engdahl who provided us with new data of focal mechanisms. We are grateful to the Indonesian government for collaboration and permission to work in its territorial seas. We also want to thank Hans Thybo, Warren B. Hamilton and an anonymous reviewer for their scientific comments and constructive reviews of this paper.

References

- Berglar, K., Gaedicke, C., Franke, D., Ladage, S., Klingelhoefer, F., Djajidhardja, Y.S., 2010. Structural evolution and strike-slip tectonics off north-western Sumatra. *Tectonophysics* 480, 119–132.
- BGR, 2006. Research Cruise SO190 Leg 1, SINDBAD. Cruise Report and Preliminary Results. Federal Institute For Geosciences And Natural Resources, Hannover. Archives No. 0.126.718.
- Briggs, R.W., Sieh, K., Meltzner, A.J., Natawidjaja, D., Galetzka, J., Suwargadi, B., Hsu, Y., Simons, M., Hananto, N., Suprihanto, I., Prayudi, D., Avouac, J.-P., Prawirodirdjo, L., Bock, Y., 2006. Deformation and slip along the Sunda Megathrust in the great 2005 Nias-Simeulue earthquake. *Science* 311. doi:10.1126/science.1122602.
- Calvert, A.J., Ramachandran, K., Kao, H., Fisher, M.A., 2006. Local thickening of the Cascadia forearc crust and the origin of seismic reflectors in the uppermost mantle. *Tectonophysics* 420, 175–188. doi:10.1016/j.tecto.2006.01.021.
- Collot, J.-Y., Agudelo, W., Ribodetti, A., Marcaillou, B., 2008. Origin of a crustal splay fault and its relation to the seismogenic zone and underplating at the erosional north Ecuador-south Colombia oceanic margin. *Journal of Geophysical Research* 113, B12102. doi:10.1029/2008JB005691.
- Davies, R.J., Brumm, M., Manga, M., Rubiandini, R., Swarbrick, R., Tingay, M., 2008. The East Java mud volcano (2006 to present): an earthquake or drilling trigger? *Earth and Planetary Science Letters* 272, 627–638.
- DeMets, C., Gordon, R.G., Argus, D.F., 2010. Geologically current plate motions. *Geophysical Journal International* 181, 1–80. doi:10.1111/j.1365-245X.2009.04491.x.
- Deville, E., Guerlais, S.-H., Callec, Y., Gribouard, R., Huyghe, P., Lallemand, S., Mascle, A., Noble, M., Schmitz, J., the collaboration of the Caramba Working Group, 2006. Liquefied vs stratified sediment mobilization processes: insight from the South of the Barbados accretionary prism. *Tectonophysics* 428, 33–47. doi:10.1016/j.tecto.2006.08.011.
- Dickinson, W.R., 1977. Tectono-stratigraphic evolution of subduction-controlled sedimentary assemblages. In: Talwani, M., Pitmann III, W.C. (Eds.), *Island Arcs, Deep Sea Trenches and Back-Arc Basins*. Maurice Ewing Series 1. American Geophysical Union, Washington D.C., pp. 33–40.
- Dickinson, W.R., 1995. Forearc basins. In: Busby, C.J., Ingersoll, R.V. (Eds.), *Tectonics of Sedimentary Basins*. Blackwell Science, pp. 221–261.
- Dickinson, W.R., Seely, D.R., 1979. Structure and stratigraphy of forearc regions. *American Association of Petroleum Geologists Bulletin* 63, 2–31.
- Engdahl, E.R., DeShon, H.R., Bilek, S., Villasenor, A., Thurber, C.H., 2007. Assessment of well-constrained seismicity and focal mechanisms in the Andaman-Sumatra-Java subduction systems. *EOS Transactions, American Geophysical Union* 88 (52) Fall Meet. Suppl., Abstract S23D-01.
- Franke, D., Schnabel, M., Ladage, S., Tappin, D.R., Neben, S., Djajidhardja, Y.S., Müller, C., Kopp, H., Gaedicke, C., 2008. The great Sumatra-Andaman earthquakes – imaging the boundary between the ruptures of the great 2004 and 2005 earthquakes. *Earth and Planetary Science Letters* 269, 118–130.
- Hall, R., 2002. Cenozoic geological and plate tectonic evolution of SE Asia and the SW Pacific: computer-based reconstructions, model and animations. *Journal of Asian Earth Sciences* 20, 353–431.
- Hall, R., Smyth, H.R., 2008. Cenozoic arc processes in Indonesia: identification of the key influences on the stratigraphic record in active volcanic arcs. In: Draut, A.E., Clift, P.D., Scholl, D.W. (Eds.), *Formation and Applications of the Sedimentary Record in Arc Collision Zones*. Geological Society America, Special Paper, V 436. doi:10.1130/2008.2436(03).
- Hamilton, W., 1979. Tectonics of the Indonesian region. *Geological Survey Professional Paper* 1078. : 1 plate. U.S. Government Printing Office, Washington, D.C., 345 pp.
- Hamilton, W.B., 1988. Plate tectonics and island arcs. *Geological Society of America Bulletin* 100, 1503–1527.
- Hamilton, W.B., 2000. Driving mechanism and 3-D circulation of plate tectonics. *Special Paper* 433. *The Geological Society of America*, pp. 1–25. doi:10.1130/2007.2433(01).
- Hamzah, L., Puspito, N.T., Imamura, F., 2000. Tsunami catalog and zones in Indonesia. *Journal of Natural Disaster Science* 22 (1), 25–43.
- Harris, R.A., 1991. Temporal distribution of strain in the active Banda orogen: a reconciliation of rival hypotheses. *Journal of Southeast Asian Earth Sciences* 6, 373–386.
- Heine, C., Müller, R.D., Gaina, C., 2004. Reconstructing the lost Tethys Ocean basin: convergence history of the SE Asian margin and marine gateways. In: Clift, P., et al. (Ed.), *Continent-Ocean Interactions Within East Asian Marginal Seas. : Geophysical Monograph Series*, Vol. 149. American Geophysical Union, Washington D.C., pp. 37–54.
- Heirtzler, J.R., Cameron, P., Cook, P.J., Powell, T., Roeser, H.A., Sukardi, S., Veevers, J.J., 1974. The Argo Abyssal Plain. *Earth and Planetary Science Letters* 41, 21–31.
- Henstock, T.J., McNeill, L.C., Tappin, D.R., 2006. Seafloor morphology of the Sumatran subduction zone: surface rupture during megathrust earthquakes? *Geology* 34, 485–488.
- Karig, D.E., Sharman, G.F., 1975. Subduction and accretion in trenches. *Geological Society of America Bulletin* 86, 377–389.
- Kopp, H., 2002. BSR occurrence along the Sunda margin: evidence from seismic data. *Earth and Planetary Science Letters* 197, 225–235.
- Kopp, H., Kukowski, N., 2003. Backstop geometry and accretionary mechanics of the Sunda margin. *Tectonics* 22. doi:10.1029/2002TC001420.
- Kopp, H., Flueh, E.R., Klaeschen, D., Bialas, J., Reichert, C., 2001. Crustal structure of the central Sunda margin at the onset of oblique subduction. *Geophysical Journal International* 147, 449–474.
- Kopp, H., Flueh, E.R., Petersen, C.J., Weinrebe, W., Wittwer, A., Scientists, Meramex, 2006. The Java margin revisited: evidence for subduction erosion off Java. *Earth and Planetary Science Letters* 242, 130–142.

- Korenaga, J., Holbrook, W.S., Kent, G.M., Kelemen, P.B., Detrick, R.S., Larsen, H.-C., Hopper, J.R., Dahl-Jensen, T., 2000. Crustal structure of the southeast Greenland margin from joint refraction and reflection seismic tomography. *Journal of Geophysical Research* 105, 21591–21614.
- Ladage, S., Gaedicke, C., Barckhausen, U., Heyde, I., Weinrebe, W., Flueh, E.R., Krabbenhoef, A., Kopp, H., Fajar, S., Djajadihardja, Y., 2006. Bathymetric survey images structure off Sumatra. *EOS Transactions, American Geophysical Union* 87 (17), 165.
- Lutz, R., Gaedicke, C., Berglar, K., Schlömer, S., Franke, D., Djajadihardja, Y.S., submitted for publication. Petroleum systems of the Simeulue forearc basin off Sumatra, Indonesia. *American Association of Petroleum Geologists Bulletin*.
- Masson, D.G., Parson, L.M., Milsom, J., Nichols, G., Sikumbang, N., Dwiyanto, B., Kallagher, H., 1990. Subduction of seamounts at the Java Trench: a view with long-range sidescan sonar. *Tectonophysics* 185, 51–65.
- Müller, C., Kopp, H., Djajadihardja, Y.S., Barckhausen, U., Ehrhardt, A., Engels, M., Flueh, E.R., Gaedicke, C., Keppler, H., Lutz, R., Lüschen, E., Neben, S., Seeber, L., Dzulkaena, D.P.S., 2008. From subduction to collision: the Sunda–Banda arc transition. *EOS Transactions, American Geophysical Union* 89 (6), 49–60.
- Nicolcas, A., 1989. Structures of Ophiolites and Dynamics of Oceanic Lithosphere. Kluwer Academic Publishers, Dordrecht. 367 pp.
- Park, J.-O., Tsuru, T., Kodaira, S., Cummins, P.R., Kaneda, Y., 2002. Splay fault branching along the Nankai subduction zone. *Science* 297, 1157–1160.
- Planert, L., Kopp, A., Lueschen, E., Mueller, C., Flueh, E.R., Shulgin, A., Djajadihardja, Y., Krabbenhoef, A., 2010. Lower plate structure and upper plate deformational segmentation at the Sunda–Banda arc transition, Indonesia. *Journal of Geophysical Research* 115, B08107.
- Rutherford, E., Burke, K., Lytwyn, J., 2001. Tectonic history of Sumba Island, Indonesia, since the Late Cretaceous and its rapid escape into forearc in the Miocene. *Journal of Asian Earth Sciences* 19, 453–479.
- Samuel, M.A., Harbury, N.A., Bakri, A., Banner, F.T., Hartono, L., 1997. A new stratigraphy for the islands of the Sumatran Forearc, Indonesia. *Journal of Asian Earth Sciences* 15, 339–380.
- Sandwell, D.T., Smith, W.H.F., 1997. Marine gravity data from GEOSAT and ERS-1 altimetry. *Journal of Geophysical Research* 102, 10039–10054.
- Schlüter, H.U., Gaedicke, C., Roeser, H.A., Schreckenberger, B., Meyer, H., Reichert, C., Djajadihardja, Y., Prexl, A., 2002. Tectonic features of the southern Sumatra–western Java forearc of Indonesia. *Tectonics* 21, 11–11–11–15. doi:10.1029/2001TC901048.
- Shulgin, A., Kopp, H., Mueller, C., Lueschen, E., Planert, L., Engels, M., Flueh, E.R., Krabbenhoef, A., Djajadihardja, Y., 2009. Sunda–Banda arc transition: incipient continent–island arc collision (northwest Australia). *Geophysical Research Letters* 36, L10304. doi:10.1029/2009GL037533.
- Sibuet, J.-C., Rangin, C., Le Pichon, X., Singh, S., Cattaneo, A., Graindorge, D., Klingelhoefer, F., Lin, J.-Y., Malod, J., Maury, T., Schneider, J.-L., Sultan, N., Umler, M., Yamaguchi, H., "Sumatra aftershocks" team, 2007. 26th December 2004 great Sumatra–Andaman earthquake: co-seismic and postseismic motions in northern Sumatra. *Earth and Planetary Science Letters* 263, 88–103. doi:10.1016/j.epsl.2007.09.005.
- Singh, S.C., Carton, H., Tapponnier, P., Hananto, N.D., Chauhan, A.P.S., Hartoyo, D., Bayly, M., Moeljopranoto, S., Bunting, T., Christie, P., Lubis, H., Martini, J., 2008. Seismic evidence for broken oceanic crust in the 2004 Sumatra earthquake epicentral region. *Nature Geoscience*. doi:10.1038/ngeo336.
- Spence, W., 1986. The 1977 Sumba earthquake series: evidence for slab pull force acting a t subduction zone. *Journal of Geophysical Research* 91 (B7), 7225–7239. doi:10.1029/JB091iB07p07225.
- Spicák, A., Hanus, V., Vanek, J., 2007. Earthquake occurrence along the Java trench in front of the onset of the Wadati–Benioff zone: beginning of a new subduction cycle? *Tectonics* 26. doi:10.1029/2005TC001867.
- Vail, P.R., Mitchum Jr., R.M., Todd, R.G., Widmier, J.M., Thompson III, S., Sangree, J.B., Bubb, J.N., Hatlelid, W.G., 1977. Seismic stratigraphy and global changes of sea level. In: Payton, C.E. (Ed.), *Seismic Stratigraphy – Application to Hydrocarbon Exploration*. The American Association of Petroleum Geologists, Tulsa, pp. 49–212.
- Van der Werff, W., 1995. Structure and morphotectonics of the accretionary prism along the Eastern Sunda – Western Banda Arc. *Journal of Southeast Asian Earth Sciences* 11, 309–322.
- Van der Werff, W., 1996. Variation in forearc basin development along the Sunda Arc, Indonesia. *Journal of Southeast Asian Earth Sciences* 14, 331–349.
- Van der Werff, W., Prasetyo, H., Kusnida, D., van Weering, T.C.E., 1994. Seismic stratigraphy and Cenozoic evolution of the Lombok Forearc Basin, Eastern Sunda Arc. *Marine Geology* 117, 119–134.
- Widiyantoro, S., Van der Hilst, R., 1997. Mantle structure beneath Indonesia inferred from high-resolution tomographic imaging. *Geophysical Journal International* 130, 167–182.

Subduction system variability across the segment boundary of the 2004/2005 Sumatra megathrust earthquakes.

A. Shulgin¹, H. Kopp¹, D. Klaeschen¹, C. Papenberg¹, F. Tilmann², E.R. Flueh¹, D. Franke³,
U. Barckhausen³, A. Krabbenhoeft¹

1. IFM-GEOMAR, Leibniz Institute of Marine Sciences, Wischhofstr. 1-3, 24148 Kiel, Germany
e-mail: ashulgin@ifm-geomar.de
Phone: +49-431-600-2660
Fax: +49-431-600-2922

2. German Research Center for Geosciences (GFZ), Telegrafenberg, D-14473, Potsdam, Germany

3. Federal Institute for Geosciences and Natural Resources (BGR), Stilleweg 2, D-30655 Hanover, Germany

Submitted to Earth and Planetary Science Letters 2012

Abstract

Subduction zone earthquakes are known to create segmented patches of co-seismic rupture along-strike of a margin. Offshore Sumatra, repeated rupture occurred within segments bounded by permanent barriers, whose origin however is still not fully understood. In this study we image the structural variations across the rupture segment boundary between the M_w 9.1 December 26, 2004 and the M_w 8.6 March 28, 2005 Sumatra earthquakes. A set of collocated reflection and wide-angle seismic profiles are available on both sides of the segment boundary, located offshore Simeulue Island. We present the results of the seismic tomography modeling of wide-angle ocean bottom data, enhanced with MCS data and gravity modeling for the southern 2005 segment of the margin and compare it to the published model for the 2004 northern segment. Our study reveals principal differences in the structure of the subduction system north and south of the segment boundary, attributed to the subduction of 96°E fracture zone. The key differences include a change in the crustal thickness of the oceanic plate, a decrease in the amount of sediment in the trench as well as variations in the morphology and volume of the accretionary prism. This suggests that the 96°E fracture zone acts as an efficient barrier in the trench parallel sediment transport, as well as a divider between oceanic crustal blocks of different structure. The variability of seismic behavior is caused by the distinct changes in the morphology of the subduction complex across the boundary, caused by the difference in the sediment supply.

Keywords:

Subduction zone; seismic tomography; crustal structure; seismogenic zone; Sumatra

1. Introduction

Since 2004, repeated large and great megathrust earthquakes along the Sumatra subduction zone have ended a ~40 year period of relative moderate ($M_w < 8.5$) global seismic activity. Studies of the $M_w = 9.1$ Sumatra-Andaman earthquake in 2004 and following events of magnitudes ≥ 8.4 in 2005 and 2007 confirmed previous observations of segmented rupture areas of earthquakes along subduction zones (Ando, 1975; Spence, 1977, DeShon et al, 2005). Offshore Sumatra, rupture occurs in discrete patches (e.g. Chlieh et al., 2007), bounded by distinct barriers. Detailed seismological studies reveal variations in the updip limit of the 2004 and 2005 ruptures, respectively (Tilmann et al., 2010). These observations imply across-strike heterogeneity in physical properties along the megathrust. The controlling physical processes, however, are still not fully understood.

The tectonics around Northern Sumatra are predominantly controlled by the subduction of the oceanic Indo-Australian plate underneath Eurasia. The current convergence rate offshore Northern Sumatra is estimated at 51 mm/y (Prawirodirdjo and Bock, 2004). The increasing obliqueness of the convergence northwards from the Sunda Strait (Moore et al., 1980; McCaffrey, 2009) results in the formation and development of a number of arc-parallel strike-slip fault systems (**Fig. 1**). The most significant are the Sumatra and the West Andaman fault systems, accommodating arc-parallel strain (Sieh and Natawidjaja, 2000) offshore central-southern Sumatra. For the Mentawai fault system (Diament et al., 1992; Malod and Kemal, 1996; Lelgemann et al., 1999; Berglar et al., 2010), recent findings suggest deformation dominated by backthrusting (Singh et al., 2010; Singh et al., 2011).

The oceanic plate is characterized by prominent tectonic features observed in the bathymetry and magnetic data (Sclater and Fisher, 1974): north-south trending fracture zones enter the trench around 96°E and 97°E (Deplus et al., 1998). In addition, the Wharton Ridge, representing the southwest-northeast trending segments of a fossil spreading axis, is approaching the trench offshore Nias. Reflection seismic studies have revealed the presence of a pre-décollement reflector in the 2004 rupture area, which terminates in the vicinity of the 2004-2005 rupture segment boundary (Dean et al., 2010) and is absent in the 2005 segment. This indicates contrasting plate boundary shear zones and prism properties in the two segments (Dean et al., 2010). Bathymetric studies show that the frontal slope offshore Nias is steeper and

that the morphology generally has a rougher appearance along this segment of the margin, compared to the adjacent southern areas (*Henstock et al., 2006; Kopp et al., 2008; Graindorge et al., 2008*). This observation suggests lateral variations in material strength and mechanical properties. This lateral heterogeneity may be associated with various factors, e.g. variations in fluid pressure (*Lallemand et al., 1994*) or cyclic changes from frontal accretion to sediment underplating (*Gutscher et al., 1998*).

The “seismic unzipping” of the Sumatra margin since 2004 offers the unique opportunity to investigate the relationship between interseismic coupling and the mechanical properties of the megathrust including the nature of asperities and barriers to megathrust ruptures. The 2004 earthquake asymmetrically ruptured to the north over a distance of more than 1200 km, while the 2005 event showed a bidirectional rupture. However, there is a clear delineation between these events, located underneath the island of Simeulue (*Ammon et al., 2005; Subarya et al., 2006; Gahalaut et al., 2006; Briggs et al., 2006*). Franke et al. (2008), based on bathymetry and multichannel seismic (MCS) data, proposed the segment boundary running NE-SW through the island of Simeulue, as discussed earlier by Briggs et al. (2006) (**Fig. 1**). The observed location of the pivot line (a proxy to the downdip limit of the rupture area) of the pre-2005 earthquake net uplift on Simeulue (*Meltzner et al., 2006*) spatially correlates with the proposed segment boundary.

A number of possible scenarios were suggested for the formation of segment boundaries: these include mechanical discontinuities in the subducting plate (*Spence, 1977; Aki, 1979*); topographic relief on the oceanic plate such as seamounts, ridges or fracture zones (*Bilek et al., 2003; Collot et al., 2001; Bilek, 2010*) and tectonic structures in the overriding plate (*Ryan and Scholl, 1993; Collot et al., 2004*). For northern Sumatra, Subarya et al. (2006) suggested that the segment boundary between the 2004-2005 patches is linked to the subduction of the north-south striking 96°E fracture zone on the oceanic plate, based on the coseismic slip modeling results. This fracture zone was identified from magnetic studies (*Sclater and Fisher, 1974*), as well as from the bathymetry data seaward of the trench; in the vicinity of the trench no anomalous relief is observed, due to increase of sediment fill. In an MCS profile presented by Franke et al., (2008) (their Fig. 5) the fracture zone is manifested by an area of low/absent reflectivity from the top of the oceanic crust, as well as in the thinning of the sedimentary cover.

The rupture patterns of the 2004 and 2005 events have been documented in a number of studies (e.g. *Ammon et al., 2005; Briggs et al., 2006; Galahaut et al., 2006; Chlieh et al., 2007; Sibuet et al., 2007; Tilmann et al., 2010*) and both events range among the most intensely studied earthquakes globally. In addition to the varying lateral extent of the rupture planes, the most striking difference is the variation in the updip limit of seismogenic rupture. The 2004 rupture area offshore Northern Sumatra experienced co-seismic slip to shallow depth underneath the accretionary prism. Contrarily, the 2005 rupture concentrated deeper in the system, underneath the transition from the forearc high to the forearc basin (*Tilmann et al., 2010*) and is comparable to most megathrust events worldwide. The analysis of the aftershocks activity of the 2004 and 2005 earthquakes document this major change in the depth of seismic activity across the proposed segment boundary (*Tilmann et al., 2010*). The separation between the northern area with prevailing shallow seismicity from the southern part, where the deeper earthquakes are observed (**Fig. 1**), is roughly collocated with the active seismic profile described in this study. *Pesicek et al. (2010)* found that the aftershocks just offshore the Banyak island group (**Fig. 1**) show an arc type distribution following variations in the trench geometry. They report a southward steepening of the dip of the downgoing oceanic plate in the distribution of the deep (>50 km) aftershocks.

The shallow and deep structure of the southern portion of the 2004 rupture was investigated using active seismic methods (*Franke et al., 2008; Singh et al., 2008; Dessa et al., 2009; Dean et al., 2010; Klingelhoefer et al., 2010; Gulick et al., 2011*). The area of the 2005 rupture is seismically not as intensely studied; however, high-resolution bathymetry mapping has been conducted in both segments in a multinational effort (e.g. *Ladage et al., 2006; Henstock et al., 2006; Graindorge et al., 2008; Kopp et al., 2008; Krabbenhoef et al., 2010*). The key reported observations include variations in the age of the incoming oceanic plate. The upper plate forearc Moho has been reported at a depth of 20 km in the northern domain (*Dessa et al., 2009; Klingelhoefer et al., 2010*) with possible deepening in the south to a depth of ca. 23-24 km (*Simoës et al., 2004*). Changes in the age of the oceanic plate and the amount of sediment (*Hippchen and Hyndman, 2008*) and also in the sediment properties (*Dean et al., 2010*) govern the regional thermal regime as suggested by thermal modeling (*Klingelhoefer et al., 2010*). As the thermal regime has a primary effect on the width of the seismogenic zone (150°C for the updip limit (*Moore et*

al., 2007) and 350°C-450°C for the downdip limit (*Hyndman and Wang, 1993; Hyndman and Wang, 1995*)), the variations in the thermal state would be associated with differences in the depth extent of the seismogenic zone. Observations of co-seismic slip and afterslip of the 2004 earthquake are based on GPS data (*Chlieh et al., 2007*) and are related to coral and satellite-derived uplift rates (*Meltzner et al., 2006*) and aftershock locations (*Klingelhoefer et al., 2010*), which support the thermal models for the updip limit of the seismogenic zone. The downdip limit of seismogenic rupture is reported to be at 48 km depth and hence located deeper than forearc Moho (22-23 km) (*Hsu et al., 2006*), which is commonly used to define the downdip limit of a seismogenic zone. These observations suggest that the 2004 rupture extended along the contact zone of the underthrusting oceanic plate and the forearc mantle, implying that the forearc mantle wedge is not serpentinized. Also, *Sibuet et al. (2007)* discuss that most of the shallow co-seismic motion during the 2004 rupture may have been not along the megathrust but may have transferred to a splay fault, which considerably contributed to tsunamigenesis.

In this work we present the deep structural image of the Sumatra margin south of Simeulue Island in the 2005 rupture area (**Fig. 1**). We compare our results to seismic images acquired near the southern termination of the 2004 rupture area north of Simeulue Island (*Klingelhoefer et al., 2010*) to quantify the crustal-scale changes across the proposed segment boundary and possible effects on the variations in the seismogenic behavior.

2. Data

The dataset used in this study consists of a multi-channel seismic (MCS) and collocated wide-angle refraction/reflection profiles (**Fig. 1**). The seismic data were collected within the SeaCause project during SO186 cruise of RV “Sonne” offshore Northern Sumatra in 2006. The reflection profile data (MCS line BGR06-135) were acquired to reveal and constrain the structure of the sedimentary fill as well as the fault deformation patterns. MCS processing included pre-stack processing and pre-stack depth migration. A time-and-space-variant frequency filter was applied prior to a spherical divergence correction and a predictive deconvolution. Normal moveout correction and velocity analysis was followed by multiple suppression and common-depth-point stacking. For the pre-stack depth migration, a scheme combining common reflection point gathers and focusing analyses is used in assessing the seismic velocity field

(Mackay and Abma, 1993). The pre-stack depth migrated data are shown in **Figure 2**. In this study it is further used in the interpretation of the shallow structures, due to much higher resolution compared to wide-angle data, and to constrain the starting model for the seismic tomography.

In total 24 ocean bottom seismometers (OBS) (Bialas and Flueh, 1999) were deployed along a 255 km long profile with an average spacing of 10 km, providing uniform coverage. The processing of the ocean bottom data included the localization of the ocean bottom instruments using the arrival information of the direct water wave and precise shot geometry. A time-gated deconvolution was applied to remove the predictable air bubble reverberations in order to improve the signal-to-noise ratio. Finally, a time and offset-variant Butterworth filter, in which the pass-band moves towards the lower frequencies as record time and offset increases, was applied to consider frequency changes caused by signal attenuation. Clear seismic phase arrivals were recorded on all stations within 50 km offsets; for some stations clear traveltimes are available up to 100 km offset. **Figure 3** provides examples of the data quality and the recorded phases as well as picked travel times (reflection and refraction phases). Stations located on the oceanic plate recorded clear arrivals of the oceanic sedimentary (Psed1/2) and crustal (Pg) phases (**Fig. 3a**). The reflections from the Moho (PmP) and from the top of the oceanic crust (PtopP) were also recorded, permitting to constrain the crustal structure of the incoming oceanic plate in great detail (**Fig. 3a & b**). The stations located on the forearc high and in the forearc basin show records of several sedimentary phases (Psed1/2) as well as crustal phases (Pg) (**Fig. 3c & d**). A number of reflected phases were identified and picked from these stations, including reflections from the oceanic Moho (PmP), top of the oceanic crust (PtopP), and the forearc basement reflections (PfbP) (**Fig. 3d**). Pn mantle phases were recorded on stations 45, 26, 59, 58 and 56 (**Fig. 3d**), providing the opportunity to define the velocity in the uppermost mantle. The final wide-angle dataset included ~15,000 first arrival traveltimes and ~4,000 reflection traveltimes.

3. Modeling

3.1 Seismic tomography

The crustal structure was modeled by the joint refraction/reflection 2D tomography code “Tomo2D” (Korenaga et al., 2000). We applied a “top-to-bottom” approach with a simple layered starting model. We

chose a grid spacing of 250 m in the horizontal direction. Vertical spacing increased with depth from 50 m at the seafloor to 330 m at 40 km depth. The correlation length parameters were defined as 1 km x 0.2 km (horizontal x vertical) at the top and linearly increasing to 8 km x 4 km at 40 km depth. Initially, the model was constrained only for the near offsets; then the depth extent of the rays was increased to include the deeper sections of the model space. Simultaneously, the positions of the reflectors were obtained, based on the inversion of the available reflection phases. The structure and the geometry of the sediments for the starting model were adopted from the collocated pre-stack depth migrated MCS profile, thus constraining the upper section of the model in detail. In addition, the position of the top of the oceanic crust in the tomographic inversion was controlled by the MCS depth migrated image (*Fig. 2*). The generalized procedure during the inversion was as follows: constraining the interface geometry based on the corresponding MCS depth section; inverting the near offset refracted phases to verify the consistency between datasets; fixing the upper section of the model with a weight of 1000 compared to the deeper sections. Then, we ran the inversion for the velocity and reflector geometry for the next depth layer. Subsequently, we fixed the obtained layer structure and repeated the previous step for the following deeper layer. Finally, we kept the entire crustal structure fixed and inverted for the velocity in the upper mantle. The final Vp model along the profile is shown in *Figure 4*.

3.2 Resolution tests

Several tests were performed to analyze the resolution of the obtained intermediate and final models. Initially, we used a forward ray shooting method to compute the traveltimes for the first arrival and reflected phases through our final models. The comparison of the seismic sections and the calculated traveltimes for several stations is shown in *Figure 3*. The calculated traveltimes, as predicted by the tomographic Vp velocity model, are in a good agreement with the recorded seismic sections. All the refracted phases, including Pg, Pn, and sedimentary phases Psed1/2 fit the observed arrivals. The reflection phases (PmP, PtopP, PfbP, and PmfcP, *see above, or Figure 3 for annotation*) also match the recorded data.

Checkerboard resolution tests provide information on the spatial and amplitude resolution, which is dependent on the given ray geometry and the velocity distribution. Small perturbations ($\pm 5\%$) with a

checkerboard pattern are added to the final Vp model. Using the same source-receiver geometry as in the tomographic inversion, synthetic traveltimes are computed through the perturbed medium. Next, in order to recover the initial perturbation pattern, the tomography is recomputed based on the synthetic traveltimes, with small (\pm pick uncertainty) random noise added. The results are presented in **Figure 5**. Three different anomaly sizes were used in the tests: 5x2.5 km, 10x5 km and 20x10 km (horizontal x vertical size). For all of them perturbation values of $\pm 5\%$ are used. For the small size perturbation we are able to recover the amplitude and size of the anomaly for the upper 5 km below sea floor (bsf), which roughly corresponds to the thickness of the sedimentary cover except across the consolidated accretionary prism. For the forearc basin, along the north-eastern portion of the profile, it is possible to recover the perturbations up to 8 km bsf, corresponding to the upper crust of the Sumatra block. Despite the presence of the high resolution MCS data, this test is essential for confirming that the given ray geometry is resolving adequately the shallow structures and does not produce extra errors in the deeper sections of the model. For the middle size anomaly the entire accretionary prism and Sumatra basement is recovered, but not the downgoing oceanic crust. Finally, the entire model space was only recovered by the largest size perturbation. In addition to the checkerboard test, a comparison of the refraction tomography with the MCS-derived velocity field was performed (**Fig. 5d**). For the shallow portion of the profile where the MCS data provide higher resolution and precision, the differences between the two methods yield comparable Vp distributions. For the major part of the profile the difference between the models are on average ~ 50 - 70 m/s. The maximum variations are observed at the structural interfaces, as the tomography tends to smooth the Vp field and the resolution is incomparably weaker. The maximum variations of ~ 150 m/s account for the limited quantity of the wide-angle record sections, the defined grid spacing of the tomography model, and the picking precision of the traveltimes.

3.3 Gravity modeling

Forward 2D gravity modeling was performed based on the final preferred velocity model, to verify that the structural model does not contradict gravity observations. The seismic velocities of the tomographic model were converted to densities using empirical and experimental relationships (*Carlson and Herrick, 1990; Christensen and Mooney, 1995*). The model space was extended laterally by 100 km

and down to a depth of 70 km, where the deep seismicity constrains the position of the downgoing oceanic plate. The mantle was modeled with a constant density of 3.35 g/cm^3 with the exception of the mantle wedge where a density of 3.30 g/cm^3 was used (**Fig. 6**). The study area covers a wide range in bathymetry (6000 m to 70 m water depth) as well as being located across a chain of forearc islands, so strong 3D effects are to be expected. However, as the aim of the gravity modeling is to confirm the tomography results and not to create a stand-alone model, pure 2D modeling is used. Despite these simplifications, we obtain a reasonable fit to the data, where the misfit does not exceed 20-25 mGal at the edges of the profile (**Fig. 6**). The key observation is that gravity modeling requires the forearc Moho to be at a minimal depth of 25 km.

3.4 Local seismicity relocation

A pseudo 3D model was constructed based on the refraction model by extruding the model in the profile-perpendicular direction but following the curved geometry of the trench; additionally the actual topography is respected in the construction of the 3D model. The seismicity catalogue of Tilmann et al. (2010) is relocated within this model using a nonlinear search method for the maximum likelihood location (NonLinLoc, Lomax et al., 2000) using P waves only, or assuming V_p/V_s values between 1.70 and 1.82. For well-located events (colored circles in Figures 1&7), the differences in depth and horizontal location between the P-only relocations and the relocations with various V_p/V_s ratios were minor and in generally smaller than the difference between the 3D relocation and the original location in the minimum 1D model. The locations shown in the figures assume a V_p/V_s ratio of 1.74, which gave close to the minimum rms.

4. Results and Discussion

Our interpretation is based on the results of the tomographic inversion and the pre-stack depth migrated reflection image shown in **Figures 2** and **4**, which will be discussed starting from the south-west towards Sumatra in the north-east.

In the south-west portion of the profile, 8 km thick oceanic crust overlain by a sedimentary cover enters the trench. Sediment thickness ranges from ca. 1 km on the outer rise and increases to up to 3.5 km at the deformation front (offset 50 km in **Fig. 2**). The observed sedimentary cover thickness is in good

agreement within both our datasets, and also fits the observed values on MCS lines BGR06-118 and BGR06-119 located offshore Simeulue (*Franke et al., 2008*) (**Fig. 1**). The MCS data show horizontally well stratified sediments cut by normal faults (**Fig. 2a**). The oceanic Moho is dipping from 13 km depth at the southwestern termination of the profile to 15 km depth below the deformation front (**Fig. 4**). The V_p distribution within the oceanic crust corresponds to a velocity profile characteristic for mature oceanic crust (*White et al., 1992*): increasing from 4.7 km/s at the basement to 5.9 – 6.0 km/s at 2 km depth below the basement, corresponding to the upper – lower crust transition, and finally increasing to 6.9 – 7.0 km/s at the Moho. The structure of the oceanic crust does not vary significantly along the profile.

The frontal prism extends from the deformation front (offset 51 km) to ~85 km offset and is characterized by thrust faulting resulting from active accretion of trench sediment (**Fig. 2**). The frontal prism is bounded by the accretionary prism located landwards (**Fig. 2**). The boundary between the frontal prism and the older accretionary wedge is imaged in the seismic velocity field (**Fig. 4**). The frontal prism shows V_p velocities ranging from 2 km/s below the seafloor to 4.2 km/s at the top of the oceanic plate with a general increase of the V_p away from the trench, due to compaction. The accretionary wedge is characterized by higher V_p values with less lateral variability, varying from 2 km/s at the top to 5.4 km/s, characterizing highly compacted, lithified and possibly metamorphosed material near the plate interface.

The observation that the frontal prism fronts a tectonically less active, older accretionary prism is supported by bathymetric studies, showing much smoother morphology on the accretionary prism compared to the lower slope (*Kopp et al., 2008*). The spatial correlation of the updip limit of the seismogenic zone with the changes in the morphology of a margin was shown by the dynamic Coulomb model of Wang and Hu (*2006*). Offshore Sumatra, based on morphology observations, the updip limit is located at around 110 km offset at a depth of 14 km (**Fig. 7**), which correlates with the location of the slope break, also suggested by the bathymetry analysis of Krabbenhoft et al., (*2010*). The location of the updip limit of the seismogenic zone is additionally supported by the relocation of seismicity in the area (**Fig. 7**).

A well-developed forearc basin underlain by Sumatra basement dominates the morphology northeast of offset 160-170 km (**Fig. 2b**). The sedimentary basin fill reaches a thickness of 3.5 km above the

depocenter. The deep pre-Neogene sedimentary strata (Berglar *et al.*, 2010) are tilted trenchward. An unconformity separates the pre-Neogene strata from more recent deposits, suggesting a complex episodic basin formation (Berglar *et al.*, 2010). The geometry of the basin is controlled by the Sumatra basement and bounded by the accretionary prism at around 175 km offset. This boundary also correlates with the location between the surface traces of the West Andaman and Mentawai fault zones, resolved in the bathymetry and MCS datasets (Berglar *et al.*, 2010). It is also possible that the structure is governed by backthrusts (Singh *et al.*, 2010 & 2011), as observed e.g. in the Aceh basin (Chauhan *et al.*, 2009). The surface trace is approximately located above the contact zone of the downgoing oceanic plate and the Sumatra basement and is traced southward to the tip of southern Sumatra and offshore Sunda Strait (Kopp *et al.*, 2001). Seismic Vp velocities are increasing within the sedimentary layers from 1.7 km/s near the seafloor to 3.5 km/s at the top of the Sumatra basement (**Fig. 4**). Vp velocities range from 5.0 km/s at the basement down to 6.0-6.1 km/s at a depth of 6 km below the basement, corresponding to the transition to the lower crust of the Sumatra block. The lower crust shows Vp velocities increasing from 6.2 km/s at the top to 7.0 km/s at the plate interface. The geometry and the depth of the forearc Moho are not recovered in our seismic dataset. However, based on the gravity modeling discussed above the Moho is likely found at a depth of ca. 25 – 27 km.

We compare the obtained crustal structure model south of the segment boundary of the 2004-2005 rupture areas (Franke *et al.*, 2008) to the SAGER profile published by Klingelhoefer *et al.* (2010), located to the north (see **Figure 1** for locations; see **Figure 7** for the profile comparison). The compared profiles were modeled using different techniques, based on different data acquisition setups. In addition, within our dataset only few Pn arrivals are available, which limits seismic sampling of the upper mantle on our profile compared to the SAGER data. This causes difficulties in one-to-one comparison of the small features.

Principal changes are observed in the structure of the incoming Indo-Australian plate as well as in the sediment supply at the trench. In the north, 5 km thick oceanic crust is subducting, posing a large contrast to the 8 km thick crust modeled in southern domain. Furthermore, in the 2004 rupture area the oceanic crust is overlain by ca. 3-3.5 km of sediment, reaching 5 km at the trench. In the southern domain, the

sedimentary cover is much thinner: 3 km thick in the trench and less than 1 km on the incoming oceanic plate. This observation is also consistent with the results of Dean et al. (2010), showing the shallowing of the oceanic basement towards the southeast and linking the changes in prism structure to variations in the lithological and rheological properties of the incoming trench sediments. This implies that the 96°E fracture zone is not only separating the oceanic crustal blocks of different thickness, but also acts as a barrier in the sediment transport along the trench. In addition, we see differences in the size and structure of the accretionary prism and possibly of the Sumatra block. Along the southern profile, the frontal prism and accretionary wedge reach a total width of ca. 130 km, while the SAGER profile documents a lateral extent of the accretionary complex exceeding 170 km. The velocity structure within the accretionary complexes is comparable in the range of values, but a frontal prism is not clearly recovered in the SAGER data. However, well-developed frontal prisms bounded by splay faults are documented along both segments in high-resolution bathymetry data (Henstock et al., 2006; Kopp et al., 2008). The geometry of the accretionary complexes also varies between the profiles. The distinct differences in accretionary prism geometry documented by the two seismic profiles shown in **Figure 7** as well as variations in material properties as discussed by Dean et al. (2010) are suggested to be linked to the changes in updip limit of seismicity as described by Tilmann et al. (2010).

The SAGER profile shows a maximum depth of the accretionary prism of 21 km, while on our profile it does not exceed 17 km. This suggests that below the accretionary prism the dip of the oceanic plate is lower in the northern segment, compared to south of Simeulue. The lateral increase of V_p values (around 200-220 km profile distance) in the accretionary prism on the SAGER profile towards the Sumatra block is also not observed on our profile, where the seismic velocities slightly decrease when approaching the Sumatra basement. This observation could be linked to the presence and activity of the West Andaman and/or Mentawai fault zones. In the northern domain, the West-Andaman fault is located around 260-270 km (SAGER profile **Fig. 7**), showing only minor V_p decrease around it. This would imply that in the southern segment the fault area is more active and thus produces extra fluid inflow into the accretionary complex, resulting in a decrease in seismic velocities.

The structure of the Sumatra crust shows a possible change across the segment boundary: the northern segment is characterized by a relatively thin crust with a flat Moho located at around 20 km depth, while the southern segment shows a much thicker crust with the Moho dipping towards Sumatra (in the southern segment the forearc Moho is not resolved in seismic data, and the thickness constrains are based on gravity modeling discussed above).

5. Conclusions

The wide-angle deep sampling tomographic model in the 2005 Sumatra earthquake rupture area, additionally constrained by gravity and MCS data reveals the crustal scale structure of the Sunda margin between Simeulue and Banyak islands. The major results obtained are: the oceanic plate carries a thin sedimentary cover (<1 km), except for the trench fill. The thickness of the oceanic crust is about 8 km and uniform along the profile. The active frontal prism of a width of ca. 35 km is bounded by the ca. 85 km wide accretionary prism. The relocated seismicity at the decollement coincides with the suggested position of the updip limit of the seismogenic zone ca. 65 km away from the trench.

The distinct differences in incoming oceanic plate structure and the accretionary complex structure observed in the two refraction seismic profiles located north and south of Simeulue Island support the existence of a segment boundary between the 2004 and 2005 rupture areas. The segment boundary is attributed to the subduction of the 96°E fracture zone. (In addition, the increase in crustal thickness southwards from Simeulue might suggest that the location of the segment boundary is determined not only by the features present on the oceanic plate, but might also spatially correlate to the changes in the crustal thickness of the overriding plate. This observation might also explain the increase in the dip of the oceanic slab from north to south, which is observed in the deep seismicity (*Pesicek et al., 2010*), and which is also visible on the seismic profiles.) Furthermore, fracture zone presents a natural separator between the blocks of oceanic crust of different thickness, as well as an efficient barrier to the trench parallel sediment transport. Such obstacle results in the difference of the amount of sediment present on the oceanic plate (3.5 km vs. <1 km) and in the trench (5 km vs. 3 km). This affects the width of the accretionary complex which is much narrower in the 2005 rupture segment, as well as being 4 km thinner,

resulting in ca. 35% volume difference. This observation suggests that in the northern segment the sediment in the accretionary prism are consolidated to higher state at the decollement, which is also inferred from the velocity profiles. Higher compaction state would result in the strengthening of the material and thus in the increased width of the seismogenic zone in the 2004 rupture area. The shift of the updip limit closer to the trench in the case of 2004 vs. 2005 earthquakes, thus could be attributed to the amount of sediment entering the system. Furthermore, the variability in the thickness of the accretionary prism as well as its consolidation state is affecting the thermal and permeability regimes: the key parameters in defining the behavior of the megathrust (*Hippchen and Hyndmann, 2008*). In addition, the thickness of the subduction channel, influencing the coupling effect at the plates interface when bathymetric features are present on the oceanic plate (*Ruff, 1989; Contreras-Reyes and Carrizo, 2011*), is also sediment supply dependent. All together, these factors determine the slip behavior of the megathrust. The slip of the 2004 earthquake propagated much closer to the trench (*Ishii et al., 2005; Ammon et al., 2005*) in contrast to the “normal” 2005 rupture, which is in agreement with the position of the updip limit of the seismogenic zone; thus explaining the drastic differences in the size of generated tsunamis (*Satake and Tanioka, 1999*). Summarizing, the sediment supply at the trench, which is one of the controlling factors regarding the evolution of the subduction complex at accretive subduction zones is also likely a key parameter controlling the width of the seismogenic zone (consequently, earthquakes and tsunami magnitudes).

Acknowledgements

We would like to thank the crew of R/V Sonne and the SeaCause Working group for their enormous help in collecting and processing of the data. We express great gratitude to Jun Korenaga for the discussion of seismic tomography and the Tomo2D code. The SeaCause project is funded by the German Federal Ministry of Education and Research (BMBF) under grant 03G0186B. A. S. wishes to thank the Petersen-Stiftung for their funding to complete this study.

References

- Aki, K., 1979. Characterization of barriers on an earthquake fault. *J. Geophys. Res.* 84, 6140–6148.
- Ammon, C. J., Ji, C., Thio, H.K., et al., 2005. Rupture process of the 2004 Sumatra-Andaman earthquake. *Science*. 308, 1133–1139, doi:10.1126/science.1112260.
- Ando, M., 1975. Source mechanisms and tectonic significance of historical earthquakes along the Nankai Trough, Japan. *Tectonophysics*. 27, 119–140.
- Berglar K., Gaedicke C., Franke D., Ladage S., Klingelhoefer F., Djajadihardja Y.S., 2010. Structural evolution and strike-slip tectonics off north-western Sumatra. *Tectonophysics*. 480, 119-132.
- Bilek S., Schwartz S., DeShon H., 2003. Control of seafloor roughness on earthquake rupture behavior. *Geology*. 31, 5, 455-458.
- Bilek, S., 2010. The role of subduction erosion on seismicity, *Geology*. 38, 5, 479-480, doi:10.1130/focus052010.1.
- Briggs, R.W., Sieh, K., Meltzner, A.J., et al., 2006. Deformation and slip along the Sunda megathrust in the great 2005 Nias-Simeulue earthquake. *Science*. 311, 1897–1901.
- Carlson, R.L., and Herrick, C.N., 1990. Densities and porosities in the oceanic crust and their variations with depth and age. *J. Geophys. Res.* 95, 9153–9170.
- Chauhan, A. P. S., Singh S.C., Hananto N.D., Carton H., Klingelhoefer F., Dessa J.-X., Permana H., White N.J. and Graindorge D., 2009. Seismic imaging of forearc backthrusts at northern Sumatra subduction zone. *Geophys. J. Int.* 179(3), 1772 – 1780, doi:10.1111/j.1365-246X.2009.04378.x.
- Chlieh, M., Avouac, J.-P., Hjorleifsdottir, V., et al. 2007. Coseismic slip and afterslip of the great Mw 9.15 Sumatra-Andaman earthquake of 2004, *Bull. Seismol. Soc. Am.* 97, S152– S173, doi:10.1785/0120050631.
- Christensen, N.I., and Mooney, W.D., 1995. Seismic velocity structure and composition of the continental crust: A global view. *J. Geophys. Res.* 100, 9761–9788.
- Collot, J.-Y., Marcaillou, B., Sage, F., Michaud, F., Agudelo, W., Charvis, P., Graindorge, D., Gutscher, M.-A., Spence, G., 2004. Are rupture zone limits of great subduction earthquakes controlled by upper plate structures? Evidence from multichannel seismic reflection data acquired across the northern Ecuador–southwest Colombia margin. *J. Geophys. Res.* 109, B11103. doi:10.1029/2004JB003060.
- Contreras-Reyes, E., Carrizo, D., 2011. Control of high oceanic features and subduction channel on earthquake ruptures along the Chile–Peru subduction zone. *Earth and Planet. Sci.*, 186, doi:10.1016/j.pepi.2011.03.002.
- Curry, J.R., 2005. Tectonics and history of the Andaman Sea region. *J. Asian. Earth. Sci.* 25, 187-232.
- Dean, S.M., McNeill, L.C., Henstock, T.J., Bull, J.M., Gulick, S.P.S., Austin, J.A., Bangs, N.L.B., Djajadihardja, Y.S., Permana, H., 2010. Contrasting Decollement and Prism Properties over the Sumatra 2004-2005 Earthquake Rupture Boundary. *Science*. 329, 5988, pp207-210.
- Deplus, C., Diament, M., Hebert, H., Bertrand, G., Dominguez, S., Dubois, J., Malod, J., Patriat, P., Pontoise, B., Sibilla, J.-J., 1998. Direct evidence of active deformation in the eastern Indian oceanic plate. *Geology*, 26, 131–134.
- DeShon, H.R., Engdahl, E.R., Thurber, C.H., Brudzinski, M., 2005. Constraining the boundary between the Sunda and Andaman subduction systems: Evidence from the 2002 M-w 7.3 Northern Sumatra earthquake and aftershock relocations of the 2004 and 2005 great earthquakes. *Geophys. Res. Lett.* 32, 24, DOI: 10.1029/2005GL024188.
- Dessa, J.-X., Klingelhoefer, F., Graindorge, D., Andre´, C., Permana, H., Gutscher, M.-A., Chauhan, A., and Singh, S., 2009. Megathrust earthquakes can nucleate in the forearc mantle: Evidence from the 2004 Sumatra event. *Geology*, 37, 659–662, doi:10.1130/G25653A.1.
- Diament, M., Harjono, H., Karta, K., Deplus, C., Dahrin, D., Zen Jr., M.T., Gérard, M., Lassal, O., Martin, A., Malod, J., 1992. Mentawai fault zone off Sumatra: a new key to the geodynamics of western Indonesia. *Geology*, 20 (3), 259–262.
- Franke, D., Schnabel, M., Ladage, S., Tappin, D.R., Neben, S., Djajadihardja, Y., Mueller, C., Kopp, H. & Gaedicke, C., 2008. The great Sumatra-Andaman earthquakes-imaging the boundary between the ruptures of the great 2004 and 2005 earthquakes. *Earth Planet. Sci. Lett.*, 269, 12, doi:10.1016/j.epsl.2008.01.047.
- Galahaut, V.K. and Catherine, J.K., 2006. Rupture characteristics of 28 March 2005 Sumatra earthquake from GPS measurements and its implications for tsunami generation. *Earth planet. Sci. Lett.*, 249, 39–46.
- Graindorge, D., Klingelhoefer, F., Sibuet J.-C., et al., 2008. Impact of the lower plate on upper plate deformation at the NW Sumatran convergent margin from seafloor morphology. *Earth Planet. Sci. Lett.*, 275, 201 – 210, doi:10.1016/j.epsl.2008.04.053.
- Gulick, S.P.S., Austin, J.A., McNeill, L.M., Bangs, N.L., Martin, K.M., Henstock T.J., Bull J.M., Dean, S.M., Djajadihardja, Y.S., and Permana, H., 2011. Thick indurated sediments extend updip rupture propagation during 2004 Sumatra earthquake. *Nature Geoscience*, 4 (7), doi:10.1038/NNGEO1176.
- Gutscher, M.-A., Kukowski, N., Malavielle, J. & Lallemand, S., 1998. Episodic imbricate thrusting and underthrusting: analog experiments and mechanical analysis applied to the Alaskan Accretionary Wedge. *J. Geophys. Res.*, 103, 10161-10176.
- Henstock, T.J., McNeill, L.C., Tappin, D., 2006. Seafloor morphology of the Sumatran subduction zone: surface rupture during a mega-thrust earthquakes? *Geology*, 34, 485–488.
- Hippchen, S., and Hyndman, R.D., 2008. Thermal and structural models of the Sumatra subduction zone: Implications for the megathrust seismogenic zone. *J. Geophys. Res.* 113, B12103, doi:10.1029/2008JB005698.
- Hsu, Ya-Ju., Simons, M., Avouac, J.-P., et al., 2006. Frictional afterslip following the 2005 Nias-Simeulue earthquake, Sumatra. *Science*, 312 (5782), doi: 10.1126/science.1126960.

- Ishii, M., Shearer, P.M., Houston, H., Vidale, J.E., 2005. Rupture extent, duration, and speed of the 2004 Sumatra-Andaman earthquake imaged by the Hi-Net array. *Nature* 435, 933-936.
- Klingelhoefer, F., Gutscher, M.-A., Ladage, S., Dessa, J.-X., Graindorge, D., Franke, D., Andre', C.H., Permana, T.Y., and Chauhan, A., 2010. Limits of the seismogenic zone in the epicentral region of the 26 December 2004 great Sumatra-Andaman earthquake: Results from seismic refraction and wide-angle reflection surveys and thermal modeling. *J. Geophys. Res.* 115, B01304, doi:10.1029/2009JB006569.
- Kopp, H., Weinrebe, W., Ladage, S., et al., 2008. Lower slope morphology of the Sumatra trench system. *Basin Res.* 20, 519–529.
- Kopp, H., Flueh, E.R., Klaeschen, D., Bialas, J., Reichert, C., 2001. Crustal structure of the central Sunda margin at the onset of oblique subduction. *Geophys. J. Int.* 147, 449-474.
- Korenaga, J., Holbrook, S., Kent, G., Kelemen, P., Detrick, R.S., Larsen, H.-C., Hopper, J.R., Dahl-Jensen, T., 2000. Crustal structure of the southeast Greenland margin from joint refraction and reflection seismic tomography. *J. Geophys. Res.* 105, doi:10.1029/2000JB900188.
- Ladage, S., Gaedicke, C., Barckhausen, U., Heyde, I., Weinrebe, W., Flueh, E.R., Krabbenhoef, A., Kopp, H., Fajar, S., Djajadihardja, Y., 2006. Bathymetric survey images structure off Sumatra. *EOS Trans. AGU* 87 (17), 165.
- Lallemand, S.E., Schnürle, P., and Malavieille, J., 1994. Coulomb theory applied to accretionary and nonaccretionary wedges: Possible causes for tectonic erosion and/or frontal accretion. *J. Geophys. Res.* 99(B6), 12,033–12,055, doi:10.1029/94JB00124.
- Lomax, A., Virieux, A.J., Volant, P., & Berge, C., Thurber, C. H. & Rabinowitz, N. (*ed.*), 2000. Probabilistic earthquake location in 3D and layered models: Introduction of a Metropolis-Gibbs method and comparison with linear locations. *Advances in Seismic Event Location*, Kluwer, Amsterdam, 101-134
- Mackay S. and Abma, R., 1993. Depth-focusing analysis using a wave-front-curvature criterion. *Geophys.* 58, 8, pp 1148-1156.
- Malod, J.-A., and Kemal, B.M., 1996. The Sumatra Margin: Oblique subduction and lateral displacement of the accretionary prism. *Geol. Soc. Spec. Publ.* 106, 19– 28, doi:10.1144/GSL.SP.1996.106.01.03.
- McCaffrey R., 2009. The tectonic framework of the Sumatran subduction zone. *Annu. Rev. Earth Planet. Sci.* 37, pp 345-366.
- Meltzner, A. J., Sieh, K., Abrams, M., Agnew, D.C., Hudnut, K.W., Avouac, J., and Natawidjaja, D.H., 2006. Uplift and subsidence associated with the great Aceh-Andaman earthquake of 2004. *J. Geophys. Res.* 111, B02407, doi:10.1029/2005JB003891.
- Moore, G.F. and Curray, J., 1980. Structure of the Sunda trench lower slope off Sumatra from multichannel seismic reflection data. *Mar. Geophys. Res.* 4, 319-340.
- Moore, J.C., Rowe, C., and Meneghini, F., 2007. How accretionary prisms elucidate seismogenesis in subduction zones, in *The Seismogenic Zone of Subduction Thrust Faults*, edited by T. H. Dixon and J. C. Moore, pp. 15–40, Columbia Univ. Press, New York.
- Peacock, S.M., and Hyndman, R.D., 1999. Hydrous minerals in the mantle wedge and the maximum depth of subduction thrust earthquakes. *Geophys. Res. Lett.* 26, 2517– 2520, doi:10.1029/1999GL900558.
- Pesicek, J.D., Thurber, C.H., Widiyantoro, S., Zhang, H., DeShon, H.R. and Engdahl, E.R., 2010. Sharpening the tomographic image of the subducting slab below Sumatra, the Andaman Islands and Burma. *Geophys. J. Int.* 182: 433–453. doi: 10.1111/j.1365-246X.2010.04630.x
- Prawirodirdjo, L., and Bock, Y., 2004. Instantaneous global plate motion model for 12 years of continuous GPS observations. *J. Geophys. Res.* 109, B08405. doi:10.1029/2003JB002944.
- Ruff, L., 1989. Do trench sediments affect great earthquake occurrence in subduction zones? *Pure Appl. Geophys.* 129, 263–282, doi:10.1007/BF00874629.
- Ryan, H.F., and Scholl, D.W., 1993. Geologic implications of great interpolate earthquakes along the Aleutian arc. *J. Geophys. Res.* 98, 22135–22146.
- Satake, K., and Tanioka, Y., 1999. Sources of tsunami and tsunamigenic earthquakes in subduction zones. *Pure Appl. Geophys.* 154, 467 - 483.
- Sclater, J.G. and Fisher, R.L., 1974. Evolution of the east-central Indian Ocean, with emphasis on the tectonic setting of the Ninetyeast Ridge. *Geol. Soc. Am. Bull.* 85, 683-702
- Sibuet, J.-C., Rangin, C., Le Pichon, X., et al., 2007. 26th December 2004 great Sumatra-Andaman earthquake: Co-seismic and post-seismic motions in northern Sumatra. *Earth Planet. Sci. Lett.* 263, 88– 103, doi:10.1016/j.epsl.2007.09.005.
- Simoes, M., Avouac, J.P., Cattin, R., and Henry, P., 2004. The Sumatra subduction zone: A case for a locked fault zone extending into the mantle. *J. Geophys. Res.* 109, B10402, doi:10.1029/2003JB002958.
- Sieh, K. and Natawidjaja, D., 2000. Neotectonics of the Sumatran fault, Indonesia. *J. Geophys. Res.* 105 (B12), doi: 10.1029/2000JB900120
- Singh, S.C., Carton, H., Tapponnier, P., et al., 2008. Seismic evidence for broken oceanic crust in the 2004 Sumatra earthquake epicentral region. *Nature Geosci.* 1(11), 777–781. doi:10.1038/ngeo336.
- Singh, S.C., Hananto, N.D., Chauhan, A.P.S., Permana, H., Denolle, M., Hendriyana, A., Natawidjaja, D., 2010. Evidence of active backthrusting at the NE Margin of Mentawai Islands, SW Sumatra. *Geophys. J. Int.* 180(2), doi: 10.1111/j.1365-246X.2009.04458.x
- Singh S.C., Hananto N.D., Chauhan A.P.S., 2011. Enhanced reflectivity of backthrusts in the recent great Sumatran earthquake rupture zones. *Geophys. Res. Lett.* 38, doi: 10.1029/2010GL046227
- Spence, W., 1977. The Aleutian arc: tectonic blocks, episodic subduction, strain diffusion, and magma generation. *J. Geophys. Res.* 82, 213–230.

Subarya, C., Chlieh, M., Prawirodirdjo, L., et al., 2006. Plate-boundary deformation associated with the great Sumatra-Andaman earthquake. *Nature*. 440, 46–51.

Tilmann, F.J., Craig, T.J., Grevemeyer, I., Suwargadi, B., Kopp, H. and Flueh, E.R., 2010. The updip seismic/aseismic transition of the Sumatra megathrust illuminated by aftershocks of the 2004 Aceh-Andaman and 2005 Nias events. *Geophys. J. Int.* 181: 1261–1274. doi: 10.1111/j.1365-246X.2010.04597.x.

Wang, K. and Hu, Y., 2006. Accretionary prisms in subduction earthquake cycles: The theory of dynamic Coulomb wedge. *J. Geophys. Res.* 111(B6), doi:10.1029/2005JB004094

White, R.S., McKenzie, D., and O’Nions, R., 1992. Oceanic crustal thickness from seismic measurements and rare earth element inversions, *J. Geophys. Res.* 97, 19,683–19,715, doi:10.1029/92JB01749.

Figures

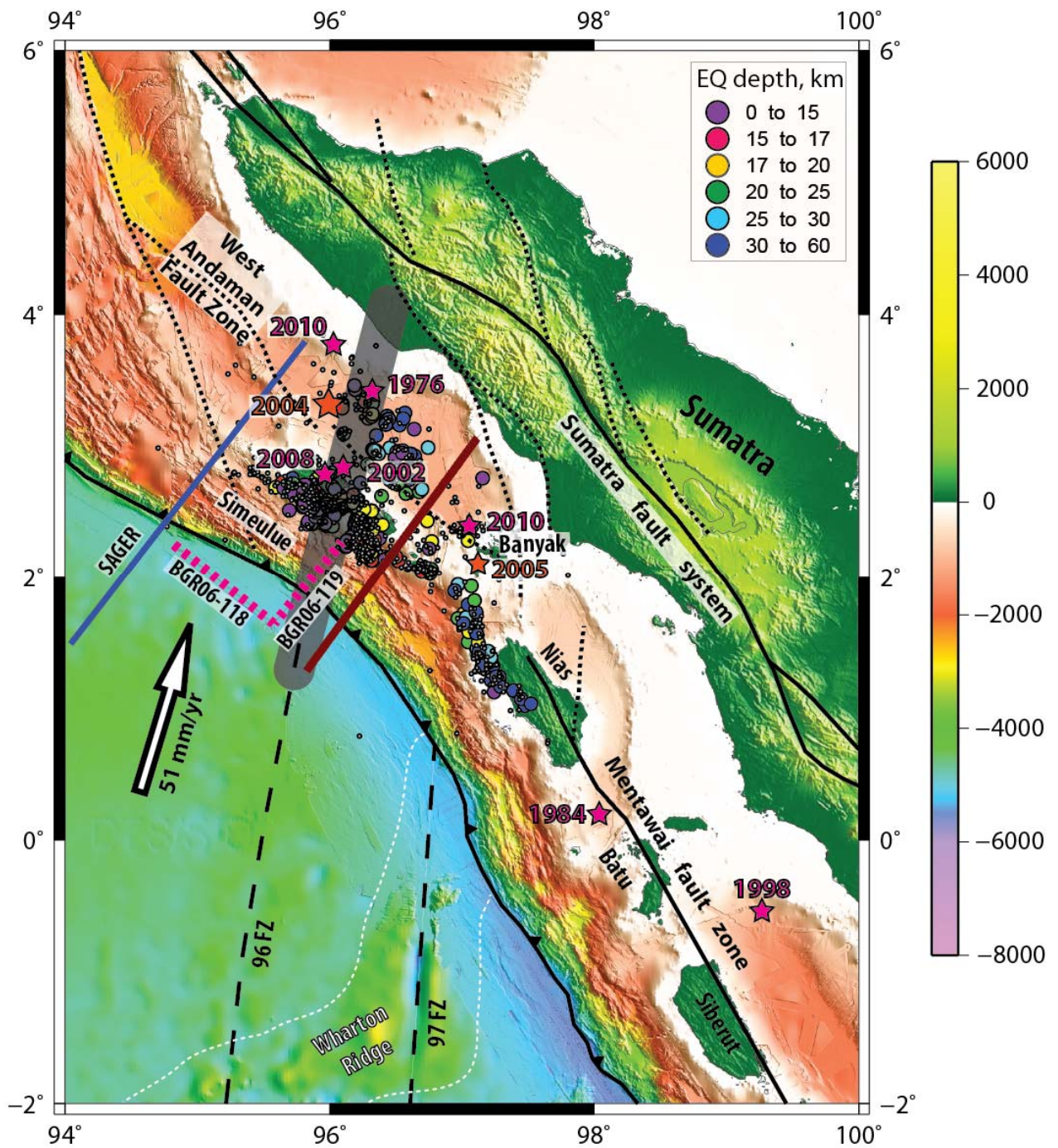


Figure 1. Map of the study area offshore Northern Sumatra. The location of the wide-angle and the collocated MCS profiles described in this study are shown by red line. The arrow shows the plate convergence vector. Major faults are shown by black solid and dashed lines (after Curray, 2005). Hypocenter locations of $M_w \geq 7.0$ earthquakes are shown by magenta stars. The local seismicity relocated

in a pseudo 3D model (recorded for 3 month in 2006, see text) is shown by depth color-coded circles (rms < 0.1 s, seismicity with poor depth constrains is shown by gray circles; after *Tilmann et. al., 2010*). The proposed segment boundary between the rupture areas of the 2004 and 2005 earthquakes is shown by thick gray line (*Franke et. al., 2008*). Dashed white lines mark the extent of the Wharton Ridge in the vicinity of the trench. Bold black dashed lines are the fracture zones on the oceanic plate identified from the bathymetric and magnetic data. Blue line – seismic profile SAGER shown on **Figure 7** from *Klingelhoefer et al., 2010*. Dashed magenta lines – MCS profiles described in *Franke et. al., 2008*.

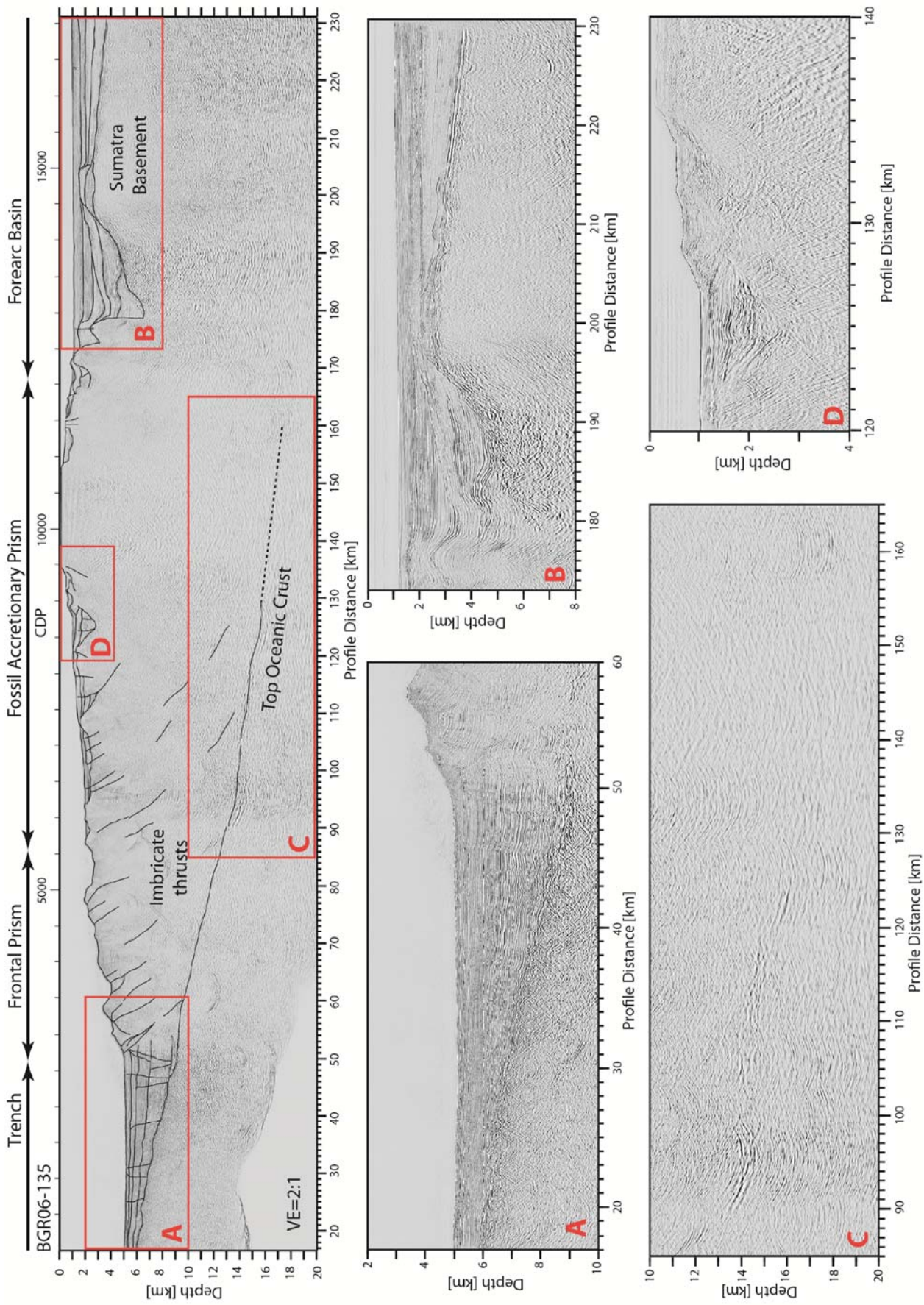
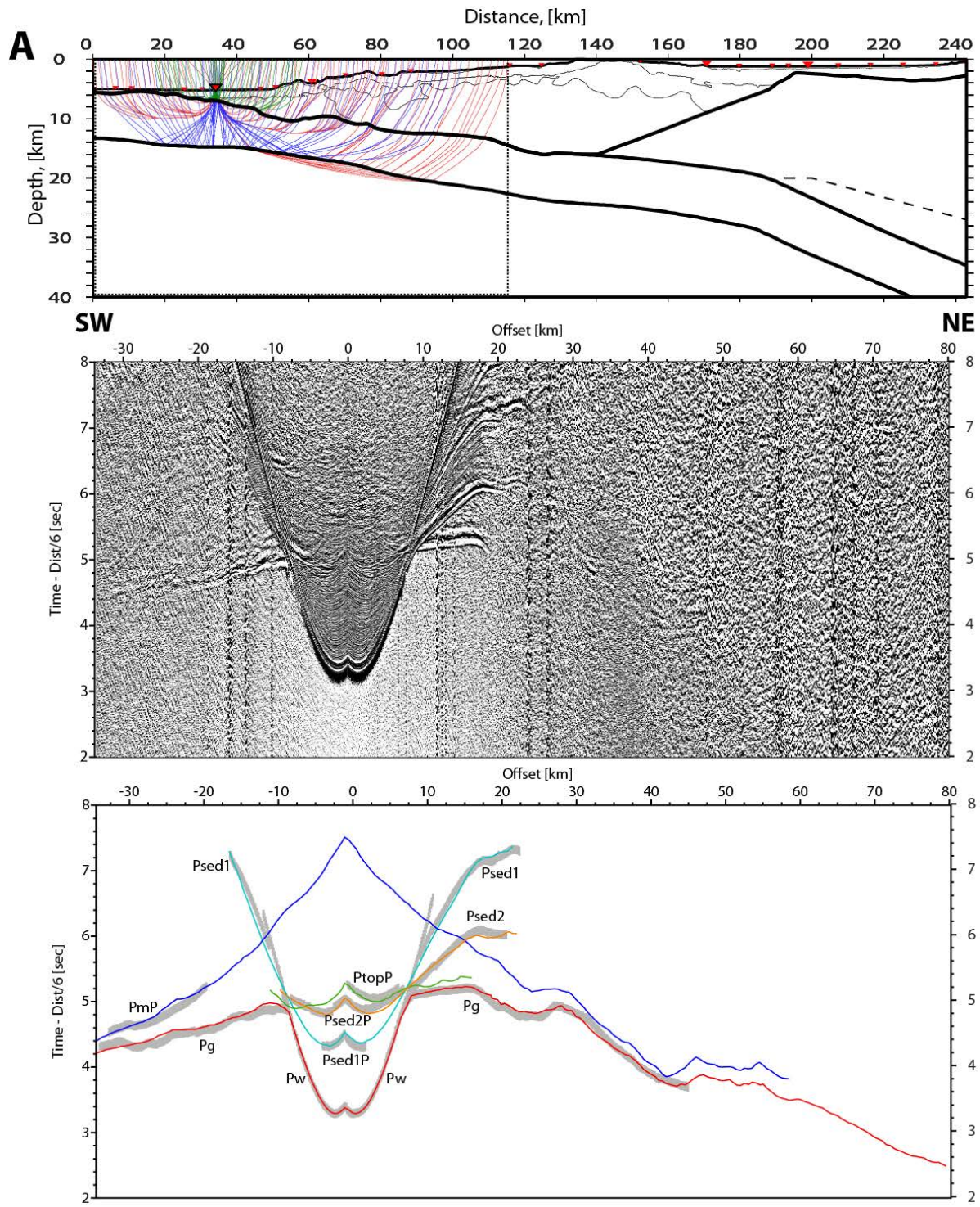
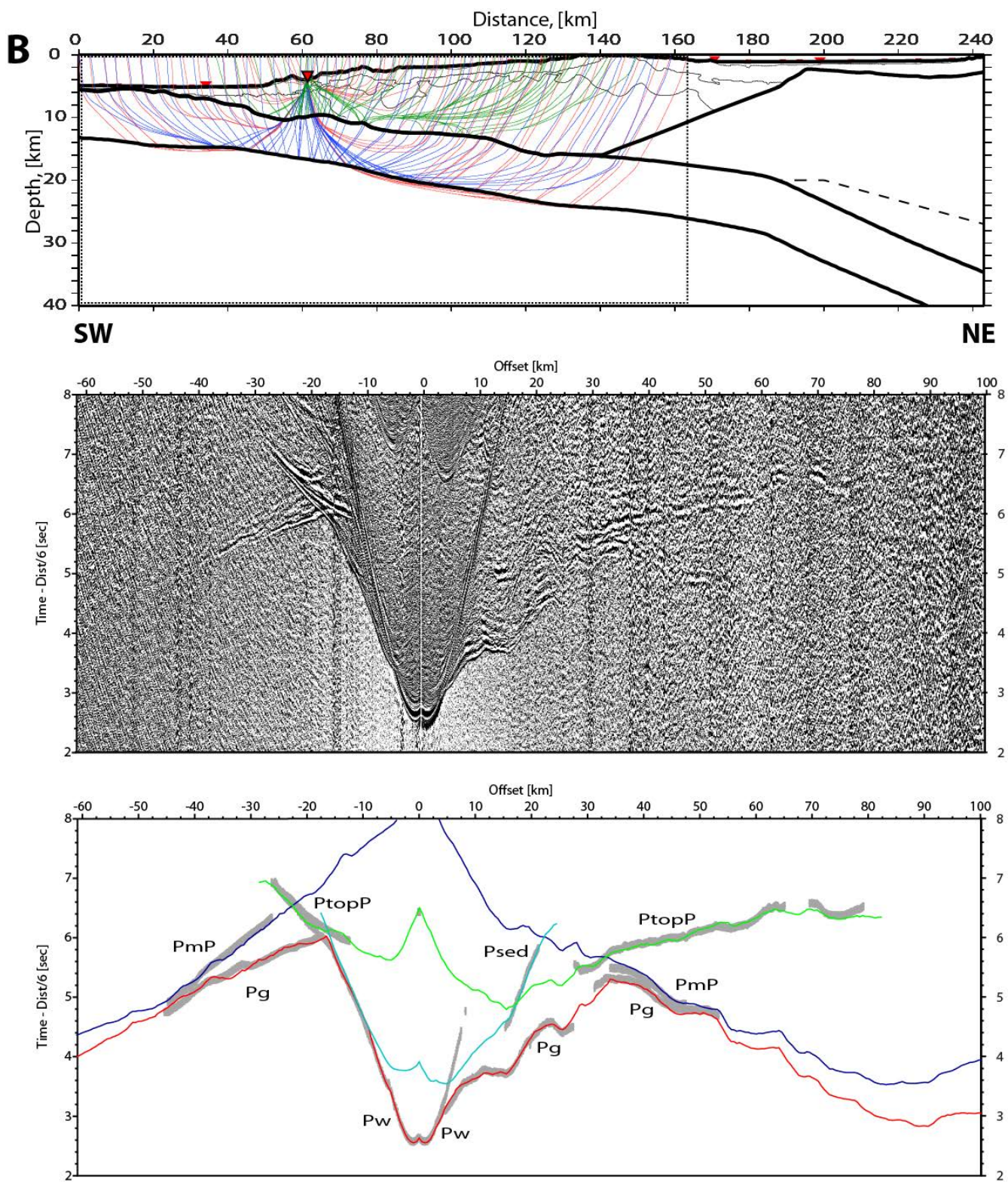
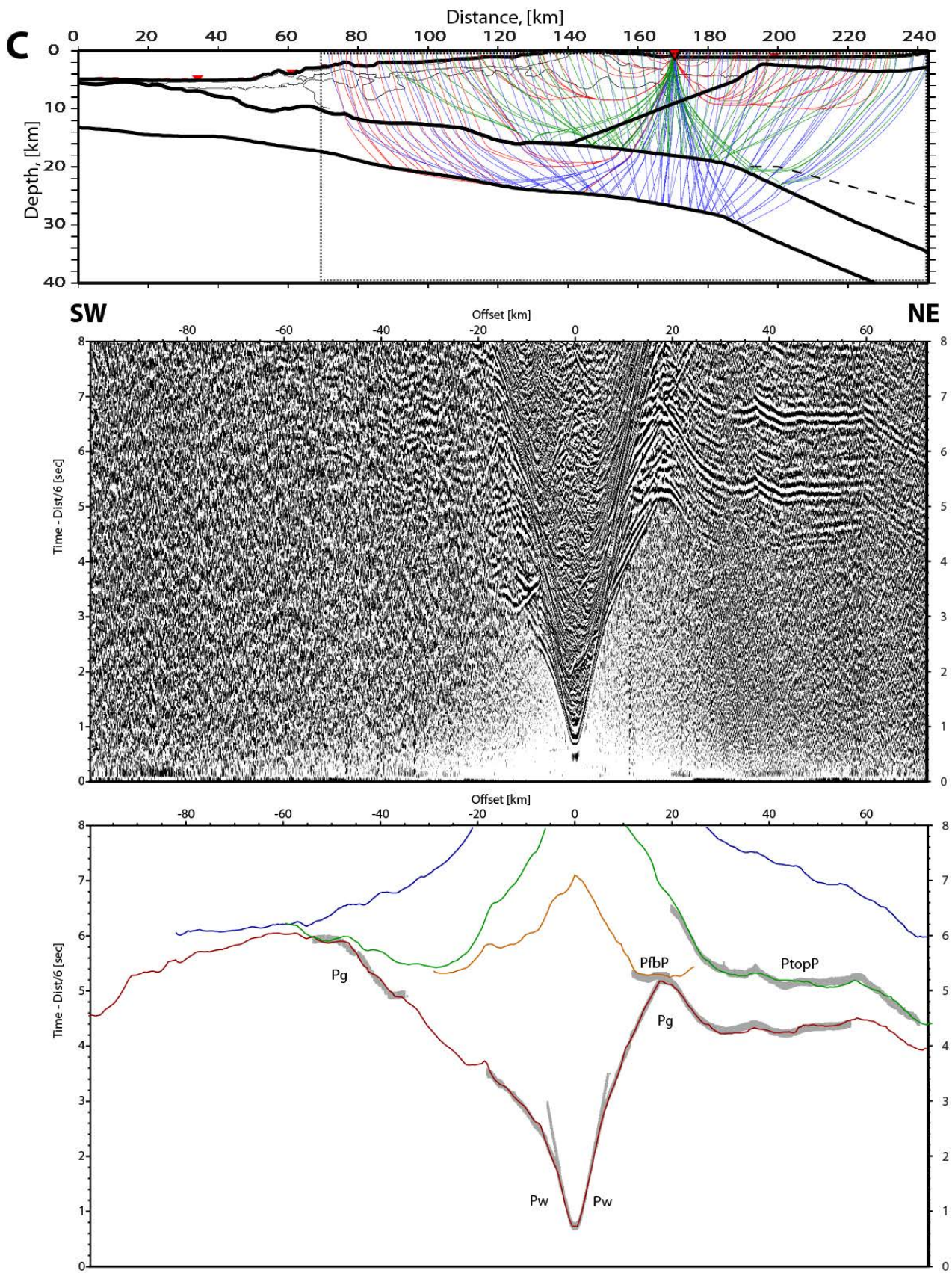


Figure 2. Pre-stack depth-migrated seismic section (BGR06-135) collocated with the wide-angle profile. Top panel shows the entire section with the line-drawing interpretation overlain. Bottom panels are the zoom-ins on the selected areas of the profile: A) oceanic plate, B) forearc basin, C) deep section of the contact with oceanic crust, D) slope break area around forearc high.







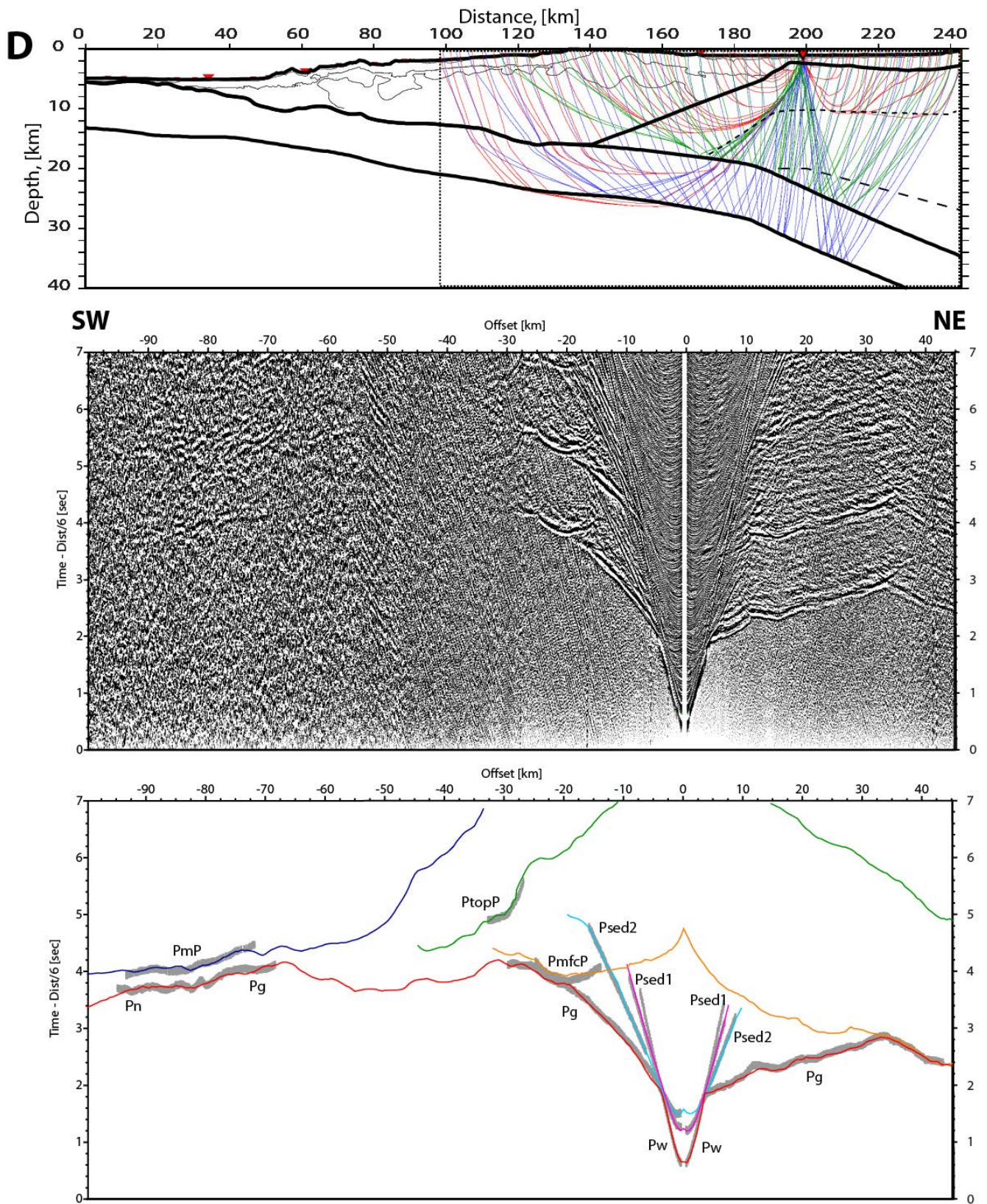


Figure 3. Data examples for four ocean bottom stations and the corresponding seismic rays obtained with forward modeling approach, locations are marked in *Figure 4*. Top plots show the schematic final

model with the OBS marked by red triangles, seismic rays are shown by colorcode: red – refractions, blue – PmP mantle reflections, green – PtopP reflection from the top of the oceanic crust, dotted box shows the lateral extent of the data sections. Middle panels show the data sections plotted with a reduction velocity of 6 km/s. Bottom panels show the picked traveltimes (gray lines, thickness corresponds to the pick uncertainty), color lines are the forward predicted traveltimes for selected phases computed through the final tomography model. The phases: Pw – direct water wave, Pg – crustal refraction, Pn – mantle refraction, Psed1/2 – refracted waves in the sedimentary layers, PmP – Moho reflection, PtopP – reflection from the top of the oceanic crust, PfbP- reflection from the top of forearc basement, PmfcP – reflection from forearc upper/lower crust boundary.

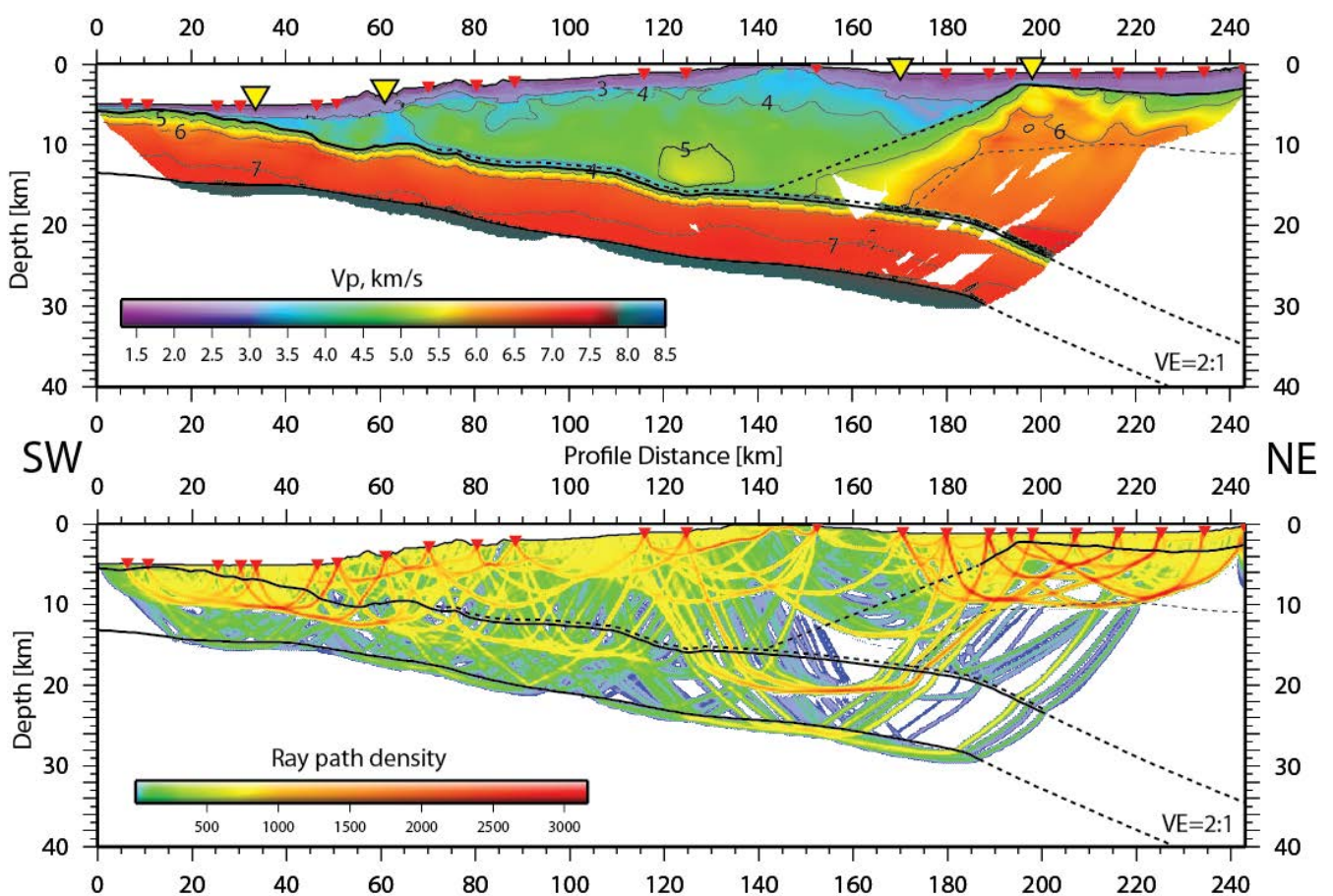


Figure 4. Tomographic inversion offshore northern Sumatra. Top panel: Vp distribution along the profile, with the black lines showing the position of the reflectors (dashed lines – reflectors which are poorly constrained). Bottom panel shows the final ray path coverage during the tomographic inversion. Yellow triangles on middle panel show the location of the ocean bottom stations described in *Figure 3*.

The low-velocity layer on top of the oceanic crust is a remnant of the input model and not required by the data.

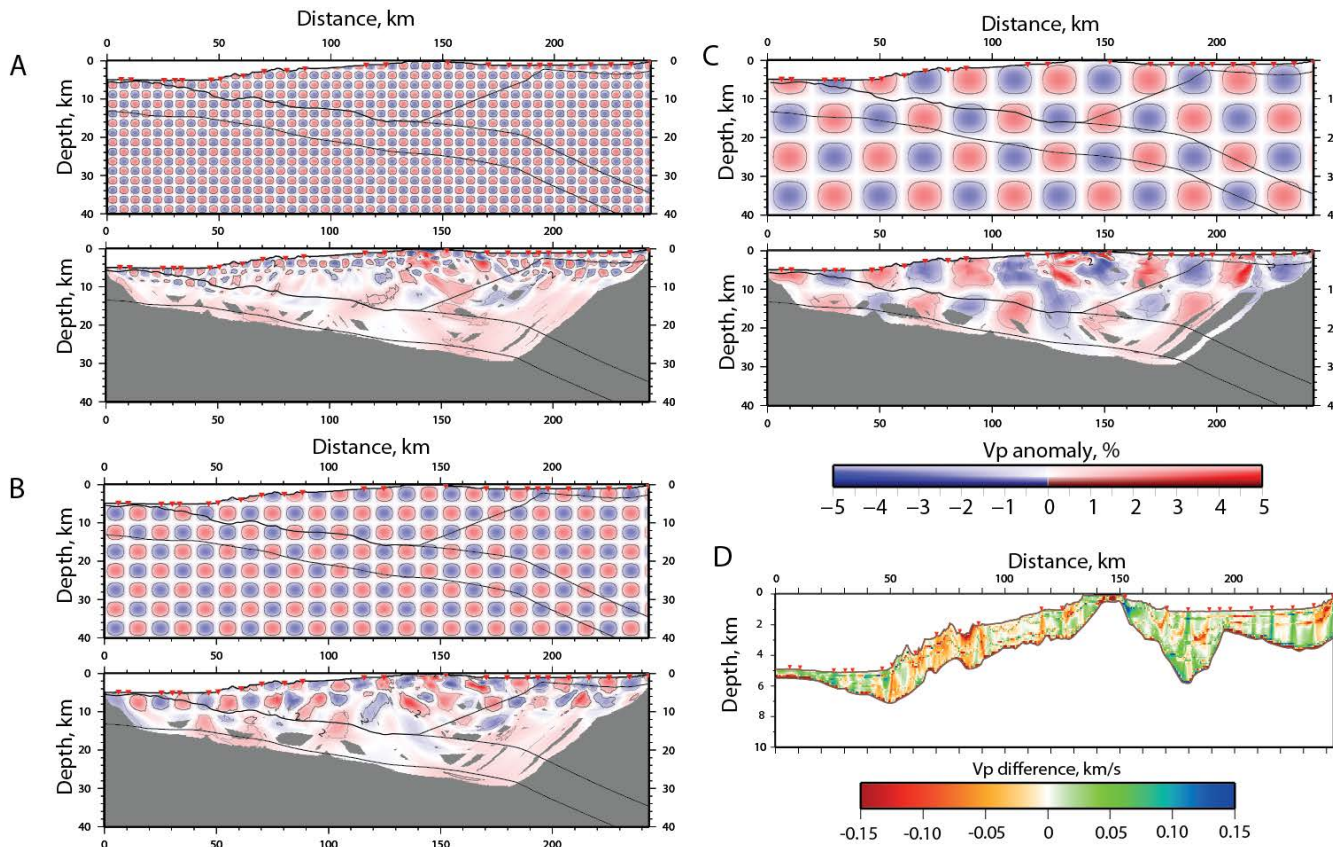


Figure 5. Results of the checkerboard tests A, B, and C. For all tests $\pm 5\%$ anomaly of different size was added to the final tomography model. The upper panels show the checkerboard test pattern for each test, while the bottom panels show the recovery of patterns. The size of the anomalies are A) 5×2.5 km B) 10×5 km and C) 20×10 km. Black lines show the position of the reflectors obtained during tomographic inversion. D) The comparison of the velocity in the shallow part of the model between wide-angle tomography and pre-stack MCS focusing analysis; in the white area Vp from the focusing analysis is not resolved.

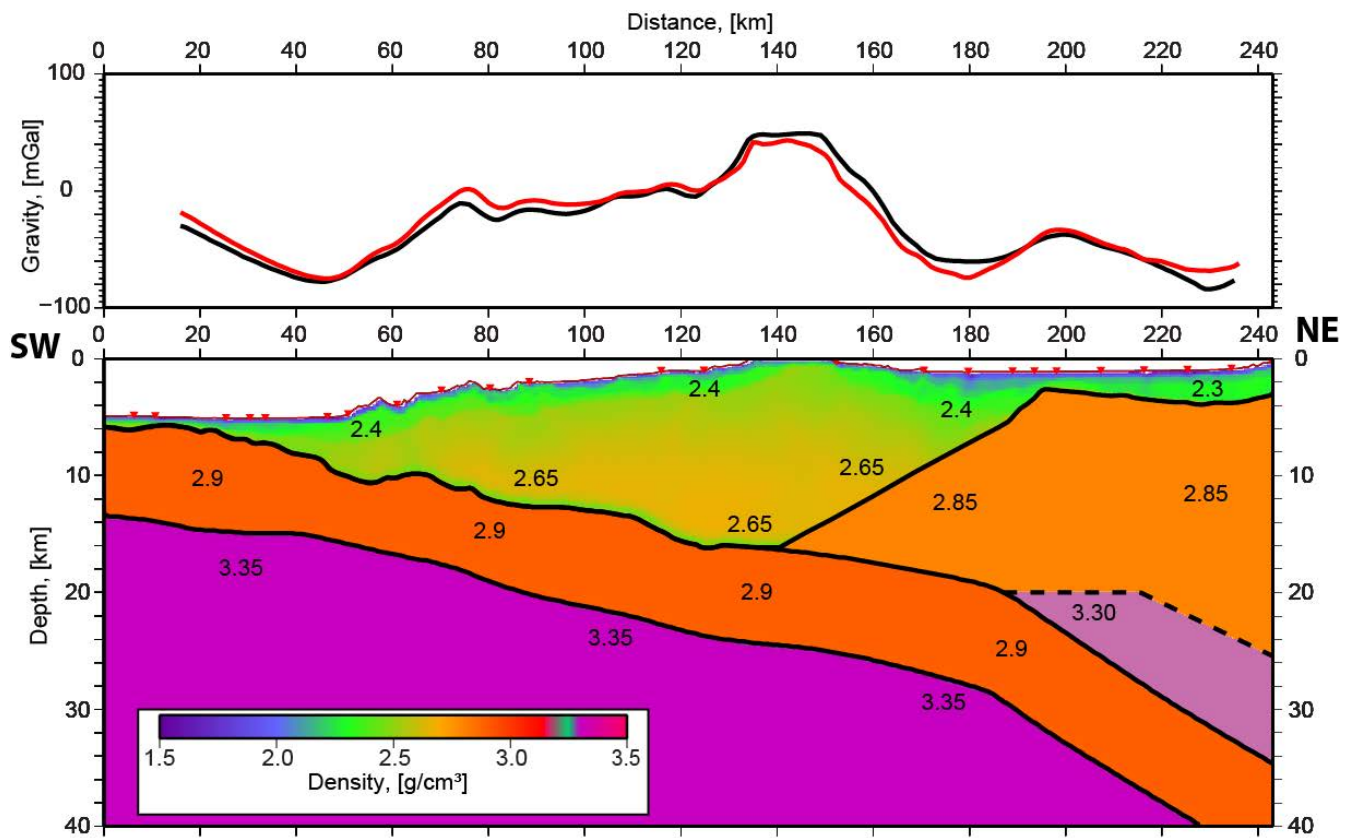


Figure 6. Forward gravity model based on tomographic image. The final preferred velocity model is converted to density and the gravity response is computed. The top panel shows the ship gravity data (black), and the model response (solid red). The bottom panel shows the density model, values are in g/cm^3 . A pure 2D approach is used in the gravity modeling.

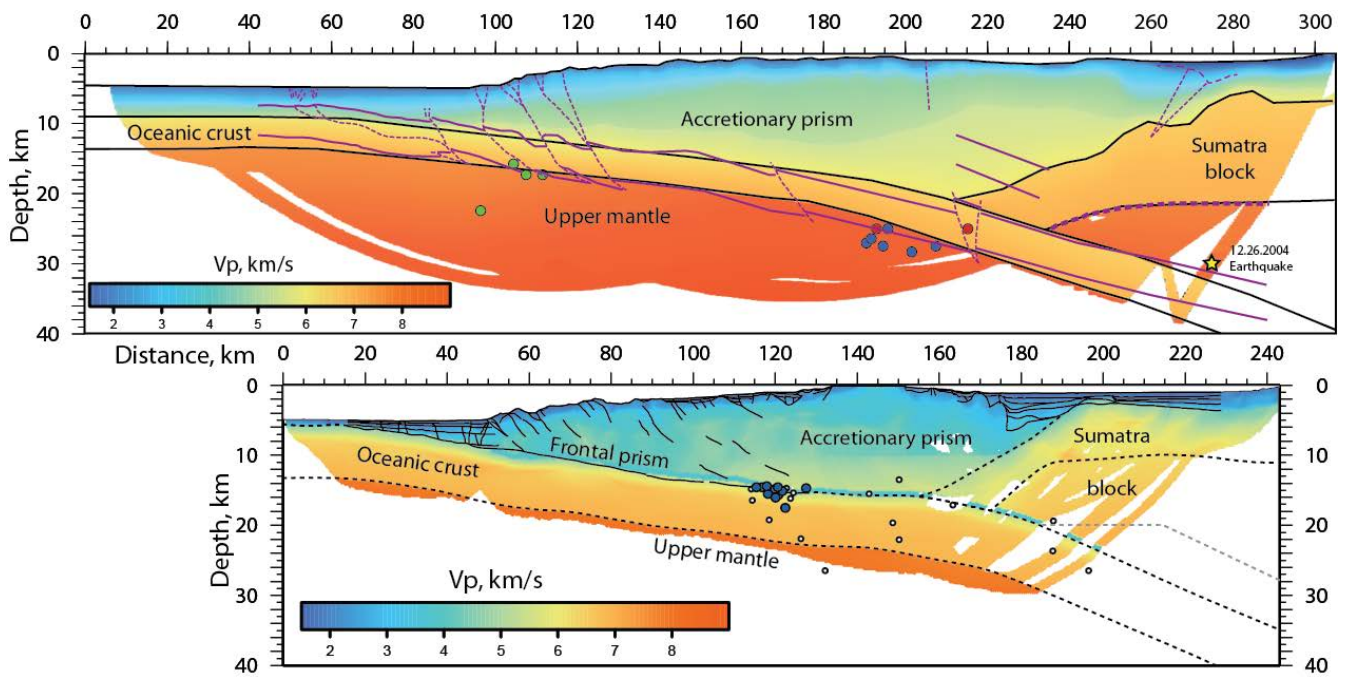


Figure 7. Comparison of the crustal structure along two adjacent segments offshore Sumatra. Identical scale and color-code are used for both models. **Top panel:** background model modified after Klingelhofer *et al.*, 2010 (location is shown by blue line in **Figure 1**). Line-drawing interpretation: black - from Klingelhofer *et al.*, 2010; blue - based on Singh *et al.*, 2008 (**Figure 4**). Aftershocks from within ± 50 km are projected onto the profile: steep frontal thrust events (green), thrust events below the Simeulue plateau (blue) and steep thrusts (red) (adapted from Singh *et al.*, 2008). **Bottom panel** represents the model obtained in this study: black lines are the line-drawing from the MCS profile, the dashed lines are the reflectors constrained by the tomography and gravity modeling. Circles are the projection of the seismicity onto the line of the profile within the ± 10 km corridor (seismicity of Tilmann *et al.*, 2010 relocated in a pseudo 3D model based on the refraction model, see text). Blue circles are well-constrained hypocenters. The low-velocity layer on top of the oceanic crust is not required by the data.

CURRICULUM VITAE

Name Alexey Shulgin
Date and Place of Birth December 1, 1982 Moscow, Russia
Citizenship Russia

1989-1999 School 1282, Moscow, Russia

1999-2005 M.S. in physics - Physics Department, Lomonosov Moscow State University, Russia

2005-2006 M.S. in Earth and Planetary Science - Earth and Planetary Science department, University of California Berkeley, USA

2006 Visiting Scientist at University of Copenhagen, Denmark

2006-present Ph.D. Geomar, Kiel, Germany
During the Ph.D. study:

- Participated in 7 marine expeditions. Total duration ca. 9 months.
- 6 peer-reviewed publications
- 23 abstracts at international conferences (AGU, EGU, IGC, DGG)